

Masterarbeit
Optimal Strategies for Exploring Near-by Stars
RT-MA 2020/15
Author:
Johannes Lebert



Betreuer:

Andreas Hein
Initiative for Interstellar Studies

Martin Dziura
Lehrstuhl für Raumfahrttechnik / Institute of Astronautics
Technische Universität München



Acknowledgments

I want to thank my supervisor Andreas Hein from the Initiative for Interstellar Studies, who gave me the possibility to work on this specific topic and allowed me to develop and realize my own ideas in great liberty. I really enjoyed our regular discussions and learned a lot, not least how to derive the time delay of the sunset between Paris and Munich.

Furthermore, I would like to thank Martin Dziura from the Chair of Astronautics at the Technical University of Munich, who agreed to supervise the thesis formally and provided me with all relevant resources. Without him, this thesis would not have been possible.

Zusammenfassung

Entdeckungen von Exoplaneten und kontinuierliche Technologiefortschritte im vergangenen Jahrzehnt lassen den Gedanken an interstellare Reisen und Forschungsmissionen weiter aufleben. Während bereits etliche Sondenkonzepte vorgeschlagen und geeignete Technologien diskutiert wurden, sind Studien zu geeigneten Erkundungsstrategien nur vereinzelt zu finden und mitunter lückenhaft.

Die vorliegende Arbeit befasst sich mit der Entwicklung optimaler Strategien zur Erforschung nahegelegener Sterne. Hierfür wird die Strategieplanung interstellarer Forschungsmissionen als bi-kriterielles Multi-Vehikel Open Routing Problem mit Profiten formuliert. Zur Lösung des resultierenden Optimierungsproblems wird ein angepasster hybrider multi-kriterieller genetischer Algorithmus verwendet. Im Rahmen der Missionsmodellierung wird eine konstante Reisegeschwindigkeit der Sonden von 10 % der Lichtgeschwindigkeit angenommen. Ferner bewegen sich die Sonden auf geradlinigen Trajektorien und beschränken sich auf Flyby-Missionen. Die zugrundeliegenden Sternmodelle basieren auf Daten des zweiten Gaia Release (Gaia DR2) und umfassen bis zu 10,000 Sterne. Dies entspricht einem kugelförmigen Volumen mit einem Radius von 110 Lichtjahren um die Sonne. Im Kontext der Sternmodellierung wird ein allgemeines Konzept für eine Sternmetrik vorgeschlagen, die jedem Stern einen gewissen Wert zuweist, abhängig von seinem potentiellen Beitrag zum übergeordneten Missionsziel. Außerdem wird ein Testmodell mit einer exakt gleichmäßigen Sternverteilung generiert, um den Algorithmus zu validieren und einzustellen.

Es zeigte sich eine erhebliche Verbesserung der Algorithmusperformance, wenn zu Beginn die Zeitbeschränkung vorübergehend aufgehoben wird, welche die maximalen Routenlänge begrenzt. Für das Testmodell generiert der Algorithmus dann Lösungen, die im Bereich einer Abweichung von 10 % zur theoretischen Ideallösung liegen. Eine qualitative Analyse der Gaia-basierten Sternmodelle ergab eine annähernd gleichmäßige räumliche Verteilung der Sterne, lässt man Effekte infolge von Binär- sowie Mehrfachsternsystemen außen vor.

Für eine vorgegebene Sondenanzahl ergibt sich ein weitestgehend linearer Zusammenhang zwischen Missionszeit und der Anzahl besuchter Sterne. Für eine bestimmte Missionszeit steigt die Anzahl besuchter Sterne mit zunehmender Sondenanzahl m gemäß $\sim m^{0.6}$. Die Sondenanzahl beeinflusst ferner die Sternauswahl und Routenstruktur: Für hohe Sondenanzahlen werden bevorzugt nahegelegene Sterne ausgewählt, für niedrigere Sondenanzahlen werden dagegen auch weiter entfernte Sterne berücksichtigt und kürzere Transferdistanzen ermöglicht. Dadurch ergeben sich folgende Schlussfolgerungen für mögliche interstellare Explorationsstrategien: Im Fall eines geringen Energiebudgets (bspw. begrenzte Treibstoffmenge) und zur Erforschung weiter entfernter Sterne bieten sich niedrige Sondenanzahlen an. Im Gegensatz dazu ermöglichen hohe Sondenanzahlen eine vergleichsweise schnelle Erforschung von Sternen in der unmittelbaren Sonnenumgebung auf Kosten einer weniger ressourcenoptimalen Routenwahl. Für eine solche Strategie würden sich daher eher kleinskalige Sondenkonzepte eignen, die keinen Treibstoff mitführen müssen. Im Fall hoher Sondenanzahlen ist gemäß der hergeleiteten Beziehung zwischen Stern- und Sondenanzahl der Einsatz schwarmbasierter Sondenkonzepte zu erwägen, um Ballungseffekte zu vermeiden.

Abstract

Driven by exoplanet discoveries and the ongoing progress in related technologies, the idea of interstellar travel and exploration has gained momentum in the recent decade. While there are already various suggestions for probe concepts and considerations on relevant technologies, only few, limited research activities on suitable exploration strategies exist.

This thesis derives optimal strategies for exploring near-by stars. The problem of interstellar exploration mission design is formulated as bi-objective multi-vehicle open routing problem with profits. The resulting optimization problem is addressed with an adapted hybrid multi-objective genetic algorithm. The underlying generic mission model assumes probes travelling at a constant velocity of 10 % of the speed of light along straight-lined trajectories with restriction to flybys. The used star models are based on the second Gaia data release (Gaia DR2) and contain a maximum of 10,000 stars. This corresponds to a spherical domain around Sol with a radius of 110 light years. In the star modelling context, a stellar metric is suggested to assign each star a score according to its potential contribution to the entire mission return. Furthermore, a test model with an exact uniform star distribution is built to validate and adjust the algorithm.

It is found that the algorithm performance can be improved significantly by means of an initial relaxation of the time constraint, which limits the maximum route length. Applied to the test model, the algorithm generates a solution with a deviation of 10 % to the ideal value. A qualitative analysis of the Gaia based star models revealed a uniform distribution of stars, excluding the effect of binary or multiple star systems.

Assuming a constant probe number, a linear relation between mission duration and number of explored stars is observed. For a given mission duration, the number of explored stars increases with probe number m according to $\sim m^{0.6}$. Furthermore, star selection and route structure are found to differ with probe number: While high probe number missions focus on stars in the immediate solar neighborhood, low probe number missions include more distant stars, enabling shorter transfers along the route. From these observations, the following conclusions for interstellar exploration strategies are inferred: If the energy resources are limited (e. g. due to low fuel reserves) and the exploration mission is not restricted to very nearby stars, low probe numbers are more efficient. Contrarily, high probe numbers allow for a faster exploration of the nearest stars at the expense of less resource-optimal transfers, which represents a suitable strategy for small-scale, remotely propelled probe concepts. Given the derived scaling law characteristics it is recommended to consider swarm-based probe concepts to mitigate crowding effects when planning high probe number missions.

Table of Contents

PREFACE	1
1 INTRODUCTION	2
1.1 Motivation and Context	2
1.2 Thesis Objectives and Research Questions	4
1.3 Thesis Structure	6
2 LITERATURE SURVEY	7
2.1 Interstellar Exploration Approaches	8
2.1.1 Large-Scale and Single-Probe Concepts	8
2.1.2 Swarm-Based and Small-Scale Concepts	9
2.1.3 Self-Replicating Probes	11
2.1.4 The Role of Artificial Intelligence in the Interstellar Exploration Context	12
2.1.5 Flyby vs. Rendezvous – The Problem with Decelerating and Unknown Stellar Medium Characteristics	13
2.1.6 Exploration Strategies and Comparison of Different Approaches, Concepts and Parameters	14
2.2 Star Systems in the Solar Neighborhood	19
2.2.1 Classification of Stars	19
2.2.2 Reference Systems and Stellar Kinematics	21
2.2.3 Galaxy Models in Interstellar Exploration Approaches	23
2.2.4 Stellar Databases and Catalogues	25
2.2.5 Scientific Areas of Interests - Stars and their Propensity to Host (Habitable) Planets	26
2.3 Survey on Relevant Optimization Algorithms and Related Problems	33
2.3.1 Optimization Algorithms as Part of Interstellar Exploration Strategies	33
2.3.2 The Global Trajectory Optimization Competition	34
2.3.3 Other Algorithms used for Interstellar Exploration or Interplanetary Spaceflight	36
2.3.4 Multi-Target Rendezvous Problems	38
2.3.5 Other Global Optimization Approaches inspired by Nature	39
2.4 Summary Literature Survey	40
2.5 Research Gaps and Refined Thesis Objectives	42
3 DEFINITION OF THE OPTIMIZATION PROBLEM FRAMEWORK	43
3.1 Analysis of Problem Structure and Reduction to Minimum Set of Variables	43
3.2 Variable Assignment and Problem Classification	46
3.2.1 Allocation of Variables to the Optimization Problem	46
3.2.2 Identification of the Optimization Problem Class	47
3.3 Implications of Variable Selection and Problem Class for Literature Survey Results	49
3.3.1 Implications for Probe Concept and Technology	49
3.3.2 Implications for Star Catalogue Selection	49

3.3.3	Implications for Optimization Algorithm Selection	51
3.4	Mathematical Formulation of the Bi-Objective Multi-Vehicle Open Routing Problem with Profits	52
4	CREATION OF MISSION AND STAR MODELS	55
4.1	Description of the Mission Model	55
4.1.1	Probe and Mission Architecture Model Specifications	55
4.1.2	Considerations on Trajectory Modelling	56
4.2	Building a Star Model of the Solar Neighborhood Based on Gaia Data	59
4.2.1	Defining the Reference Frames	59
4.2.2	Investigating the Impact of Stellar Motion	59
4.2.3	Star Selection and Filtering Procedure	61
4.2.4	Star Mission Score - Developing a Stellar Metric	63
4.3	Building a Simplified Test Model for Algorithm Testing and Parameter Adjustment	65
5	IMPLEMENTATION OF AN ADAPTED HYBRID MULTI-OBJECTIVE GENETIC ALGORITHM	67
5.1	Algorithm Terminology and Definitions	67
5.1.1	Genetic Encoding of the Problem	67
5.1.2	Defining Metrics for Solution Quality Evaluation	68
5.2	Description of the Optimization Procedure	73
5.2.1	Selection of Parents	73
5.2.2	Generating Children	74
5.2.3	Evolving Population	78
5.2.4	Local Search Operation	78
5.3	Algorithm Overview – Presentation of the Preliminary Pseudocode	80
6	APPLYING THE ALGORITHM TO THE SIMPLIFIED TEST MODEL	81
6.1	Preliminary Analysis of the Model	81
6.2	Parameter Variation and Algorithm Adjustment	82
6.2.1	Variation of Time Constraint Settings	82
6.2.2	Implementation of Convergence Check and Variation of Crossover and Mutation Rates	89
6.2.3	Variation of Population Size and Local Search Operation Intervals	92
6.3	Revised Pseudocode based on Test Problem Outcomes	93
7	APPLYING THE REVISED ALGORITHM TO THE GAIA BASED STAR MODELS	95
7.1	Results for 10,000 stars	95
7.1.1	Preliminary Analysis of the Model - Spatial Star Distribution	95
7.1.2	Variation of Probe Number for Given Algorithm Configuration	100
7.1.3	Variation of Algorithm Parameter for Given Probe Number	109

7.2	Results for 1,000 Stars	114
7.2.1	Preliminary Analysis of the Model - Spatial Star Distribution	114
7.2.2	Variation of Probe Number for Given Algorithm Configuration	115
7.3	Comparison of Different Model Results	122
7.3.1	Comparison of the Models	122
7.3.2	General Comparison of the Solutions and Linearity Effects	123
7.3.3	Probe Number Doubling Effects	124
7.3.4	Convergence Behavior	126
7.3.5	Star Selection Analysis	127
8	DISCUSSION	132
8.1	Discussion on Selected Models and Algorithm	132
8.1.1	Assumption on Mission Concept and Probe Technology	132
8.1.2	Star Model Limitations	133
8.1.3	Algorithm Limitations: Remarks on Solution Quality and Reliability	134
8.2	Implications of the Results for Exploration Strategies and Mission Planning	135
8.2.1	Linearity vs. Non-Linearity	135
8.2.2	The Relation between Probe Number, Mission Duration and Mission Return	136
8.2.3	The Effect of Probe Number on the Star Selection	140
8.3	Further Implications for Star Model and Algorithm	143
8.3.1	Implications for Star Model: Remark on the Spatial Star Distribution	143
8.3.2	Implications for Algorithm: Initial Relaxation of the Time Constraint	143
9	CONCLUSIONS AND REMARKS ON FUTURE WORK	145
9.1	Summary and Main Outcomes	145
9.1.1	Main Results	145
9.1.2	Simplifications and Known Weaknesses	146
9.1.3	Main Conclusions for Future Optimization Procedures and Interstellar Exploration Strategies	146
9.2	Evaluation of the Research Questions	147
9.3	Future Work	149
A	REFERENCES	151

List of Figures

FIGURE 1-1: OVERVIEW OF EXISTING PROBES THAT HAVE REACHED OR ARE ABOUT TO REACH THE INTERSTELLAR MEDIUM (NOT TO SCALE, TRAJECTORIES NOT EXACT) ([5], ADAPTED)	3
FIGURE 1-2: OVERVIEW OF THESIS OBJECTIVES AND HOW THEY ADDRESS VARIOUS RESEARCH QUESTIONS.....	5
FIGURE 1-3: THESIS CONCEPT OVERVIEW AND STRUCTURE	6
FIGURE 2-1: OVERVIEW OF LITERATURE SURVEY ELEMENTS	7
FIGURE 2-2: HYPOTHETIC MISSION TO TAU CETI BY SWARM-BASED PROBES SUGGESTED BY [22]. THE SCENARIO INCLUDES A RECONNAISSANCE MISSION AT KUIPER BELT FOR IN-SPACE TESTING OF THE SYSTEM OPERABILITY.....	10
FIGURE 2-3: NUMBER OF EXPLORED STARS VS. TIME FOR REPRODUCING AND NON-REPRODUCING PROBES (FROM [29], ADAPTED).....	16
FIGURE 2-4: FRACTION OF VISITED SYSTEMS VS. PROBE SUCCESS PROBABILITY PER PARSEC, CONSIDERING A TOTAL NUMBER OF 40 TARGETS [26]	18
FIGURE 2-5: CLASSIFICATION OF STARS ACCORDING TO SPECTRAL CHARACTERISTICS [3, P. 132].....	19
FIGURE 2-6: HERTZSPRUNG-RUSSELL DIAGRAM OBTAINED FROM GAIA MISSION [69]	20
FIGURE 2-7: GALACTIC COORDINATE SYSTEM WITH GALACTIC LONGITUDE l AND GALACTIC LATITUDE b (BACKGROUND IMAGE TAKEN FROM [70])	21
FIGURE 2-8: STELLAR DISTANCES FROM SOL WITH TIME OBTAINED FROM THE INTEGRATION OF THE N-BODY EQUATIONS OF MOTION OVER 15,000 YEARS [73].....	22
FIGURE 2-9: APPROXIMATED ORBITAL AND ESCAPE VELOCITY WITH DISTANCE FROM GALACTIC CENTER INCLUDING THE INFLUENCE OF MAJOR GALAXY MASS COMPONENTS (MBH = SUPERMASSIVE BLACK HOLE), TAKEN FROM [75] (ADAPTED).....	23
FIGURE 2-10: SIMPLIFIED GALAXY MODEL (ONE QUADRANT) USED IN [28], A SIMILAR MODEL IS USED IN [27].....	24
FIGURE 2-11: HERTZSPRUNG-RUSSEL DIAGRAM FOR STARS WITHIN 150 PC FROM SUN, WITH STELLAR RADII LESS THAN 100 SOLAR RADII WHICH HAS BEEN DETERMINED INTERFEROMETRICALLY WITH RANDOM UNCERTAINTIES SMALLER THAN 5 % [83, P. 39]	27
FIGURE 2-12: PROPERTIES THAT POSSIBLY IMPACT PLANETARY HABITABILITY - FONT COLOR INDICATES DIRECTLY OBSERVABLE CHARACTERISTICS (BLUE) AND PROPERTIES DERIVED FROM THEORETICAL MODELING (ORANGE) AND MODELING INTERPRETATION (GREEN) (FROM [100], ADAPTED)	29
FIGURE 2-13: HABITABLE ZONES FOR DIFFERENT SPECTRAL STAR TYPES [103]	30
FIGURE 2-14: THE HABITABLE ZONE (HZ) FOR DIFFERENT STAR CLASSES AND TIDAL LOCKING THRESHOLD FOR THE ORBITAL DISTANCE [99]	31
FIGURE 2-15: K STARS AS "SWEET SPOT" BETWEEN M STARS AND G STARS [109].....	32
FIGURE 2-16: METHODOLOGY AND ALGORITHMS USED IN PREVIOUS TRAJECTORY OPTIMIZATION COMPETITIONS	36
FIGURE 2-17: INTERACTION AND DEPENDENCIES BETWEEN DIFFERENT MISSION DRIVERS FROM A HIGH-LEVEL PERSPECTIVE	41
FIGURE 3-1: PROCEDURE TO BUILD THE OPTIMIZATION FRAMEWORK	43
FIGURE 3-2: PARAMETER MAP OF THE CONSIDERED PROBLEM	44
FIGURE 3-3: VARIABLE MAP AFTER REDUCTION TO THE MINIMUM SET OF PARAMETERS; EXCLUDED ELEMENTS ARE GREYED OUT	46
FIGURE 3-4: PARAMETER SET USED WITHIN THE OPTIMIZATION CONTEXT, COLOR SCHEME ACCORDING TO EACH ELEMENT'S ROLE IN THE OPTIMIZATION	47
FIGURE 3-5: VISUALIZATION OF THE PROBLEM: FROM A SET OF LOCATIONS WITH REWARD s_i A SUBSET IS SELECTED WHICH IS CONNECTED VIA A ROUTE.....	47
FIGURE 3-6: EXTENSION OF THE PROBLEM BY ALLOWING MULTIPLE ROUTES (ROUTE 1 IN RED, ROUTE 2 IN GREEN).....	48
FIGURE 3-7: TOP: PREDICTED PROBABILITY THAT A SOURCE IS DETECTED BY GAIA AS FUNCTION OF MAGNITUDE, BELOW: THE COMPLETENESS OF THE GAIA DR2 FOR GIVEN MAGNITUDES (CROWDING EFFECTS NOT INCLUDED) [88].....	50

FIGURE 3-8: EXAMPLE OF TWO MISSIONS A AND B WITH SAME MISSION RETURN BUT DIFFERENT MISSION DURATION.....54

FIGURE 4-1: INTERSTELLAR TRAJECTORY SEGMENTS ACCORDING TO THE DIFFERING GRAVITATIONAL POTENTIAL (PRINCIPLE SKETCH, NOT TO SCALE) – BLUE: PROBE TRAJECTORY, GREY: GALACTIC POTENTIAL, YELLOW: POTENTIAL DUE TO STAR A, RED: POTENTIAL DUE TO STAR B56

FIGURE 4-2: SKETCH OF A FLYBY TRAJECTORY WITH ACTUAL HYPERBOLIC ORBIT (BLUE) AND ASSUMPTION OF A STRAIGHT-LINE TRAJECTORY (GREEN), dp REFERS TO THE PERIASTRON DISTANCE, a TO THE SEMI-MAJOR AXIS AND h TO THE IMPACT PARAMETER.....57

FIGURE 4-3: STRAIGHT TRAJECTORY VS. CURVED TRAJECTORY, ASSUMING CONSTANT ACCELERATION AND VELOCITY.....58

FIGURE 4-4: ORIENTATION OF THE CARTESIAN REFERENCE SYSTEM (X, Y, Z) (RED) WITH RESPECT TO GALACTIC COORDINATES (L, B) AND OBJECT DISTANCE (D)59

FIGURE 4-5: DISTRIBUTION OF HIGHEST DENSITY INTERVAL FOR STAR POSITION ESTIMATES60

FIGURE 4-6: FILTERING PROCEDURE: 1.: SELECTION OF NEAREST 25,000 STARS FROM GAIA DR2, 2.: APPLYING FILTER STEPS 1 AND 2 (15,856 STARS LEFT), 3.: APPLYING FILTER STEP 3 (11,981 STARS LEFT, FROM WHICH THE 10,000 NEAREST STARS ARE SELECTED)61

FIGURE 4-7: GENERIC STELLAR SCORE CONCEPT63

FIGURE 4-8: CALCULATION PROCEDURE OF THE STELLAR SCORE65

FIGURE 4-9: 2D GRID OF THE STELLAR TEST MODEL, EACH BLUE DOT REPRESENTS ONE STAR66

FIGURE 4-10: 3D MODEL OF THE TEST PROBLEM: 9260 UNIFORMLY DISTRIBUTED STARS WITHIN A CUBE-SHAPED VOLUME OF 120 LY SIDE LENGTH66

FIGURE 5-1: EVOLUTIONARY ALGORITHM TERMINOLOGY AND ENCODING OF EXPLORATION MISSION TERMS68

FIGURE 5-2: CONCEPT OF PARETO FRONT AND PARETO DOMINANCE, THE BLUE CROSSES INDICATE POSSIBLE SOLUTIONS IN THE SEARCH SPACE69

FIGURE 5-3: CONCEPT OF CROWDING DISTANCE FOR A SOLUTION i , THE FILLED DOTS FORM A SUBSET OF SOLUTIONS WITH THE SAME PARETO RANK ([195])70

FIGURE 5-4: PSEUDOCODE FOR CROWDING DISTANCE CALCULATION (FROM [195], ADAPTED); THE TERM $J_m(i)$ REFERS TO THE EVALUATION OF INDIVIDUAL i WITH RESPECT TO OBJECTIVE J_m 70

FIGURE 5-5: OVERVIEW AND MAIN FUNCTIONS OF THE GENETIC ALGORITHM73

FIGURE 5-6: TOURNAMENT PROCEDURE.....74

FIGURE 5-7: GENERATING CHILDREN BY REPLICATION AND CROSSOVER PROCEDURE: FROM EACH PARENT THE BEST ROUTE (BASED ON FITNESS RATIO σ) IS SHARED WITH EACH CHILD; DUPLICATES IN THE REMAINING ROUTES ARE ELIMINATED75

FIGURE 5-8: MUTATION PROCEDURE: MUTATION OPERATIONS (BLUE) ARE CARRIED OUT RANDOMLY (RAND(0,1) GENERATES A RANDOM NUMBER BETWEEN 0 AND 1); SUBSEQUENT MODIFICATIONS (ORANGE) MAY BE REQUIRED TO AVOID CONSTRAINT VIOLATION (ADOPTED FROM [193], MODIFIED)76

FIGURE 5-9: CHILD SUFFERING FROM HIGH DISCREPANCIES IN TRAVEL TIME, LEADING TO POOR SOLUTION FITNESS.....77

FIGURE 5-10: CHILD IMPROVEMENT PROCEDURE.....77

FIGURE 5-11: EVOLVING PROCEDURE BASED ON NON-DOMINATED SORTING AND CROWDING RANKING (FROM [195], ADAPTED)78

FIGURE 5-12: LOCAL SEARCH PROCEDURES (ONE-POINT OPERATION AS EXAMPLE, WORKFLOW EQUIVALENT FOR TWO-POINTS AND TWO-OPT OPERATION).....79

FIGURE 5-13: PRELIMINARY ALGORITHM PSEUDOCODE (THE “%” SYMBOL IN THE IF-CONDITION FOR PERFORMING THE LOCAL SEARCH REFERS TO THE MODULO OPERATOR).....80

FIGURE 6-1: SOLUTION SET FOR EACH RUN CONSIDERING DIFFERENT T_{max} ACTIVATION AND CUTTING TIME, THE IDEAL SOLUTION IS GIVEN AS REFERENCE84

FIGURE 6-2: UPPER PLOT: NUMBER OF DIFFERENT EXPLORED STARS PER GENERATION; LOWER PLOT: NUMBER OF NEW STARS IN SUBSEQUENT GENERATION COMPARED TO PREVIOUS GENERATION.....85



FIGURE 6-3: VISUALIZATION OF ROUTES FOR SELECTED SOLUTIONS WITH SIMILAR MISSION RETURN FROM RUN 5 AND RUN 6 (BOTH AFTER 2000 GENERATIONS); EACH COLOR REFERS TO ONE ROUTE86

FIGURE 6-4: MEAN FITNESS RATIO OF POPULATIONS VS. GENERATION NUMBER FOR RUNS WITH DIFFERENT T_{max} ACTIVATION AND CUTTING TIMING, ADDITIONALLY THE IDEAL VALUE OF 0.067 IS GIVEN AS REFERENCE.....87

FIGURE 6-5: POPULATION MEAN FITNESS RATIO VS. GENERATIONS FOR VARIATION OF CROSSOVER RATE, MUTATION OPERATION PROBABILITIES AND IMPROVEMENT OPERATION PARAMETER90

FIGURE 6-6: REVISED PSEUDOCODE BASED ON TEST PROBLEM RESULTS (THE “%” SYMBOL IN THE IF-CONDITION FOR PERFORMING THE LOCAL SEARCH REFERS TO THE MODULO OPERATOR)94

FIGURE 7-1: OVERVIEW AND HIGH-LEVEL STRUCTURE OF CHAPTER 795

FIGURE 7-2: DISTRIBUTION OF GALACTIC LONGITUDE, EACH BEAM REFERS TO AN INTERVAL WITH A SIZE OF 10° 96

FIGURE 7-3: COMPARISON OF GALACTIC LATITUDE COORDINATE AND RANDOM UNIFORM DISTRIBUTION97

FIGURE 7-4: CUMULATIVE HISTOGRAM FOR DISTANCE VALUES; RANDOM DISTRIBUTION REPRESENTED BY CUBIC CURVE98

FIGURE 7-5: DISTRIBUTION OF THE MINIMUM TRANSFER DISTANCE BETWEEN TWO STARS; INTERVAL SIZE OF 0.25 LY99

FIGURE 7-6: FINAL SOLUTIONS FOR DIFFERENT PROBE NUMBERS, THE LOWER CHART SHOWS A ZOOMED SECTION FROM THE COMPLETE UPPER PLOT101

FIGURE 7-7: MISSION RETURN VS. MISSION DURATION FOR SELECTED RUNS CONSIDERING SHORT-TERM MISSIONS102

FIGURE 7-8: VISUALIZATION OF SELECTED SOLUTIONS WITH SIMILAR MISSION RETURN, EACH COLOR REFERS TO ONE ROUTE, EACH NODE INDICATES AN EXPLORED STAR - LEFT: RUN FOR 512 PROBES, RIGHT: RUN FOR 8 PROBES103

FIGURE 7-9: RATIO OF MINIMUM NUMBER OF STARS REQUIRED TO DEPLOY ALL AVAILABLE PROBES AND PROBE NUMBER.....104

FIGURE 7-10: COMPARISON OF TWO EXAMPLE MISSIONS WITH DIFFERENT PROBE NUMBER BUT EQUIVALENT MISSION RETURN AND DURATION.....105

FIGURE 7-11: EFFECT OF PROBE NUMBER DOUBLING ON THE MISSION RETURN – UPPER RIGHT PLOT: MISSION RETURN VS. MISSION DURATION FOR DIFFERENT PROBE NUMBERS; UPPER LEFT PLOT: EXTRACTION OF SELECTED SOLUTIONS AT 2000 AND 4000 YEARS MISSION DURATION; LOWER PLOT: INCREASE IN MISSION RETURN AFTER DOUBLING THE PROBE NUMBER.....106

FIGURE 7-12: PLOT OF THE FIRST DERIVATIVE OF THE SCALING LAW WITH RESPECT TO PROBE NUMBER (EQ. (7-2))107

FIGURE 7-13: POPULATION MEAN FITNESS RATIO VS. GENERATIONS FOR RUNS WITH VARIED PROBE NUMBER, NOTE THE LOGARITHMIC Y-AXIS SCALE108

FIGURE 7-14: RESULTS FOR ALGORITHM PARAMETER VARIATION FOR A GIVEN PROBE NUMBER OF 4110

FIGURE 7-15: POPULATION MEAN FITNESS RATIO OVER GENERATIONS FOR RUNS WITH CONSTANT PROBE NUMBER OF 4.....111

FIGURE 7-16: RESULTS FOR ALGORITHM PARAMETER VARIATION FOR A GIVEN PROBE NUMBER OF 512113

FIGURE 7-17: ANALYSIS OF THE SPATIAL STAR DISTRIBUTION IN THE 1,000 STARS MODEL.....114

FIGURE 7-18: RESULTING SOLUTION FITNESS FOR VARIOUS PROBE NUMBERS CONSIDERING A MODEL WITH 1000 STARS.....116

FIGURE 7-19: EFFECT OF PROBE NUMBER DOUBLING ON THE MISSION RETURN CONSIDERING 1000 STARS MODEL – UPPER RIGHT PLOT: MISSION RETURN VS. MISSION DURATION FOR DIFFERENT PROBE NUMBERS; UPPER LEFT PLOT: EXTRACTION OF SELECTED SOLUTIONS FOR 2000 AND 4000 YEARS MISSION DURATION; LOWER PLOT: INCREASE IN MISSION RETURN AFTER DOUBLING THE PROBE NUMBER117

FIGURE 7-20: POPULATION MEAN FITNESS RATIO OVER TIME FOR 1000 STARS MODEL WITH VARYING PROBE NUMBER.....118

FIGURE 7-21: NORMALIZED MISSION RETURN DISTRIBUTION FOR THE CONSIDERED RUNS119



FIGURE 7-22: AVERAGE TRANSFER DISTANCES VS. MISSION RETURN FOR VARIOUS PROBE NUMBERS	120
FIGURE 7-23: DISTRIBUTION OF THE TRANSFER DISTANCES FOR SELECTED SOLUTIONS, EACH BIN REPRESENTS AN INTERVAL SIZE OF 1 LY	121
FIGURE 7-24: COMPARISON OF SPATIAL STAR DISTRIBUTION BETWEEN BOTH MODEL	123
FIGURE 7-25: COMPARISON OF SOLUTION FITNESS FOR DIFFERENT PROBE NUMBERS WITH RESPECT TO THE STAR MODELS (DOTS INDICATE THE USAGE OF THE 1,000 STARS MODEL, STAR SYMBOLS REPRESENT RUNS FROM THE 10,000 STARS MODEL)	124
FIGURE 7-26: COMPARING DOUBLING FACTORS FOR DIFFERENT STAR MODELS.....	125
FIGURE 7-27: COMPARISON OF THE DERIVED SCALING LAW WITH THE ALGORITHM RESULTS OBTAINED FOR GIVEN MISSION DURATION AND FROM DIFFERENT MODELS.....	126
FIGURE 7-28: MEAN FITNESS RATIO FOR SELECTED RUNS CONSIDERING THE TWO MODELS WITH DIFFERENT STAR NUMBER	127
FIGURE 7-29: STAR FRACTION USED BY SUBSEQUENT INDIVIDUAL	128
FIGURE 7-30: ROUTES COMPARISON FOR DIFFERENT SOLUTIONS FROM BOTH MODELS CONSIDERING 4 PROBES.....	129
FIGURE 7-31: NUMBER OF DIFFERENT STARS WITHIN ONE GENERATION FOR DIFFERENT PROBE NUMBERS AND STAR MODELS OVER THE OPTIMIZATION PROCEDURE.....	130
FIGURE 7-32: NUMBER OF NEW STARS IN NEXT GENERATION COMPARED TO PREVIOUS GENERATION CONSIDERING RUNS WITH 4 PROBES FROM DIFFERENT MODELS	131
FIGURE 8-1: COMPARISON OF TWO DIFFERENT MISSIONS A AND B WITH SWARM-BASED CONCEPT TO AVOID CROWDING EFFECTS - EACH COLOR REPRESENTS ONE PROBE, THE BLUE DOTS INDICATE EXPLORED STARS	139
FIGURE 8-2: FIRST DERIVATIVE OF THE SCALING LAW WITH RESPECT TO THE PROBE NUMBER AND RECOMMENDATION FOR SWARM-BASED CONCEPTS BASED ON QUALITATIVE ANALYSIS OF THE SCALING LAW	140
FIGURE 8-3: COMPARING RUNS WITH SIMILAR MISSION RETURN BUT DIFFERENT PROBE NUMBER.....	141
FIGURE 8-4: STRATEGY RECOMMENDATIONS BASED ON MISSION CONSTRAINTS AND REQUIREMENTS INCLUDING SUITABLE PROBE CONCEPTS FROM LITERATURE.....	142
FIGURE 8-5: PRINCIPLE OF DIFFERENT APPROACHES TO SELECT/BUILD THE GENERATION STAR SET – TOP-DOWN CORRESPONDS TO INITIAL RELAXATION OF THE TIME CONSTRAINT, BOTTOM- UP REFERS TO ACTIVE TIME CONSTRAINT FROM THE BEGINNING	144

List of Tables

TABLE 2-1: EXPLORATION SCENARIOS FOR NON-REPRODUCING AND REPRODUCING PROBES DESCRIBED IN [29].....	15
TABLE 2-2: STELLAR SYSTEMS WHICH ARE SUGGESTED AS PRIME TARGETS FOR INTERSTELLAR EXPLORATION BY [34, P. 34]	28
TABLE 3-1: DIFFERENCES IN PROBLEM FORMULATION TO ORIGINAL APPROACH AND AFFECTED EQUATIONS.....	52
TABLE 6-1: SPECIFICATION OF INPUT DATA AND ALGORITHM PARAMETER, X VALUES INDICATE A PARAMETER VARIATION	82
TABLE 6-2: PARAMETER VARIATION CONCERNING T_{max} ACTIVATION AND CUT OPERATION TIMING	83
TABLE 6-3: SOLUTION QUALITY RELATIVE TO THE IDEAL VALUE FOR EACH RUN TOGETHER WITH THE RELEVANT PARAMETERS, RUN 6 CONSIDERED TO BE MOST EFFICIENT.....	88
TABLE 6-4: SPECIFICATION OF INPUT DATA AND ALGORITHM PARAMETER CORRESPONDING TO RUNS INVESTIGATING CROSSOVER AND MUTATION PARAMETER, X VALUES INDICATE A PARAMETER VARIATION	89
TABLE 6-5: VARIATION OF PARAMETERS CORRESPONDING TO RUNS INVESTIGATING CROSSOVER, MUTATION PARAMETER AND CHILDREN IMPROVEMENT OPERATION PARAMETER	89
TABLE 6-6: RESULTS FOR VARIATION OF CROSSOVER RATE AND MUTATION OPERATION PROBABILITIES.....	91
TABLE 6-7: SPECIFICATION OF INPUT DATA AND ALGORITHM PARAMETER CORRESPONDING TO RUNS INVESTIGATING POPULATION SIZE AND LOCAL SEARCH INTERVAL IMPACT, 'X' INDICATES A PARAMETER VARIATION.....	92
TABLE 6-8: RESULTS FOR PARAMETER VARIATION CONSIDERING PROBE NUMBER, POPULATION SIZE AND LOCAL SEARCH INTERVAL	92
TABLE 7-1: STRUCTURE OF THE DISTANCE MATRIX.....	98
TABLE 7-2: SPECIFICATION OF INPUT DATA AND ALGORITHM PARAMETER, 'X' INDICATES A PARAMETER VARIATION	100
TABLE 7-3: SPECIFICATION OF INPUT DATA AND CONSTANT ALGORITHM PARAMETER, 'X' INDICATES A PARAMETER VARIATION.....	109
TABLE 7-4: VARIATION OF PARAMETER FOR GIVEN PROBE NUMBER OF 4.....	109
TABLE 7-5: SPECIFICATION OF INPUT DATA AND CONSTANT ALGORITHM PARAMETER, 'X' INDICATES A PARAMETER VARIATION.....	112
TABLE 7-6: VARIATION OF PARAMETER FOR GIVEN PROBE NUMBER OF 512.....	112
TABLE 7-7: FIXED INPUT PARAMETERS AND ALGORITHM PARAMETERS	115
TABLE 7-8: INPUT DATA AND ALGORITHM CONFIGURATION.....	122
TABLE 9-1: RESEARCH QUESTIONS AND CORRESPONDING THESIS CHAPTERS.....	149

Symbols

a	m	semi-major axis (also specified in solar radii)	r_{merge}	-	merge rate
a_{grav}	m/s^2	acceleration due to gravity	r_{mission}	-	mission return
b	$^\circ$	galactic latitude	r_{shuffle}	-	shuffle rate
c	m/s	speed of light	r_{swap}	-	swap rate
d	ly	distance	S_i	-	stellar score
d_{ij}	ly	distance between star i and j	t_{ij}	y	travel time between star i and j
d_p	m	periastron distance (also specified in solar radii)	t_{mission}	y	mission duration
d_{travel}	ly	travel distance	T_m	y	travel time for probe m
g	-	generation number	T_{max}	y	max. travel time (time constraint)
g_{max}	-	max. number of generations	U_{ip}	-	position of star i in route p
h	m	impact parameter (also specified in solar radii)	v	m/s	velocity (often specified as fraction of the speed of light)
J_1	-	first objective function (mission return)	x_{ijp}, y_{ip}	-	binary decision variables
J_2	y	second objective function (mission duration)	ε	-	normalized mission return distribution factor
l	$^\circ$	galactic longitude	σ	y^{-1}	fitness ratio
m	-	probe number	σ_{mean}	y^{-1}	mean fitness ratio
n	-	number of stars	\mathcal{M}	-	variable set
p	-	travel route	\mathcal{M}_{min}	-	minimum variable set
P	-	population	\mathcal{M}_{opt}	-	variable set for optimization
P_{children}	-	children population			
P_{max}	-	max. population size			
P_{parent}	-	parent population			
$q_{\text{exploration}}$	-	exploration sequence			
r_{cross}	-	crossover rate			
$r_{\text{imp_cut}}$	-	improvement cut rate			
$r_{\text{loc_search}}$	-	local search interval			

Abbreviations

ACO	Ant Colony Optimization
ACT	Advanced Concepts Team
AI	Artificial Intelligence
ARI	Astronomisches Rechen-Institut
BCRS	Barycentric Celestial Reference System
DR1	Data Release 1
DR2	Data Release 2
ESA	European Space Agency
FK	Fundamentalkatalog
GTOC	Global Trajectory Optimization Competition
ICRS	International Celestial Reference System
HZ	Habitable Zone
MBH	Supermassive Black Hole
NNH	Nearest-Neighbor Heuristic
PSO	Particle Swarm Optimization
RECONS	Research Consortium On Nearby Stars
SOI	Sphere of Influence
TOP	Team Orienteering Problem
TSP	Traveling Salesman Problem
USNO	United States Naval Observatory
VRP	Vehicle Routing Problem

Preface

How can one imagine interstellar exploration strategies? To provide a comfortable entry into this admittedly rather ambitious topic, the readers are invited to imagine their next, hopefully well-deserved holiday trip to a destination of their choice. We assume a safe and trouble-free travel before arriving and completing the check-in procedure at the hotel. Now plans want to be made for the next days or weeks, unless not already done in advance: Which are the most interesting spots, e. g. are there any museums, churches or other historical building that deserve a visit? Less culturally interested readers may look for stunning landscapes and pristine beaches, others for restaurants and bars to discover the local cuisine. However, as everyone can confirm by experience, holidays are generally too short: Hence, the number of destinations that can be visited during one trip is limited; furthermore, constraints are imposed due to monetary considerations. To satisfy a maximum of the tourist's needs and ensure an enjoyable trip, a careful planning is required addressing several questions: What are the most interesting destinations and where are they located? Can I use any vehicle to go there? Is there special equipment required to enjoy a certain destination at its best (e. g. a camera for museums, a surfboard for the beach)?

Based on these questions, one needs to prioritize and select suitable target destinations according to personal preferences. In some cases, trade-offs might be necessary: Is it worth travelling to the very fascinating but distant castle, when it is possible to visit the less interesting but nearby opera house and the neighboring museum at the same time? Can I even merge selected destinations, that are at least to some extent compatible concerning equipment and vehicle, into one route to save time?

The result from above considerations is a travel plan or, keeping it more abstract and generic, a strategy, which is designed to guarantee the best travel experience with the given resources. However, in some cases, e. g. due to insufficient budget or travel restrictions, one needs to wait for the realization of his or her strategy and is limited to imaginary travels in the meantime. The good thing about imaginary travelling is that there are no restrictions on distances – so why not going a bit farther and imagining travelling across our galaxy and exploring stars? In fact, the considerations to develop a suitable exploration strategy are very similar to the planning of an enjoyable holiday trip as described above: By changing the wording from destinations to star systems, from equipment such as surfboards to scientific instrumentation such as telescopes and routes to trajectories, the holiday trip turns into an exploration strategy.

Of course, it is not as simple as that; interstellar travel and exploration provide a lot more challenges which still need to be solved. Compared to an ordinary holiday travel (unless during a pandemic), its realization may appear at least ambitious, one might state that it is even unfeasible given the current, limited technological capabilities. But, in analogy to the holiday trip considerations under the present circumstances with travel restrictions: Why not starting to make plans now to be prepared once it is feasible?

1 Introduction

1.1 Motivation and Context

The idea of travelling to another star originates from the time when humanity became aware of stars as distant objects, which dates back to the 18th century [1]. Although by definition interstellar travel refers to space flight between stars [2], in most cases the primary objects of interests are the planets that are potentially hosted by the target star instead of the star itself, which is in particular driven by the search for habitable planets or even extraterrestrial life. Interstellar travel is differentiated from interplanetary travel, which considers travelling between planets within a certain star system, and intergalactic travel, which represents the hypothetical idea of visiting other galaxies. Compared to interplanetary travel, which has already been accomplished by humanity, interstellar travel involves much larger scales: The nearest star, Proxima Centauri, is located at a distance of roughly 270,000 AU [3], while the entire solar system has a radial extension of about 100 AU, taking the distance of the heliopause as reference [4].

The comparably high distances between the stars entail very large travel times which are the reason why, up to the present, discussions on interstellar travel are dominated by theoretical concepts and ideas. There is a handful of existing probes (see Figure 1-1), that have reached or are about to reach the interstellar medium, e. g. the Voyager 1, which was launched 1977 and is currently the most distant human-made object from earth with a distance of about 150 AU [5]. However, all probes are still very far from approaching or even exploring a star system – literally far (in terms of distance) but also concerning the technology: None of these probes has been designed to perform an interstellar exploration mission; in fact, they have already accomplished their mission and now, left to themselves, continue their travel. Moreover, their velocity is not high enough to reach any other star in reasonable time: Considering again Voyager 1, which is currently traveling at 3.5 AU/y [6], it would arrive at Proxima Centauri after more than 77,000 years. Hence, the realization of interstellar travel at reasonable timescales in its original idea, which is travelling to another star, appears to be reserved to future generations.

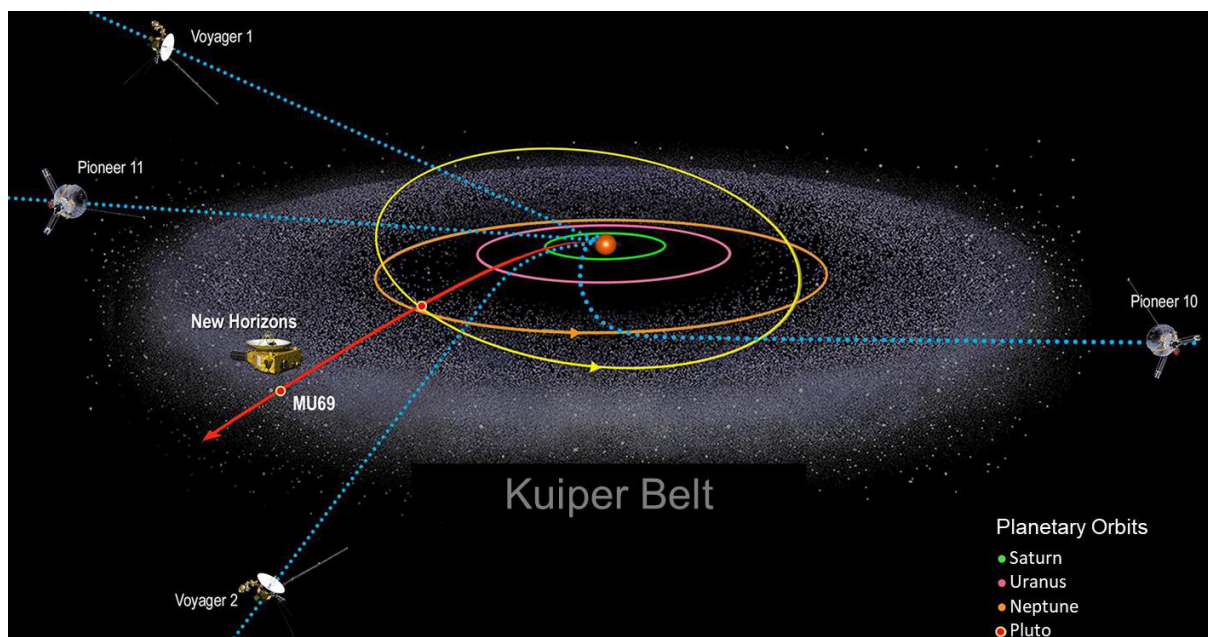


Figure 1-1: Overview of existing probes that have reached or are about to reach the interstellar medium (not to scale, trajectories not exact) ([5], adapted)

However, driven by exoplanet discoveries and the ongoing progress in related technologies, the traction for interstellar travel and exploration has gained momentum in the recent decade: As an example, consider the Breakthrough Starshot program which had been launched only few months before the detection of an exoplanet in the Alpha Centauri system in 2016 was announced [7] [8]. Being part of the Breakthrough Initiatives the Starshot concept consists of a gram-scale probe which is equipped with a laser propelled lightsail. Accelerated to a travel velocity of 20 % of the speed of light [9], the probe would reach its target, the Alpha Centauri system, after 20 years. Assuming further traction and extrapolating the current trends, it can be expected that the idea of interstellar travel may shed some of its very hypothetic and speculative nature within the next decades, at least regarding unmanned probes.

On the path towards the feasibility of interstellar spaceflight, there are still various challenges waiting to be solved, ranging from the probe concept itself to the general strategy of the exploration mission. Some technological aspects are already addressed in existing literature, such as the propulsion system [10, 11], replicability [12, 13], the role of artificial intelligence [14], or the overall feasibility of interstellar travel [15]. Among the suggested probe concepts, huge differences in scale are found, ranging from nanoprobes weighting only few grams [16] to large-scale spacecrafts with weights of several [17] or even thousands of tons [18]. In some cases also roadmaps [19, 20] and missions to a single target are suggested, typically focusing regions beyond the heliopause [21] or near-by stars such as Tau Ceti [22], the Alpha Centauri star system [23–25] or Barnard's star [18].

However, only few studies derive strategies for exploring a large number of star systems or exploration sequences. Of those, most make rather simplistic assumptions in terms of type of spacecraft used [26], the type of star system [27, 28] and the optimization methods [28–30]: No further considerations on probe technology (e. g. propulsion system, probe mass) and mission architecture (e. g. rendezvous maneuver) with respect to the implications for the exploration strategy are made. Star systems are

not distinguished based on their characteristics (e. g. propensity to host planets) and typically assumed to follow a simple spatial distribution instead of using true data from observations. The optimization methods, which are applied to the problem to derive optimal exploration strategies, are mostly based on simple approaches such as nearest-neighbor heuristics: Apart from a simulated annealing algorithm no advanced optimization approaches are considered. Following a generic approach, this thesis attempts to extend existing work by making use of current knowledge of interstellar spacecraft and nearby star systems to derive trends for new interstellar exploration strategies based on optimization algorithms.

1.2 Thesis Objectives and Research Questions

The overarching objective of this thesis is to develop strategies for the exploration of star systems in the solar neighborhood (approximately 10^3 - 10^4 stars), based on optimization algorithms, taking advantage of current knowledge of exoplanets and interstellar spacecraft. From this main objective, the following subordinate goals and tasks can be derived, which address various research questions:

- Identification and review of relevant literature: This task is required to identify parameters which are part of interstellar exploration approaches and strategies. Furthermore, data sources for the modelling and possible solution methods need to be found. It addresses the first research question, which asks for relevant parameters and variables in the interstellar exploration context, e. g. what are possible travel velocities of interstellar probes?
- Definition of the optimization problem: Based on the previous results, the most relevant parameters need to be identified and used to define and formulate the optimization problem. Furthermore, the problem needs to be classified in order to identify suitable optimization methods. With this subgoal, the research question concerning the formulation of interstellar exploration strategies as optimization problem is answered, which is strongly linked to the question on the corresponding problem class.
- Creation of an optimization model: The optimization model is required as part of the solution approach. It includes the star model, where current knowledge and recent observations on star systems can be incorporated. Hence, this step addresses two research questions: The first one, more generally, regarding the integration of recent stellar observations into the exploration strategy and the second one, more specific, concerning the value of a star system for a given mission. This includes questions on the structure of the solar neighborhood (are there any clusters?) and how the star distribution might affect the exploration strategy.
- Application of an optimization algorithm: By means of the optimization algorithm a solution for the described problem will be found. It requires the selection of a suitable method and its adaption for the considered problem. Therefore, it answers the research question on the algorithm type which can be used to solve the described problem class.

- Deduction of exploration strategies based on the optimization results:** This goal is expected to represent the main outcome of the thesis. It addresses the research question on the impact of mission design parameters on the exploration strategy and star selection. For instance, is there any dependency between the probe number and the optimum star exploration sequences?

Figure 1-2 summarizes the objectives and addressed research questions.

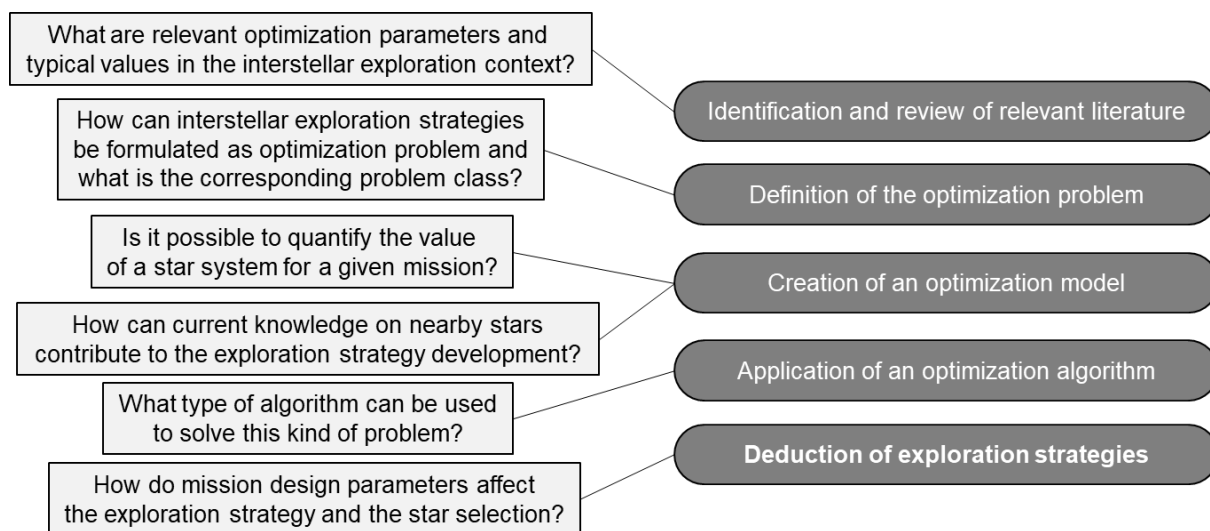


Figure 1-2: Overview of thesis objectives and how they address various research questions

The objectives and tasks stated above will be refined and specified later based on the literature survey results.

1.3 Thesis Structure

In Figure 1-3, the thesis concept is illustrated. From the beginning, the thesis is thematically divided into three cross-cutting areas of concern, which are recurring throughout the entire thesis: Interstellar exploration approaches, star systems in the solar neighborhood and related problems and relevant optimization algorithms.

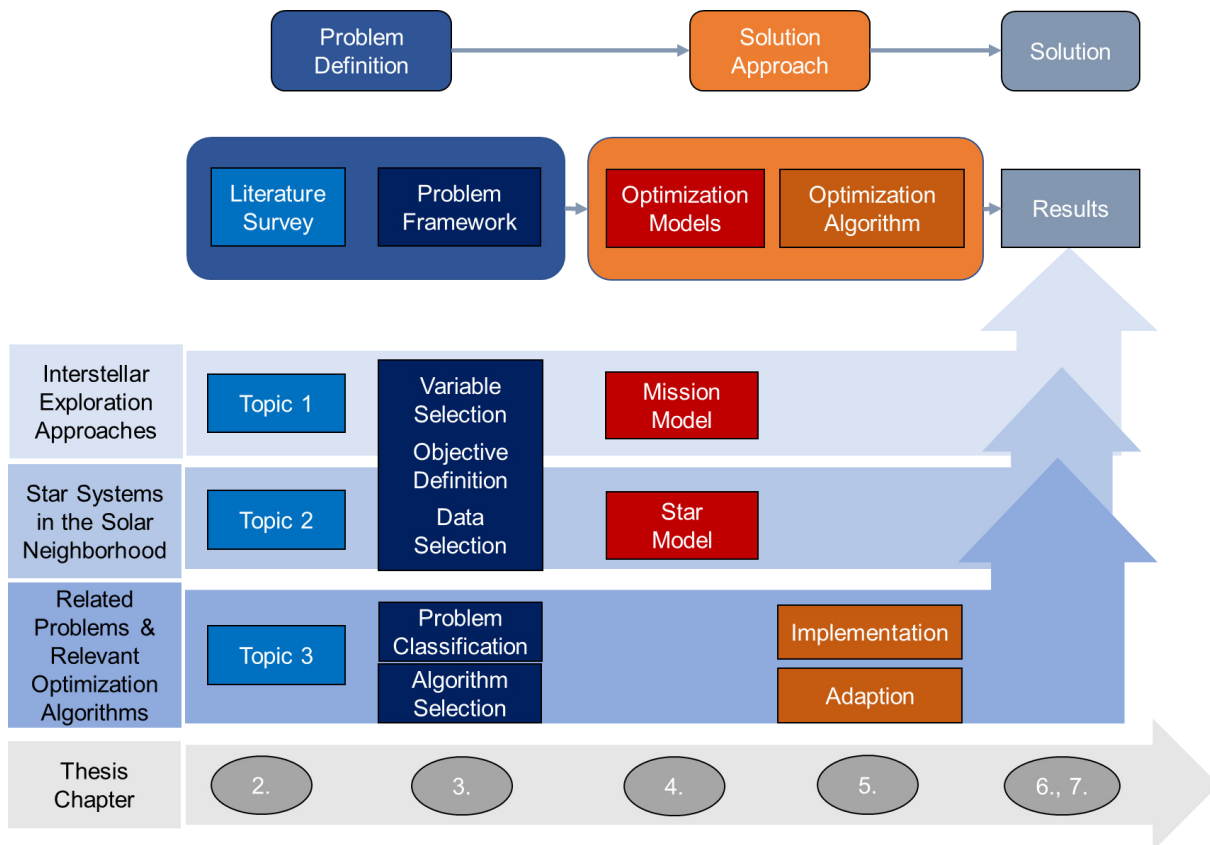


Figure 1-3: Thesis concept overview and structure

From the highest-level perspective, the thesis can be structured into three main components which are addressed subsequently: It starts with the definition of the optimization problem, which is then encountered by suitable approaches to provide a solution to the previously stated problem. The problem definition, as indicated by the second layer, is composed of the literature survey and the problem framework. The solution approach contains the models, particularly mission and star model, and the algorithm which is used to generate the results that build the problem solution. Note the strict separation of optimization model (mission and star model) and optimization algorithm, which is adopted from [31], where the optimization model is independent from the optimization algorithm.

2 Literature Survey

As already indicated during the presentation of the thesis structure, the literature survey consists of three parts:

- **Interstellar exploration approaches:** This literature provides the main input for the optimization framework and the mission model. It contains a review of mission concepts, probe technologies and mission architectures that have been suggested in the literature with respect to interstellar exploration.
- **Star systems in the solar neighborhood:** The review on nearby stars serves as basis for the star model, which is later used as part of the solution approach. It includes some astrophysical basics, e. g. star classification and characteristics, and an overview of star databases and catalogues.
- **Relevant optimization algorithms and related problems:** The results of this survey are used to identify the problem class and to find a suitable optimization algorithm to solve the given problem. It starts with related problems and algorithms that are applied in interstellar exploration and settlement optimization, but later also other areas of application are included.

Figure 2-1 provides an overview of the literature survey elements and its main contents. A brief explanation follows below.

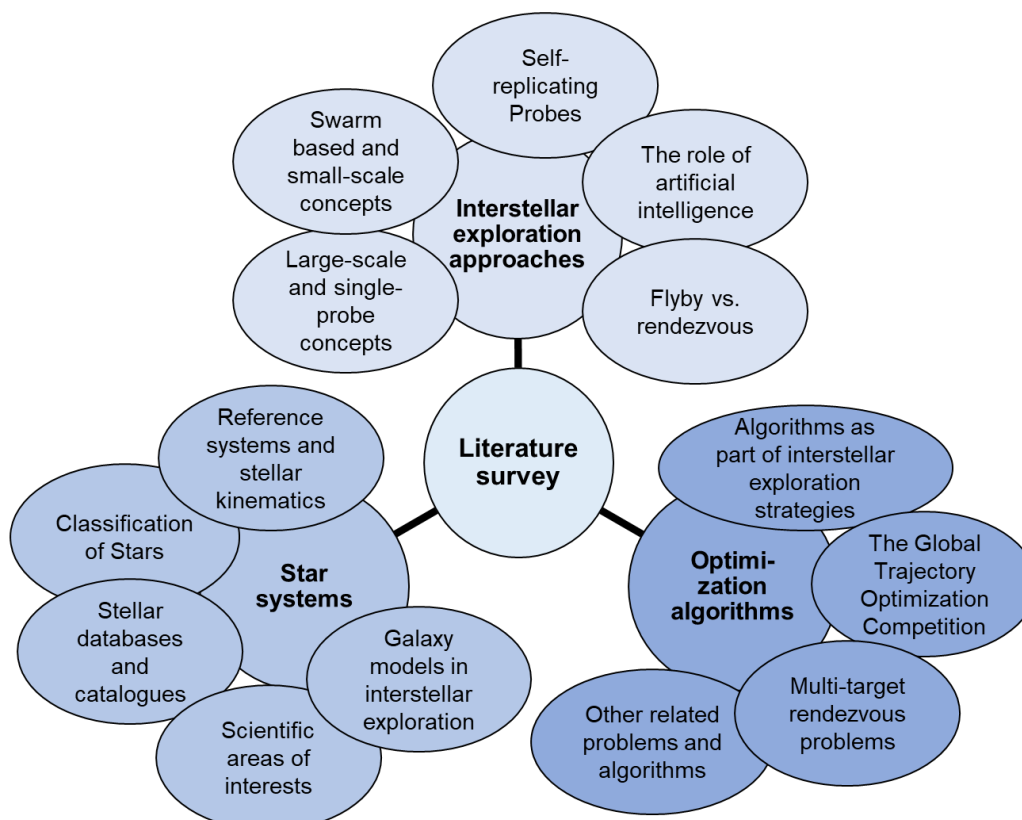


Figure 2-1: Overview of literature survey elements

As shown in Figure 2-1, the first topic concerning **interstellar exploration approaches** is divided into several subtopics. The subtopics include general probe concepts for interstellar exploration, relevant technologies, and mission architecture concerns. The probe concepts are grouped according to the concept size into large-

scale, single-probe concepts and small-scale, swarm-based concepts. With respect to technologies, self-replicability and the relevance of artificial intelligence in the interstellar exploration context is addressed. The survey on mission architecture focus on the challenges of rendezvous compared to flybys including considerations on the impacts from the unknown stellar medium.

The second topic, **star systems in the solar neighborhood**, covers different fields: It starts with some basics on astrophysics, which includes the classification of stars, reference systems and stellar kinematics. Furthermore, stellar databases and catalogues are reviewed, also modelling approaches of the galaxy or galactic sections are investigated. Another aspect that is addressed in this topic are the scientific areas of interest regarding star systems.

The third topic, concerning **optimization algorithms**, attempts to identify similar problems and suitable optimization methods. Therefore, it investigates optimization approaches in the interstellar exploration context and reviews methods from the Global Trajectory Optimization Competitions. Furthermore, related problems are considered, which includes multi-target rendezvous problems but also generic problems such as the Traveling Salesman Problem and suitable solution approaches.

2.1 Interstellar Exploration Approaches

As explained earlier, the topic of interstellar exploration approaches is divided into several subtopics. Due to the large differences in scale, suggested probe concepts are categorized into large-scale and small-scale approaches. The large-scale section covers probes weighting hundreds of kilograms and more, while the small-scale approaches include probes down to the gram-scale. Additionally, the large-scale concepts typically focus on single-probe missions, whereas the smaller probes often correspond to swarm-based mission concepts. Note that in some cases, both approaches are combined, i. e. when a large spacecraft transports a swarm of smaller exploration probes.

2.1.1 Large-Scale and Single-Probe Concepts

One of the first comprehensive studies addressing interstellar exploration has been the Project Daedalus [18]. The study considers a flyby mission to Barnard's star using a two-staged vehicle with nuclear pulse propulsion. Assuming a coast velocity of about 12 % of the speed of light, the vehicle would arrive after 50 years. Within the context of this thesis the vehicle itself can be considered as a large-scale concept, featuring an initial weight of 54,000 t and a length of 190 m. Three decades later, a successor study called Icarus was initiated [32], which aims to redesign the entire Daedalus systems and to reconsider some of the assumptions made in [18].

A different propulsion system is suggested by Forward [17]: He considers two different unmanned exploration missions based on laser-pushed lightsails. The first one will be a flyby mission to Alpha Centauri using a 1000 kg lightsail with a diameter of 3.6 km, which accelerates the probe to 11 % of the speed of light. The successor mission, where discoveries from the flyby will be incorporated, includes a rendezvous at the target system. For that purpose, an additional lightsail section is required, which will be used to decelerate the main section (consisting of payload and smaller lightsail section) when approaching Alpha Centauri. Compared to the first flyby mission, the

system's size and weight increase drastically (100 km diameter, more than 800 t weight). Although traveling at higher speed (21 % of the speed of light), the mission duration will be roughly the same, which is due to the deceleration process.

In [33], Garrett et al. identify key requirements for long-lasting interstellar missions. As a best-case scenario, they propose a 40 to 50 year mission followed by rendezvous and entering an orbit near the target star instead of doing a flyby to enable further investigation. The required deceleration phase imposes significant constraints on the propulsion system, they conclude. Candidates for propulsion systems include nuclear based engines (such as nuclear fission and nuclear fusion), laser-driven sail and antimatter engines [34, pp. 45-57]. Among these, nuclear fusion propulsion is considered as optimal for automated exploration missions allowing for low mass ratios and due to its comparably high technological readiness. However, like conventional chemical propulsion-based systems, nuclear fusion requires additional systems for storage and reactions, leading to larger and more massive configurations, compared to directed energy approaches such as laser beams [35]. A review on solar sails, which gain momentum from solar radiation pressure and thus not require the transportation of fuel, is provided by Gong and Macdonald [11]. In a similar manner, electric solar wind sails make use of the solar winds to accelerate, allowing for travels to the solar system boundaries [36]. Cohen et al. [25] introduce a new method, designated as "Direct Fusion Drive", allowing for an interstellar mission to the Centauri System with subsequent orbiting around a local planet.

2.1.2 Swarm-Based and Small-Scale Concepts

High energy requirements are one of the major problems of large-scale spacecraft. To save both cost and resources, Matloff [37, pp. 61-69] presents two options: The first one, lowering energy requirements by reducing velocity, would lead to unacceptable mission durations. Alternatively, he suggests minimizing the size of the spacecraft to micro scale by making use of nanotechnology, thus reducing weights from 1 ton to less than 1 kg. This also allows the deployment of multiple probes for swarm-based exploration, as suggested by Baumann [22]. He considers a hypothetical mission to Tau Ceti consisting of a swarm of unmanned exploration probes (see Figure 2-2).

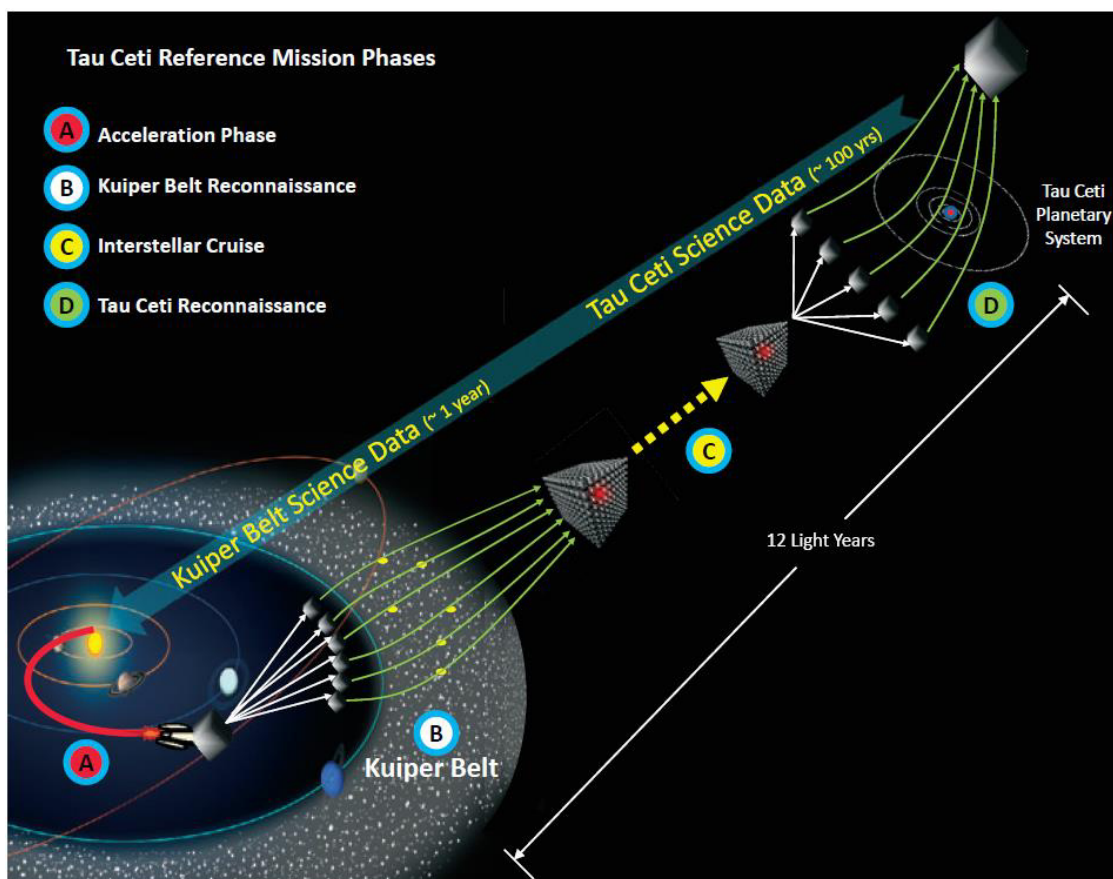


Figure 2-2: Hypothetic Mission to Tau Ceti by swarm-based probes suggested by [22]. The scenario includes a reconnaissance mission at Kuiper Belt for in-space testing of the system operability

The probes are assumed to travel about 100 years with 12 % of the speed of light using plasma and/or nuclear propulsion and power systems. These technologies have been tested successfully on small-scale but operability on larger scale has still to be shown. However, it seems questionable, whether speeds of that order are reachable by using the mentioned propulsion technologies. After arriving at the destination, the probes are planned to do a one-week lasting fly-through of the system to take measurements and acquire data, which will be sent back to earth. Decelerating the probes allowing for entering an orbit would double both mission time and vehicle mass. The advantage of such a swarm-based concept is the capability of investigating dispersed sites after being launched and transported to the destination within one common system. The probes operate independently but are also able to collaborate and support each other (e. g. by repair operations), if required. The capability of autonomous repair increases resilience and thus success probability of the mission. The challenge of self-repairing is also addressed by Moon et al. [38]. Considering nano-spacecrafts, they present a technology to heal space electronics from damage due to ionization radiation, hot carrier and tunnel stress. As a result, lifetime and reliability is increased.

A similar concept to [22], amongst others, is suggested in [39], where different scales of spacecraft, from gram level (referred to as "WaferSats") up to the 100 ton range are considered. As one option, a mother ship packed with several hundred WaferSats which will be dropped after reaching the target system is presented. The data collected by the WaferSats will be transmitted to the mother ship before send back to earth.

Decelerating the probes down to orbit speed (which is about 0.01 % of the speed of light) is identified as one major challenge and considered to be unsolvable with techniques such as magnetic coupling, using stellar wind or the stars photon pressure. Therefore, a flyby mission is suggested as a first scenario, enabling the development of braking strategies based on new findings on the stellar environment. The aspect of data transfer is also addressed by Messerschmitt et al. [40]. They suggest relaying swarms of low-mass probes to return scientific observational data back to earth.

Another study which considers a small scale probe with 23 g total mass is presented by Hein et al. [23]. Propelled by a laser beam, the probe will travel to Alpha Centauri at 10 % of the speed of light and collect optical data during a flyby which will be send back to earth. Similarly, the Breakthrough Starshot Initiative suggests to deliver a 1 g scientific payload to the Centauri system [9]. Also beam-driven, the probe is planned to be accelerated up to 20 % of the speed of light. More than three decades earlier Forward [24] already presented his lightweight probe concept "Starwisp". The Starwisp probe consists of a mesh sail (weighting 14 g) with microcircuits (4 g) and is powered by a microwave beam, which could be generated by solar-power satellite. Being accelerated at 115 g, the probe will reach a velocity of 20 % of the speed of light within one week. After 21 years, it will reach Alpha Centauri to do a flyby and send high-resolution pictures back to earth. Matloff [41] rethinks the idea of solar-power satellites by introducing non-stationary power stations, which follow the probes to enable higher thrust rates. The concept of lightsails is also part of a study conducted by Kulkarni et al. [16], where they consider gram-scale spacecrafts that are accelerated up to 20 % of the speed of light. However, it is highlighted that this technology is not limited to small-scale spacecrafts. Another important outcome concerns the lightsail design, which turned out to be optimal (in terms of maximal spacecraft velocity) when its mass equals the spacecraft mass. The effect of photon recycling, which is discussed to maximize the energy transfer, is found to be stronger in case of low-speed missions compared to relativistic speeds.

According to Crawford [42], small scale probes accelerated by earth-based lasers are the only feasible exploration approach in near-future, although having only limited scientific value due to their low mass. Larger probes, which would enable more sophisticated exploration tasks, require a space-based civilization being able to harvest material and energy resources of the solar system. His rather pessimistic estimation is supported by Millis [43]: By extrapolating trends from past space activities and energy considerations Millis expects a first interstellar exploration probe not to launch before 2500. As an example, he considers a 75-year lasting rendezvous mission to Alpha Centauri with a probe weighting about 10 t.

2.1.3 Self-Replicating Probes

The concept of self-replicating probes, also called von Neumann probes, is suggested recurrently when it comes to interstellar exploration or space exploration in general [12, 13, 44–46], also with respect to the Fermi paradox [47, 48]. Being able to produce copies of themselves, they may reduce the time for interstellar exploration or even colonialization drastically. A prototype of an autonomous self-replicating robot has already been built and tested on earth [49], however, self-replicating probes are still rather theoretical. Freitas [45], for instance, describes a self-replicating probe concept based on the Daedalus vehicle presented in [18]. Compared to the original version, the

payload is assumed to double to enable reproduction. In addition, the mission profile changes, as the probe has to slow down to start reproduction activities when reaching its target star instead of doing a flyby as originally proposed. The deceleration of the probe is planned to be conducted by the configuration stage 1 and 2, hence an additional stage “0” is required for the acceleration, which will be larger than the Daedalus configuration itself. After entering a parking orbit around the target star, a smaller probe will be released and landed on a moon. Once landed, its main function is to build a manufacturing complex, which in turn will produce a new, self-replicating Daedalus probe every 500 years.

Another, more recent example of a self-replicating probe concept is presented by Borgue and Hein [12]. They address the question of near-term feasibility of such a concept considering small spacecrafts based on technologies that are currently available or at least expected to be available soon. It is concluded, that within the next 10 years a partially self-replicating, small-scale probe could be launched, which is capable of replicating 70 % of its mass. Complex electronic parts such as microchips are not produced and must be provided by the initial probe.

In [13], Stephenson combines the self-replicability of the probes with an bio-inspired approach. Referred to as self-replicating, self-improving probes, his concept includes an evolutionary process, where experiences and new information are included into the manufacturing process. Thus, instead of producing exact copies of themselves, the probes will develop continuously, which provides a certain degree of intelligence.

2.1.4 The Role of Artificial Intelligence in the Interstellar Exploration Context

A recurring topic in the field of interstellar travel or exploration is the application of artificial intelligence (AI) which also allows for autonomous operations. The capability to operate autonomously is required due to the large distance between earth and the probe. Drivers and a system architecture with respect to interstellar exploration or colonialization are described by Hein [50]. According to him, power requirements for the payload and the capabilities of power generation and heat rejection are the key challenges to be addressed. Given the high computational cost and power requirements, he proposes to place the probe in an orbit close to the star to provide sufficient power for computing before continuing with exploration. Considering a 2050-2060 timeframe, a payload with computational power comparable to human brains would weight from dozens of tons up to 100 t, he concludes.

An earlier study on the topic of artificial intelligence is provided by Freitas et al. [51]. They consider various space missions including an autonomous space exploration system. It was found that the three, traditional sequential stages of exploration (in particular: reconnaissance, exploration and intensive studies) can be merged into one single discovery phase to reduce mission time. For this purpose, the probes will be equipped with an advanced machine intelligence, enabling an automated hypothesis formation, which is regarded as essential for interstellar exploration.

In [14], Hein and Baxter classify probe concepts according to their degree of intelligence. They present four types with different skills, two of them are relevant within the scope of this thesis; in particular, the “Explorer” probe, being able to perform a predefined mission within known environment (such as the Daedalus and Icarus concepts) and the more sophisticated “Philosopher”, which is capable of designing own

scientific missions in unexplored environment and doing in-situ manufacturing based on local resources. Özkural [52] introduces the concept of semi-autonomous agents to enable intelligent control of the spacecraft within a mission framework to Tau Ceti and Gliese 667C. He defines an AI agent as “abstraction of an intelligent animal, which acts in an environment in an intelligent manner”. A human-level AI technology is expected to be feasible by 2030, allowing for a probe launch in 2040 after ten years of training and simulation. Beside the communication latency, particularly the challenge of high uncertainty which demands for high adaption capabilities can be encountered by intelligent probes.

With respect to agent modeling in the space exploration context, Graziano et al. [53] define the concept of artificial curiosity. Their concept addresses the question to decide autonomously, what to explore, by assessing the interestingness of observations. Sievers and Madni [54] address the need of autonomous, on-board decision making by presenting a contract-based approach, which is bio-inspired by immune system responses and reaction of attacked social insect colonies. Being embedded into a swarm-based concept, it also yields higher resilience and reliability.

2.1.5 Flyby vs. Rendezvous – The Problem with Decelerating and Unknown Stellar Medium Characteristics

One major challenge for interstellar exploration missions is the deceleration of the probe before reaching its target system. By entering an orbit, the scientific value of the mission could be increased significantly, compared to conducting only a flyby. To encounter this problem, Andrews and Zubrin [55] suggests the use of magnetic sails. By making use of interplanetary or interstellar plasma winds, magnetic sails are considered as valuable addition to other propulsion systems such as fusion rockets or laser lightsails. The combination of lightsail and electric sail is also proposed by Perakis and Hein [56], as both technologies benefit mutually due to their different optimal velocity regimes: The efficiency of magnetic sails increase with velocity, whereas electric sails operate more efficiently at lower speeds. Decelerating from 5 % of the speed of light to interstellar velocities would take about 29 years when both sail technologies are used, 35 years with electric sails and 40 years with magnetic sails, they elaborate, assuming a constant spacecraft mass. Gros [57], however, argues that magnetic sails, which might be useful for deceleration, would increase the spacecraft weight significantly, which in turn lays down new requirements on the acceleration process. Hence, providing that mission duration is not a critical factor, which allows the probe to travel with comparably low speed (about 0.3 % of the speed of light), a deceleration with subsequent orbiting and exploration phase would be possible. Otherwise, he concludes, only flyby missions are realizable. Heller and Hippke [58] present an alternative approach to decelerate interstellar light sails based on a combination of gravitational assist and photon pressure. Assuming a maximal injection speed of about 4.6 % of the speed of light and a light sail carrying a 10-gram payload, this method enables multiple stellar flybys in the Alpha Centauri system with successive deceleration, followed by entering into an orbit around Proxima. The described method is modified and improved in [59], additionally a catalogue is presented, where results for rendezvous missions to other nearby stars are provided. Interestingly, a mission to Sirius A has the shortest trip time (69 years assuming 12.5 % of the speed of light), although being located roughly twice as far as Alpha Centauri.

This is due to the high luminosity of Sirius A, which is capable of absorbing more kinetic energy than other fainter stars and thus allows for comparably high arrival velocities.

From a more general perspective, Lingam and Loeb [60] highlight that electric sails are superior to light sails for most star systems due to the higher stellar wind pressure. Near K- and M-dwarfs, speeds up to 500 km/s are reachable; on a longer time scale also relativistic speeds are possible by repeated encounters with the stellar systems. Deceleration is enabled by activating the electric sail within the interstellar medium.

The local interstellar medium and its characteristics, which are not known in detail, are discussed by Crawford [61] as part of the Project Icarus study group. Given the high level of uncertainty, he concludes that first-generation probes should be designed rather conservatively with respect to assumptions on the interstellar medium. Hence, when considering decelerating systems, he recommends assuming the lowest plausible density whereas analyses on particle impacts should be conducted based on the highest plausible density. The danger of damage due to collision with particles and interaction with gas for relativistic probes is assessed by Hoang et al. [62]. As an example mission, they consider a journey to Alpha Centauri at 0.2 % of the speed of light. They found that interstellar gas and dust might damage the probe surface up to a depth of 0.1 mm or 0.5 mm, respectively. Gram-scale spacecrafts are expected to be destroyed completely when colliding with dust grains larger than 15 μm . To protect the spacecraft, they suggest using needle-like configurations, appropriate materials or shielding layers.

2.1.6 Exploration Strategies and Comparison of Different Approaches, Concepts and Parameters

From a high-level perspective Vulpetti [63] presents different scenarios for interstellar exploration by discussing the feasibility of interstellar travel: While fast round-trip travels are considered to be rather improbable in the near-future, one-way flights at relativistic speeds or slower expansions based on replicating robots are assumed to be more realistic. Valdes and Freitas [29] compare exploration strategies based on self-replicating probes and nonreproducing ones. The underlying exploration models, strategies and parameters are summarized in Table 2-1.

Table 2-1: Exploration scenarios for non-reproducing and reproducing probes described in [29]

	Non-reproducing probes	Reproducing probes
Model of the galaxy	Large number of small, equal volume cells containing n target stars	Small number m of large, equal volume cells
Exploration strategy	Each volume cell is explored by one single probe	Each volume cell is assigned to one daughter probe, which may divide the cell further and assign each of them to her daughter probes or subsequent generations
	After completing the exploration of its cell, the probe stops operating	Each probe explores only one single star system
	All probes are launched subsequently from origin	Only one single reproducing probe is launched from origin
Parameters		
Interstellar cruise velocity	10 % of the speed of light	
Residence time (exploration time per star)	1 year	
Time to produce probe at origin	10 years	100 years
Time to reproduce new probes in space	-	$500 (1+m^{-1})$ years

The reproducing probe concept is based on the approach described earlier by Freitas [45], accordingly probes do not replicate themselves directly but need to build a factory at the target system, which produces new probes. Regarding the non-reproducing approach, automated messenger probes are considered which are mentioned by Bracewell [64] within the context of extraterrestrial technologies for space exploration.

Figure 2-3 shows the result of their analysis. In the diagram, the number of explored star systems (N) is plotted as function of exploration time (T). Two additional horizontal lines indicate distances of 100 and 1000 light years in the Galactic Disk. The dotted line refers to the exploration strategy based on self-replicating probes. For non-replicating probes, several cases are considered depending on the number of stars which are visited by one probe. The dashed line indicates the optimum scenario for non-replicating probes, as there exists an optimal value for n which corresponds to a certain exploration time T .

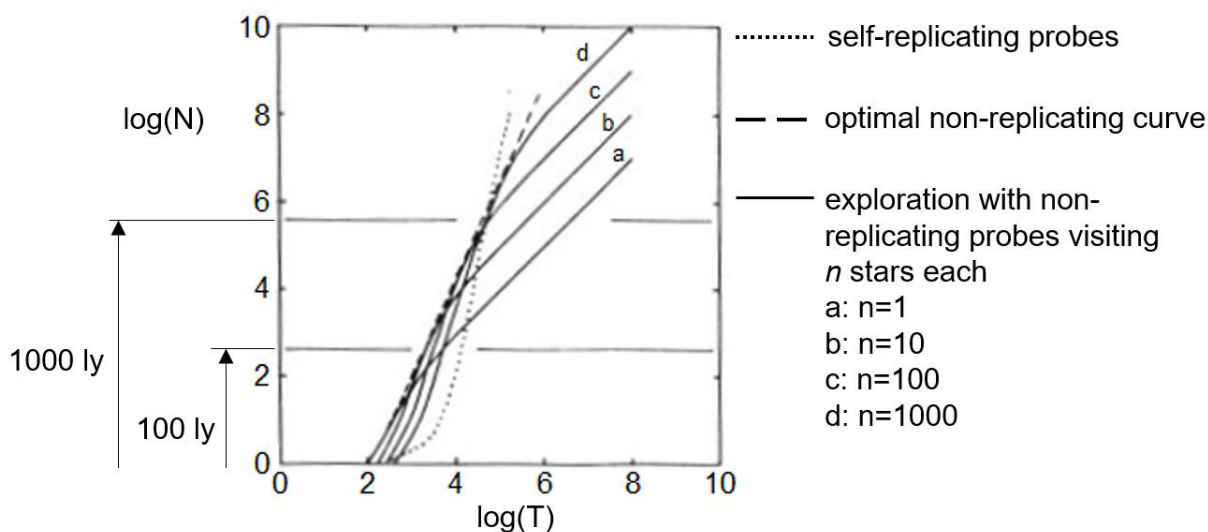


Figure 2-3: Number of explored stars vs. time for reproducing and non-reproducing probes (from [29], adapted)

It is found that, considering short term exploration programs ($T < 10^4$ years) with limited number of target systems ($N < 10^3$ stars), non-replicating probes are superior to those with self-replicating capabilities. With increasing mission time and number of stars, however, self-replicating probes perform better. As another outcome they show that self-replicating probes benefit from high stellar number density and high cruise velocities. Residence time is found to have only small impact, same holds for the number of self-replicating probes launched from origin.

To minimize exploration time, they conclude that a combination of both approaches might be the most promising strategy. Generally, it is stated that for nearby systems non-reproducing probes are more effective than reproducing ones and vice versa. The threshold for cost-effectiveness varies from 10^2 - 10^6 stars, depending on the exploration strategy and effectiveness criteria.

Limits of this study are the rather simple model of the galaxy assuming a homogenous star distribution and, particularly concerning the non-reproducing probe, the lack of information on the probe concept. Hence, some of the assumptions might be reconsidered and could bring different results.

In [27], Bjørk describes an approach to explore the Milky Way using space probes that transport a swarm of smaller exploration subprobes to a destination star (similar to [22]). After arriving there, 4-8 subprobes are released and start to explore the nearest 40,000 stars by traveling to the nearest star that has not been visited yet. After all 40,000 stars are covered, the subprobes return to the destination star and couple to their host probe, which then will travel to a new star region for subsequent exploration. All probes are assumed to travel with 10 % of the speed of light, which is low enough to neglect relativity effects but still fast enough to enable reasonable interstellar travel time (order of years). The exploration of stars by the smaller subprobes is done via flybys to save energy and time. To avoid that stars are explored twice, each subprobe is assigned a certain corridor of height, where it is allowed to travel. Similarly, each host probe must stay within a predefined region defined by the angle with respect to the Galactic Center. Considering one quadrant of the galaxy, which has about 65,000 systems with 40,000 stars each, exploration time would range in the orders of

10^8 to 10^9 , depending on the number of host probes and subprobes. Although exposing some weaknesses (such as the assumption, all probes will operate without fails or defects over 10^8 years), his concept is revisited by Cotta and Morales [28].

In [65], Frisbee investigates the impact of mission parameters such as vehicle acceleration, maximum and cruise velocity on mission time, mass and power budget. It is found that mission parameters depend strongly on the propulsion technology: Mass, power, thrust and acceleration correlate strongly for antimatter rockets or fusion ramjets, whereas light sails allow for arbitrarily high power and thrust without a significant increase of vehicle mass. However, with increasing mission distance, light sail area and mass are growing with square, whereas ramjet or antimatter engines only require thicker shielding, which entails lower mass increase. When it comes to mission time, travelling to nearby stars might be less time efficient compared to longer travels, as due to the shorter acceleration and deceleration period the vehicle cannot reach its maximum velocity for cruising. Another outcome is, that the impact of acceleration on the entire mission time is comparably high for values smaller than 0.1 g and almost negligible from 1 g upwards, assuming a cruise velocity of 50 % of the speed of light. A similar result is obtained by Singh et al. [66], who describe an exploration mission to Luhman 16 based on an unmanned probe powered by gas core nuclear reactors: Under the assumption of constant terminal velocity, it is found, that travel duration does not depend on the acceleration rates (considering scenarios with constant acceleration of 1 g and 3 g, respectively). By taking account of relativistic effects they further show that with increasing flight velocity on-board travel time is reduced drastically.

Cartin [26] examines the effect of parameters like cruise speed, success probability and number of target stars and launched probes on the exploration of the solar neighborhood. The probes are assumed to travel with a constant speed and use gravitational assist for trajectory deflection, resulting in hyperbolic orbits. Like other approaches described above, each probe is assigned one or more target systems at launch, which are visited subsequently without rendezvous. Concerning the probe concept itself, he decides for large-scale spacecrafts without self-replicating capability, which are stand-alone systems and more robust compared to smaller vehicles, but also more costly in terms of construction time and resources. Representing the more conservative approach, however, some of the results are also valid for small-scale systems.

He found, that doubling the number of probes or cruise velocity reduces the mission time to complete the same exploration by half. Another outcome is the proportional correlation between number of target stars and mission time: Accordingly, doubling the targets also doubles the exploration time. Involving a success probability factor shows, that only up to a certain value a higher number of probes will increase the number of visited targets (see Figure 2-4).

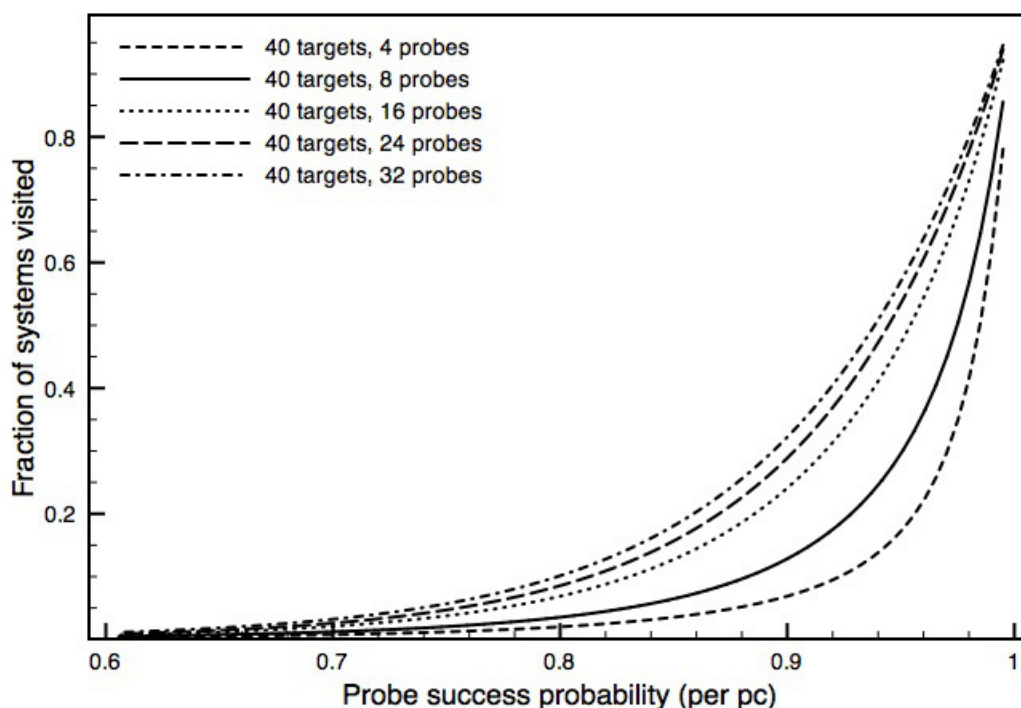


Figure 2-4: Fraction of visited systems vs. probe success probability per parsec, considering a total number of 40 targets [26]

For instance, assuming a success probability of 90 % per parsec and number of 40 targets planned to be visited by eight probes, about five targets can be expected to be explored successfully. Doubling the number of probes would add four more explored targets, however, to obtain three more successful visits, 16 additional probes must be deployed.

As most of the described exploration strategies omit orbit dynamics, Forgan et al. [30] suggest the use of slingshot maneuvers, which allow the spacecraft to gain velocity without fuel cost. Based on a single probe concept, he compares three different approaches: firstly, traveling from the origin star to nearest neighbor with Δv only depending on acceleration/deceleration of the engines (“powered” scenario); secondly, a slingshot assisted travel to nearest neighbor where the spacecraft only has to accelerate once to maximum velocity (“slingshot” scenario); and thirdly, a slingshot assisted travel to that star, which allows for the highest velocity boost (“maxspeed” scenario). He demonstrates that, taking the first scenario (“powered”) as reference, travel time can be cut by two orders of magnitude when using the “slingshot” scenario and by a factor of 2 considering the “maxspeed” scenario. However, total travel time remains large (order of 10^8 years for “slingshot” scenario), due to the comparably low maximum velocity (0.003 % of the speed of light) and the high number of target systems (10^6 stars). Another, earlier study on the effect of near flybys to accelerate space probes is done by Surdin [67]. According to his model, accelerating a probe to 10,000 km/s in the solar neighborhood would take 100,000 years and 100 years at the Galactic Center.

2.2 Star Systems in the Solar Neighborhood

This section presents the literature survey on star systems. It starts with some astrophysical basics concerning the classification of stars, followed by an introduction of reference systems and stellar kinematics. Afterwards, approaches for galactic models are investigated, before an overview of star catalogues and databases is provided. Finally, the scientific areas of interests concerning star systems and corresponding stellar characteristics are surveyed.

2.2.1 Classification of Stars

Commonly, stars are classified according to their spectral characteristics, as shown in Figure 2-5.



Figure 2-5: Classification of stars according to spectral characteristics [3, p. 132]

Roughly speaking, the effective temperature decreases from “O” class to “M” type stars. For each star class, a number of luminosity types are distinguished, indicated by roman numerals from 0 to VII, where 0 refers to the highest luminosity. A detailed description of each class can be found in literature [3, pp. 125-175, 68, pp. 327-337] and is thus omitted here. Plotting surface temperature against luminosity, yields the Hertzsprung-Russel Diagram, shown in Figure 2-6. Included are more than 4 million stars within 5,000 light years from the sun with data obtained from the Gaia Mission [69].

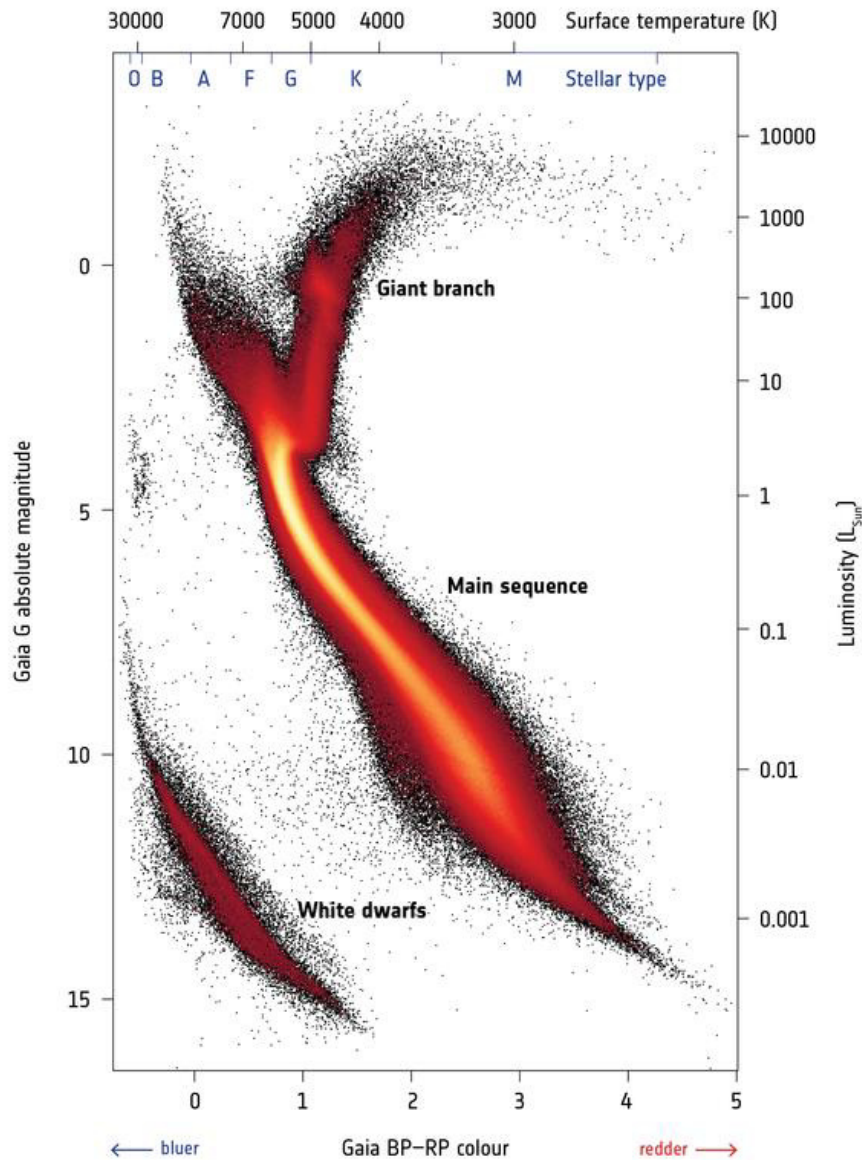


Figure 2-6: Hertzsprung-Russell Diagram obtained from Gaia Mission [69]

As seen, stars are not distributed uniformly, but follow a certain pattern, such as the main sequence, which is a diagonal stripe from bottom right to upper left. Along the main sequence, which includes 90 % of all stars within the Milky Way Galaxy, mass and diameter increase with luminosity [3, pp. 189-190]. As there is a negative correlation between the star mass and its lifetime, highly massive stars are difficult to find and observe despite their high luminosity – it is assumed that the entire milky way contains only about 20,000 of O-type main sequence stars [3, p. 144]. Accordingly, M-stars, with an average mass of about half a solar mass, are the most prevalent spectral star type. [3, p. 164]

2.2.2 Reference Systems and Stellar Kinematics

Depending on the current problem and specific needs, various systems are common to define an object's position. For the investigation and description of stellar distributions within the Milky Way, the galactic coordinate system can be used [68, pp. 5-11], which is a spherical system. Like the geographic coordinate system on earth, the galactic coordinate system is composed of a galactic longitude l , which is in the plane of the galaxy, and a galactic latitude b in the perpendicular direction, positive towards north and negative towards south (see Figure 2-7). [4, p. 389]

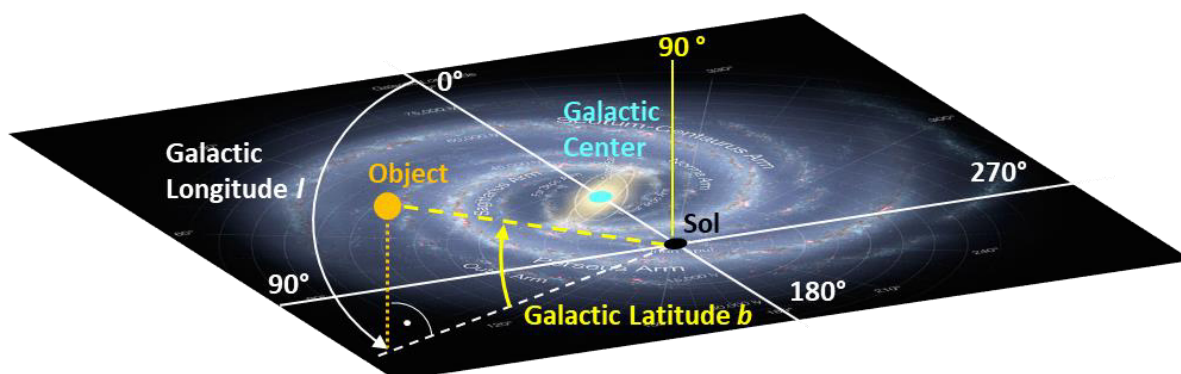


Figure 2-7: Galactic Coordinate System with galactic longitude l and galactic latitude b (background image taken from [70])

As all measurements are done from the solar system, the origin is placed in Sol instead of the galactic center, hence the longitude $l = 0^\circ$ gives the direction from Sol towards the galactic center. [71, p. 257] The distance, which is the third coordinate and required to define the position of an object, is mostly omitted in this context. [68, p. 6]

Alternatively, stellar objects can be located using the International Celestial Reference System (ICRS), which has its origin in barycenter of the solar system. Its axes are defined by 212 extragalactic radio sources (quasars and active galactic nuclei) without observable intrinsic angular motions. Accordingly, the system is space-fixed and not related with a certain epoch. Nevertheless, the ICRS is aligned closely with the Earth's mean equator and equinox of J2000.0 (error of 0.02 arcsec). Note, that strictly speaking there is a difference between a reference system and a reference frame, as a system can be realized by several frames: For instance, the ICRS is realized by the International Reference Frame (ICRF) or, with less accuracy, by the Hipparcos Celestial Reference Frame. [72]

The motion of stars is composed of a radial velocity component and the so-called proper motion. The radial velocity can be measured using the Doppler effect: Positive values (red shift) indicate that the star is moving away from the sun, while for negative values (blue shift) the star is approaching the sun. The proper motion describes the star motion on the celestial sphere and is typically given as angular velocity. The ratio of proper motion and parallax yields the tangential velocity, which is added to the radial velocity to obtain the spatial velocity of the star. [4, p. 176]

The relative motion of the stars is visualized in Figure 2-8 which shows the relative distances between selected, nearby stars and Sol considering a timeframe of 15,000 years.

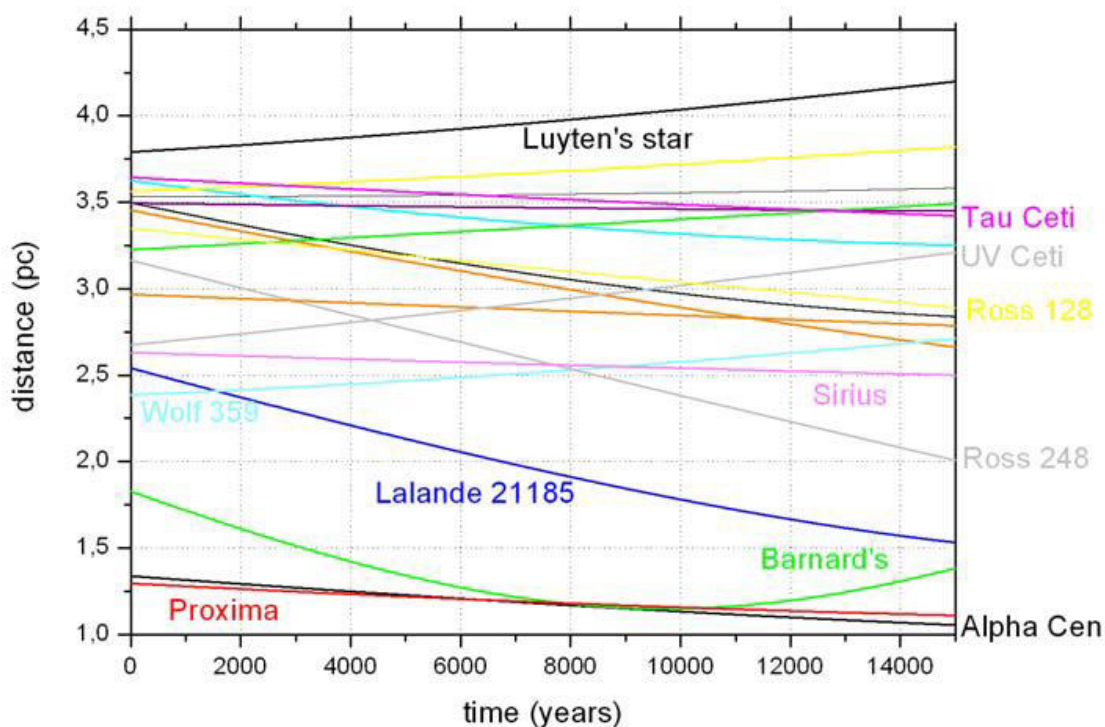


Figure 2-8: Stellar distances from Sol with time obtained from the integration of the N-body equations of motion over 15,000 years [73]

For instance, in roughly 8,000 years Barnard's Star is expected to replace Proxima Centauri as nearest star temporarily (for a few hundred years), before Alpha Centauri will take over the position of the closest star.

Beside the described, relative motion, stars are rotating around the galactic center. There is also an unknown number of so-called hypervelocity stars, which are unbound and travel across the galaxy at much higher speeds compared to the local escape velocity. However, the classification of an observed object as hypervelocity star is still part of current research and typically based on probabilities. Moreover, recent studies [74] utilizing data from the Gaia second release indicate, that most of the candidates previously assumed to be unbound turned out to be bound with high probability and thus no hypervelocity stars.

The velocity of the bounded stars depends on the orbit and the distance from the galactic center. Due to the distributed galaxy mass, there exists no simple function for this correlation. Instead, an approximation is required, e. g. by decomposing the galaxy mass into its main components supermassive black hole (MBH), bulge, disk and halo. This has been done by Brown [75] (see Figure 2-9).

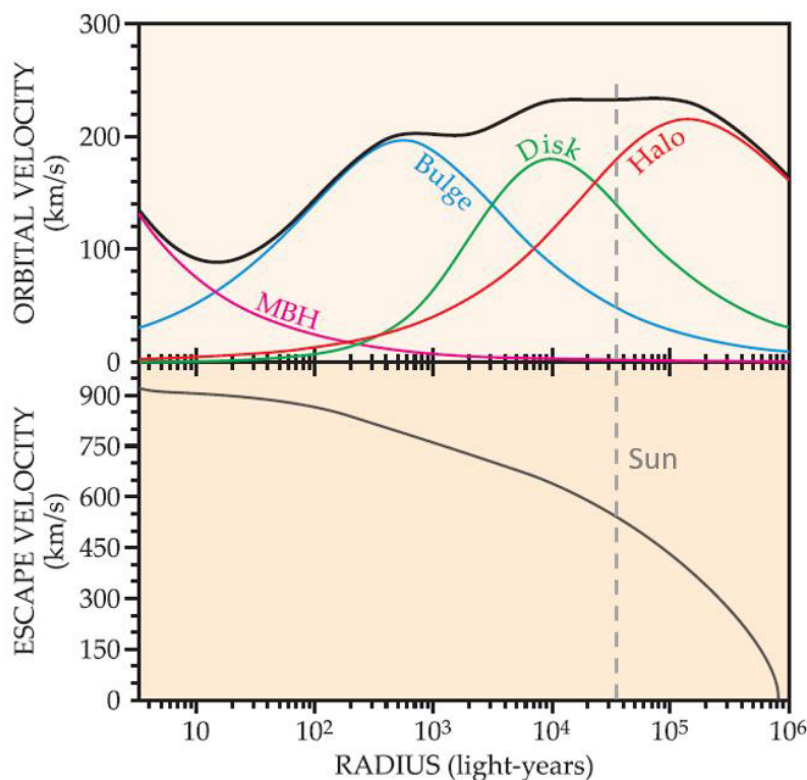


Figure 2-9: Approximated orbital and escape velocity with distance from galactic center including the influence of major galaxy mass components (MBH = supermassive black hole), taken from [75] (adapted)

From Figure 2-9 it can be derived, that the maximum orbital velocity occurs between disc and halo, within the region of the sun, which orbits at around 230 km/s around the galactic center. The escape velocity in that region is roughly about 550 km/s. These values are also valid in close solar proximity (say ± 100 light years), which is the region of interest in this thesis.

2.2.3 Galaxy Models in Interstellar Exploration Approaches

Valdes and Freitas [29] use a very simple galactic model to analyze various exploration strategies. They assume a homogenous and infinite distribution of star systems defined by $4.3 \cdot 10^{-4} \frac{stars}{ly^{-3}}$ in the Galactic Disk (considering 10 % of all stellar classes to be habitable). The model described in Bjørk [27] assumes an exponential decline of the stellar density with increasing distance from the Galactic Center, a similar model is used in [28] (see Figure 2-10). Only stars within the Galactic Habitable Zone are considered, which is defined by a thin annular area with distance from 3 – 11 kpc from the Galactic Center.

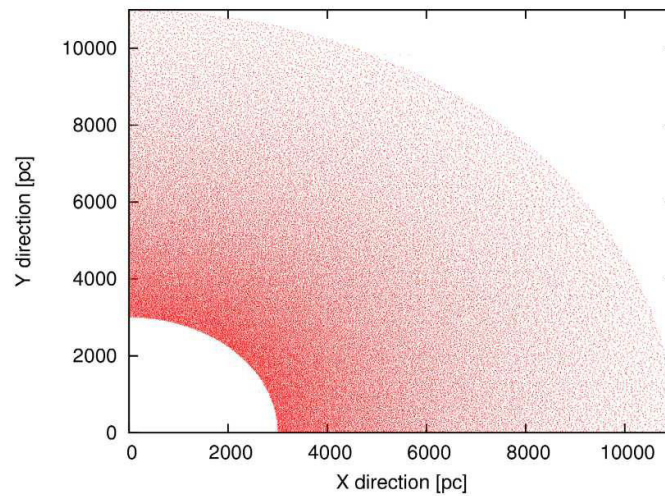


Figure 2-10: Simplified galaxy model (one quadrant) used in [28], a similar model is used in [27]

Forgan et al. [30] assumes a uniform distribution of one million stars with a density of 1 star per cubic parsec. The star position is fixed; however, each star possesses a certain velocity vector to calculate the slingshot dynamics. Contrarily, Cartin [26], who focus on a lower number of stars, uses real data for his model of the solar neighborhood. As the previous approaches he assumes all star systems to maintain a constant position.

As seen, real data is only relied on when considering a low number of stellar systems [26], for higher count rather simple star distribution models are used instead [27, 29, 30]. The motion of the stars is neglected in each model; even if the effect of slingshot maneuvers is investigated only a velocity vector for each star is included without having any impact on the star position.

2.2.4 Stellar Databases and Catalogues

From past until nowadays, it has been common practice to incorporate star data and information about stellar objects into catalogues or data archives. Those databases are updated regularly according to discoveries and new findings from space missions. One mission in the stellar categorization context was the Hipparcos space astrometry mission, launched 1989 and led by the ESA. Data generated from observations and calculations are incorporated in the Hipparcos Catalogue, which provides more than 118,000 star positions with high precision and magnitudes up to 12.4. More than 1,000,000 stars with less precise position data are listed in the Tycho Catalogue. The Tycho 2 Catalogue, which was published 2000, includes more than 2,500,000 stars, covering 99 % of all stars with magnitude up to 11. ([76], [77]) On their search for extraterrestrial intelligence, the SETI institute developed a catalog named “HabCat”. It contains more than 17,000 stars selected from the Hipparcos Catalogue, 75 % of them within 140 pc distance from sun. [78]

FK 6 (Fundamentalkatalog 6), which is provided by the Astronomisches Rechen-Institut (ARI) in Heidelberg, combines the results from 200 years of earth-based observations with data from the Hipparcos Catalogue. It contains data for more than 4000 single stars. [79] Two further databases from the ARI are the ARIHIP, which is more extensive than FK6, and the ARICNS (Astronomisches Rechen-Institut Catalog of Nearby Stars), which focus on nearby stars in the solar neighborhood within up to 25 parsecs distance from earth. [80]

The solar neighborhood is also the subject of investigation of the Research Consortium On Nearby Stars (RECONS). Amongst others, they provide a list of the nearest 100 stellar systems (status from 2012) [81]. [82, pp. 472-475] compiles a similar list with older status. Another dataset of nearby stars with distances up to 150 parsecs is given in [83, pp. 24-38]. Knapp [84] describes double or multiple star systems within 10 parsecs based on latest data (status from 2020).

One of the most recent and extensive catalogues is the Gaia Archive, where observations from the ongoing Gaia mission by ESA are collected. The first release, Gaia Data Release 1 (Gaia DR1), has more than 1.1 billion entries, including results from Hipparcos and Tycho 2 Catalogue. [85] The second and latest release¹, Gaia Data Release 2 (Gaia DR2), contains more than 1.6 billion objects, most of them (1.3 billion) including position on the sky, parallax and proper motion. Contrarily to the first release, data from Tycho 2 are not incorporated anymore, instead only observation from the Gaia mission are considered. However, there are still limits in terms of completeness of the catalogue: Bright stars of magnitude $G \leq 7$ are not covered completely, hence there is still a fraction of stars missing. Furthermore, 20 % of the stars with a proper motion $\geq 0.6 \frac{\text{arcsec}}{\text{year}}$ are not included. [87] Regarding fainter stars, Gaia DR2 is 99 % complete to a magnitude limit from 18.9 – 21.3 depending on the position on the sky, as stated by Boubert and Everall [88]. Based on the Gaia data, there are various approaches to derive further information on the objects: For instance, Bailer-Jones et al. [89] estimate the distance of the objects using primarily parallax data or Andrae et al. [90] derive further parameters such as effective temperature and radius for 77 million sources.

¹Note: An early, third Gaia Data Release (GAIA EDR3) was published in December 2020, a full release is planned for 2022 [86].

Another, more specific mission to be named in this context is the Kepler mission, which was carried out by the NASA. While the Gaia mission follows a rather general investigation and observation approach, the Kepler mission focused on the discovery of habitable exoplanets and their hosting stars. Based on the observation of transits, it required a continuous monitoring of stars, which imposed restrictions on the field of view. Therefore, only a certain section of the galaxy could be considered. In order to maximize the number of stars (more than 150,000), a region of the Cygnus and Lyra constellations was selected for observation. After a technical issue, the Kepler mission was terminated and followed by K2, which allowed for a varying field of view. [91]

The United States Naval Observatory (USNO) provides further catalogues, such as the UCAC2 (USNO CCD Astrograph Catalog, for stars with magnitudes between 8-16) or the USNO-B Catalog (more than 1 billion entries). They offer also a merged dataset referred to as NOMA (Naval Observatory Merged Astrometric Dataset) which includes data from Hipparcos, UCAC2, Tycho 2 and USNO-B. [92] The Sloan Digital Sky Survey is an ongoing project with the scope of mapping the universe, however, to date it covers only one third of the sky [93].

2.2.5 Scientific Areas of Interests - Stars and their Propensity to Host (Habitable) Planets

With respect to interstellar spaceflight, there exist mainly four different areas of scientific interest and potential explorations [94]: The first one is the interstellar medium encountered during the travel to a target star (can be investigated en route); secondly, the astrophysical characteristics of the target star; then studies on the planetary system (if existing) and finally, linked to the planetary studies but now from a biological perspective, the search for any life that may have evolved. Generally, most discussions on interstellar travel and exploration are driven by the search for habitable exoplanets or extraterrestrial life. Hence, in this thesis the scientific interest of a star system is assumed to be determined by the occurrence of exoplanets and their habitability with respect to the stellar characteristics.

2.2.5.1 The Probability of a Star for Hosting Planets

When assessing stellar systems with respect to the presence of exoplanets, some general tendencies can be derived: Von Braun and Boyajian [83] present an overview of nearby stars and, where known, their exoplanets. They incorporate any star with stellar radius smaller than 100 solar radii, determined interferometrically with random uncertainties smaller than 5 %, out to a distance of 150 pc from sun into a Hertzsprung-Russel-Diagram (Figure 2-11). Stellar radii are represented by the diameter of each data point, based on a logarithmic scale. The data point color indicates the occurrence of exoplanets: Blue circles are exoplanet-hosting stars, grey circles not (or at least not known to do so).

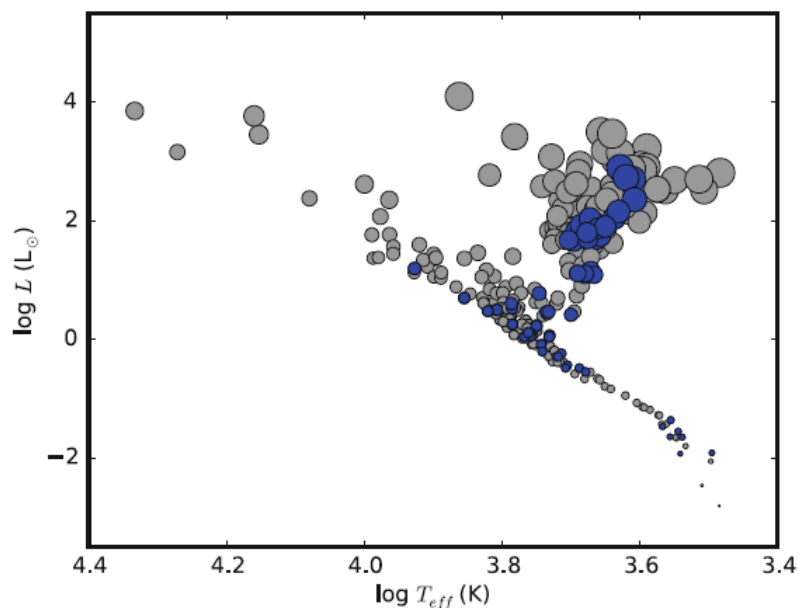


Figure 2-11: Hertzsprung-Russel Diagram for stars within 150 pc from sun, with stellar radii less than 100 solar radii which has been determined interferometrically with random uncertainties smaller than 5 % [83, p. 39]

From Figure 2-11 it is concluded that there is no systematic difference between stars, which are hosting planets and stars without planets (or not known to host planets). This is due to the high level of uncertainty (does the star really host no planets or are they not discovered yet) but also expected, as planets only represent a small fraction of the entire system mass. [83, p. 54] A similar result is obtained by Fressin et al. [95]: Considering Kepler data, they state, that there is no functional dependence between the planet occurrence rate and the host star spectral type, mass or temperature. In contrast, Mulders et al. [96] found (also based on Kepler data) an increase in planet occurrence rate towards cooler stars: According to him, Planets around M stars are occurring twice as frequently compared to G stars and thrice compared to F stars.

Based on Gaia and Kepler Data, Maliuk and Budaj [97] investigate the spatial distribution of exoplanet candidates in the solar neighborhood and near open clusters. After eliminating for gradients, which are assumed to result from single unobserved planets orbiting faint stars, they derive a homogeneous distribution of exoplanets within the considered regions, apart from a slight decline with distance for F stars. Within the closer solar neighborhood, several systems are expected to host exoplanets. Some examples including further characteristics are given in Table 2-2.

Table 2-2: Stellar systems which are suggested as prime targets for interstellar exploration by [34, p. 34]

Stellar system	Distance in light years from Earth	Remarks
Alpha Centauri	4.3	Closest system. Triple (G0, K5, M5). Component almost identical to Sun. High probability of “life bearing” planets
Barnard’s Star	6	Closest system known to have one, and perhaps two or more planetary companions. Very small, low luminosity red dwarf (M5)
Lalande 21185	8.2	Red dwarf star (M2) known to have a planet
Epsilon Eridani	10.8	Single star system; slightly smaller and cooler than the Sun (K2), may have a planetary system similar to the solar system
Procyon	11.3	Large, hot white star (F5), second only to Altair in luminosity (within 20 light years). System contains small white dwarf
Tau Ceti	11.8	Single star system, similar in size and luminosity to the Sun (G4). High probability of possessing a “Solar-like” planetary system
Gliese 876	15	Red dwarf star with confirmed planetary system composed of four planets

2.2.5.2 The Probability of a Star for Hosting Habitable Planets

Beside the debate on stars and their propensity to host planets in general, another important aspect in this context is the probability of hosting habitable planets. Early work in this field was done by Dole [98], who calculated several probabilities of the occurrence of habitable planets for a given star more than half a century before. However, the question regarding the habitability of exoplanets is still discussed conversely and part of current research. In [99], relevant factors for habitable Earth-like planets are reviewed, similar work is done by Meadows and Barnes [100]. One of the key drivers are the stellar characteristics, as shown in Figure 2-12. Due to the focus of this thesis, which is not on planetary science but on stellar exploration, they are regarded as the most relevant, other aspects are omitted. Most of these properties can be derived from observation (as indicated in Figure 2-12 by the blue font), a telescope with sufficient power provided.

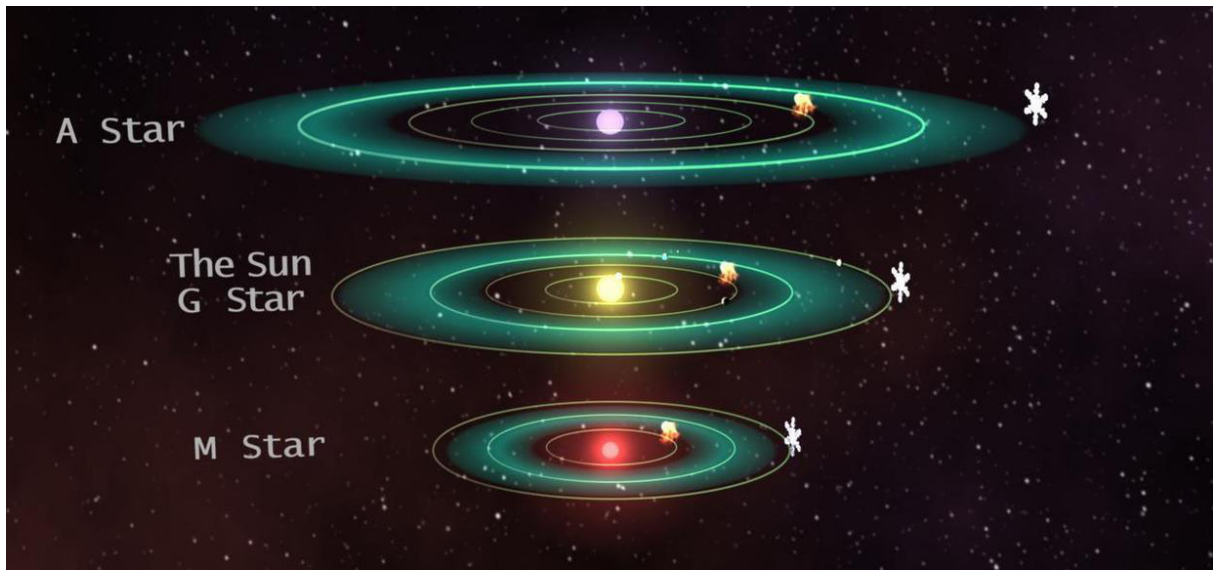


Figure 2-13: Habitable zones for different spectral star types [103]

As shown, the habitable zone increases while moving outwards with higher surface temperatures of the host star. Based on an empirical habitable zone definition, Cantrell et al. [104] derive a ranking for nearby stars depending on their spectral class. Representing a range of more than 30 light years from sun, they assessed a sample of 4 A stars, 6 F stars, 21 G stars, 35 K stars and 400 M stars. As the number of M stars is not completely known up to this distance, it was scaled based on known data from closer neighborhood. They conclude that M stars are most likely to host earth-like planets, which is mostly due to their large number, followed by K, A, G and F stars. Their analysis does not include O and B stars, as there are no examples within the next 30 light years. Conversely, Bignami and Sommariva [34, p. 34] argue that, considering M stars, habitable planets are only possible within orbits close to the star, which are less stable. Hence, closely orbiting planets may get tidally locked with one side permanently facing towards the star and thus less hospitable (Figure 2-14).

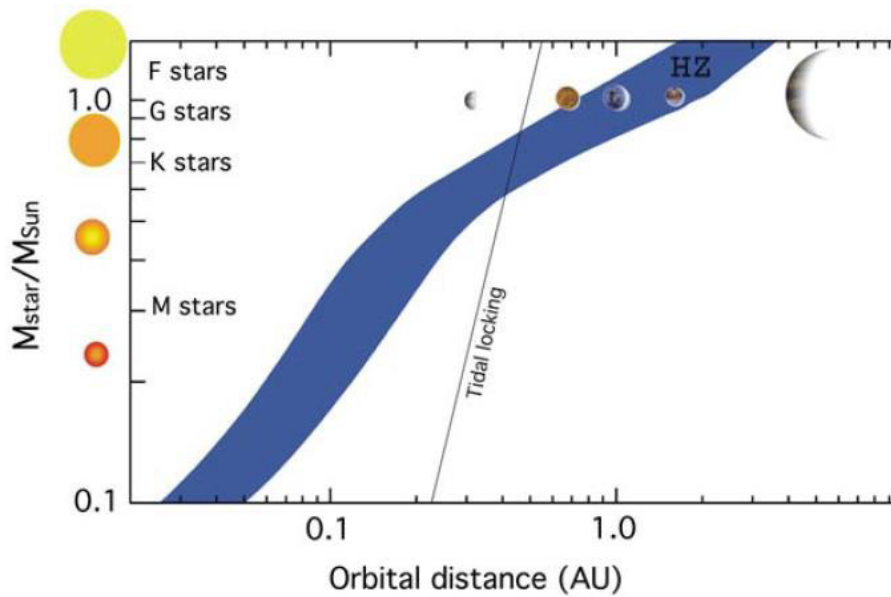


Figure 2-14: The habitable zone (HZ) for different star classes and tidal locking threshold for the orbital distance [99]

This issue is also addressed by other studies, such as Kopparapu et al. [105] or Lammer et al. [99] who emphasize the hostile effects of a tidal lock, which leads to a reduced magnetic field and thus a higher exposure to cosmic radiation. In addition, the slow rotation rate may result in a partial or complete loss of atmosphere with time.

However, another, previous analysis by Kopparapu [106] states that there might exist more earth-like planets orbiting M stars than assumed, supporting the result from [104]. Similarly, Scalo et al. [107] perform a study on the habitability of planets orbiting M stars and suggest a more optimistic estimation regarding the viability near M stars.

A recent study performed by Arney [108] finds K stars to be the most promising candidates for hosting habitable planets, as they represent a “sweet spot” between the smaller M stars and larger G stars: Compared to M stars, they emit less harmful radiation due to the lower stellar activity while featuring longer lifetimes than G stars (see Figure 2-15).

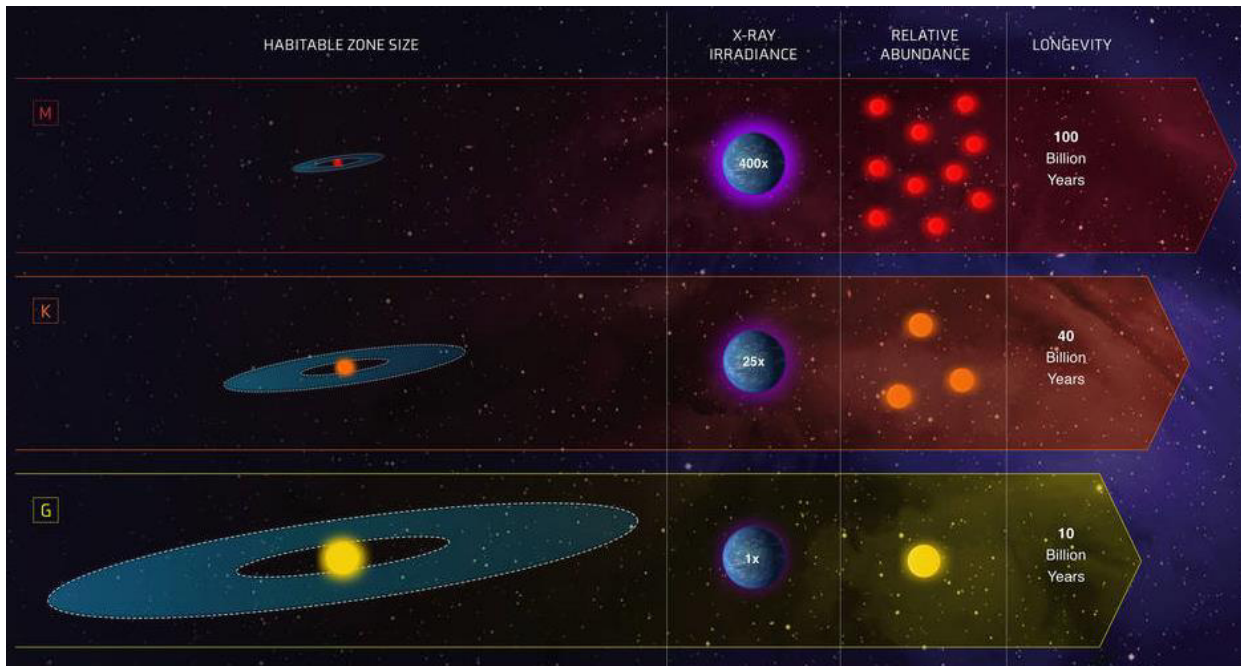


Figure 2-15: K stars as “sweet spot” between M stars and G stars [109]

The effect of stellar activity on the habitability of exoplanets is also addressed by Atri [110]. In accordance with [108] he states that the occurrence of flares on young, fast-rotating M stars is up to 100 times more frequent compared to a G star.

Extensive studies in the search for habitable exoplanets have also been performed by the SETI Institute. As one result, they developed a catalog of nearby habitable stellar systems which is based mainly on the Hipparcos Catalogue but also includes information from other catalogues [78]. Their habitability criteria used for selecting stars capture stellar properties like age, mass and variability but also the planetary capability of forming and supporting liquid water. In particular, they applied several filters and cuts on magnitude and spectral type, e. g. O, B and A stars and F stars earlier than F5 are excluded.

2.3 Survey on Relevant Optimization Algorithms and Related Problems

The last chapter of the literature survey is dedicated to optimization methods and related optimization problems. First, interstellar exploration strategies which have already been introduced in chapter 2.1 are reinvestigated, now with respect to the used optimization approach. Then, solution strategies and methods from the Global Trajectory Optimization Competitions are presented before further algorithms used in the context of interstellar or interplanetary travel are reviewed. Afterwards, a survey on multi-target rendezvous problems is conducted, followed by a short overview of other, nature-inspired global optimization approaches.

2.3.1 Optimization Algorithms as Part of Interstellar Exploration Strategies

The exploration approach suggested by Cotta and Morales [28], mentioned in chapter 2.1.6, uses a nearest-neighbor heuristic (NNH) with two local improvement strategies (1-opt and 2-opt) for the selection of the next star to be explored. The first one (1-opt) examines, whether the entire exploration time can be reduced by reassigning the last visited star to another probe. The 2-opt procedure modifies the planned route by removing two edges and reconnecting them in a different way. If this modification leads to a reduction of the tour length, the modification is adopted and the procedure is repeated. By using these two improvement approaches, the entire exploration time is reduced by 10 %. The nearest-neighbor method is also used by Bjørk [27] to maximize the number of explored stars as a function of time. However, as a result, some of the stars in the vicinity of the original star system are skipped and not visited.

The exploration strategy in Cartin [26], is based on a simulated annealing algorithm. The underlying objective function calculates the Euclidean norm of the individual travel time of a single probe, which results in similar travel times for each probe. Contrarily to the NNH, the simulated annealing method also allows for a temporary worsening of a solution, which is necessary to find a better (global) minimum instead of only a local one. However, the acceptance of poor solutions decreases during the optimization process. To enable a comparison between different approaches, two further algorithms based on heuristics (“fastest speed” and “shortest time”) are implemented: According to the “fastest speed” method, the star, which maximizes the cruise velocity is selected for subsequent exploration. Basically, this is a function of the gravitational deflections, as the impact of the star’s gravity on the probe trajectory is considered. Using the shortest time approach, the next star to be visited is selected according to the shortest travel time, which is determined by both gravitational deflections and distance. The exact optimal solution for a simple case with one single probe exploring a low number of targets is obtained from a branch-and-bound algorithm. It is found that both heuristic approaches perform rather poor, however, they are much faster to compute compared to the simulated annealing algorithm, which was run for a number of 60 trials. Forgan [30] presents three different scenarios, two are based on a nearest-neighbor heuristic whereas the third one uses the “fastest speed” heuristic (as described in [26]). Considering the scenarios which allowed for slingshot maneuvers, the NNH was performing better than the “fastest speed” heuristic.

2.3.2 The Global Trajectory Optimization Competition

The Global Trajectory Optimization Competition (GTOC) is a recurring contest to solve various complex trajectory problems. The most recent competition problem from 2019 (GTOC X) addressed the colonialization of the galaxy [111]. One approach, submitted by the Advanced Concepts Team (ACT) from the European Space Agency (ESA), used a concurrent tree search algorithm [112]. A tree, within this context referred to as settlement tree, is grown from a root node, which represents the first settlement by a spaceship. Subsequently settled stars add further nodes to the tree, which will grow continuously with time. In the beginning, a fleet of spacecrafts is launched to start the settlement process, hence various settlement trees are grown, which together form a settlement forest. Beside choosing favorable departure settlement stars (which defines the root node of each settlement tree), the selection process of subsequent star settlements determines the quality of the solution. For instance, naive greedy searches based on minimal transfer time or minimal thrust requirements result in clustering or reduces the number of settled stars. Furthermore, growing each tree individually bears the risk of overlapping, which leads to less efficiency in the settlement process. For that reason, a concurrent tree search approach was used, where all settlement trees are built simultaneously.

The selection process of stars to be settled includes a filter to reduce the possible target stars, otherwise computation time would be excessive due to the high number of stars. Filter criteria are primarily derived from boundary conditions, which are incorporated in the merit function. In addition, stars are ranked according to a phasing value, indicating the quality of transfers more reliably than the Euclidean distance. To save further computation time, every calculated transfer is written into a look-up table, which can be used later instead of repeating the computation. After each settlement step, several strategies are applied to yield better results, such as lowering thrust (referred to as Δv – refinement or leaf stretching).

Another solution on GTOC X is presented in [113], where set-covering problems are formulated within several zones of the galaxy to solve for the optimal distribution of settled stars, which is required to be uniform. Settlement trees are grown using a beam best-first search method and refined afterwards with a genetic algorithm for transfer time improvement. Zhang et al. [114] develop a solution to the settlement problem deploying a breadth first search algorithm. Conversely to the beam best-first search method, all neighbors of one node at its level are explored before extending the tree to the next, deeper level. As done in the other approaches described above, the derived settlement tree is refined afterwards for further optimization via local improvements, such as node replacements (settled stars are replaced by other, near-by stars unless outer constraints are violated), branch reconstruction and Δv optimization. The best approach to solve the GTOC X problem was delivered by Luo et al. [115]. They split the optimization process into four subsequent steps where different optimization techniques are applied: At the beginning, settlements pods are created by using differential evolution before suitable target systems are selected by means of genetic algorithms. Then, selected target systems are connected to build settlement trees. The growth of settlement trees, which is considered to be similar to the minimum spanning tree problem, is based on ant colony optimization. Afterwards, the resulting trees are refined locally by reconfiguring single nodes and arrival times are improved, involving again differential evolution and sequential quadratic programming methods.

A review of optimization methodologies from past GTOCs and its Chinese equivalent (CTOC) is provided by Li et al. [116]. They present the competition topics of each year and the solution method of the winning team. Depending on the problem, which typically features large search spaces and complex objective functions, in most cases a combination of several algorithms turned out to deliver the best solution instead of relying on just one single method. A common approach to encounter the challenge of global optimization and high complexity is the use of a hierarchical optimization strategy: The entire optimization problem is split into two sub-problems, one focusing on the global search of optimal target sequences and the other on the local optimization of the trajectories. The global search problem itself is built from a search model, with simplifications regarding mission and dynamics to improve efficiency by reducing complexity, and an appropriate optimization algorithm. Algorithms used to solve the global search problem can be grouped according to three main categories: Branch-and-bound algorithms, evolutionary algorithms and hybrid algorithms.

Branch-and-bound algorithms form a sub-group of the tree search algorithm class already mentioned earlier. Being commonly used for sequence searching, they are less appropriate when multiple optimization problems, such as multiple spacecraft exploration, are considered. In those cases, evolutionary algorithms turned out to perform better. Within the field of evolutionary algorithms, mainly three different methods have been used in this context, namely genetic algorithms, particle swarm optimization (PSO) and ant colony optimization (ACO). Compared to tree searches, genetic algorithms can be more efficient in terms of computational effort, as less calculations are required. However, compared to other evolutionary methods, its computational efficiency is rather low. PSO algorithms are especially good at finding sequences with multiple targets and other optimization objects involved. Due to its poor local optimization characteristics, it should be combined with a local optimizer method for better convergence. The ant colony optimization shows good performance for problems structured similar to the traveling salesman problem with a large search space. Hybrid algorithms are approaches where methods from different algorithm families are combined; e. g. using a branch-and-bound method for sequence optimizing before deploying an evolutionary method for further refinement of the solution.

Approaches to solve for the second sub-problem (concerning local trajectory optimization) are categorized according to the underlying propulsion principle into low-thrust trajectory and multiple-impulse transfer optimization techniques. Low-thrust trajectory problems can be addressed with indirect or direct methods, also new approaches such as evolutionary neurocontrol have been developed. Multi-impulse transfers can be considered as nonlinear programming problem and as such are solvable via well-established tools.

The explanations given above are summarized and structured in Figure 2-16, all information is taken from [116]. To keep the diagram concise, not all methods are included.

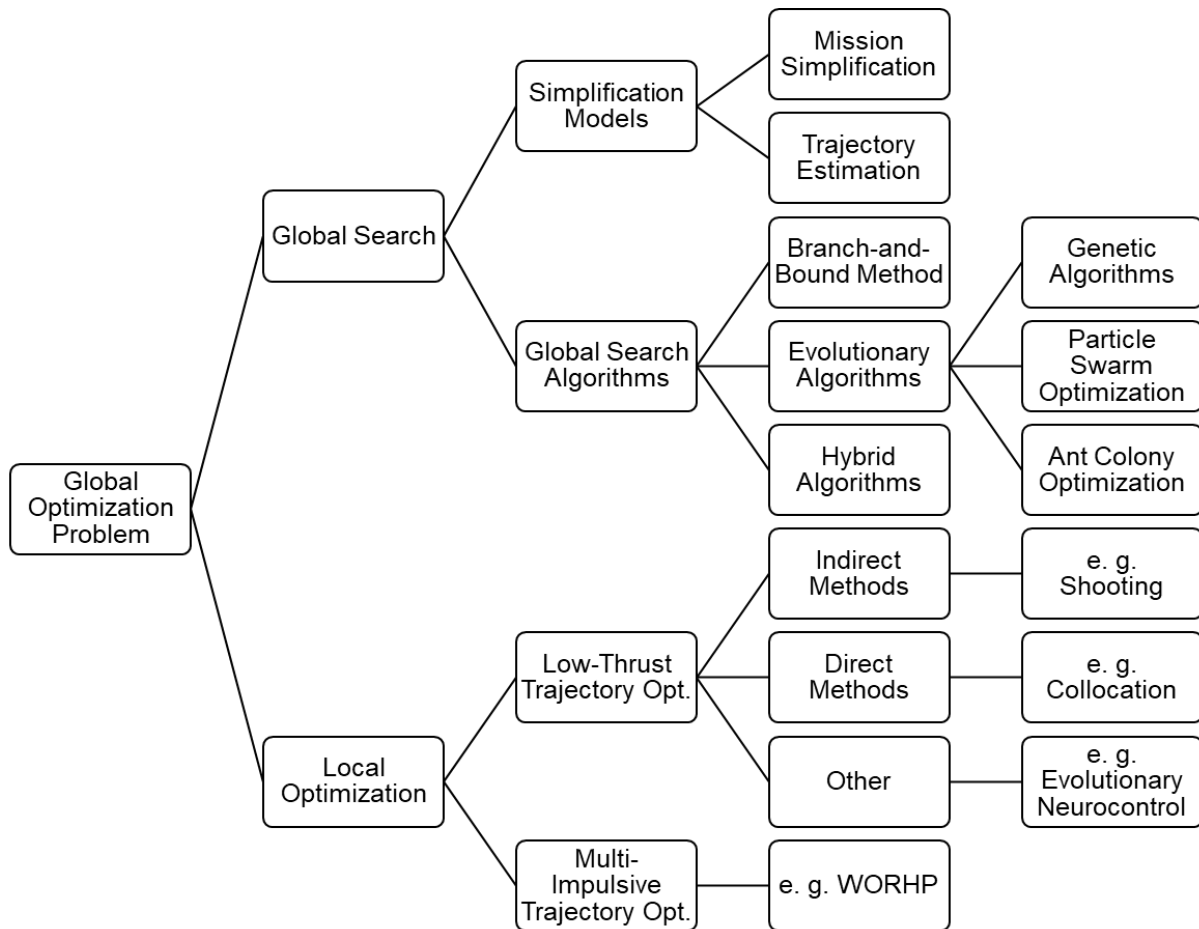


Figure 2-16: Methodology and algorithms used in previous trajectory optimization competitions

Another study to be named in this context is presented by Izzo et al. [117]. It introduces some basic approaches when encountering a GTOC problem in general, before becoming more specific by developing a solution on the 7th GTOC (multiple-asteroid rendezvous mission).

2.3.3 Other Algorithms used for Interstellar Exploration or Interplanetary Spaceflight

An extension to heuristics such as NHH, which are typically problem-specific, are the meta-heuristics, that follow a more generic strategy. One popular, well-established method are genetic algorithms, which belong to the class of bio-inspired, evolutionary algorithms and are widely used for trajectory and orbit transfer optimization [118–120], including interstellar travel with relativistic rockets [121]. A common approach to increase the optimization performance is the combined use of different algorithms, also referred to as hybridization, as recommended by Vinkó and Izzo [122]. They demonstrate, that applying standard, standalone solvers on global trajectory optimization problems yields poor results compared to the collaborative use of different solver methods. Some of the reference problems proposed in [122] are addressed in [123] by involving a Basin Hopping scheme. Wagner and Wie [124] present a hybrid variant of genetic algorithms, where a gradient-based solver is integrated for local optimum search. The hybridization of genetic algorithms by including a local optimization technique is widely adopted, as done by Hartmann et al. [125] and

Selvaraj [126], both focusing on optimal Earth-Mars transfer and rendezvous trajectories. By hybridizing evolutionary algorithms with a systematic branching strategy, Vasile and De Pascale [127] present a novel technique addressing multiple gravity-assist trajectory design problems. In [128] the hybrid multiagent approach is formulated more generally for global trajectory optimization, considering also bi-impulsive orbital transfers.

Evolutionary neurocontrol is another field of hybrid algorithms to solve for low-thrust trajectory optimization problems [129–132]. Being a combination of genetic algorithms and neural networks, it is particularly useful for global optimization without initial guess to avoid entrapment in local optimums.

Olympio [133] provides a detailed study on scenarios for the planet sequence design problem considering gravity-assisted low-thrust interplanetary transfers. In a similar manner to the earlier described, hierarchically strategy to solve trajectory optimization competition problems, the problem is approached from two different ways: At first, a global optimization problem is considered, where the optimum scenario is found by iterating on possible planet sequences. Trajectories are estimated by means of a low thrust model; impulsive interplanetary trajectories are considered separately. The second approach focuses on local optimization of the trajectory problem, particularly involving swing-by maneuvers.

The optimization problem of multi-spacecraft trajectories, formulated as multi-objective, multi-agent global optimization problem, is addressed by Napier et al. [134]. They present a novel technique based on a coupled approach instead of dividing the problem into subproblems which are solved separately for each spacecraft. Several constraints are investigated, such as sharing one launch vehicle, minimum number of identical flybys or minimum number of shared trajectory phases.

Izzo et al. [135] provide an overview on recent developments of artificial intelligence methods applied to spacecraft guidance dynamics and control. They focus on evolutionary optimization, tree searches and machine learning, which includes deep learning and reinforcement learning. The basic idea behind each method is explained and, when available, relevant scenarios from literature are given. Evolutionary algorithms comprise several subgroups of mostly nature-inspired algorithms, such as the aforementioned genetic algorithms (representing Darwinian evolution) or ant colony optimization. They are used to tackle both single- and multiple-objective, continuous problems but also combinatorial problems with higher complexity, e. g. planning the sequence of planetary encounters. With increasing size of the search space, however, evolutionary algorithms suffer performance. In that case, and whenever it is possible to assemble the solution of the global problem from several smaller sub-problems, tree searches are the method of choice. A typical challenge addressed by tree searches are complex combinatorial problems, such as multiple flybys or rendezvous, which involve two different optimization layers: An outer layer, which searches for the optimum sequence and an inner layer consisting of the trajectory optimization itself, while both layers influence each other. Machine learning represents a rather new class of optimization approaches in this context, compared to the well-established evolutionary algorithms. Generally, these methods require a large set of training data, which may be difficult to obtain in some cases. However, the capability of reinforcement learning to react on unexpected events is highly beneficial when operating in unknown environments. In [136] a machine learning method, more

precisely a deep artificial neural network, is studied with respect to interplanetary trajectory design, considering an Earth-Mars orbital transfer as test case.

Another extensive study on tools for global optimization problems with respect to mission design and analysis is provided by Di Lizia et al. [137, 138]. Problem categories are identified according to propulsion system (two-impulse vs. low thrust) and the number of planetary bodies. A set of optimization algorithms is selected and applied to several test cases to evaluate their performance on the different problem classes.

Myatt et al. [139] conduct a similar analysis, focusing on novel methods. Considered problems include planet transfers and multiple gravity assists, with and without deep space maneuvers. Among the tested algorithms, differential evolution turned out to be most efficient. Furthermore, a gravity assist space pruning algorithm is introduced, which is a new method adapted for the global optimization of multiple gravity assist trajectories (also described in [140]).

2.3.4 Multi-Target Rendezvous Problems

A typical application where multi-target rendezvous problems are encountered is during space debris removal missions. Yang et al. [141] present an autonomous planning tool based on a combination of genetic algorithm and back propagation neural network. While the genetic algorithm is used to obtain optimal rendezvous sequences and accurate transfer trajectory, the trained neural network provides approximations of the optimal trajectory parameters. Other approaches to achieve favorable target sequences include modified genetic algorithms [142], ant colony optimization [143, 144], tree search techniques such as branch and bound algorithms [145, 146] and beam search [147], or reinforcement learning based methods [148]. A combination of genetic algorithm and ant colony optimization is also proposed, referred to as evolving elitist club algorithm [149]. Due to its similarity to the well-known Traveling Salesman Problem (TSP), the multi-target rendezvous problem is commonly formulated as dynamic TSP variant [150, 151] or as Vehicle Routing Problem [152, 153]. Afterwards, techniques such as evolutionary algorithms [154, 155] are applied to obtain a solution to the former problem.

Another typical space optimization problem, which has a problem structure very similar to the space debris removal problem, are multiple-asteroid rendezvous missions. Due to the strong analogy, optimization approaches are similar to the methods mentioned previously, e. g. genetic algorithms [156], search-and-prune algorithms [157], deep neural networks in conjunction with Monte Carlo Tree Search [158] or hybrid methods combining particle swarm optimization and differential evolution [159].

Federici et al. [160] optimize an impulsive multi-rendezvous trajectory design problem based on a bi-level approach, which is similar to the hierarchical strategy described earlier. The outer-level, combinatorial problem comprises target sequence search and rough trajectory estimation and is solved by means of a genetic algorithm. The full transfer trajectory optimization defines the inner-level problem. Both problem levels go hand in hand and, in theory, require a simultaneous solving procedure. Practically, however, the solution from the outer-level problem serves as an initial guess for the inner-level, full trajectory optimization, which is solved subsequently.

Circling back to the TSP, a lot of research has been conducted and various algorithms has been developed and tested, as many real-world problems can be reduced to a TSP or TSP variant, reaching from 3D print trajectory planning [161] to DNA sequencing [162]. An extensive overview of TSP applications and relevant algorithms is given in [163], TSP variants and different solving approaches are provided by [164].

The Vehicle Routing Problem (VRP), already mentioned previously, can be considered as generalization or extension of the traditional TSP. In its classical formulation, the VRP is defined by a set of arcs and vertices, which e. g. represent cities or customers to be served - analogously to the TSP. The first vertex, conversely to the TSP, is considered as a depot or base, which is the starting and ending point of each tour. As another slight difference to the TSP typically a fleet of vehicles is considered, which have a limited delivery capacity. As the TSP, it is extensively studied and there exist lots of different applications and variants, e. g. dynamic VRPs [165, 166] or multi-depot VRPs [167]. Nalepa [168] provides a rich survey on various VRPs and solving methods.

Another TSP variant addressing multi-target rendezvous optimization is the class of orienteering problems. An overview on this problem class is provided by Vansteenwegen et al. [169]. Orienteering is an outdoor sport, where participants have to visit a set of targets which are distributed within a given area. Each target point is assigned with a certain score, which is earned by the participator once the target is visited. As the time is limited, it is not possible to visit each target, hence competitors need to find a route consisting of selected targets in order to maximize the overall score. [170] The classical orienteering problem is very similar to the VRP and thus sometimes also referred to as VRP with profits. Variants include additional constrains in form of time windows which restrict the accessibility of certain targets [171] or the team orienteering problem, where multiple participants or vehicles are considered [172]. In both cited papers, evolutionary algorithms are used to solve the optimization problem, however, also ant colony optimization approaches are common methods ([173], [174]). An application example of the orienteering problem, in particular the variant with additional time window constraint, is the design of tourist trips: Similar to the original orienteering problem, from a given set of points of interests a subset must be selected and arranged as tour in order to maximize the tourist satisfaction. A survey on suitable algorithms addressing the tourist trip design problem is provided by Gavalas et al. [175].

2.3.5 Other Global Optimization Approaches inspired by Nature

Nature has served traditionally as extensive source for models and algorithms to solve complex problems, such as evolutionary algorithms. A selection of further nature-inspired approaches that have not been mentioned yet is provided by Siddique and Adeli [176]. Elbeltagi et al. [177] compare five different evolutionary algorithms by testing them against two benchmark problems. They found Particle Swarm Optimization to perform best in terms of success rate and solution quality. PSO in combination with natural selection is proposed by [178] to encounter the challenge of multi-robot exploration in unknown environments. Generally, PSO is commonly used within hybridization schemes, e. g. together with genetic algorithms [179] (also referred to as Breeding Swarm algorithm [180]), or by including a Kalman Filter [181] or a self-organized criticality extension [182] to improve convergence. Hybridization in the

context of evolutionary algorithms has generated a subclass of so-called memetic algorithms, which are introduced by Moscato [183] and tested successfully against the TSP by Merz and Freisleben [184].

2.4 Summary Literature Survey

Various concepts have been proposed in the context of unmanned interstellar travel, differing in scale (both time and size) and pursuing different strategies. Most of them consider a mission to a single star system, sequential explorations of multiple star systems are presented rather seldomly. Within the interaction of concept, technology and mission objectives several tradeoffs have to be made: Small-scale probes are less expensive in terms of manufacturing costs and propulsion/power requirements but provide only limited capacity for scientific payload, thus limiting the scientific value of a mission. Conversely, large-scale spaceships with extended investigation capabilities are associated with high-performance propulsion and power systems.

Considering the mission itself, one has to decide between conducting a rendezvous maneuver at the target system or performing a simple flyby: A rendezvous increases complexity and mission time (due to the deceleration period) but allows for extensive exploration and investigation operations (yielding higher scientific return). Furthermore, it provides access to resources which can be used for reproducing. Flyby missions, contrarily, are less complex, faster and allow for slingshot maneuvers but offer limited exploration possibilities without access to resources apart from the interstellar medium. Regarding the propulsion technologies, it can be categorized between systems powered from remote sources (e. g. light sails) and integrated concepts, where the fuel has to be transported or produced aboard. Whereas integrated propulsion systems typically are part of large-scale spaceships, small-scale concepts are propelled remotely due to size and mass constraints. Swarm-based concepts describe a fleet of collaborative small-sized probes, which possibly, but not necessarily, are transported by a single, large-scale mothership. Like self-replicating probes, they gain relevance with increasing number of exploration targets and improve the mission success probability due to higher resilience and redundancy compared to single probe approaches.

A map with some of the key mission drivers is provided in Figure 2-17. Arrows indicate correlations with the arrow direction representing the causal dependence.

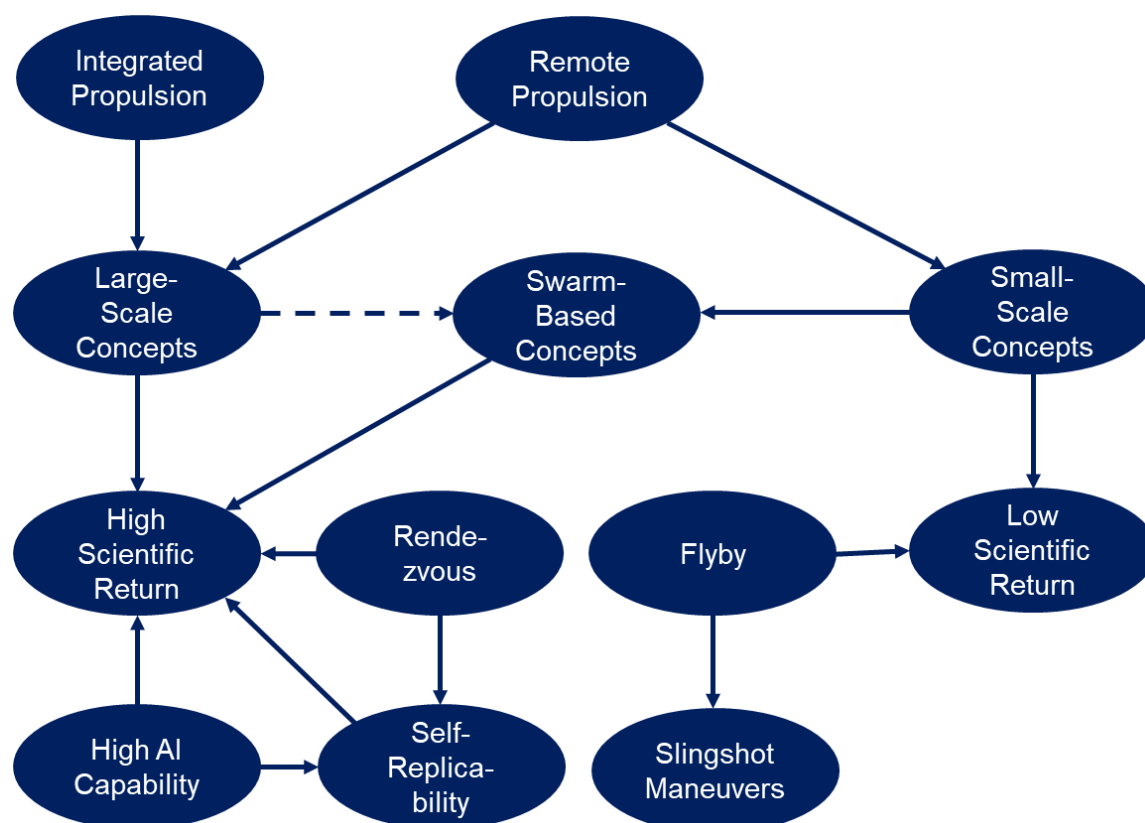


Figure 2-17: Interaction and dependencies between different mission drivers from a high-level perspective

Concerning star systems, a selection of star catalogues resulting from several observation missions has been presented and might serve as data source for the star models (e. g. Gaia DR2, which is the most recent and accurate). Considering modeling approaches, different strategies are found: With increasing number of stars, rather simple star distribution models are assumed (e. g. homogenous or exponential decline of stellar density). Only if the number of included stars is limited (e. g. by focusing on the immediate solar neighborhood), the underlying model relies on real star position data. The assignment of scientific values to a certain star system turns out to be challenging: Whereas it is possible to determine a habitable zone with respect to a certain star, the relation between stellar characteristics and the exoplanet occurrence rate is still discussed. The same holds for the aspect of habitability, where converse studies are found. Hence, there is still a need for further research and observation. Especially a better understanding of the planetary formation process and more data on exoplanets would increase the reliability of predictions on habitable planet occurrence. From what is known today, only trends can be derived, e. g. exoplanets are assumed to follow a homogenous spatial distribution and K stars are expected to support habitability in contrast to high-massive stars. Furthermore, it must be noted that many observations and estimations suffer from a selection bias, which results from the detection method and the observed objects. [185]

To sum up the survey on optimization problems and algorithms, some general strategies can be derived: A common approach to reduce the complexity of multi-objective rendezvous problems is the hierarchical division of the entire problem into two subproblems, specifically global search and local optimization. Both subproblems

are then treated differently, depending on technological boundary conditions (low-thrust vs. impulse) and the optimization objectives. Among the algorithms, which are used for similar problems, hybrid variants typically perform better than standalone solvers. While the problem of interplanetary trajectory optimization has been studied extensively, there exists only few research on advanced interstellar exploration optimization, apart from approaches in the GTOCs framework or missions to close targets. Hence, the search for similar problems needs to be extended to further areas, that at first glance have nothing in common with interstellar exploration but from a more abstract perspective have a very similar problem structure. In particular, the TSP is a very suitable example of a well-established and extensively studied optimization problem with various applications in different areas. Hence, formulating a specific, novel scenario as a common, well-established problem opens access to a large pool of possible optimization approaches.

2.5 Research Gaps and Refined Thesis Objectives

Based on the literature survey, the main research gaps on interstellar exploration strategies can be identified and stated as follows:

- Limitation to certain probe concept or simplistic assumptions on technology
- Focus on low number of target stars, single-target missions or very large number of stars
- Assumption of simplified star distribution model
- Undefined optimization problem of interstellar exploration
- Restriction to limited optimization methods

The research gaps can be used to refine the thesis objectives from chapter 1.2: The overarching goal of this thesis is to derive optimal strategies for interstellar exploration missions, considering a number of 1,000-10,000 stars in the solar neighborhood. Conversely to other studies in this field, the analysis will be based on real star position data instead of using simple distribution models. Furthermore, the question regarding scientific values of stars and their systems will be addressed and included in the modelling procedure.

Earlier work in the interstellar exploration context typically is limited to a certain technology and considers only few target stars. Those approaches will be extended by finding optimal sequences of numerous exploration targets and investigating the impact of mission-related parameters on the exploration strategy, e. g. the effect of number of probes on exploration sequence and selection of target stars. Following a generic approach, this thesis is not meant to identify new technologies or develop novel probe concepts, instead it is making use of the large pool of existing approaches and ideas to define framework and boundary conditions of a generic optimization problem. This ensures validity of the derived results across various concepts.

The solution to this problem will be found via the application of suitable algorithms, which may stem from similar, space-related applications or other fields. In that context it remains interesting to observe, in which kind the problem class (and thus the selection of appropriate algorithms) is affected by the decision for a certain concept or mission parameter.

3 Definition of the Optimization Problem Framework

In this section, the optimization framework is built based on the findings from the literature survey. The approach is visualized in Figure 3-1, starting from upper left.

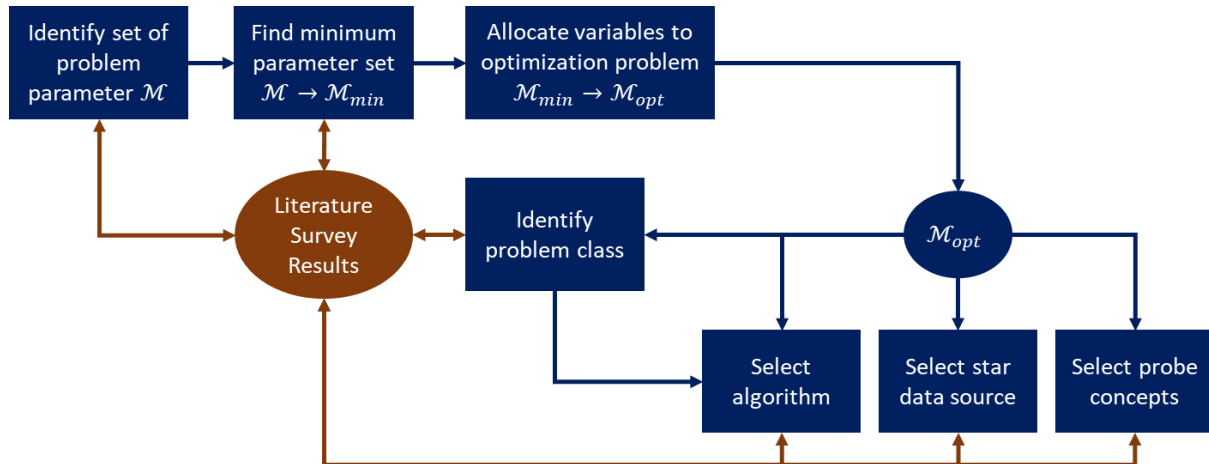


Figure 3-1: Procedure to build the optimization framework

First, relevant problem parameters are derived, which are then used to find the minimum set of variables \mathcal{M}_{min} . In a subsequent step, each variable is classified according to its function within the optimization context. The resulting set \mathcal{M}_{opt} is then used to identify suitable approaches from the literature survey; the selection of an optimization algorithm requires further the identification of the problem class. Most of the described steps are performed under involvement of the literature survey results, as indicated in Figure 3-1.

3.1 Analysis of Problem Structure and Reduction to Minimum Set of Variables

In order to identify suitable solution approaches, the considered problem and its structure needs to be analyzed first. Similar to the concept map derived in chapter 2.4 (see again Figure 2-17), the problem can be structured with respect to relevant parameters and variables. Figure 3-2 provides an overview of the relevant parameters and mission architecture considerations including the correlations, indicated by means of arrows. The elements are colored according to their subgroup of the problem, which are categorized similar to the literature survey:

- Elements in orange represent the probe concept, focusing on the propulsion technology. This includes parameters which are directly related with the propulsion system (such as thrust T and specific impulse I_{sp}), but also variables which are indirectly affected by the propulsion technology, as the probe mass m_{probe} or the required acceleration time t_{acc} determined by the provided Δv_{acc} .
- Input corresponding to the star systems is indicated with black color. The relevant parameters of the star dataset can be reduced to the star position x_i and the value of a star system denoted with s_i .

- Mission parameters and architecture design considerations are indicated with blue color. The criterion of belonging to this subgroup is that the element either depends on parameters from more than one subgroup (e. g. the travel time t_{travel}) or that it is a variable related with mission design (e. g. the exploration sequence of stars $q_{exploration}$).

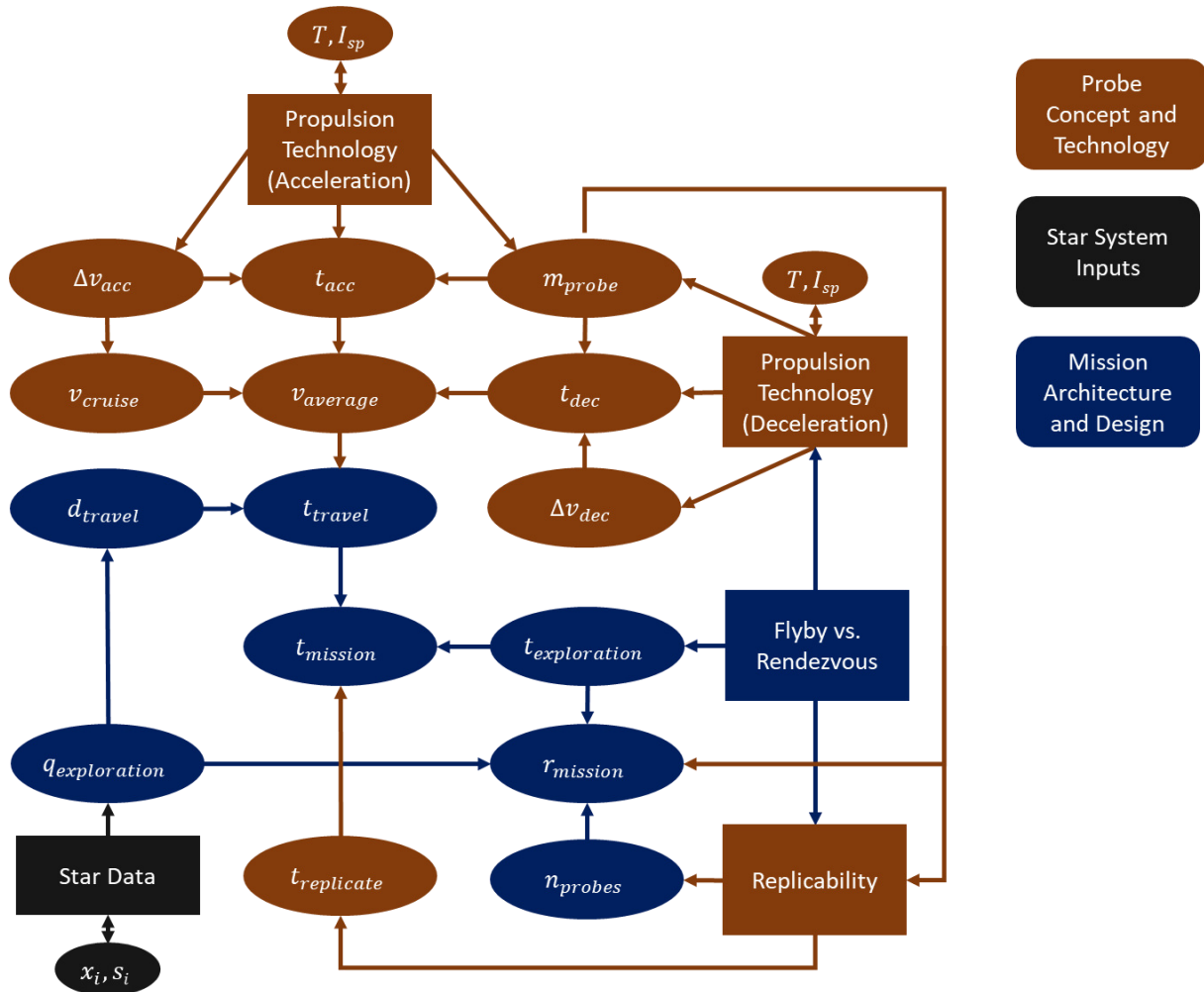


Figure 3-2: Parameter map of the considered problem

Given the problem complexity, the map is not intended to be a comprehensive and complete representation of all mission parameters: In particular, the possibility of slingshot maneuvers and the degree of probe intelligence, which is an important factor for mission return and replicability, are excluded a priori. Same holds for the arrows indicating the correlation, which are restricted to the most relevant ones (e. g. m_{probe} has also an impact on the required replication time $t_{replicate}$). Furthermore, in some cases the separation between the subgroups is not clear, for instance the replicability is both part of probe concept and mission design. Nevertheless, the map serves as a first analysis of the considered problem structure and allows some early conclusions:

Concerning the mission design variables, two sinks can be identified, where correlations are ending while there are no outgoing arrows, namely the mission duration $t_{mission}$ and mission return $r_{mission}$. Hence, both elements can be interpreted

as central results determined by various parameters of the problem and as such represent suitable objective function candidates.

Another observation is that the parameter $v_{average}$, representing the average travel velocity of the probe, includes implicitly most of the concept parameters. This property allows a further simplification of the problem by eliminating the corresponding probe concept parameters. An additional simplification of the problem is done by restricting the mission architecture to flyby missions. This decision helps to further reduce complexity but is also justified by findings from literature: Though limiting the scientific return of the mission, flybys are still appropriate for initial reconnaissance of planets [94] and as such represent a valid contribution to the mission return. Due to the restriction to flybys, the applicability of self-replicating probes is limited; hence, the replicability element is eliminated from the map. Again, this reduces the problem complexity but is also in accordance with results from literature: Considering short-term missions within the solar neighborhood non-replicating probes are found to be more efficient than replicating ones. [29]

Another important consequence of flyby-only missions is that there is no need to account for deceleration and acceleration periods, which are an essential element of rendezvous missions. Hence, the travel velocity of probes is assumed to be constant, which is a common practice in literature on interstellar exploration (for instance, see again Cartin [26]). By further neglecting the impact of probe mass on the mission return, the variable map from Figure 3-2 can be updated as shown in Figure 3-3. Now it contains the minimum set of variables required to describe the given problem in its simplest form. The parameters eliminated due to the reduction procedure and simplifications are greyed out.

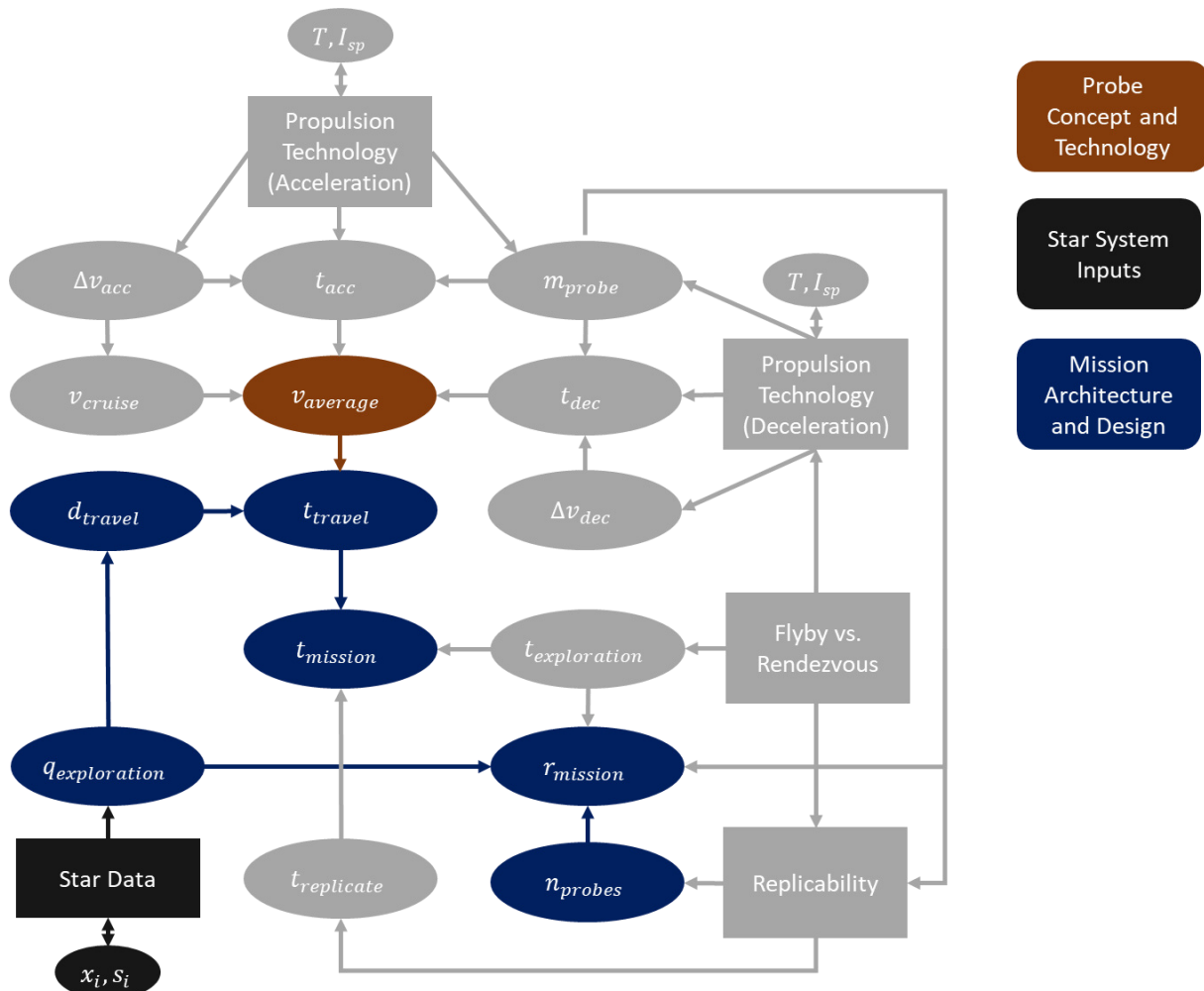


Figure 3-3: Variable map after reduction to the minimum set of parameters; excluded elements are greyed out

As indicated by Figure 3-3 the resulting problem structure and complexity has been simplified significantly. Still, each subgroup is represented by at least one variable.

3.2 Variable Assignment and Problem Classification

In this section the optimization variables are defined by means of the results from the previous subchapter. Furthermore, the class of the optimization problem is identified.

3.2.1 Allocation of Variables to the Optimization Problem

Based on the derived minimum set of variables, the optimization problem to be solved is constructed as follows: In accordance with the observations made already from Figure 3-2, the mission parameters $t_{mission}$ and $r_{mission}$ are selected as objectives. The probe number n_{probes} and average travel velocity $v_{average}$ are chosen as input parameters and need to be specified externally. Same holds for the stellar parameters s_i and x_i . The travel time represents an internal variable, as it can be derived from $v_{average}$ and d_{travel} . d_{travel} , in turn, depends on the star exploration sequence $q_{exploration}$, and is thus also considered as internal variable. As remaining variable, $q_{exploration}$ is chosen as decision variable and as such to be determined by the

algorithm. The final set of parameters is shown in Figure 3-4. Note that the color scheme is changed compared to the previous figures, as now the colors indicate each element's role in the optimization context.

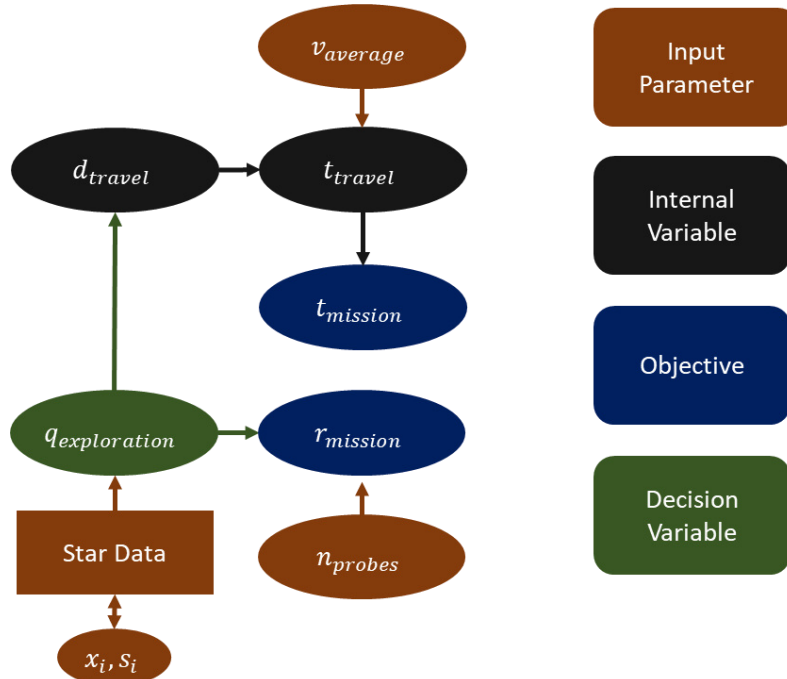


Figure 3-4: Parameter set used within the optimization context, color scheme according to each element's role in the optimization

3.2.2 Identification of the Optimization Problem Class

By dissociating the problem from the interstellar exploration context, a first abstraction level is obtained. On this level, the problem can be described as follows: From a set of locations, each assigned with a certain reward s_i , a subset shall be selected and then arranged in form of a route (see Figure 3-5). The route is evaluated based on two criteria: Its total reward, which is the sum of all rewards from locations that are included in the route and the time, which is required for passing the route. As optimization objectives, the total reward shall be maximized while keeping the route time minimal.

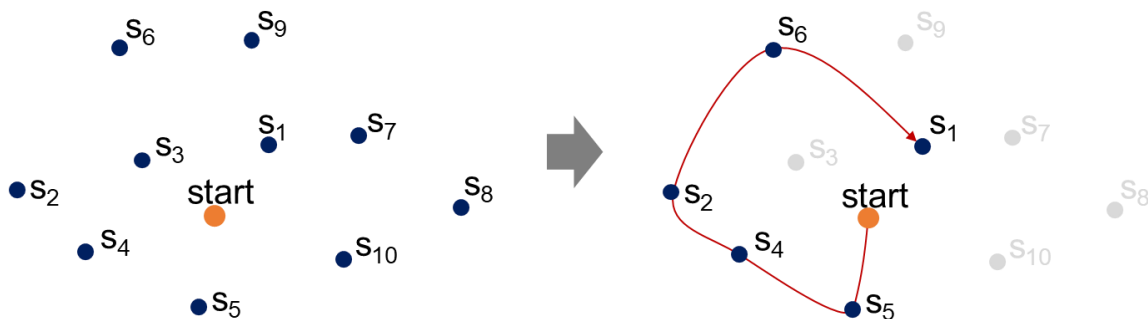


Figure 3-5: Visualization of the problem: From a set of locations with reward s_i a subset is selected which is connected via a route

Considering the abstract problem definitions above together with its visualization in Figure 3-5, the problem reveals strong similarities to the TSP and particularly to some of its variants, e. g. the selective TSP, tourist trip design problem, vehicle routing problem or orienteering problem.

So far, the problem is restricted to a single route. Extending the given problem by allowing the construction of several routes that are passed simultaneously yields a slightly different problem class, which is very similar to the team-orienteering problem. It is visualized in Figure 3-6.

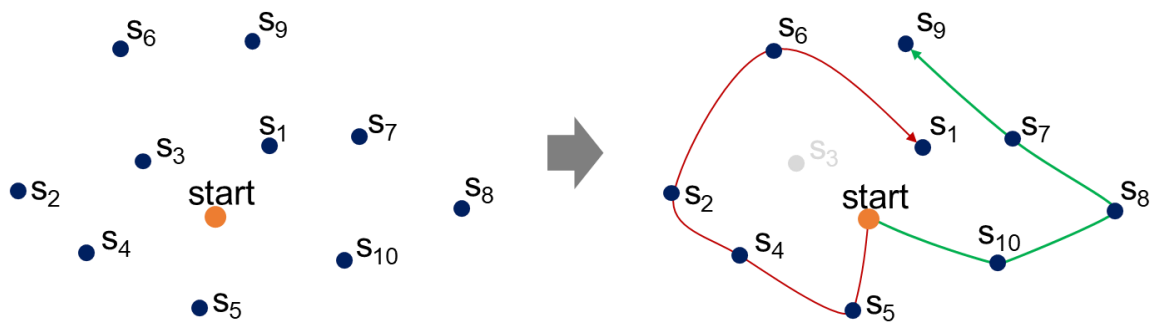


Figure 3-6: Extension of the problem by allowing multiple routes (route 1 in red, route 2 in green)

However, appearing to be very similar to the mentioned problems, there are two main differences:

- In most of the classical approaches the time is not used as an objective but only as a constraint representing a time budget (e. g. the orienteering problem), yielding a single-objective problem. For those cases, the time required for completing a certain route is not involved in the route evaluation unless the time constraint is violated. Hence, two routes with the same profit but different time are considered as equal if both are completed within the given time budget. However, in the exploration context one would certainly prefer the route with shorter time. Therefore, the time is considered as second objective beside the profit, which leads to a bi-objective problem. Note that this does not exclude the possibility of applying a time constraint to limit the maximum route time.
- A common constraint in routing problems (also for orienteering problems) is the prescription of a target destination or end position, commonly denoted as depot. Each participant or vehicle must return to this point after completing its route or arrange its route in a way that it ends at the given final target. For the problem considered here, this is assumed to be not required, therefore it is referred to as open routing problem.

With the given explanations, the considered problem can be categorized as bi-objective multi-vehicle open routing problem with profits. It consists of mainly two tasks, which are firstly the selection of a subset of targets to be visited and secondly the determination of a visit sequence by arranging the selected targets into a route.

The considered problem can be categorized as bi-objective multi-vehicle open routing problem with profits.

3.3 Implications of Variable Selection and Problem Class for Literature Survey Results

Based on the problem structure derived in the previous chapters, suitable approaches to solve for the given problem can be identified from the survey presented in chapter 2. This includes considerations on probe concepts, star catalogues and optimization algorithms.

3.3.1 Implications for Probe Concept and Technology

Considerations on the first search field (chapter 2.1) are incorporated primarily by means of the input parameters $v_{average}$ and n_{probes} . Due to the strong simplifications and restriction to these two variables, the possibilities to distinguish between technologies or compare probe concepts are limited. Concerning $v_{average}$, there is a natural limit defined by the speed of light. The velocity regime suggested in literature for interstellar flyby missions typically ranges from 10-20 % of the speed of light without being restricted to a certain technology or concept. However, considering mission architectures with a high number of probes it can be expected that small-scale probes are preferred over the very large-sized spaceships. An exception might be a “hybrid” concept, where one or few large mother ships are used to transport a swarm of small probes. Leaving this hybrid approach aside, suitable probe concepts are the Starwisp probe or the concept suggested by the Breakthrough Starshot Initiative, just to give two examples. Furthermore, as these concepts rely on remote propulsion technology, they are assumed to be more appropriate for long-term flyby-only missions. Concepts with integrated propulsion typically need to transport the fuel (adverse for long-term missions) or produce fuel aboard by harvesting resources (limited due to the restriction to flybys).

To sum up, given the low number of variables, various probe concepts and technologies are compatible with the considered optimization problem. This entails the advantage that the results of the optimization are not restricted to a certain concept or technology but are valid for various approaches.

3.3.2 Implications for Star Catalogue Selection

The second search field, dedicated to nearby star systems, is represented by the input parameter star data, which provides the star values s_i and positions x_i . The required stellar properties are provided by most of the catalogues presented in chapter 2.2.4 or at least can be derived from the published data. Hence, further criteria need to be involved in order to choose the most suitable source, such as completeness, accuracy and accessibility of the data. The Kepler mission, for instance, which focus on the search of exoplanets and their host stars, would serve as suitable source to identify interesting exploration targets, but lacks from completeness, as its observations are restricted to a certain sky region. Same holds for the ongoing Sloan Digital Sky Survey project, which to date covers only one third of the sky. Other catalogues with focus on nearby stars are limited to a certain range and thus do not contain enough stars, e. g. ARICNS or the list from RECONS. The Gaia DR2 outperforms the other catalogues in terms of completeness and accuracy. E. g., compared to the Hipparcos catalogue, which has a magnitude limit of 12.4 the Gaia DR2 covers also much more fainter stars.

Considering brighter stars, however, its completeness is limited, as shown in Figure 3-7.

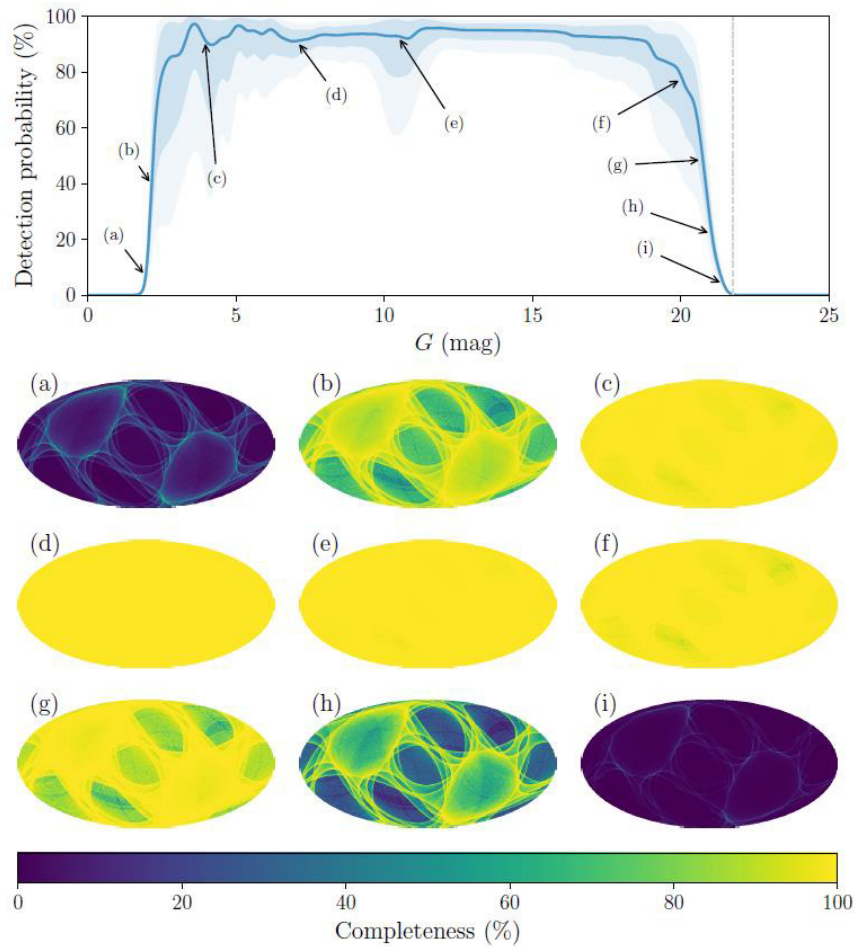


Figure 3-7: Top: predicted probability that a source is detected by Gaia as function of magnitude, below: the completeness of the Gaia DR2 for given magnitudes (crowding effects not included) [88]

As indicated by the plot in Figure 3-7, the Gaia DR2 can be considered as approximately complete across a large range of magnitudes. Another advantage of the Gaia DR2 is the accessibility, as it provides a Python interface which can be used to start user-defined queries and returns the results in processable data format. Given the described benefits of the Gaia DR2, it is regarded as most suitable for the considered problem and thus selected as star data source.

The Gaia DR2 is regarded as most suitable star catalogue for the considered problem and selected as data source for the star model.

3.3.3 Implications for Optimization Algorithm Selection

The third search field, concerning optimization algorithms, corresponds generally to the entire set of variables, but particularly to the objectives and decision variables. Together with the identified problem class they are used to find a suitable algorithm to solve the given problem.

Given the large size of the problem, some of the algorithms and solution approaches presented in section 2.3 can be excluded a priori: Considering n stars there are $n!$ possibilities to arrange them in one route. By means of the binomial coefficient it can be further shown that there are $\frac{n!}{2(n-2)!}$ ways to group the stars in pairs, representing the number of possible transfers between stars under the assumption of symmetry (symmetry means, that the transfers from star A to B and from B to A are assumed to be equal in terms of travel cost). Hence, as there is a minimum number of 1,000 stars considered, any approach based on enumeration is not feasible, even though it would allow to determine the exact optimum. Same holds for branch and bound methods, as their runtime increases exponentially with problem size – in worst cast the runtime is equivalent to the enumeration approach.

Based on these considerations, heuristics or meta-heuristic methods appear to be more suitable to deal with the problem size, even though they do not guarantee to find the optimum solution. Due to the lack of an appropriate growth metric, concurrent tree search algorithms, as suggested by the ESA with respect to GTOC X, are less appropriate: For instance, using a simple nearest neighbor heuristic to grow the tree would lead to clustering and poor ending sequences of a route, as with increasing route lengths the number of unvisited stars decreases. Given the bi-objectivity of the problem, population-based algorithms could help to analyze the relation between both objectives, e. g. by means of the Pareto front: They provide a set of solutions, which can be interpreted as different but equally valued strategies, instead of just one single solution.

Considering approaches which are used to solve similar problems, such as team-orienting problems, different population-based algorithms are applied, e. g. particle swarm optimization, ant colony optimization or genetic algorithms. However, without any further information on the problem and due to the missing experience, it remains difficult to choose between these approaches. As it reveals a very strong similarity to the problem given here, finally a hybrid genetic algorithm described in [172] is selected. Note that any other population-based method, PSO or ACO, are considered as equally appropriate and thus might be used likewise – actually, it would be interesting to see if the results obtained from one of those approaches would differ, but this question is saved for further research.

A hybrid genetic algorithm as presented in [172] is selected to solve the described optimization problem.

3.4 Mathematical Formulation of the Bi-Objective Multi-Vehicle Open Routing Problem with Profits

By following, the optimization problem is formulated mathematically. Due to the similarity of the problems, most of the definitions and equations for the problem formulation are adopted from [172], however, in some cases a few modifications are necessary: For instance, in the original approach a fixed target destination is prescribed, where all vehicles must arrive after terminating their route. This constraint is eliminated in here, as there is no need to force all probes to end their route on a certain star. The two main differences between both formulations and affected equations are summarized in Table 3-1.

Table 3-1: Differences in problem formulation to original approach and affected equations

Original formulation [172]	Algorithm presented here	Affected equations
Start from node 1 ("start depot")	Start from node 0 (solar system)	Eq. (3-6) Eq. (3-7) Eq. (3-8)
Common final target destination n ("arrival depot")	Open final target choice	Eq. (3-9) Eq. (3-10) Eq. (3-11)
Optimization w.r.t. overall route times (sum of route times)	Optimization w.r.t. maximum route time of a mission	Eq. (3-13)

Assume a connected graph $G = (V, E)$ with a set of nodes $V = \{1, \dots, n\}$ and edges E , which represent the connections between each two nodes i and j . In the considered context, the nodes are representing the stars while the edges are the travel routes between the stars. Each node i provides a certain score s_i , which represents the value of the star system that will be added to the mission return if the star is visited. The travel time for a certain edge (i, j) is denoted by t_{ij} and obtained from the distance d_{ij} and travel velocity v :

$$t_{ij} = \frac{d_{ij}}{v} \tag{Eq. (3-1)}$$

Furthermore, the binary decision variable x_{ijp} is introduced, which equals 1 if the edge (i, j) is crossed along a travel route p :

$$x_{ijp} = \begin{cases} 1, & \text{if } (i, j) \in p \\ 0, & \text{otherwise} \end{cases} \tag{Eq. (3-2)}$$

Similarly, y_{ip} indicates, whether a star i is visited along p :

$$y_{ip} = \begin{cases} 1, & \text{if star } i \in p \\ 0, & \text{otherwise} \end{cases} \tag{Eq. (3-3)}$$

The position of a star i within a route is defined by u_{ip} :

$$u_{ip} = \begin{cases} \text{position of star } i \text{ in } p \text{ if } i \in p \\ 0, \text{ if star } i \notin p \end{cases} \quad \text{Eq. (3-4)}$$

The mathematical formulation of the optimization problem is then:

$$Z = \max \begin{pmatrix} J_1 \\ -J_2 \end{pmatrix} \quad \text{Eq. (3-5)}$$

Subject to:

$$\sum_{p=1}^m \sum_{i=1}^n x_{oip} \leq m \quad \text{Eq. (3-6)}$$

$$\sum_{p=1}^m y_{kp} \leq 1 \quad \forall k = 1, \dots, n \quad \text{Eq. (3-7)}$$

$$\sum_{j=1}^n x_{ijp} = y_{ip}, \quad i = \{1, \dots, n\} \setminus \{w\}, \quad p = \{1, \dots, m\} \quad \text{Eq. (3-8)}$$

$$\sum_{j=0}^n x_{jip} = y_{ip}, \quad i = \{1, \dots, n\}, p = \{1, \dots, m\} \quad \text{Eq. (3-9)}$$

$$\sum_{i=0}^n \sum_{j=1}^n t_{ij} x_{ijp} \leq T_{max}, \quad p = \{1, \dots, m\} \quad \text{Eq. (3-10)}$$

$$u_{ip} - u_{jp} + 1 \leq n(1 - x_{ijp}), \quad i, j = \{1, \dots, n\}, p = \{1, \dots, m\} \quad \text{Eq. (3-11)}$$

Eq. (3-6) ensures that a maximum number of m probes is launched from the solar system. Eq. (3-7) guarantees that each star is visited not more than once. By Eq. (3-8) and Eq. (3-9) a continuity check is implemented, ensuring that the number of vehicles arriving at a star is equal to the number of vehicles leaving that star, which excludes the possibility of replication. Note that continuity is not required, when the last star w of a route is reached. This special case is accounted for by excluding w from the input set of i in Eq. (3-8), which is different to the original formulation, where all routes are ending at the same target.

Eq. (3-10) sets a time constraint, which limits the maximum total travel time of a single tour done by one probe. By means of Eq. (3-11) subcycles for a given probe are avoided.

The objective function J_1 represents the mission return and is obtained from:

$$J_1 = \sum_{p=1}^m \sum_{i=1}^n y_{ip} S_i \quad \text{Eq. (3-12)}$$

The objective function J_2 represents the mission duration, which is defined as the maximum travel time for one route:

$$J_2 = \max \left(\sum_{i=0}^n \sum_{j=1}^n t_{ij} x_{ijp} \right), p = \{1, \dots, m\} \quad \text{Eq. (3-13)}$$

It is emphasized, that this is different to the definitions from [172], where the travel cost to be minimized is obtained from the sum of travel times. By means of the following example, this decision shall be justified: Assume two missions A and B, consisting of four probes, with the same mission return but different travel times, as shown in Figure 3-8.

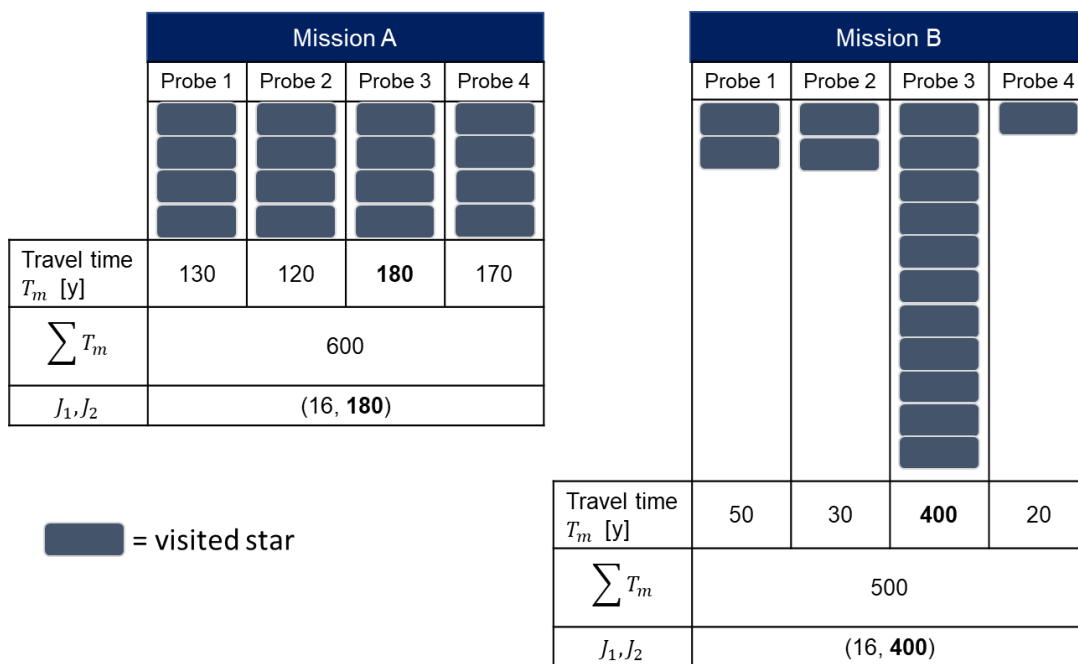


Figure 3-8: Example of two missions A and B with same mission return but different mission duration

During each mission, 16 stars are visited, which yields $J_1 = 16$ (assuming $s_i = 1 \forall i$). The maximum travel time J_2 for mission A is 180 years (probe 3) and 400 years for B (also probe 3). Hence, based on J_1 and J_2 , mission A is to be preferred over mission B, as the same mission return is obtained within a shorter mission duration. Contrarily, when the sum of travel time $\sum T_m$ is considered as cost (as originally done in [172]), mission B is superior to A. Comparing both approaches directly, mission A can be interpreted as resource-saving strategy, which tries to reduce the overall travel time by finding the shortest routes, while mission B is favoring time-optimal solutions. As such, it accepts even longer routes for a single probe, whenever it enables a reduction of the final mission time.

Within the interstellar exploration context, it is expected that resources (particularly fuel costs) are less problematic to a mission (e. g. by using solar sails) compared to the time factor, which is determined by the physical limits of travel speed and large distances. For instance, a mission lasting 10,000 years will not be contemplated even if it is resource optimal. Therefore, the time-optimal approach as described in Eq. (3-13) is used herein, which will produce solutions consisting of balanced route times (as mission A in Figure 3-8).

4 Creation of Mission and Star Models

The final optimization model is composed of several components, which are presented in this section. Following the literature survey categorization, the focus is first on the mission model, which includes the probe concept, mission architecture and trajectory modelling. Afterwards, the star model is specified: It starts with introducing the reference frame and addressing the question, whether to model stellar motion or not. Subsequently, a clean dataset of stars is ensured by performing some filter operations, before a stellar metric defining the value of a star is developed. Finally, a simplified test model is built, which is used for algorithm testing and parameter adjustment.

4.1 Description of the Mission Model

In this section the mission model is specified. It comprises the probe model with the relevant parameters and the assumptions on the mission architecture. In a second subchapter considerations on the trajectory model are presented.

4.1.1 Probe and Mission Architecture Model Specifications

The probe and mission architecture model is based on the minimum set of parameters derived already before (see again section 3.1) and only summarized here: The mission architecture is restricted to flybys, rendezvous are not allowed. Probes are not capable of replicating; hence the probe number remains constant within one mission. However, between different simulation runs the probe number is varied. The probes are assumed to travel with an average velocity of 10 % of the speed of light which is in line with suggestions from literature (for instance, see again [27] or [29]). Limited to this value, the velocity is high enough to allow interstellar travel within a reasonable timescale but still low enough to omit relativistic effects on the trajectory: Given a Lorentz factor of about 1.005, time dilatation and length contraction effects are below 1 % [186] and thus negligible in the modeling context. However, even when considering this high velocity regime, timescales for interstellar travel remain comparably large. This is due to the resulting trajectories lengths, which are set by the large distances between stars. The aspect of trajectory modeling is another important aspect and addressed in a separate subchapter.

Probes are assumed to travel at a constant velocity of 10 % of the speed of light and are limited to flyby missions.

Following the results from the reduction principle introduced previously, parameters and considerations on propulsion technology are not part of the model and optimization. Nevertheless, it must be noted, that the question of propulsion is a key driver and as such remains one of the greatest challenges to be solved to enable interstellar exploration. Being excluded from the variable set, the impact of probe mass on the mission return is also neglected.

4.1.2 Considerations on Trajectory Modelling

With respect to the gravitational potential impacting the space probe on its travel from star A to star B, the interstellar travel trajectory can be divided into two segments: Close to a star, or to be more precise within the corresponding Sphere of Influence (SOI), the individual stellar gravity characteristics is dominant and galactic potential can be neglected. In between (segment 2), the galactic potential must be considered (see Figure 4-1). Intersecting SOI are encountered rather seldomly and thus omitted here. [73]

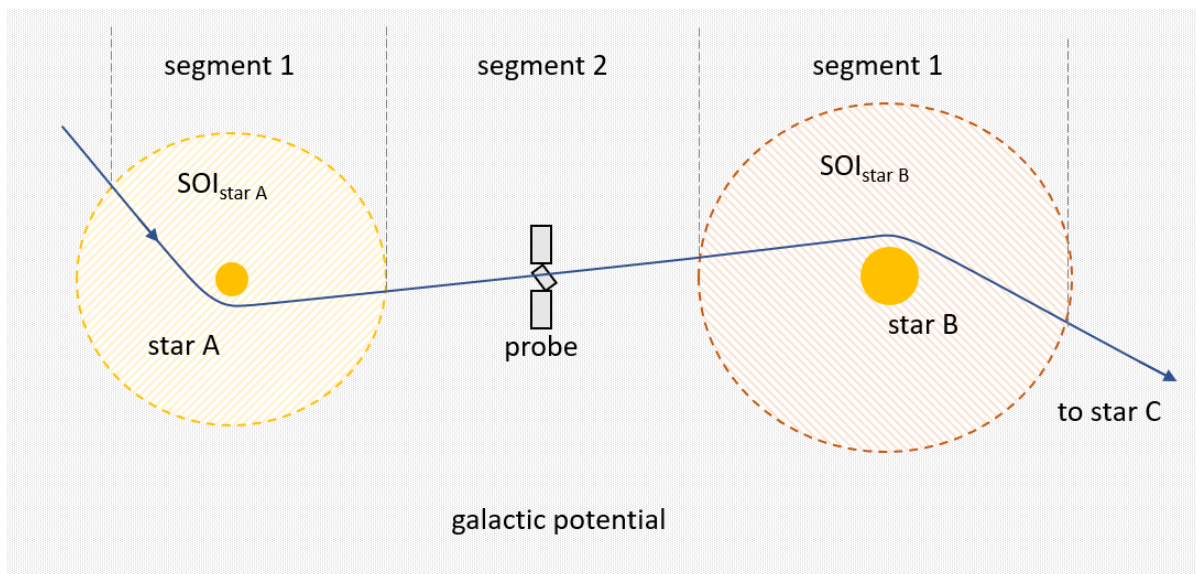


Figure 4-1: Interstellar trajectory segments according to the differing gravitational potential (principle sketch, not to scale) – blue: probe trajectory, grey: galactic potential, yellow: potential due to star A, red: potential due to star B

Inside the SOI, which corresponds to segment 1 in Figure 4-1, the probe follows a hyperbolic orbit which is due to its high travel velocity that exceeds the local escape velocities of the star systems substantially: For instance, the escape velocity of the solar system which is about 600 km/s near Sol [187] differs by more than one order of magnitude from the travel velocity of the probe. Note that the departure trajectory inside the SOI of the Sol, where the probe needs to be accelerated first before entering a hyperbolic orbit, is not considered here.

The resulting, hyperbolic flyby trajectory around the star is shown in Figure 4-2 (blue) together with a simplified, straight-line trajectory (green). The variable d_p refers to the periastron distance, which corresponds to the closest encounter between star and probe. The semi-major axis is indicated by a , the impact parameter is denoted by h . Δl refers to the length difference between one leg of the straight-line trajectory and the asymptote-based curve (grey).

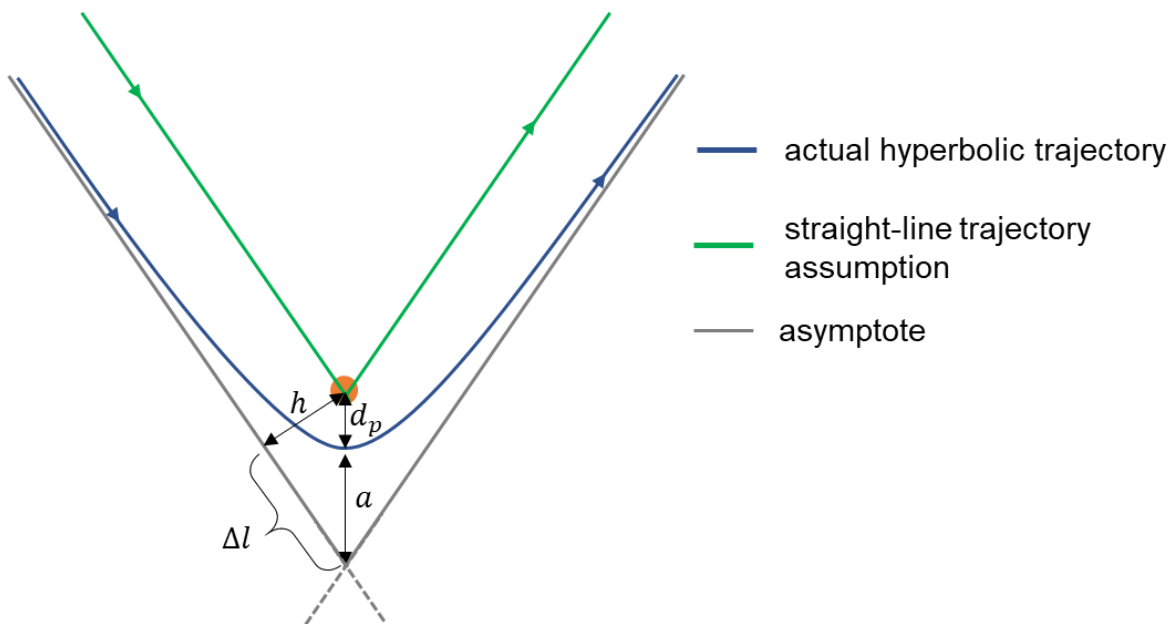


Figure 4-2: Sketch of a flyby trajectory with actual hyperbolic orbit (blue) and assumption of a straight-line trajectory (green), d_p refers to the periastron distance, a to the semi-major axis and h to the impact parameter

With increasing distance to the star, the probe trajectory approaches a straight line which is due to the hyperbolic nature of the orbit. Regarding the trajectory lengths, the actual, hyperbolic trajectory length (blue) can be assumed to range between the length of the simplified, straight-line trajectory (green) and the length of the two legs defined by the asymptotes (grey). As it is much easier to calculate, the asymptote-based curve which consists of the two straight legs is used for an estimation of the length differences.

The difference in length between the straight-line trajectory (green) and the asymptote-based curve (grey) can be calculated as follows:

$$l_{asymptote} - l_{straight} = 2 \Delta l = 2 \sqrt{(a + d_p)^2 - h^2} \quad \text{Eq. (4-1)}$$

In [188] parameters for some example hyperbolic trajectories at lower speed are provided (considering Sol) which can be used here for a rough estimation of the length differences: The perihelion distance d_p is in the range of few solar radii, the length of the semi-major axis a is roughly 20 solar radii; the impact parameter is slightly lower (11 solar radii). Inserting these values in Eq. (4-1) yields a length difference of roughly 40 solar radii. Given the transfer distances between the stars, which are in the range of light years (one light year equals roughly 10^7 solar radii), the error due to the straight-line trajectory assumption inside the SOI is negligible.

Outside the SOI (corresponding to segment 2 in Figure 4-1) the gravitational potential needs to be considered. Due to the high probe velocity, which is still higher than the local escape velocity of the Milky Way (which is about 550 km/s as shown in Figure 2-9 in the literature survey), the probe can be assumed to behave like a hypervelocity star. As such, the acceleration due to the galactic potential can be expected to have no significant impact on the trajectory curvature, at least assuming reasonable mission timescales. This can be shown by considering a simple trajectory problem:

Assume a probe traveling at constant speed v (in x -direction) within a gravitational field (see Figure 4-3). In proximity to the solar system, the acceleration a_{grav} due to the galactic potential is about $2 \cdot 10^{-10} \text{ m/s}^2$ [189]. The most impact on the trajectory curvature (representing a worst-case scenario in this context) occurs when the acceleration acts perpendicularly to v (in y -direction), as shown in Figure 4-3.

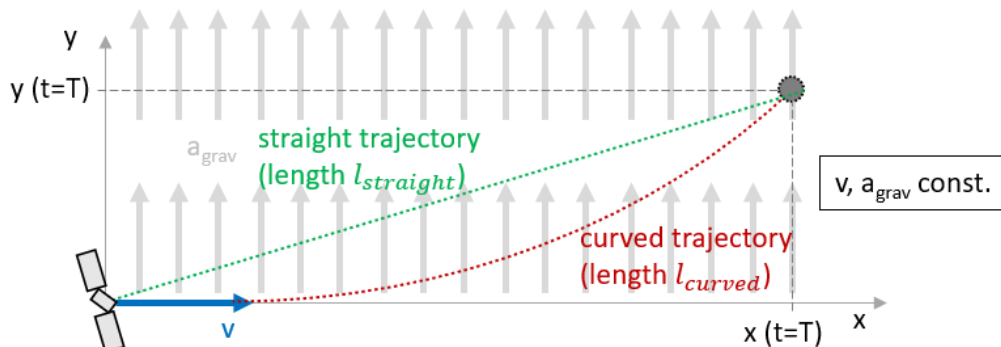


Figure 4-3: Straight trajectory vs. curved trajectory, assuming constant acceleration and velocity

The position of the probe with time t is then described by

$$\begin{pmatrix} x \\ y \end{pmatrix} = \begin{pmatrix} v \cdot t \\ \frac{1}{2} \cdot a \cdot t^2 \end{pmatrix} \quad \text{Eq. (4-2)}$$

The curved trajectory length l_{curved} after time T can be derived from the integral

$$l_{curved}(t = T) = \int_0^T \sqrt{\left(\frac{dx}{dt}\right)^2 + \left(\frac{dy}{dt}\right)^2} dt = \int_0^T \sqrt{v^2 + a^2 \cdot t^2} dt \quad \text{Eq. (4-3)}$$

Conversely, the direct uncurved trajectory length is simply obtained by

$$l_{straight}(t = T) = \sqrt{x(t = T)^2 + y(t = T)^2} \quad \text{Eq. (4-4)}$$

The equations are evaluated for different probe velocities v , considering a maximum timeframe of 1000 years. Due to the low acceleration the deviation between curved trajectory and straight line turned out to be mostly negligible. The curvature effect becomes only significant ($> 1\%$) when considering probe velocities below 10 m/s, which is very much lower than the average travel velocity of the probe.

Given the low curvature effect derived above, the probes can be assumed to travel along a straight trajectory. This model simplification is in accordance with [73], where it is stated that interstellar travel trajectories can be assumed to occur on rectilinear orbits.

Probes are assumed to travel along straight-lined trajectories.

4.2 Building a Star Model of the Solar Neighborhood Based on Gaia Data

In this section, the Gaia based star model used as part of the optimization problem is presented. Furthermore, a concept for a stellar metric is suggested, which can be used to assign each star a certain score according to its contribution to the mission return.

4.2.1 Defining the Reference Frames

The Gaia DR2 catalogue provides galactic coordinates (l, b) , which together with the distance estimates (d) from [89] build a spheric coordinate system to define an object's position in 3D space. However, in some cases, the usage of a cartesian reference system is more comfortable (see Figure 4-4). Compared to the spherical system, which is more common in astrophysics, it simplifies the distance calculations required later within the algorithm.

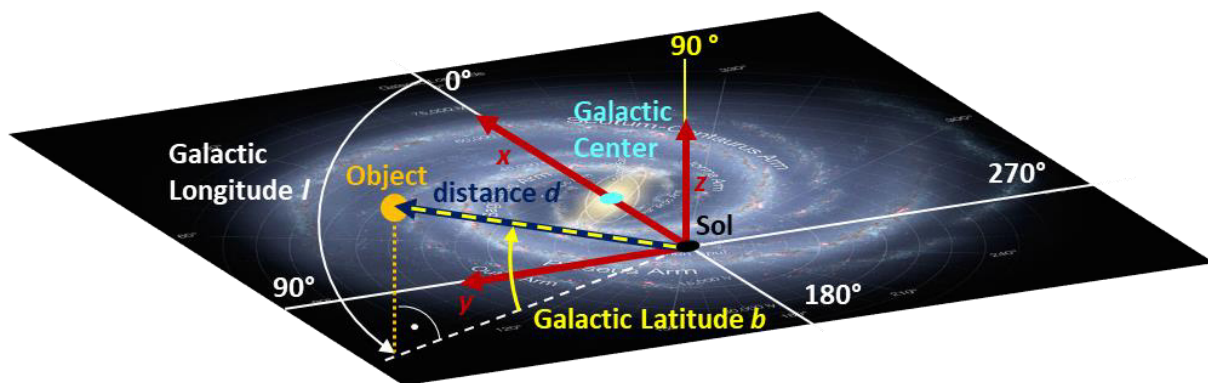


Figure 4-4: Orientation of the Cartesian Reference System (x, y, z) (red) with respect to galactic coordinates (l, b) and object distance (d)

The Cartesian coordinates (x, y, z) are derived from (l, b, d) via a coordinate transformation. Being well-known practice and basic mechanics, the transformation between the systems as well as the corresponding equations are omitted here. The technical implementation of the transformation is done by means of the Astropy Python library [190, 191]. Compared to the galactic coordinate system, the Cartesian system has the same origin, which is our solar system. Its x-axis is pointing towards the galactic center (corresponding to $l = 0^\circ$), the y-axis is aligned with $l = 90^\circ$. The z-axis is orientated towards galactic north ($b = 90^\circ$).

4.2.2 Investigating the Impact of Stellar Motion

An important feature to be included in modeling considerations is the stellar motion, as stars are not fixed but typically rotate around the galactic center. As described during the literature survey (see again chapter 2.2.2) there exist also hypervelocity stars which are unbound and traversing the galaxy faster than the local escape velocity. However, given the high degree of uncertainty and – from current knowledge – presumable low fraction of the entire star number, the aspect of hypervelocity stars is omitted in the model.

The velocity of the bounded stars depends on their orbits and distance from the galactic center. As derived by Brown [75] (see again Figure 2-9), the orbital velocity for nearby-stars is about 230 km/s, the escape velocity is roughly about 550 km/s. Assuming an



average velocity of an interstellar space probe of about 10 % of the speed of light (30,000 km/s) the stellar velocities are comparably small (factor of 0.01). However, with increasing time scales the stellar motion gains relevance, as the star position changes significantly which yields new star constellations and thus may lead to other favorable exploring sequences. For instance, considering a 7,000-year timeframe, the star position will differ by about 5 ly compared to its original position, assuming an average orbit velocity of 230 km/s. Regarding the relative stellar motion a similar range in position difference can be observed: For instance, Barnard’s Star will reduce its distance to Sol by roughly 1.6 ly within the next 7,000 years (see again Figure 2-8). Hence, the assumption of fixed star position holds only for relatively short time scales.

To enable an estimate, whether the stellar motion is significant and needs to be included in the model or not, the uncertainty of the distance estimation provided by [89] is considered: For each star, an upper bound r_{hi} and lower bound r_{lo} is given, which correspond to the highest density interval with probability 0.68. This means, that with a probability of 68 % the star distance estimation is within the interval defined by r_{hi} and r_{lo} . In Figure 4-5, a histogram is provided, where the stars are grouped according to their uncertainty interval size.

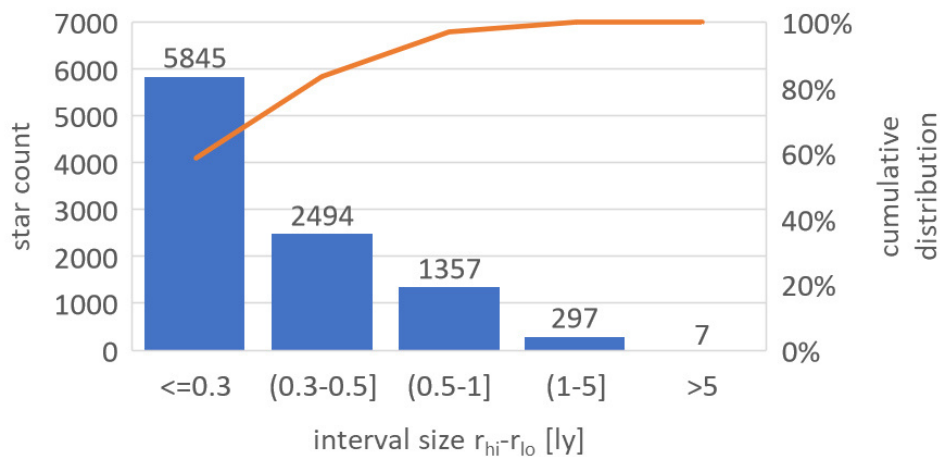


Figure 4-5: Distribution of highest density interval for star position estimates

As indicated by Figure 4-5, most of the estimations are related with highest density intervals smaller than 1 ly. In general, it can be derived, that the maximum uncertainty to be expected is in the order of a few light years. Reconsidering the above example of a 7,000-year timeframe, the effects of stellar motion on the star positions are similar in scale. Hence, the model simplification of fixed stars is considered to be valid as long as the mission timeframe remains below 7,000 years.

Within a mission timeframe below 7,000 years stars are assumed to maintain constant positions.

4.2.3 Star Selection and Filtering Procedure

The Gaia DR2 catalogue contains several reported spurious sources [192], e. g. there are 59 entries which are closer than Proxima Centauri, which is – to current knowledge – the closest star to the solar system. Accordingly, a filter procedure consisting of several steps is applied to obtain a clean dataset of stars. The filtering follows the approach suggested in [192], and is thus only summarized, for details it is referred to the relevant section and equations from the cited paper. The filtering process and its result is illustrated in Figure 4-6.

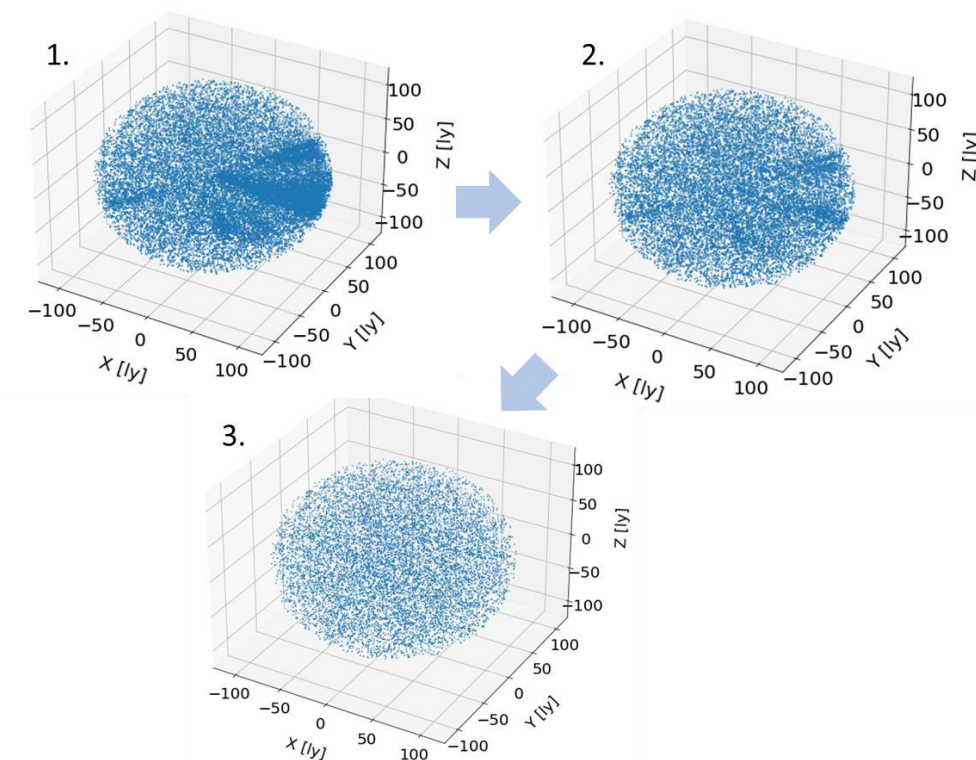


Figure 4-6: Filtering procedure: 1.: Selection of nearest 25,000 stars from Gaia DR2, 2.: Applying filter steps 1 and 2 (15,856 stars left), 3.: Applying filter step 3 (11,981 stars left, from which the 10,000 nearest stars are selected)

In Figure 4-6, the first plot contains the initial, raw dataset with the nearest 25,000 stars which is obtained by using the distance estimates from [89]. The plot indicates the presence of dense regions, which is the result of spurious data and is eliminated by following. From the first to the second plot, a filtering based on parallax error (filter step 1) and uncertainties in BP and RP fluxes (filter step 2) is applied (equivalent to equations (ii),(iii),(iv) for selection A in [192]), reducing the star number to roughly 15,850. This already yields a more homogenous distribution (see second plot in Figure 4-4), however, the denser regions are still apparent, which makes an additional filter operation necessary.

The third filter operation consists of two separate steps: A first selection is made by checking the unit weight error against a criterion derived from the stellar magnitude (equation C.1 in [192]). Secondly, sources where the flux excess factor is beyond a

certain range, which is defined by a color index (calculated from the difference of BP and RP mean magnitude) are eliminated (equation (C.2) in [192]). After applying both filter steps, 11,981 stars are remaining. From this subset, the 10,000 nearest stars are selected (using again the distance estimates from [89]) in order to obtain the final dataset, which is shown in plot 3 from Figure 4-6. Compared to the first plot, the stars are now distributed almost homogeneously. Furthermore, all entries with distances closer than Proxima Centauri have been removed through the filtering, as expected.

Note that the described filter method is rather strict, which leads to the elimination of confirmed, actually true sources, particularly after applying the third filter operation [192]. However, as the thesis focus on general strategies and deriving possible patterns, the impact of excluding some true stars is considered as less adverse to the result than including spurious data points: Particularly the highly inhomogeneous star distribution (remember the dense regions from plot 1 and 2 in Figure 4-6) may mislead the optimization algorithm, resulting in clustered exploration patterns which in real are not feasible.

The Gaia based star model represents a spherical domain around Sol with a radius of 110 ly which contains 10,000 stars.

4.2.4 Star Mission Score - Developing a Stellar Metric

In general, the value of a star or a star system depends strongly on the mission objective and the mission architecture. To ensure applicability for various missions, the concept is intended to follow a rather generic approach.

The generic concept is illustrated Figure 4-7, an explanation on the relevant entries is given below. Note that the ellipses represent examples that may differ depending on the considered mission and objectives.

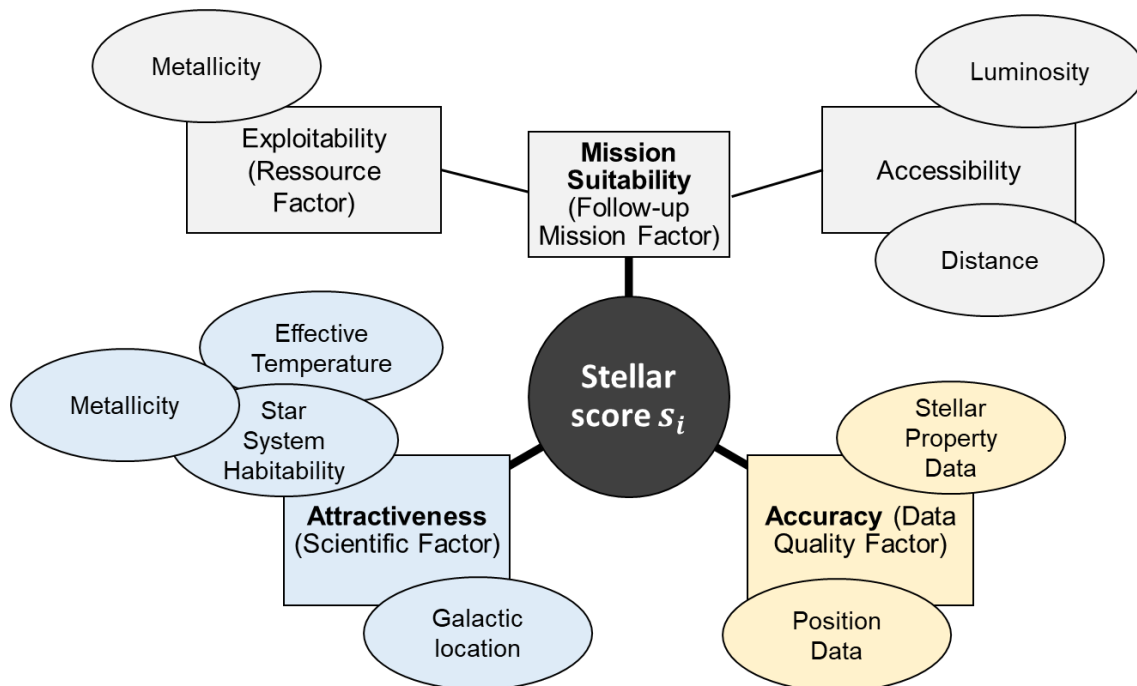


Figure 4-7: Generic stellar score concept

The stellar score is assumed to be determined by three factors that are described by following:

- **Attractiveness:** This includes all the scientific potential which is provided by the star system. Being the key driver of any interstellar mission, the aspect of habitability is assumed to be the main subject of scientific interest. As described earlier (see again chapter 2.2.5) the star system habitability is determined by various factors, which are still discussed today, e. g. the metallicity or the spectral class of the star. However, depending on the mission objectives also other factors such as the galactic location might be relevant (e. g. when focusing a certain galactic region).
- **Mission Suitability:** The mission suitability factor becomes relevant, when the considered mission (e. g. a reconnaissance mission) is part of an entire program, as it assesses the star system with respect to its suitability for subsequent missions. It is determined by two factors:
 - **Exploitability:** Here, the possibilities of resource harvesting are evaluated, e. g. for replication, repairing or fuel production.
 - **Accessibility:** This aspect tries to quantify how easy it is to reach a given star. The distance is an obvious example, as it determines not only the required travel time but also the communication latency when sending

data back to earth. Depending on the probe concept used in the subsequent mission, also the luminosity might be relevant, as it affects the deceleration period and thus overall trip time when using light sails (see again chapter 2.1.5)

It is emphasized, that the mission suitability factor needs to be set based on the subsequent mission – for the current mission, the suitability is evaluated by the optimization algorithm.

- **Accuracy:** The accuracy factor represents the reliability of the used database concerning the position and stellar properties. As the accuracy of the observation methods is limited, each data value is subject to a certain degree of uncertainty. Hence, by means of this factor, the uncertainty can be accounted for in the model. The effect of uncertainty on the stellar score can be defined according to the mission needs, as one might argue that a high degree of uncertainty makes a star system even more interesting.

Note that, depending on the setting of the factors, there is the risk of systematically preferring a certain type of stars, which leads to a bias in the results. Hence, each factor needs to be selected carefully and included into the discussion and interpretation of the results.

To determine the overall stellar score, the scores with respect to each selected category are calculated separately and then averaged. The stellar score in a given category is obtained by a normalized ranking formalism: First, the stars are ranked according to the selected category in reversed order, hence, the worst star is ranked first, while the best star is ranked last. The stellar score $s_{i,x}$ with respect to the category x is then defined by its ranking position r_i normalized by the number of stars n :

$$s_{i,x} = \frac{r_{i,x}}{n} \quad \text{Eq. (4-5)}$$

Due to the normalization, values from 0 to 1 are obtained, where 1 refers to the highest score (the best star in the selected category) and 0 to the lowest score (the worst star in the selected category).

The procedure is illustrated in Figure 4-8, taking the effective temperature as an example. For the other factors and categories, the procedure is the same.

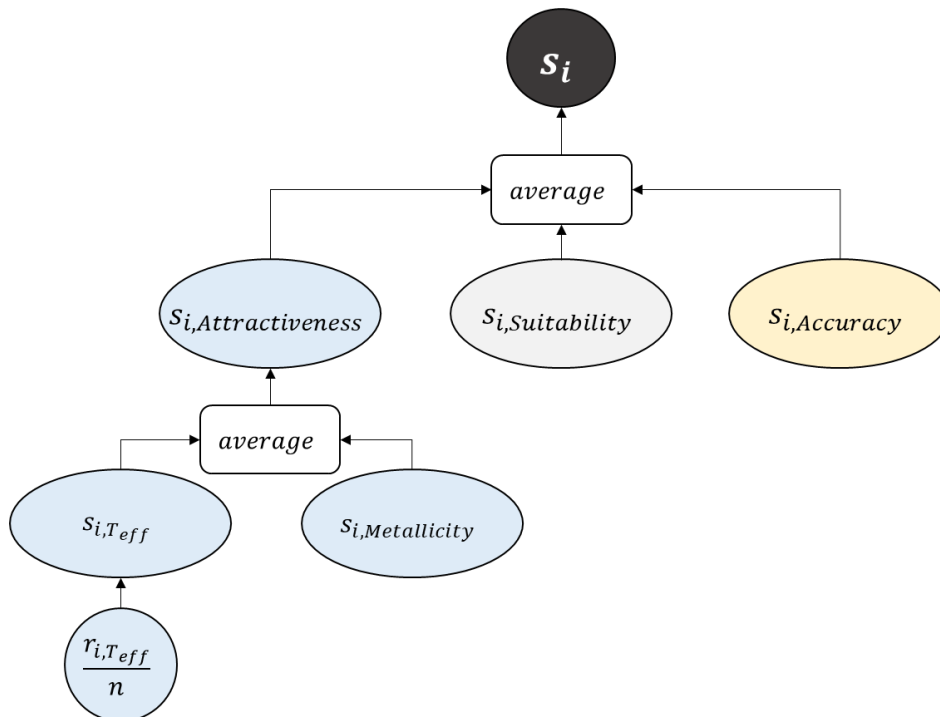


Figure 4-8: Calculation procedure of the stellar score

In the described procedure each factor is weighted equally. Depending on the mission needs, it is also possible to build a weighted sum if one of the factors has higher relevance. The derived metric represents a relative assessment of the stars, which is due to the ranking based score assignment. Hence, the same star can yield different scores when considered within different models.

4.3 Building a Simplified Test Model for Algorithm Testing and Parameter Adjustment

Before applying the algorithm to the real star data model, a test case is generated and used for testing and parameter tuning. Additionally, the test problem serves as performance check for the algorithm: It enables a comparison of the algorithm solution and the ideal solution, which is known due to the simple structure of the test problem.

The test problem is built based on similar length scales and size of the search space of the real star model, which is supposed to contain 10,000 stars with max. 110 ly distance from sol. As model domain, a cube with 120 ly side length is used to yield a similar maximum distance, which is 104 ly and reached at the cube corner. The cube volume is filled uniformly with stars, whereby the minimum distance between two stars is 6 ly. The stars are distributed within a rectangular grid, as shown in Figure 4-9.

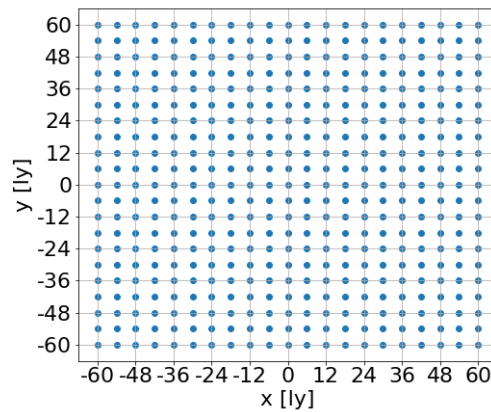


Figure 4-9: 2D grid of the stellar test model, each blue dot represents one star

The resulting 3D model of the test problem is shown in Figure 4-10. It contains 9,260 stars (21^3-1) after removing the star at the origin $[0,0,0]$, which represents Sol. Each star has a score of $s_i = 1$, hence the mission return of a solution equals the number of visited stars.

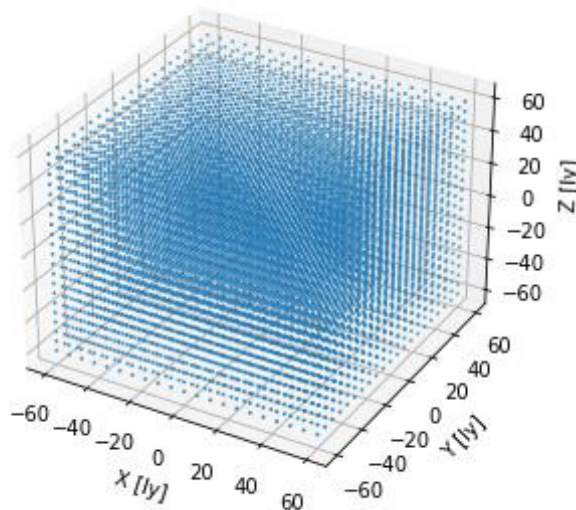


Figure 4-10: 3D model of the test problem: 9260 uniformly distributed stars within a cube-shaped volume of 120 ly side length

The test model represents a cube-shaped domain with a side length of 120 ly which contains 9,260 equally spaced stars.

5 Implementation of an Adapted Hybrid Multi-Objective Genetic Algorithm

This chapter describes the basic mechanisms of the optimization algorithm, which is implemented to solve the described problem. In the beginning, relevant terminologies and definitions are introduced, which are required due to the genetic algorithm methodology. The second subchapter explains the main functions and steps of the optimization procedure. Finally, a summary of the algorithm implementation is provided in form of a pseudocode.

5.1 Algorithm Terminology and Definitions

By following, the algorithm terminology is introduced as well as some further definitions. This includes the encoding of the optimization problem in the genetic context and metrics, which are used to evaluate the solution quality.

5.1.1 Genetic Encoding of the Problem

Before going into detail of the optimization procedure, some general definitions are required, which will encode the problem and its variables for an appropriate use within the evolutionary algorithm context. The first term to be introduced is the chromosome, which represents one possible solution of the given problem and, as such, can be interpreted as one mission suggestion. The chromosome itself consists of a number of genes. Each gene embodies a sequence of stars, which are explored as part of the suggested mission by defining a travel route. Consequently, the number of genes which are part of one chromosome is limited by the probe number, as each probe is assigned to a different route and visits different stars. Note that in general also empty routes are allowed, which corresponds to probes that are not launched.

A set of chromosomes forms a population, therefore sometimes they are also referred to as individuals. As the population undergoes an evolving process and will change with time, each population belongs to a certain generation. With increasing generation number, the population and the solutions represented by each individual will improve. Figure 5-1 illustrates the given explanations on the encoding procedure and terminology.

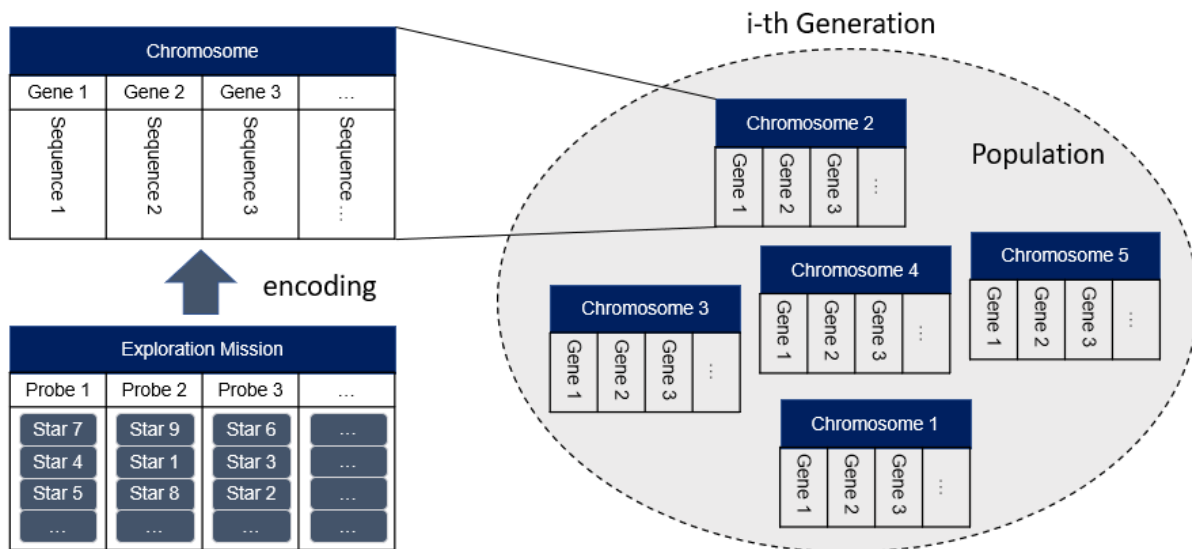


Figure 5-1: Evolutionary Algorithm Terminology and Encoding of Exploration Mission Terms

5.1.2 Defining Metrics for Solution Quality Evaluation

This subchapter introduces metrics that are used to assess the quality of a solution. It starts with the concept of Pareto dominance, which is a common practice in multi-objective optimization problems. Afterwards, the crowding distance metric is presented, which serves to generate new solutions in unexplored regions of the solution space. Finally, the solution fitness ratio is introduced which is defined by the ratio of both objectives.

5.1.2.1 Pareto Dominance and Pareto Rank

An essential tool for comparing solutions mutually is based on the principle of Pareto dominance, which is a common method to evaluate and rank solutions in multi-objective optimization problems. Roughly speaking, one solution is Pareto dominated by a second solution if the second solution allows an improvement in at least one objective function J_i without worsening in one or more of the remaining objective functions J_j . The set of non-dominated solutions (also referred to as Pareto optimal solutions) builds the Pareto front.

Figure 5-2 shows the concept of Pareto dominance and Pareto front for the considered bi-objective optimization problem with the objective functions J_1 and J_2 . As an example, an exploration mission is considered, where mission return J_1 (e. g. determined by the number of explored stars) is supposed to be optimized while keeping the entire mission duration J_2 minimal.

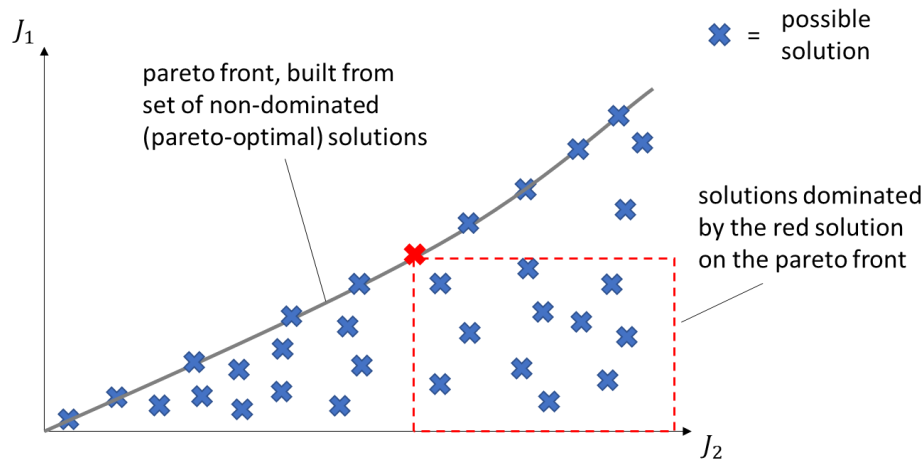


Figure 5-2: Concept of Pareto front and Pareto dominance, the blue crosses indicate possible solutions in the search space

Intuitively, both objective functions are competing: The higher the mission duration, the more stars can be visited and vice versa. This negative correlation makes it difficult to compare two different solutions with respect to their performance. In those cases, the Pareto principles tries to find subsets of optimum solutions by searching for non-dominated solutions. In the considered example, one solution i is dominated by another solution j if j either allows higher mission return in the same or in shorter time or if the same mission return is obtained in shorter time. Mathematically formulated, j dominates i if one of the two following conditions hold:

$$J_1(j) > J_1(i) \text{ and } J_2(j) \leq J_2(i) \quad \text{Eq. (5-1)}$$

or:

$$J_1(j) = J_1(i) \text{ and } J_2(j) < J_2(i) \quad \text{Eq. (5-2)}$$

The concept of Pareto dominance is used to derive the Pareto rank, which is another important quantity to evaluate the relative quality of an individual within its population. Its calculation is adopted from [193] (originally developed by Fonseca [194]) which is similar to the NSGA-II based approach [195] but easier to formulate.

The Pareto rank of an individual is determined by comparing it to all other individuals from one population and counting the number of dominating solutions. For instance, if individual A is dominated by 10 solutions, its Pareto rank equals 10. Consequently, individuals with a low rank are dominated by less solutions than individuals with a higher rank. By means of the Pareto rank, the population can be subdivided into subpopulations, e. g. individuals with rank 0 are non-dominated and form the Pareto front of the current generation.

5.1.2.2 Crowding Distance

Whenever two individuals with the same Pareto rank are compared, another criterion is required, which is referred to as the crowding distance. Generally, it favors individuals in less crowded, unexplored regions from the search space over those located in denser regions. The crowding ranking is only valid between individuals from the same Pareto rank and thus needs to be recalculated for each subpopulation

corresponding to one Pareto rank. The concept can be visualized by drawing a cuboid around the selected individual i , which is bounded by the neighboring individuals $i - 1$ and $i + 1$ (see Figure 5-3). The crowding distance value corresponding to i is then the normalized side length of the cuboid.

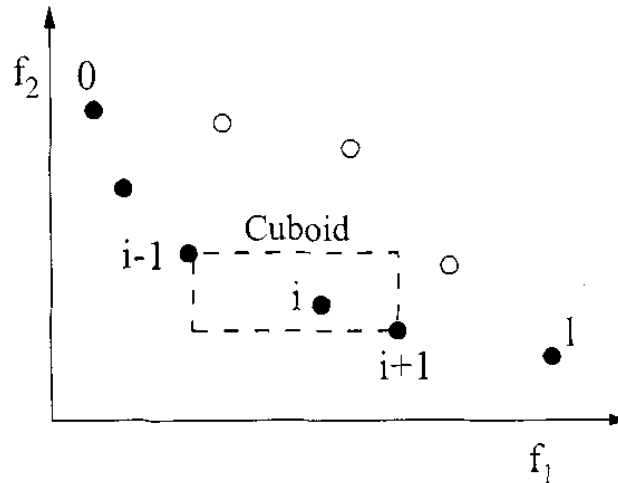


Figure 5-3: Concept of crowding distance for a solution i , the filled dots form a subset of solutions with the same Pareto rank ([195])

The calculation method follows mostly the NSGA-II approach [195] and is illustrated by means of a pseudocode in Figure 5-4. A short explanation follows below.

- (1) $l = |I|$
- (2) for each i , set $I[i]_{distance} = 0$
- (3) for each objective J_m
- (4) $I = sort(I, J_m)$
- (5) $I[1]_{distance} = I[l]_{distance} = \infty$
- (6) for $i \in \{2, \dots, l - 1\}$
- (7)
$$I[i]_{distance} = I[i]_{distance} + \frac{J_m(I[i+1]) - J_m(I[i-1])}{\max(J_m(I)) - \min(J_m(I))}$$

Figure 5-4: Pseudocode for crowding distance calculation (from [195], adapted); the term $J_m(I[i])$ refers to the evaluation of individual $I[i]$ with respect to objective J_m

In (1), the number of individuals l is determined, which form the subpopulation I corresponding to a given Pareto rank. (2) initializes the crowding distance variable and sets it to 0 for each individual. From (3), a loop is started where the crowding distance is calculated for each objective J_m . As herein two objectives are considered (mission value and time), the loop (3)-(7) will be passed twice. (4) sorts the individuals according to the objective J_m in ascending order. For instance, assuming $J_m = mission\ duration$, the individual with the shortest mission duration is placed at the first position, while the individual with the longest mission duration is located at the end. In (5), both individuals positioned at the beginning and at the end are assigned an infinite crowding distance value. As later individuals with high crowding distance values will be preferred, those boundary points will be selected and kept for further generations in almost any case.

(6) starts another loop, where now the crowding distance is calculated for the remaining individuals. This is done by measuring the distance between the two adjacent

individuals for one individual $I[i]$. The result is normalized with the maximum distance within the considered subpopulation. This is slightly different from the original approach in [195] where the global maximum distances (considering the entire population) are used for normalization. A brief explanation on this issue is provided after this paragraph – in short, this modification yields a more balanced weighting between the distances for each objective. Note that crowding distance values derived from former objectives are kept, hence new distance values (corresponding to the new objective) are added to the old distance values.

Remark on Crowding Distance Calculation

Due to the different normalization factors the final crowding distance value is a weighted sum: The larger the normalization factor $F_{normal,m}$, the smaller the distance value for one objective.

$$I[i]_{distance} = \sum_{m=1}^M \frac{J_m(I[i+1]) - J_m(I[i-1])}{F_{normal,m}} \quad \text{Eq. (5-3)}$$

Considering the two objectives mission return and time yields:

$$I[i]_{distance} = \frac{J_1(I[i+1]) - J_1(I[i-1])}{F_{normal,return}} + \frac{J_2(I[i+1]) - J_2(I[i-1])}{F_{normal,time}} \quad \text{Eq. (5-4)}$$

Hence, if one of the normalization factors is relatively large, the resulting, final crowding distance value $I[i]_{distance}$ will mostly depend on the crowding distance based on the other objective. This especially may occur, when one of the objectives is unconstrained. In the considered problem this is true, as one objective has a “natural” limit (set by the star number), while the other (mission duration) in theory is not bounded upwards (only if a time constraint is set).

In its original formulation [195], the normalization factor is defined as follows:

$$F_{normal,m} = \max(J_m(Population)) - \min(J_m(Population)) \quad \text{Eq. (5-5)}$$

Consequently, the normalization factor $F_{normal,time}$ for time-based crowding distance might grow immensely, whenever one individual from the entire population features a very long mission duration (e. g. due to mutation). Thus, the time-based crowding distance will be weighted relatively low compared to the mission-return based crowding distance.

To avoid this behavior, the normalization factor is determined from the maximum distance of the considered subset of individuals instead of the entire population:

$$F_{normal,m} = \max(J_m(I)) - \min(J_m(I)) \quad \text{Eq. (5-6)}$$

Hence, only if the poor solution is part of the subset, it will affect the normalization factor and thus the crowding distances.

5.1.2.3 Fitness Ratio

The final quantity to be introduced here as part of the solution metrics is the fitness ratio σ . The idea behind the fitness ratio is adopted from [171], where the averaged cost over nodes is used as criterion to identify the best routes within a solution.

Typically, it is considered whenever none of the previously described quantities is applicable. This is particular the case for low-level comparisons, such as comparing different routes from one solution. As its name suggests, it is defined by the ratio of both objectives:

$$\sigma = \frac{J_1}{J_2} \quad \text{Eq. (5-7)}$$

Since J_1 is dimensionless and J_2 is noted in years it can be interpreted as averaged mission return per mission year. The fitness ratio includes the concept of Pareto dominance implicitly, hence, whenever one solution or route is dominated by another, its fitness ratio is also lower. Note that in general this relation does not hold backwards: Solutions or routes with lower fitness ratio are not necessarily Pareto dominated by other solutions with higher fitness ratio.

If J_2 equals zero, e. g. in case of empty routes, Eq. (5-7) cannot be evaluated. In this case, the fitness ratio is manually set to zero, as no stars are visited, yielding zero mission return. Hence, any other solution or route which contains stars is to be preferred.

Based on the fitness ratio σ_i , which refers to an individual i , an average fitness ratio σ_{mean} can be derived. It represents the averaged fitness of a population with size P_{max} and is calculated as follows:

$$\sigma_{mean} = \frac{1}{P_{max}} \sum_{i=1}^{P_{max}} \sigma_i \quad \text{Eq. (5-8)}$$

As populations will evolve over the generations, σ_{mean} varies with time: The more dynamically the populations are evolving, the higher its variation. Typically, the evolution dynamics decreases with time while approaching the optimum and thus stabilizing σ_{mean} . Hence, the behavior of σ_{mean} indicates, whether the evolving and improving process of the population is still ongoing or already stagnating, which makes σ_{mean} a suitable convergence criterion.

5.2 Description of the Optimization Procedure

The algorithm which is implemented to solve the given problem follows mostly the approach described in [172], apart from some additional features and adaptations. In particular, the modified calculation of the second objective J_2 requires some changes with respect to the original implementation. For a better understanding, they are explained together with the corresponding algorithm sections.

The method in [172], referred to as hybrid multi-objective evolutionary algorithm, combines two different approaches: Firstly, the Non-Dominated Sorting Genetic Algorithm (NSGA-II), which is a well-established genetic algorithm used for solving multi-objective problems. Secondly, several local search methods are applied for better convergence, making the algorithm a hybrid variant.

Figure 5-5 illustrates the concept including the main functions of the genetic algorithm.

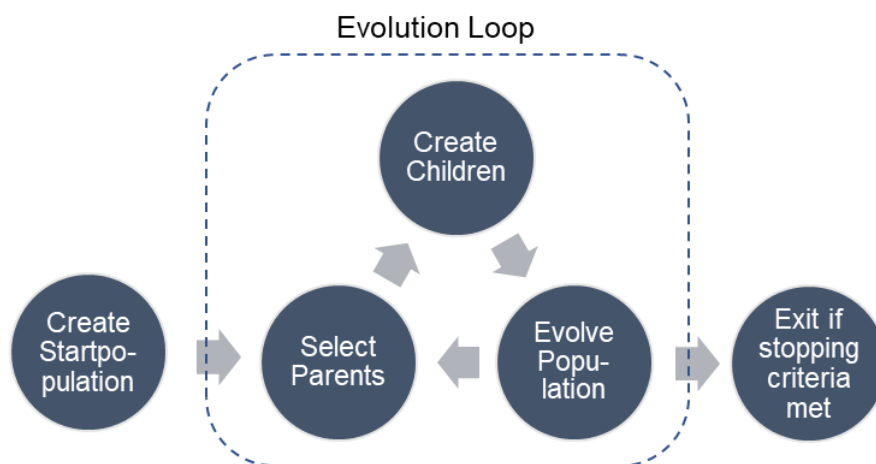


Figure 5-5: Overview and main functions of the genetic algorithm

Before the evolution loop starts, an initial population needs to be generated. This is done by randomly distributing unvisited stars to the probes of an individual until either the time constraint is violated, or all stars are assigned to a route. Then the three operations within the evolution loop are carried out subsequently: It starts with the selection of parents, which are used to generate children, before evolving the population, which again serves as pool to select new parents. According to the evolution terminology introduced in the previous chapters, the iteration of one loop is referred to as one generation. The evolution loop is stopped once a given number of generations is reached. In the subsequent chapters, the functions of the main loop are explained in more detail.

5.2.1 Selection of Parents

The parent selection process is based on a tournament procedure: Individuals are grouped randomly in pairs and compared with respect to their Pareto rank and crowding distance. The underlying tournament condition is: Lower Pareto rank beats higher Pareto rank and higher crowding distance beats lower crowding distance. Note that the Pareto rank has higher priority, therefore the crowding distance is only considered when two individuals with the same Pareto rank are compared. If two

individuals have the same Pareto rank and the same crowding distance value, the winner is selected randomly. The tournament procedure is shown in Figure 5-6.

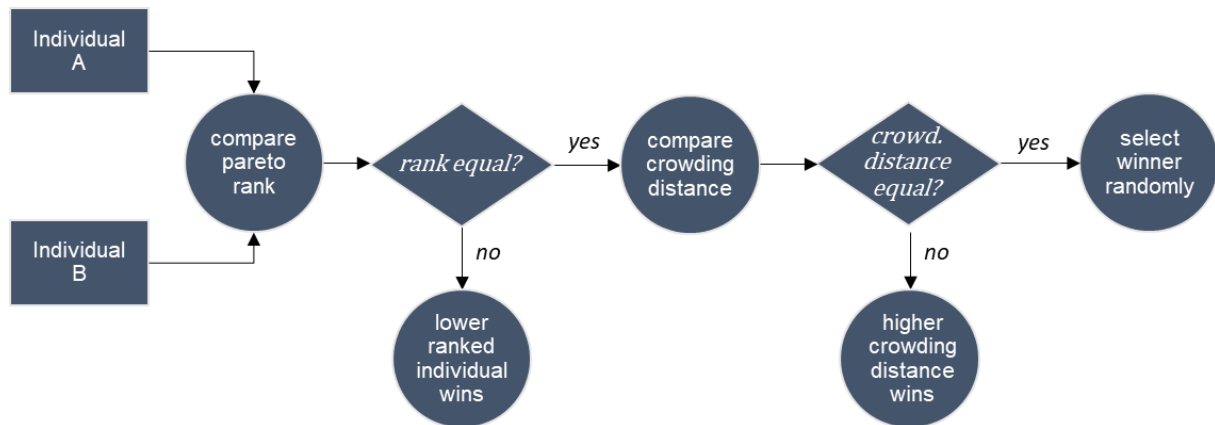


Figure 5-6: Tournament procedure

The winning individual will be included into the parent population, whereas the losing individual is kept in the general population without being involved in the children generation process. In the next step, the resulting set of winning individuals, which are forming the parent population, are used to generate children.

5.2.2 Generating Children

The children creation process consists of several steps. Firstly, two chromosomes from the parent population are chosen randomly. Then, each parent creates one offspring by replicating its genes and a so-called crossover operation. The crossover enables sharing of the best gene, so each child will receive an additional gene from the other parent. To identify the best gene from each parent, the fitness ratio criterion is used. Due to the crossover the chromosome now may contain duplicate gene entries, which means, that stars would be visited twice by different probes within one mission. As this is solution is not wanted, the inherited genes (obtained from replication) are checked for duplicates with respect to the route obtained from crossover. If there exists any, the duplicate element will be removed from the inherited gene, while the crossover gene is kept without modifications. The described children creation process is illustrated in Figure 5-7.

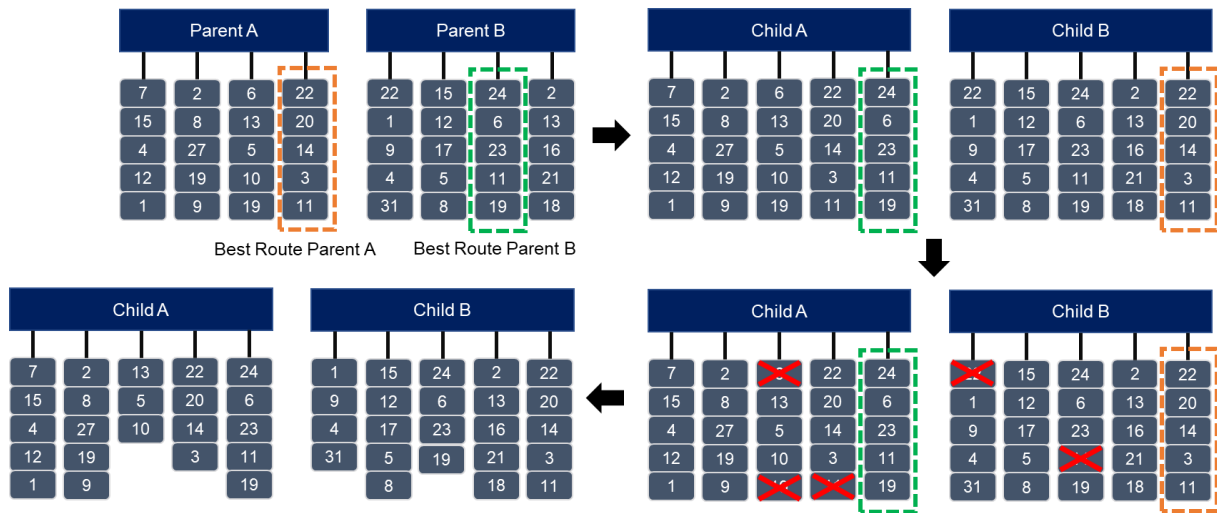


Figure 5-7: Generating children by replication and crossover procedure: From each parent the best route (based on fitness ratio σ) is shared with each child; duplicates in the remaining routes are eliminated

As seen in Figure 5-7, the gene number of the resulting children is increased by one, which conflicts with the given number of space probes. Therefore, a repair function is introduced, which deletes the worst gene (again evaluated based on the fitness ratio σ) until the desired gene number is reached.

After the repairing is finished, a mutation operation is applied to the children with a certain probability, which is defined by the mutation rate. During the mutation, different operations are possible, which are selected based on probabilistic rates. The mutation operations are:

- A) Partial Swap: Two random segments from two random routes are exchanged.
- B) Shortest Route Merge: The two shortest routes (in terms of travel time) are merged into one single route.
- C) Longest Route Split: The longest route (in terms of travel time) is split at a random position into two shorter routes.
- D) Shuffle: The stars in each route are reordered randomly.

Note that the mutation may generate non-valid solutions, which violate the mission time constraint or exceed the probe number limit. For instance, operation B) and C) reduce or increase the route number per child by one, which requires further modifications: For C), the original route number is restored by deleting the route with the worst fitness ratio (analogous to the repair function used when creating children). For B), a new, empty route slot will be created, which can be filled with unexplored stars in subsequent steps. By means of these operations a constant gene number is ensured.

If the time constraint is violated (which may occur for all operations apart from C)), either the original solution is restored (for A) and D)) or the relevant route is cut elementwise, until the mission time reaches T_{max} (for B)).

In Figure 5-8 the mutation procedure is shown.

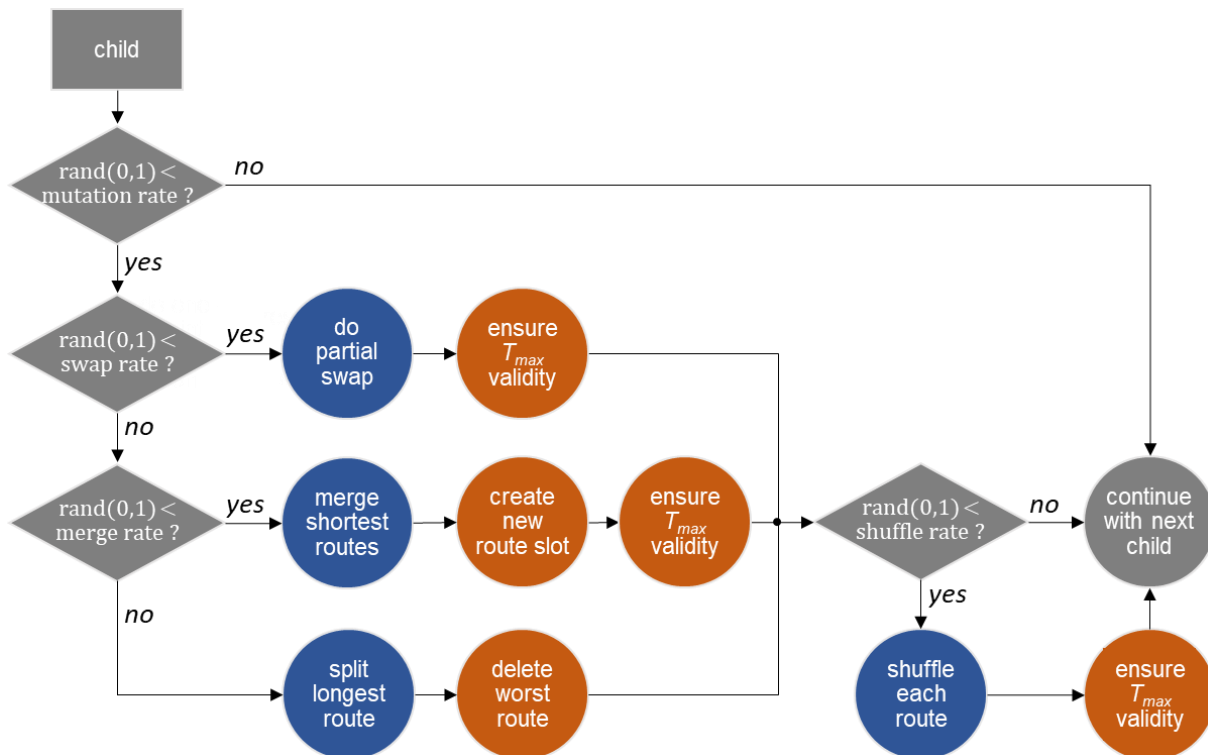


Figure 5-8: Mutation procedure: Mutation operations (blue) are carried out randomly (rand(0,1) generates a random number between 0 and 1); subsequent modifications (orange) may be required to avoid constraint violation (adopted from [193], modified)

However, depending on the parents and the mutation, the resulting children may underperform with respect to the objectives, as the travel times of their routes possibly vary significantly: For instance, assume two parents with very different mission timeframe (see Figure 5-9). Due to the route sharing, the route lengths of child A are not balanced, instead there will be one long route (inherited from parent B) and several short routes (inherited from parent A). The same issue occurs after the mutation, i. e. after merging the shortest routes, where an empty route is generated.

Bearing in mind that mission duration and thus solution fitness is determined by the longest travel time, the solution can be improved (yielding better Pareto rank) by filling up the shorter (or empty) routes with unvisited stars. The improved solution will dominate the original solution, as the star count is increased while the mission duration is kept constant. Alternatively, routes can be cut down to the shortest route lengths, which also equalizes the travel times.

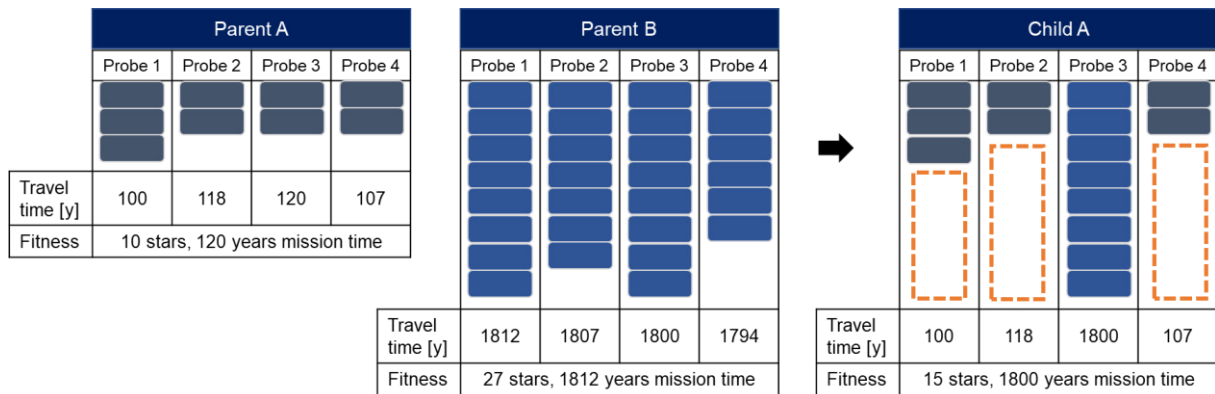


Figure 5-9: Child suffering from high discrepancies in travel time, leading to poor solution fitness

Therefore, to increase solution quality and thus survivability of the children, an improvement function is implemented, which is applied to each child. It consists of either filling up all routes (apart from the longest route) with unvisited stars until the longest route travel time is reached or cutting each route (apart from the shortest route) down to the shortest route travel time (see Figure 5-10). Again, selection between the methods is made using a probabilistic rate (cut rate), except from children containing empty routes, where a cut of all other routes is not desirable.

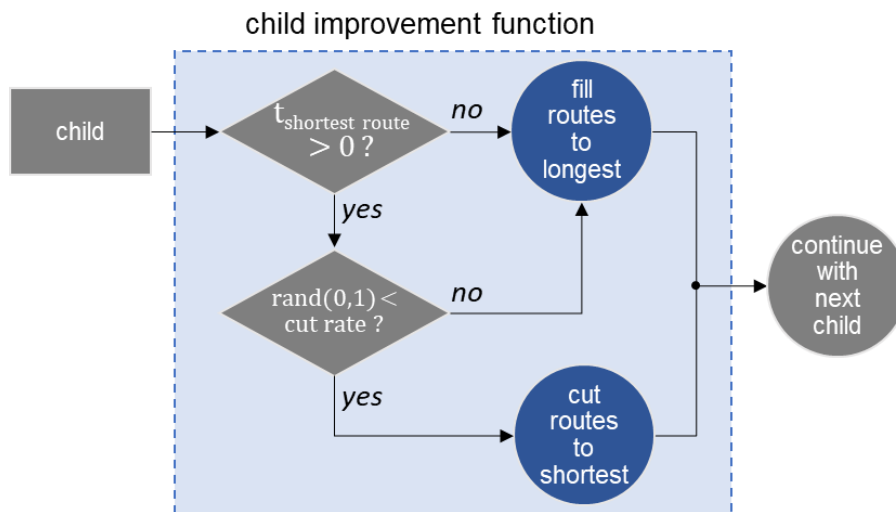


Figure 5-10: Child improvement procedure

Note that this improvement operation is not part of the original approach: As already explained in the beginning of this section, this is one of the modifications which is required due the differing calculation of J_2 . Unlike here, where unbalanced routes may yield poor solution fitness, there the ratio between the routes does not affect the overall solution quality.

The described procedure of producing children is repeated until the children population reaches a certain size, which is defined by the crossover rate. For instance, assuming a crossover rate of 1, the size of the children population equals the size of the original population. Hence, after merging both populations, the population size is doubled.

5.2.3 Evolving Population

Due to the merging of children and original population the population size increases. Therefore, another selection procedure is required, which again makes use of the Pareto rank and crowding distance (as during the population tournament, see section 5.2.1).

During the evolving process, the next generation's population is filled subsequently with individuals from the current population until the maximum population size is reached. The underlying principle is illustrated in Figure 5-11.

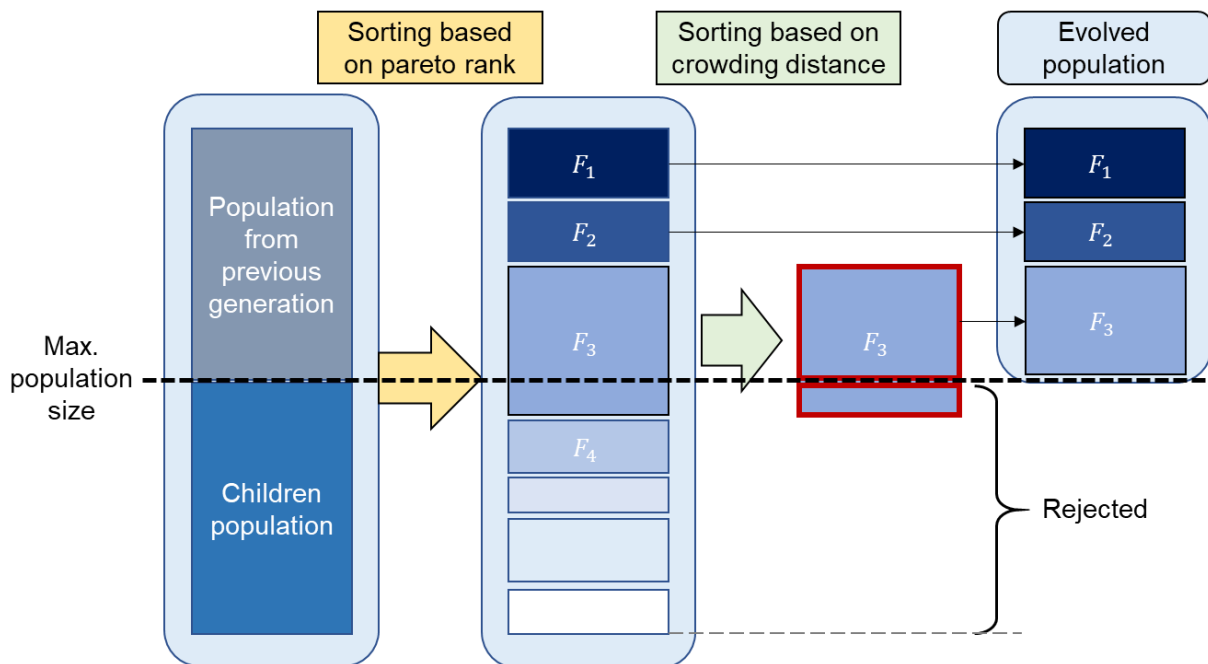


Figure 5-11: Evolving procedure based on non-dominated sorting and crowding ranking (from [195], adapted)

Firstly, individuals are sorted according to their Pareto rank. In Figure 5-11, F_i refers to a subpopulation of individuals with the same Pareto rank. Individuals with the lowest Pareto rank (F_1 in Figure 5-11) are prioritized and included first into the evolved population before individuals with higher ranks are added. Once the maximum population size is about to be reached, individuals from the critical rank (F_3 in Figure 5-11) are selected based on their crowding distance. As described earlier, individuals with high crowding distances are located in less crowded regions of the search space and thus preferred over individuals with low crowding distances. When the maximum population size is reached, the left individuals from the critical rank with lower crowding distance are rejected as well as the individuals with higher Pareto ranks (F_4 upwards in Figure 5-11).

5.2.4 Local Search Operation

Strictly speaking, the local search operation is not part of the evolutionary algorithm procedures. Instead, it represents an additional, external method to improve the solution convergence and therefore is not included in the main loop of Figure 5-5. The local search operation is a set of five methods which are applied within a regular interval to each individual from a population. The methods are described by following:

- A) One-point: An arbitrarily chosen star is switched to another position within the same route.
- B) Two-points: Two arbitrarily chosen stars switch position within the same route.
- C) Two-opt: An arbitrarily chosen route segment is inverted.
- D) Best insertion: The route is rebuilt using a nearest neighbor heuristic.
- E) Switch from longest to shortest: The last star from the longest route is removed and appended to the shortest route.

A)-D) is adopted from [172]. E) is another extension to the original algorithm and added to counteract unbalanced route times for one individual (as described in 5.2.2). The concept of E) is adopted from [28], where with the I-opt a similar local search operation is implemented.

For each individual, one of the five operations is chosen arbitrarily and then applied to all of its routes. Generally, any route modifications caused from local search operations are kept only if the overall solution is improved, which is measured by means of the fitness ratio σ (see Figure 5-12).

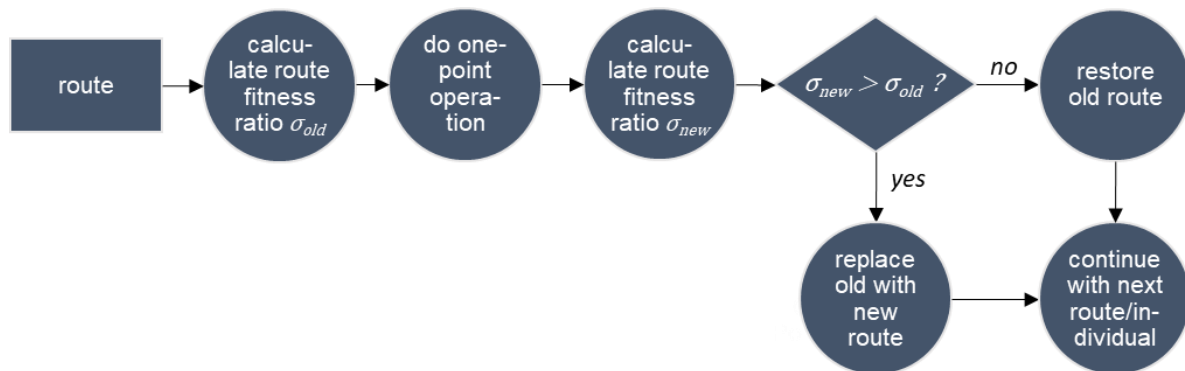


Figure 5-12: Local search procedures (one-point operation as example, workflow equivalent for two-points and two-opt operation)

5.3 Algorithm Overview – Presentation of the Preliminary Pseudocode

The complete algorithm is summarized in Figure 5-13 by means of a pseudocode. As the code might be modified during the testing and adjustment procedure, this version is referred to as preliminary pseudocode.

```

input    set of  $n$  stars with position data and star scores  $s_i$ , probe number  $m$ , travel speed  $v$ 
para-   Time constraint  $T_{max}$                 Crossover rate  $r_{cross}$                 Swap rate  $r_{swap}$ 
meters Max. generations  $g_{max}$                 Improvement cut rate  $r_{imp\_cut}$         Merge rate  $r_{merge}$ 
          Population size  $P_{max}$                 Mutation rate  $r_{mut}$                     Shuffle rate  $r_{shuffle}$ 
          Local search rate  $r_{loc\_search}$ 

output  Population of solutions  $P(g_{max})$ 

begin     $g \leftarrow 0$ 
           $P(g) \leftarrow generate\_initial\_population(P_{max}, T_{max})$ 
          while  $g < g_{max}$ :
             $P'(g) \leftarrow P(g)$ 
            while  $size(P'(g)) < (2 P_{max} r_{cross})$ ::
               $P_{parent} \leftarrow do\_tournament(P(g))$ 
               $P_{children} \leftarrow generate\_children(P_{parent})$ 
               $P'_{children} \leftarrow mutate\_children(P_{children}, T_{max}, r_{mut}, r_{swap}, r_{merge}, r_{shuffle})$ 
               $P''_{children} \leftarrow improve\_children(P'_{children}, T_{max}, r_{imp\_cut})$ 
               $P'(g) \leftarrow (P'(g) \cup P''_{children})$ 
            end
             $P(g) \leftarrow P'(g)$ 
             $P(g + 1) \leftarrow evolve\_population(P(g), P_{max})$ 
            if  $g > 1$  and  $g \% r_{local\_search} = 0$ :
               $P(g + 1) \leftarrow do\_local\_search(P(g + 1))$ 
            end
             $g \leftarrow g + 1$ 
          end
end

```

Figure 5-13: Preliminary algorithm pseudocode (the “%” symbol in the if-condition for performing the local search refers to the modulo operator)

6 Applying the Algorithm to the Simplified Test Model

This section describes the results for the test problem, based on the preliminary algorithm code as presented in Figure 5-13. It starts with a preliminary analysis on the test model before the optimization algorithm is applied. The results are used to refine the algorithm and find a suitable parameter set up, which serves as initial configuration to start with the optimization based on the Gaia star models.

6.1 Preliminary Analysis of the Model

For the preliminary analysis, an exploration mission carried out by a single space probe is considered. Assuming a constant travel speed of 10 % of the speed of light, the probe would reach the nearest star (at 6 ly distance) after 60 years. Due to the uniform star distribution, each subsequently visited star increases the mission duration by further 60 years. Dividing the number of visited stars by the mission duration yields the fitness ratio σ , which represents the average number of visited stars per year. The larger this ratio, the more stars are visited on average per year.

The optimum value is reached, when a maximum number of stars is visited within the shortest possible time. For above example of a single-probe mission, this value will be constant at $\frac{1}{60 y}$:

$$\sigma_{max, single\ probe} = \max \left(\frac{J_1}{J_2} \right) = \frac{n_{stars,visited}}{n_{stars,visited} \cdot 60 y} = \frac{1}{60 y} \quad \text{Eq. (6-1)}$$

Increasing the probe number will increase the scientific return without affecting the mission duration, as more stars can be visited within the same time. Consequently, the fitness ratio will increase as function of the probe number m :

$$\sigma_{max}(m) = \max \left(\frac{J_1}{J_2} \right) = \frac{n_{stars,visited} \cdot m}{n_{stars,visited} \cdot 60 y} = \frac{m}{60 y} \quad \text{Eq. (6-2)}$$

However, this equation holds only for small probe numbers and a limited number of visited stars, as, in general, a time-optimum transfer lasting only 60 years is not always possible: Already the travel to the first target star will last longer, when more than six probes are allowed, as there are only six stars at six light years distance (one in each axis-direction, positive and negative). As each probe is starting from the solar system, only six of them can reach a star within 60 years, the remaining probes have to choose farther stars. Similarly, when most of the stars are already explored, the allocation of new stars reachable within reasonable travel times becomes more and more challenging and potentially impossible, particularly when more probes are involved. Hence, for most cases the fitness ratio has to be interpreted as reference value, not necessarily as an exact, absolute criterion to judge the algorithm performance. Nevertheless, it helps to compare different solutions and gives a rough estimate on the deviation between optimum and calculated solution, especially for small probe and star number.

6.2 Parameter Variation and Algorithm Adjustment

In this section, several algorithm parameters are varied and investigated with respect to their impact on the solution. The solution quality is evaluated by means of the results from the preliminary model analysis (chapter 6.1).

In general, parameters and input data of optimization runs are specified in a table (e. g. see Table 6-1), following the conventions introduced in the pseudocode (Figure 5-13). The values in the table are kept constant along the selected runs while “X”-values indicate a parameter variation.

6.2.1 Variation of Time Constraint Settings

As explained in chapter 4.2.3, the value for the time constraint T_{max} limiting the maximum route time is about 7000 years for physical reasons. However, setting T_{max} already from optimization start to 7000 years turned out to impair the solution quality. Significant higher quality is reached, when the time constraint is disregarded at the beginning of the run and set active after a certain number of generations. Temporarily, this produces invalid solutions but as the activation of T_{max} is combined with a cut operation, which cuts each route down to T_{max} , the final set of solutions will satisfy the time requirements.

Within the runs described in this section, the timing effect of T_{max} activation and cut operation is investigated. This includes a staggered cutting and T_{max} activation, which means, that in a pre-step solutions are cut to a $T_{max} > 7000$ y before performing the final cut to ensure valid solutions.

In Table 6-1, the used input data and algorithm parameter are listed.

Table 6-1: Specification of input data and algorithm parameter, X values indicate a parameter variation

Input Data					
Model	Testproblem	m	4		
n	9260	v	0.1 c		
s_i	1				
Algorithm Parameter					
T_{max}	X	r_{cross}	1	r_{swap}	0.5
g_{cut}	X	r_{imp_cut}	0.05	r_{merge}	0.5
g_{max}	2000	r_{loc_search}	40	$r_{shuffle}$	0.3
P_{max}	100	r_{mut}	0.4		

As shown in Table 6-1 the first parameters to be varied are the time constraint T_{max} and the timing of the cut operation g_{cut} . The remaining algorithm parameters are either adopted from the original approach [172] (r_{cross} and the mutation parameters r_{mut} , r_{swap} , r_{merge} , $r_{shuffle}$), or set based on experimentation. Their impact is addressed in separate subchapters.

The selected parameters are varied according to Table 6-2. $T_{max,g=0}$ refers to the time constraint at start, $T_{max} = \infty$ indicates unconstrained mission duration. The second parameter $T_{max,g=g_{cut1}}$ gives the value used for the pre-cut, which is performed after g_{cut1} generations. Note that for subsequent generations the time constraint $T_{max,g=g_{cut1}}$ is active from g_{cut1} , hence the algorithm is forced to generate solution only within this time range.

Analogously, $T_{max,g=2}$ refers to the value used for the final cut. To ensure valid solutions, it is set to 7000 years and remains active until the run ends. Entries with “-“ indicate that there is no cut and time constraint activation applied, e. g. run 1 remains unconstrained with respect to mission duration whereas run 5 maintains its initial constraint until the end.

Table 6-2: Parameter variation concerning T_{max} activation and cut operation timing

Run	$T_{max,g=0}$ [y]	$T_{max,g=g_{cut1}}$ [y]	g_{cut1} [generat.]	$T_{max,g=g_{cut2}}$ [y]	g_{cut2} [generat.]
1	∞	-	-	-	-
2	∞	-	-	7000	500
3	∞	100000	300	7000	500
4	∞	100000	100	7000	300
5	7000	-	-	-	-
6	∞	100000	100	7000	150
7	∞	100000	500	7000	800

Figure 6-1 shows the resulting set of solutions for each run. The solutions are obtained by evaluating the objective functions for each individual from the final population. Additionally, the ideal curve is given as reference, which is calculated based on the maximum fitness ratio, as discussed in the preliminary analysis.

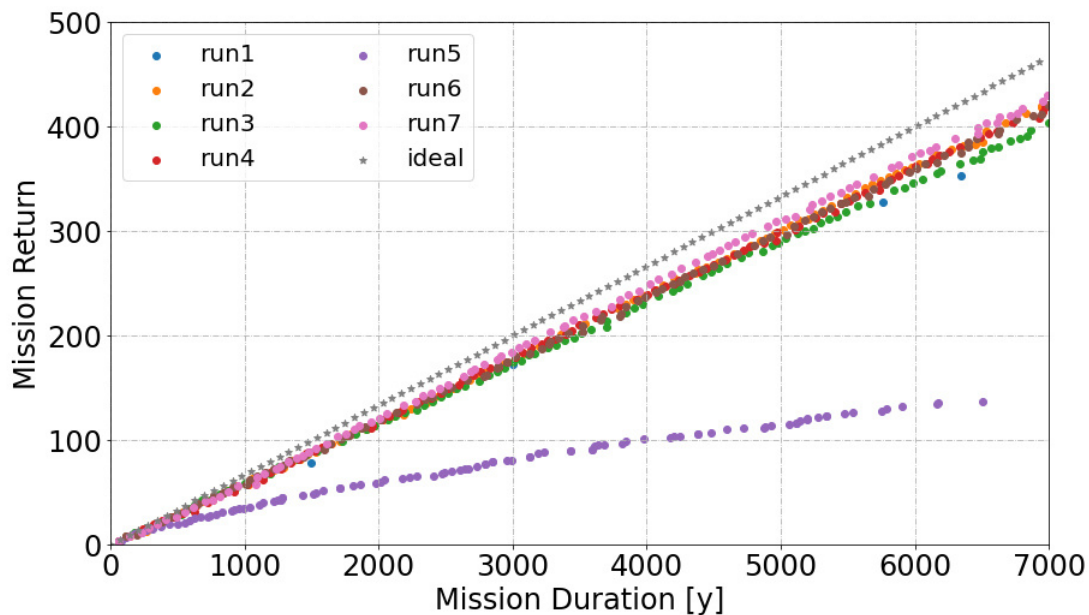


Figure 6-1: Solution set for each run considering different T_{max} activation and cutting time, the ideal solution is given as reference

Apart from run 5, all solutions are within a similar range, which indicates that the effects from different timings for constraint activation and cutting operation are rather low. For run 1, only few solutions are obtained for the considered time frame, which is due to the unconstrained mission time that spreads the population over a large timescale.

6.2.1.1 Time Constraint Effect on the Solution Quality

As already stated previously, run 5, which has an active T_{max} restriction from the beginning, performs significantly worse compared to the other runs. This is assumed to result from the strong reduction of the stars in the solution space from the beginning: In Figure 6-2, this effect is visualized by comparing the number of different stars per generation for run 5 and run 6. Additionally, a plot is given below, which shows the number of new stars compared to the previous generation. Note that to generate this data, run 5 and 6 are repeated and thus may differ slightly from the original runs, however, the general trend is not affected.

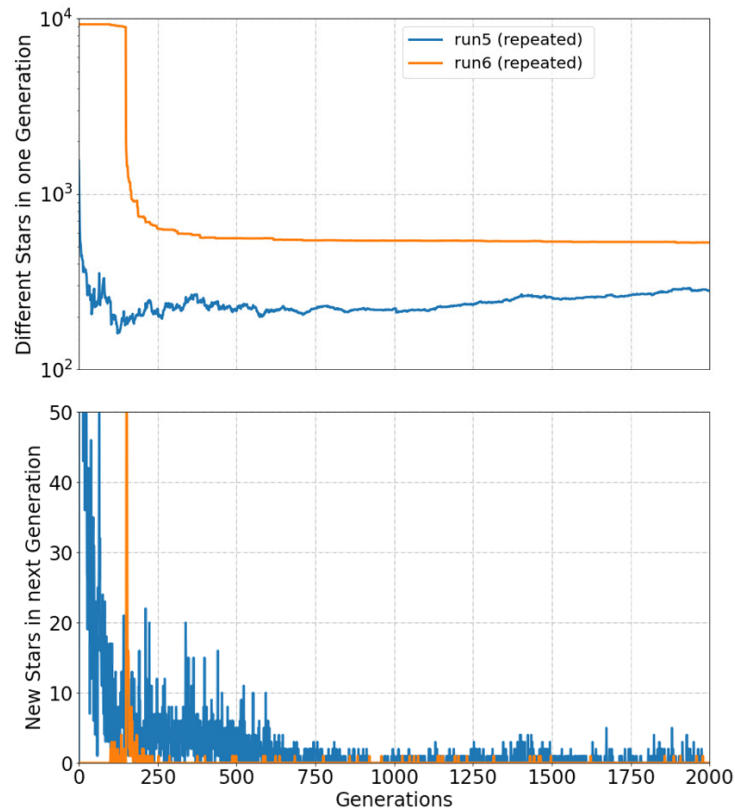


Figure 6-2: Upper plot: number of different explored stars per generation; lower plot: number of new stars in subsequent generation compared to previous generation

As each generation represents a set of missions consisting of various star exploration sequences, it also serves as a pool of stars for the subsequent generations. The only opportunity to add new stars to this pool is during the mutation operations or children improvement procedure, assuming that the corresponding child survives the evolving process. Due to the high star number, however, the probability of selecting a star and inserting it at a favorable position within a suitable exploration sequence of a viable child is rather low, given the random nature of the algorithm. This is exactly what happens in case of run 5: It starts with a small set of stars (see upper plot in Figure 6-2) which is further reduced before being enlarged very slowly with increasing generations. Hence, the routes are built subsequently by adding new stars, which requires many generations. Run 6 pursues a different strategy, where routes are built by selecting stars from the existing set without requiring new stars to be added. This leads to better solutions in faster time. A visualization of selected solution from each run is provided by Figure 6-3, considering a number of 2000 generations.

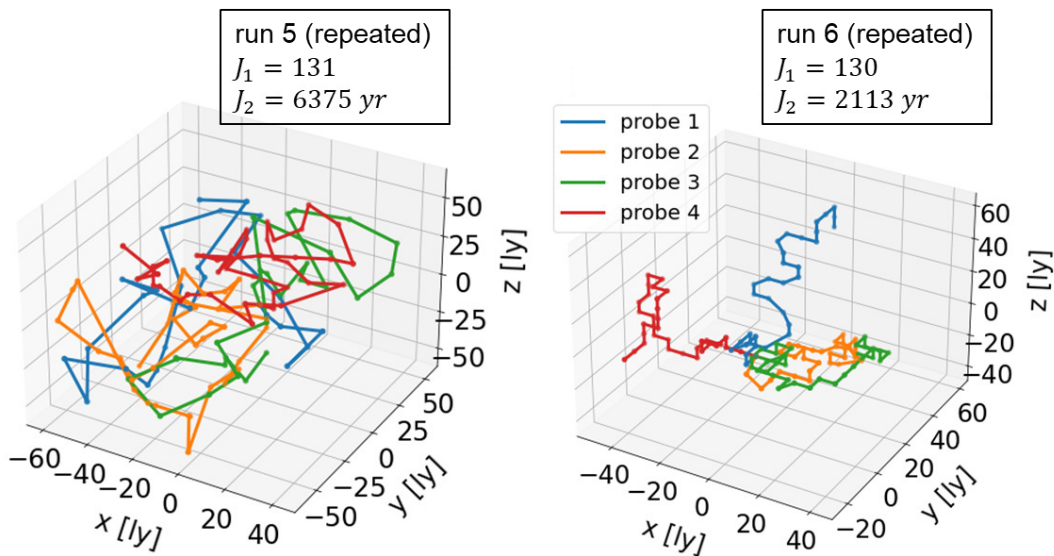


Figure 6-3: Visualization of routes for selected solutions with similar mission return from run 5 and run 6 (both after 2000 generations); each color refers to one route

Compared to run 6, in run 5 the transfers between the stars are much longer and appear to be more chaotic, since there are less stars available to build suitable routes (Figure 6-2, upper plot). As a result, the mission duration required to yield a similar mission return is more than three times higher. With increasing generation number, the routes are improved by subsequently inserting new stars, e. g. after 40000 generations the same mission return is obtained after 3430 years. In run 6, contrarily, the transfer trajectories are much shorter and reveal a more organized structure due to the higher density of selectable stars.

The solution quality can be improved significantly by means of an initial relaxation of the time constraint.

6.2.1.2 Linear Correlation and Considerations on Convergence

Another observation is the linear correlation between both objectives, which is due to the uniform star distribution. The relation is defined by the fitness ratio, which yields for the ideal case according to Eq. (6-2):

$$\sigma_{ideal}(m_{probes}) = \frac{m_{probes}}{60} = \frac{4}{60} \approx 0.067 \quad \text{Eq. (6-3)}$$

Whenever one solution reaches this fitness ratio, it represents the ideal solution.

Due to the linearity the ideal fitness ratio value is constant across the population. Hence, by means of the mean fitness ratio σ_{mean} the overall quality of a population can be evaluated. The development of σ_{mean} along the generations is shown in Figure 6-4, the ideal value of 0.067 is given as reference.

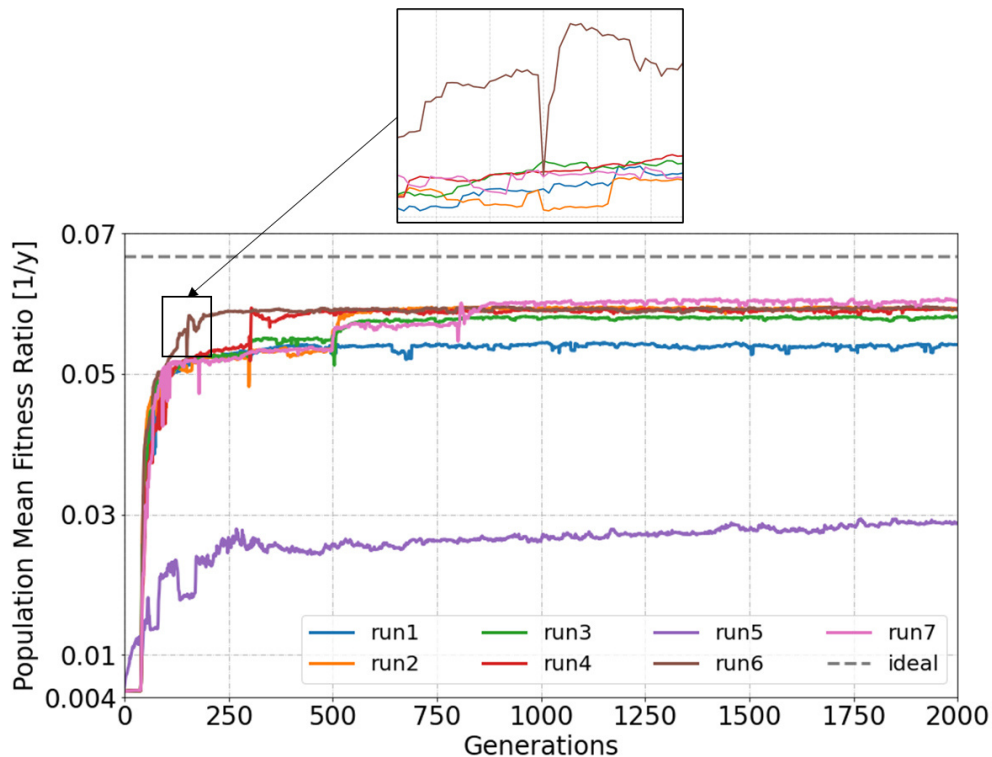


Figure 6-4: Mean fitness ratio of populations vs. generation number for runs with different T_{max} activation and cutting timing, additionally the ideal value of 0.067 is given as reference

There is a strong improvement of the solution within the first generations for run 5. The other runs initially stagnate on a low level but outpace run 5 shortly after the first local search operation is applied (after 40 generations). The cut operations can be recognized by small troughs in the plots, as due to the cutting the overall fitness is temporarily reduced (as shown in the upper plot in Figure 6-4): The cutting operation typically modifies the existing population and also the non-dominated solutions by compressing the Pareto front. Hence, the number of non-dominated solutions is reduced, as formerly non-dominated solutions (located at the end of the curve and thus affected by the cut) may now be dominated by short-term missions, where no cut was required. If the number of non-dominated solutions is smaller than the allowed population size, also dominated solutions are included in the next generation (depending on their Pareto rank, see again section 5.2.3). Due to the inclusion of the comparably worse solutions, the overall population fitness is temporarily reduced.

Another observation from Figure 6-4 is that, apart from run 5, the mean fitness ratio does not improve significantly after a certain number of generations, which indicates a stagnation in the evolving process and thus the presence of a converged solution. In its original formulation from [172], the algorithm is stopped after a certain number of generations without considering the behavior of the solution. With respect to computational resource and runtime this approach might be very inefficient if the optimum solution is found very early and not improved by further generations, as it can be observed in Figure 6-4. Therefore, a convergence check is developed to reduce unnecessary runtime and computational cost, given the large size of the problem considered here.

Technically, the convergence check is implemented by observing σ_{mean} over 200 generations and applying a moving average of size 3 to filter small fluctuations. The solution is then assumed to be converged, when the ratio of minimum $\sigma_{mean,min}$ and maximum $\sigma_{mean,max}$ over the considered sample is below 1 %. Note that a generation number of 300 is set as minimum limit in order to avoid premature convergence due to entrapment in local optimums. In case the convergence criterion is not satisfied, the algorithm stops after reaching the maximum number of generations \mathcal{G}_{max} .

6.2.1.3 General Quality and Efficiency Assessment

In Table 6-3, the final fitness ratio of each run measured after 2000 generations with respect to the ideal fitness ratio is provided. For convenience, also the relevant parameters related with T_{max} are given, furthermore the runtime is shown.

Table 6-3: Solution quality relative to the ideal value for each run together with the relevant parameters, run 6 considered to be most efficient

Run	$T_{max,g=0}$ [y]	$T_{max,g=g_{cut1}}$ [y]	g_{cut1} [gen.]	$T_{max,g=g_{cut2}}$ [y]	g_{cut2} [gen.]	$\frac{\sigma_{mean,final}}{\sigma_{ideal}}$	runtime [min]
1	∞	-	-	-	-	81 %	196
2	∞	-	-	7000	500	88 %	65
3	∞	100000	300	7000	500	87 %	54
4	∞	100000	100	7000	300	88 %	41
5	7000	-	-	-	-	43 %	22
6	∞	100000	100	7000	150	88 %	35
7	∞	100000	500	7000	800	90 %	77

The results in the table confirm the qualitative observations made from the previous figures: The solution from run 5 deviates significantly from the ideal solution, while the other runs are within a range of 80-90 %. Not that for run 1, which is unconstrained with respect to T_{max} , the ideal solution is maybe not realizable for the entire population, hence it performs slightly worse but still better compared to run 5.

Regarding the runtime, it can be stated that it correlates with the possible route length, which is limited by T_{max} . Consequently, run 5 is very fast due to the permanent constraint, while run 1 takes about 9 times longer. The runtime of the other runs depends on the timing of g_{cut} : The earlier the cut is applied, the shorter is the overall runtime.

The decision, which parameter combination is the most suitable, is based on the solution quality and runtime: Run 7 performs best, however, its runtime is more than twice compared to the runtime from run 6, which performs only slightly worse. Therefore, the parameters from run 6 are assumed to represent a good trade-off between solution quality and runtime.

6.2.2 Implementation of Convergence Check and Variation of Crossover and Mutation Rates

This set of runs is dedicated to the probability rates used for crossover, mutation and improvement operations. Additionally, the functionality of the convergence check as described before is tested. The remaining parameters are kept constant and listed in Table 6-4.

Table 6-4: Specification of input data and algorithm parameter corresponding to runs investigating crossover and mutation parameter, X values indicate a parameter variation

Input Data					
Model	Testproblem	m	4		
n	9260	v	0.1 c		
s_i	1				
Algorithm Parameter					
$T_{max,g=0}$	∞	g_{max}	2000	r_{mut}	X
$T_{max,g=g_{cut1}}$	100,000 y	P_{max}	100	r_{swap}	X
$T_{max,g=g_{cut2}}$	7000 y	r_{cross}	X	r_{merge}	X
g_{cut1}	100 gen.	r_{imp_cut}	X	$r_{shuffle}$	X
g_{cut2}	150 gen.	r_{loc_search}	40		

The parameters are varied for each run according to Table 6-5. For better transparency in each run only one parameter is varied compared to run 1 (apart from run 8).

Table 6-5: Variation of parameters corresponding to runs investigating crossover, mutation parameter and children improvement operation parameter

Run	r_{cross}	r_{mut}	r_{swap}	r_{merge}	$r_{shuffle}$	r_{imp_cut}
1	1	0.4	0.5	0.5	0.3	0.05
2	0.8	0.4	0.5	0.5	0.3	0.05
3	1	0.8	0.5	0.5	0.3	0.05
4	1	0.4	0.8	0.5	0.3	0.05
5	1	0.4	0.5	0.8	0.3	0.05
6	1	0.4	0.5	0.5	0.6	0.05
7	1	0.4	0.5	0.5	0.3	0.2
8	0.9	0.7	0.6	0.7	0.2	0.1

The plot of the final solution fitness for each run is omitted here, instead only the mean fitness ratio over the generations is shown (see Figure 6-5).

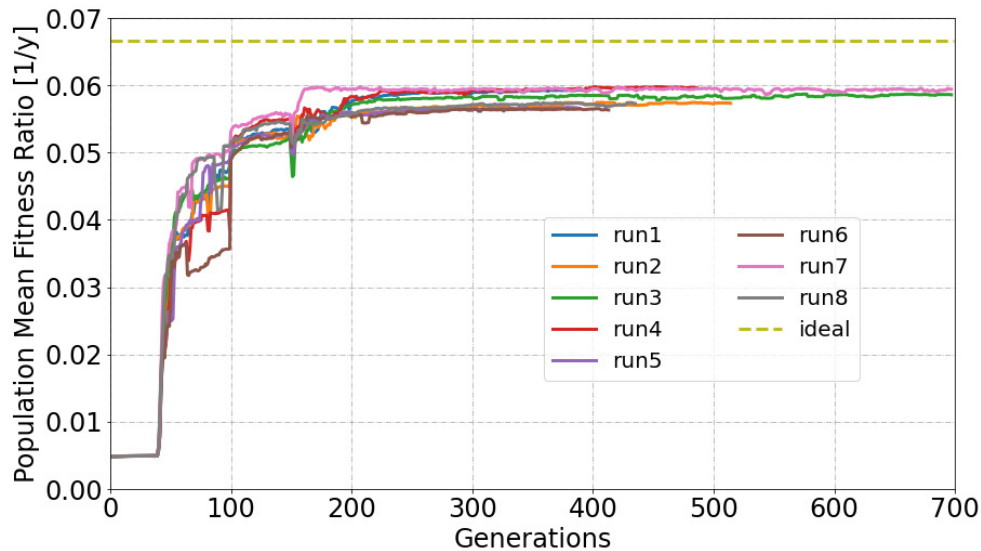


Figure 6-5: Population mean fitness ratio vs. generations for variation of crossover rate, mutation operation probabilities and improvement operation parameter

All runs stop before the maximum generation number is reached, which is due to the implemented convergence check. The criterion appears to be rather strict but kept to avoid pre-mature solutions, as the runtime is still manageable.

Based on the plots shown in Figure 6-5 the parameter variation seems to have only low effect on the solution quality. This can be confirmed quantitatively by comparing the mean fitness ratio from the final solution to the ideal fitness ratio, as done in Table 6-6. Due to the stochastic nature of the algorithm, each run is performed twice, which increases the reliability of the result. Therefore, Table 6-6 contains one column with results for set 1, a second column for set 2 (where the runs from set 1 are repeated with the identical parameters) and a third column, where both values are averaged.

Table 6-6: Results for variation of crossover rate and mutation operation probabilities

Run	r_{cross}	r_{mut}	r_{swap}	r_{merge}	$r_{shuffle}$	r_{imp_cut}	$\frac{\sigma_{mean,final}}{\sigma_{ideal}}$		
							set 1	set 2	mean
1	1	0.4	0.5	0.5	0.3	0.05	88 %	86 %	87 %
2	0.8	0.4	0.5	0.5	0.3	0.05	86 %	86 %	86 %
3	1	0.8	0.5	0.5	0.3	0.05	87 %	86 %	87 %
4	1	0.4	0.8	0.5	0.3	0.05	89 %	90 %	90 %
5	1	0.4	0.5	0.8	0.3	0.05	84 %	88 %	86 %
6	1	0.4	0.5	0.5	0.6	0.05	84 %	88 %	86 %
7	1	0.4	0.5	0.5	0.3	0.2	89 %	85 %	87 %
8	0.9	0.7	0.6	0.7	0.2	0.1	86 %	88 %	87 %

As already derived from observations from Figure 6-5, the results are fairly robust against the parameter variation. Furthermore, it can be stated that an early termination of the simulation due to the implemented convergence check does not impair the overall solution quality. Out of all runs, run 4 performs best. Consequently, the parameters from run 4 are considered to be the most suitable.

6.2.3 Variation of Population Size and Local Search Operation Intervals

In this subchapter the focus is on parameters which have not been varied yet. This includes the population size together with the probe number and the local search intervals. The constant input data and parameters are given in Table 6-7.

Table 6-7: Specification of input data and algorithm parameter corresponding to runs investigating population size and local search interval impact, 'X' indicates a parameter variation

Input Data					
Model	Testproblem	m	X		
n	9260	v	0.1 c		
s_i	1				
Algorithm Parameter					
$T_{max,g=0}$	∞	g_{max}	2000	r_{mut}	0.4
$T_{max,g=g_{cut1}}$	100,000 y	P_{max}	X	r_{swap}	0.8
$T_{max,g=g_{cut2}}$	7000 y	r_{cross}	1	r_{merge}	0.5
g_{cut1}	100 gen.	r_{imp_cut}	0.05	$r_{shuffle}$	0.3
g_{cut2}	150 gen.	r_{loc_search}	X		

Table 6-8 shows the varied parameters together with the results. Note that the ideal fitness ratio for runs with 32 probes is not realizable, as discussed in the preliminary analysis. Accordingly, the corresponding deviation values must be considered as relative values which enable a comparison between runs and not as absolute values which indicate the actual solution quality.

Table 6-8: Results for parameter variation considering probe number, population size and local search interval

Run	m	P_{max}	r_{loc_search}	$\frac{\sigma_{mean,final}}{\sigma_{ideal}}$
1	4	100	40	88 %
2	4	50	40	86 %
3	4	200	40	88 %
4	32	100	40	45 %
5	32	50	40	44 %
6	32	200	40	45 %
7	4	100	20	87 %
8	4	100	80	82 %



Regarding the population size, it can be stated that there is a negligible decline in solution quality when the population size is reduced to 50 individuals. This holds also for higher probe numbers. Run 7 and 8, which investigate the effect of more or less frequent local search operations, indicate that the reduction from 40 to 20 does not improve the overall solution quality. Conversely, doubling the interval to 80 reduces the quality significantly.

Based on the described observations, the initial configuration with a search interval of 40 generations for performing the local search operations appears to be a good choice. Similarly, the population size of 100 individuals seems to represent a fair initial value to start with when the Gaia based star model is considered.

6.3 Revised Pseudocode based on Test Problem Outcomes

Based on the findings from the test problem runs the preliminary pseudocode is revised as shown in Figure 6-6. Compared to the preliminary pseudocode, two major modifications are made: The first one concerns the time constraint implementation, the second one the convergence check.

input set of n stars with position data and star scores s_i , probe number m , travel speed v

Parameters

Initial time constraint $T_{max,g=0}$	Max. generations g_{max}	Mutation rate r_{mut}
1st cut generation number $g_{cut,1}$	Population size P_{max}	Swap rate r_{swap}
2nd cut generation number $g_{cut,2}$	Crossover rate r_{cross}	Merge rate r_{merge}
1st cut time constraint $T_{max,g=g_{cut,1}}$	Local search rate r_{loc_search}	Shuffle rate $r_{shuffle}$
2nd cut time constraint $T_{max,g=g_{cut,2}}$	Improvement cut rate r_{imp_cut}	

output Population of solutions $P(g)$

begin

```

 $g \leftarrow 0$ 
 $T_{max} \leftarrow T_{max,g=0}$ 
 $P(g) \leftarrow generate\_initial\_population(P_{max}, T_{max})$ 
while  $g < g_{max}$ :
  if  $g = g_{cut,i}$ :
     $T_{max} \leftarrow T_{max,g=g_{cut,i}}$ 
     $P(g) \leftarrow cut\_routes(P(g), T_{max})$ 
  end
   $P'(g) \leftarrow P(g)$ 
  while  $size(P'(g)) < (2 P_{max} r_{cross})$ :
     $P_{parent} \leftarrow do\_tournament(P(g))$ 
     $P_{children} \leftarrow generate\_children(P_{parent})$ 
     $P'_{children} \leftarrow mutate\_children(P_{children}, T_{max}, r_{mut}, r_{swap}, r_{merge}, r_{shuffle})$ 
     $P''_{children} \leftarrow improve\_children(P'_{children}, T_{max}, r_{imp\_cut})$ 
     $P'(g) \leftarrow (P'(g) \cup P''_{children})$ 
  end
   $P(g) \leftarrow P'(g)$ 
   $P(g+1) \leftarrow evolve\_population(P(g), P_{max})$ 
  if  $g > 1$  and  $g \% r_{local\_search} = 0$ :
     $P(g+1) \leftarrow do\_local\_search(P(g+1))$ 
  end
  if  $do\_convergence\_check(P(g+1)) = True$ :
    stop algorithm and return  $P(g+1)$ 
  end
   $g \leftarrow (g+1)$ 
end

```

end

Figure 6-6: Revised pseudocode based on test problem results (the “%” symbol in the if-condition for performing the local search refers to the modulo operator)

7 Applying the Revised Algorithm to the Gaia based Star Models

In this section, the revised algorithm as presented at the end of the previous chapter (Figure 6-6) is applied to the star models built from Gaia data. Two different models are considered: One large-size model containing 10,000 stars as defined in 4.2 and a smaller one with 1,000 stars. The smaller model is obtained from the 10,000 stars model by simply selecting the 1,000 nearest stars. For each model, several analyses are performed, as shown in Figure 7-1. Finally, the results of both models are compared. Note that in both models the stellar scoring metric is not incorporated, hence the mission return is equal to the number of explored stars.

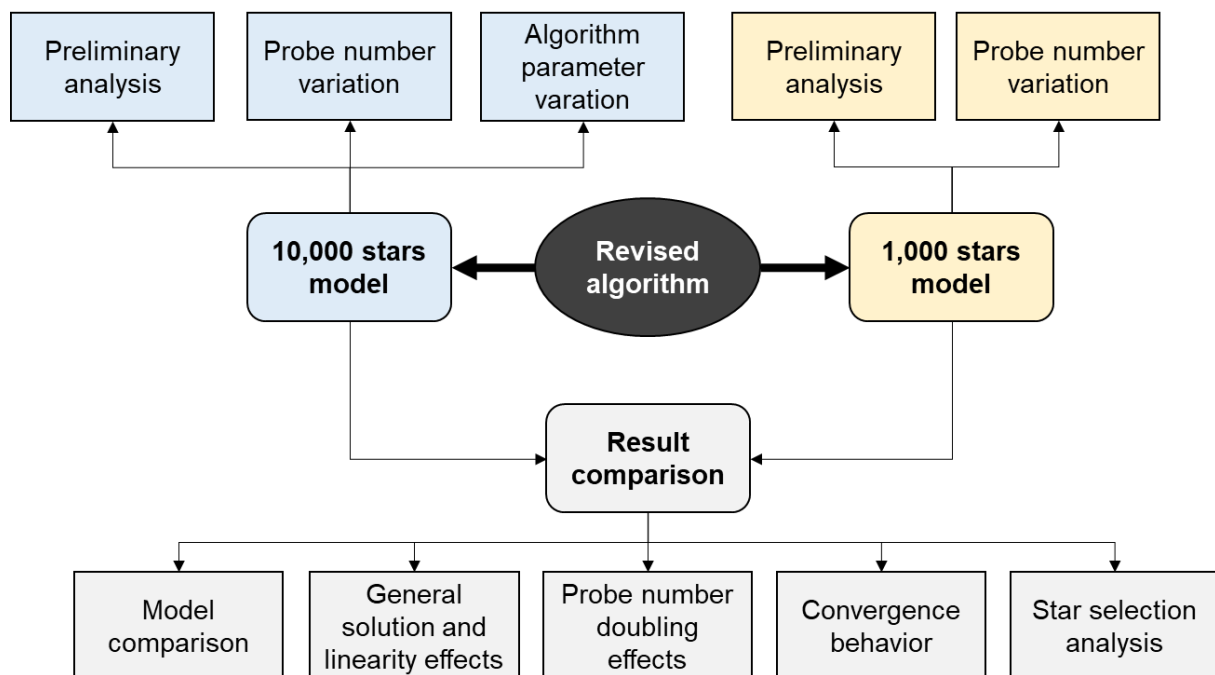


Figure 7-1: Overview and high-level structure of chapter 7

7.1 Results for 10,000 stars

The results for the 10,000 stars model are structured as follows: At the beginning the model is analyzed with respect to the spatial star distribution. Then selected parameters are varied, which comprises the probe number and algorithm parameters.

7.1.1 Preliminary Analysis of the Model - Spatial Star Distribution

The preliminary analysis focus on the spatial star distribution. Therefore, the star locations are analyzed with respect to their coordinates. Due to the spherical model domain spherical coordinates are considered, which are galactic longitude, latitude and distance. Furthermore, the transfer distance for each star to its nearest neighbor star is investigated.

7.1.1.1 Distribution of the Galactic Longitude

The distribution of the galactic longitude is analyzed by dividing the entire range of 0-360° into 72 equal-sized intervals, yielding an interval size of 5°. Depending on their longitude, stars are assigned to a certain interval and counted. The resulting histogram is shown in Figure 7-2.

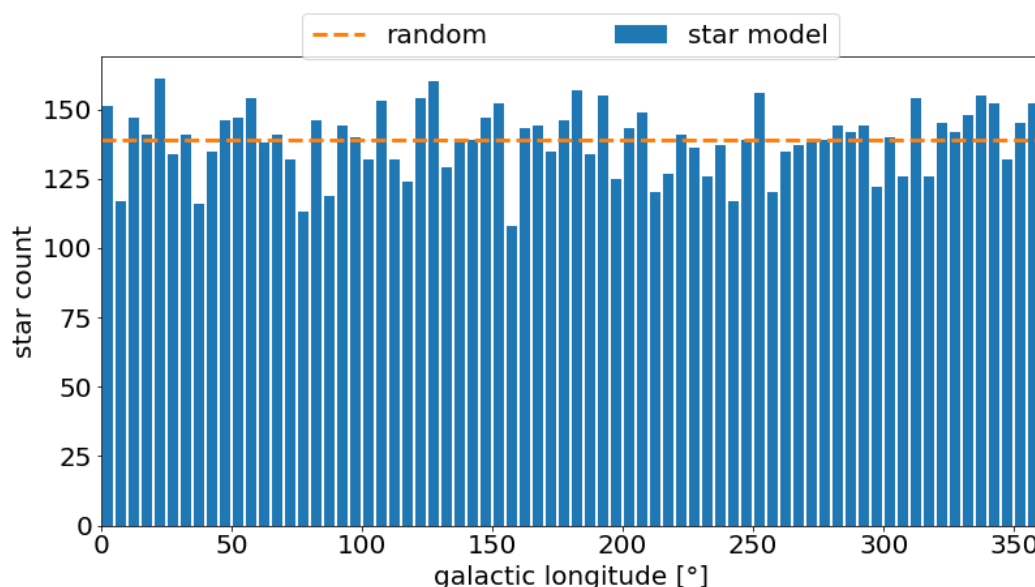


Figure 7-2: Distribution of galactic longitude, each beam refers to an interval with a size of 10°

From the histogram in Figure 7-2 it can be derived that the galactic longitude follows approximately a uniform distribution.

7.1.1.2 Distribution of the Galactic Latitude

The analysis of the galactic latitude distribution follows the same approach as the longitude. From the range of -90° to 90° now 90 equal-sized intervals are built, yielding an interval size of 2°. Note that conversely to the longitude, the spherical characteristics of the system must be involved in the distribution analysis of the latitude. Hence, the star count of a uniform distribution is not constant for all latitude values (as it was for the longitude) but decreases towards the poles. In [196], an approach to model a random distribution of the latitude is presented, which is adopted here. The resulting curve together with the star model data is shown in Figure 7-3.

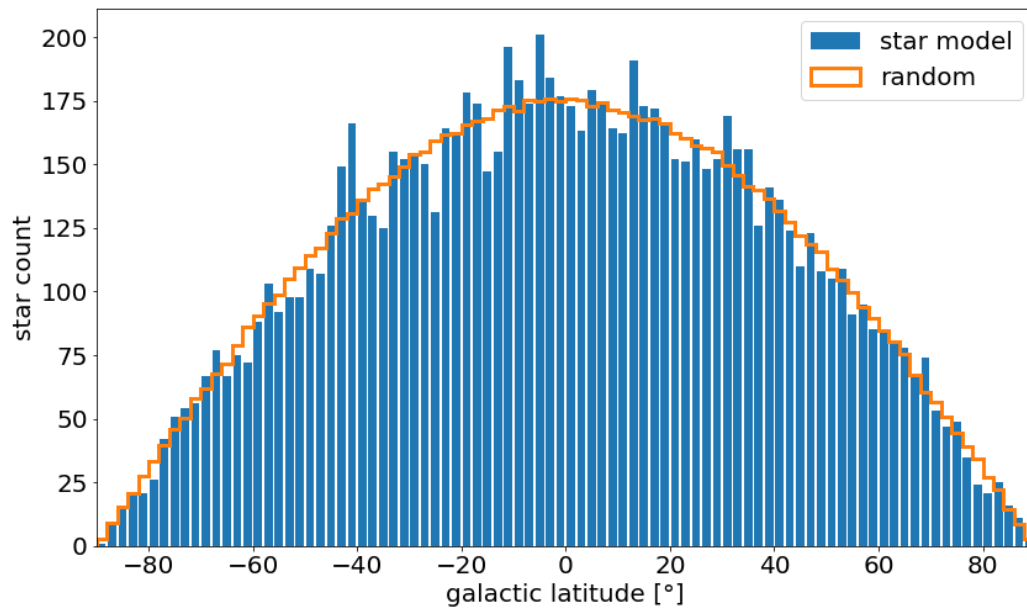


Figure 7-3: Comparison of galactic latitude coordinate and random uniform distribution

Based on Figure 7-3, an approximately uniform distribution of the latitude can be assumed.

7.1.1.3 Distribution of the Estimated Distance Values

To analyze the distribution of the distances to Sol a cumulative histogram is used. Hence, each bin indicates the number of stars with smaller or same distance for a considered distance value. Accordingly, the final bin at 110 ly, which is the maximum distance in the model, includes all 10,000 stars. In Figure 7-4, the resulting histogram is given together with the theoretical curve derived from a random uniform distribution. Note that due to the cubic increase of a spheric volume with radius ($V \sim r^3$) the random distribution curve has a cubic course.

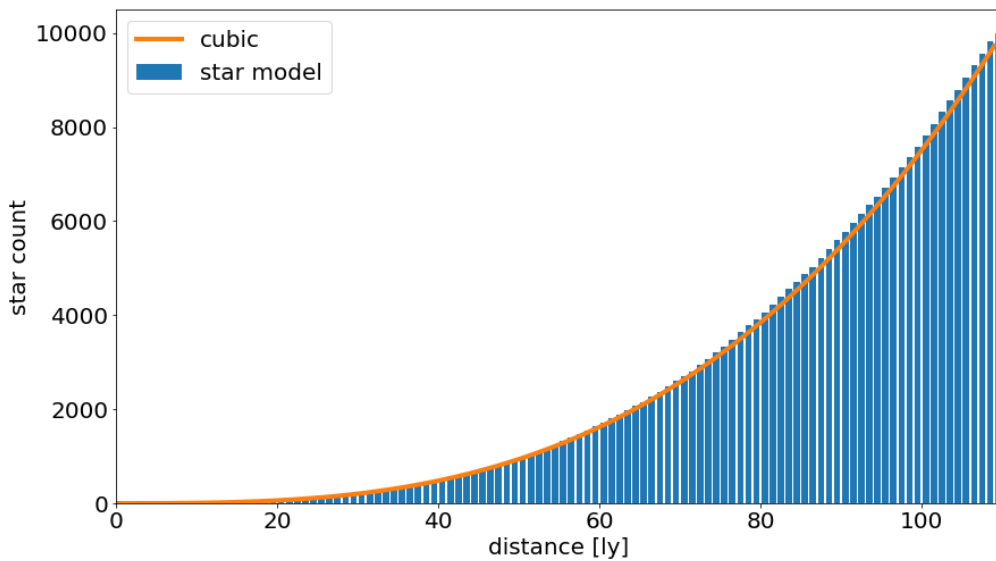


Figure 7-4: Cumulative histogram for distance values; random distribution represented by cubic curve

As indicated by the plot, the distances to Sol can be assumed to follow a uniform distribution.

7.1.1.4 Distribution of the Minimum Transfer Distances between Stars

As final distribution analysis the minimum distances between the stars are considered. The analysis is done by means of the distance matrix, which represents a look-up table where each possible transfer $d_{i,j}$ between two stars i and j is calculated. Note that due to the symmetry assumption $d_{i,j}$ equals $d_{j,i}$, hence the distance matrix is symmetrical.

Table 7-1: Structure of the distance matrix

	1	2	j	...	N
1	-	$d_{1,2}$	$d_{1,j}$...	$d_{1,N}$
2	$d_{2,1}$	-	$d_{1,j}$...	$d_{2,N}$
i	$d_{i,1}$	$d_{i,2}$	-	...	$d_{i,N}$
...	-	...
N	$d_{N,1}$	$d_{N,2}$	$d_{N,j}$...	-

From each row in the distance matrix, the minimum value is extracted and stored separately, yielding a new array which contains for each star the transfer distance to its nearest neighbor star. This new array is used to create a histogram which is plotted in Figure 7-5. The interval size is 0.25 ly, e. g. the second bar represents the number of stars that have a transfer distance between 0.25-0.5 ly to it nearest neighbor.

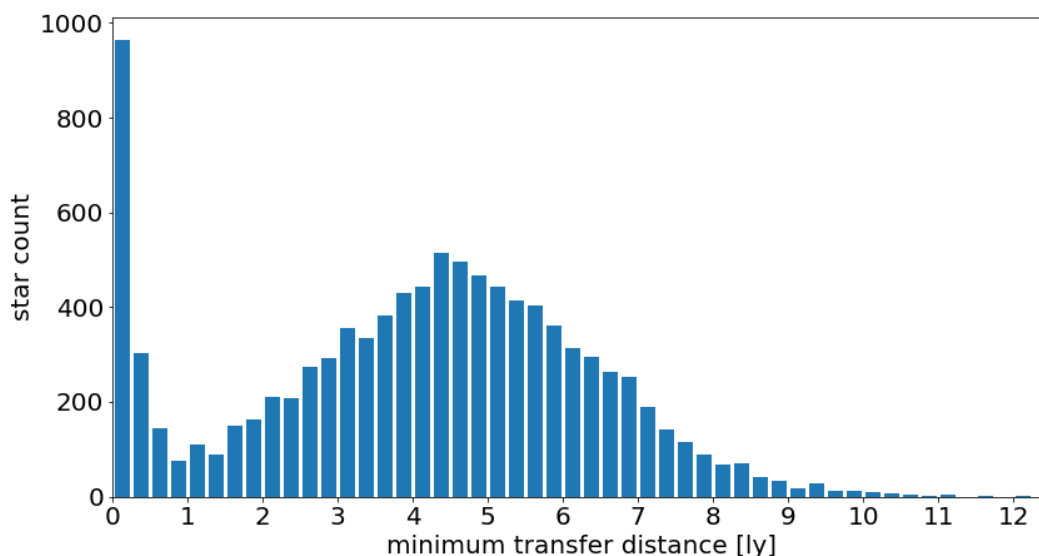


Figure 7-5: Distribution of the minimum transfer distance between two stars; interval size of 0.25 ly

The minimum transfer distances range from 0 to 12 ly. The distribution appears to resemble a Poisson distribution, apart from a large number of very short transfers smaller than 0.75 ly. This phenomenon is expected to be caused by the presence of binary or multiple star systems, as in the Gaia release each star source is treated as single star [192]. Hence, from Figure 7-5 it can be stated that more than 10 % of the stars in the model are part of a binary or multiple star system. In fact, multiple star systems are even more prevalent: 40 - 60 % of the stars in the Milky Way are estimated to form multiple systems [3, p. 109]. The deviation between model and estimations are assumed to result from the limited resolution of the Gaia observations and due to the filtering procedure: As very close binary systems may produce spurious results, those stars are eliminated during the filtering (for more details on binaries and multiple star systems in the Gaia release it is referred to [192]).

Based on a qualitative analysis of the coordinates, stars appear to follow a uniform spatial distribution but are not equally spaced due to the presence of multiple star systems.

7.1.2 Variation of Probe Number for Given Algorithm Configuration

Table 7-2 lists the parameters that are kept constant along this set of runs. As indicated, solely the probe number is varied.

Table 7-2: Specification of input data and algorithm parameter, 'X' indicates a parameter variation

Input Data					
Model	Gaia Star Model	m		X	
n	10,000	v		0.1 c	
s_i	1				
Algorithm Parameter					
$T_{max,g=0}$	∞	g_{max}	1500	r_{mut}	0.4
$T_{max,g=g_{cut1}}$	100,000 y	P_{max}	200	r_{swap}	0.8
$T_{max,g=g_{cut2}}$	7000 y	r_{cross}	1	r_{merge}	0.5
g_{cut1}	100 gen.	r_{imp_cut}	0.05	$r_{shuffle}$	0.3
g_{cut2}	150 gen.	r_{loc_search}	40		

The parameters are adopted from the test problem results, with some minor changes: The population size is increased to 200 compared to the suggestions from chapter 6 to obtain a higher density of solutions along the front, particularly regarding the cases with high probe number. The maximum generation number is set to 1500 to reduce the maximum runtime of one optimization run.

A set of 9 runs with different probe numbers is considered. Starting with 2 probes, the probe number is doubled for each run, which yields a probe number of 512 for run 9.

7.1.2.1 General Solution Overview

In Figure 7-6, the final populations from each run are evaluated with respect to the objectives. Due to the algorithm behavior, the curves define the estimated Pareto front for the given problem. Each dot represents one individual from the final population.

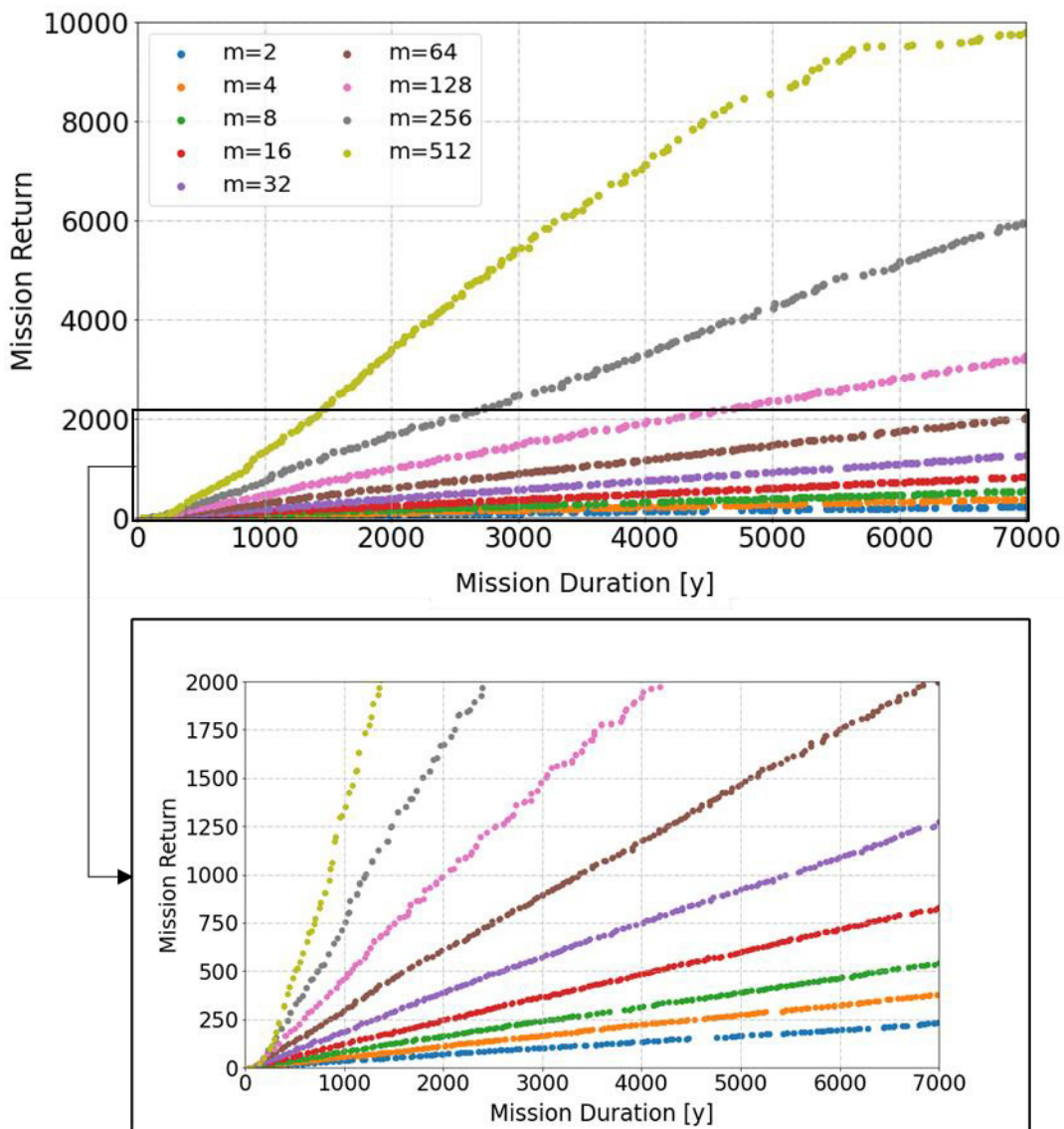


Figure 7-6: Final solutions for different probe numbers, the lower chart shows a zoomed section from the complete upper plot

From Figure 7-6, several observations can be made: As expected, the mission return for a given mission duration increases with probe number. Furthermore, there appears to be a linear relation between both objectives for a given probe number.

For a given probe number, in most instances a linear relation between mission duration and number of explored stars is observed.

Driven by the crowding distance criterion, individuals are distributed uniformly along each curve. The presence of small gaps (e. g. for run 1 ($m = 2$) near 4600 years) is due to the probabilistic nature of the algorithm together with the convergence criterion and the limited population size. This can be easily shown by repeating the run with the same parameters, where former gaps are filled. A closer comparison between the curves (zoomed section in Figure 7-6) reveals that with increasing probe number there

is a slightly higher fluctuation along the curve while for small probe numbers the curves are smooth. This may indicate poor convergence and requires further analysis based on the mean fitness ratio.

7.1.2.2 Linearity and Impact on Routes and Star Selection

In general, for a given probe number the mission return increases linearly with mission duration, apart from two exceptions: The first one is the flattening of the curve of run 9 (considering 512 probes) towards higher mission duration, say 5000 years upwards. This phenomenon is assumed to result from the restriction of the model to 10,000 stars, which may cause a saturation effect: Considering solutions with high probe number and mission duration (upper right region in the plot), only few stars are remaining, that have not been explored yet. Unlike in the beginning, where the probes could select suitable targets from a large pool of unexplored stars, they are now forced to add stars with less favorable transfer trajectories to their route. Hence, when approaching the maximum star number of the model an increase of mission return is more expensive in terms of mission time. The presumption, that this effect is induced by the model and not due to real star constellations, needs further verification in following subchapters.

The second exception to the linear behavior concerns again the high probe number runs but now related with very short-term missions. This solution region in the lower left corner in the plot from Figure 7-6 is shown again in Figure 7-7 with higher resolution and for selected runs to ensure clarity.

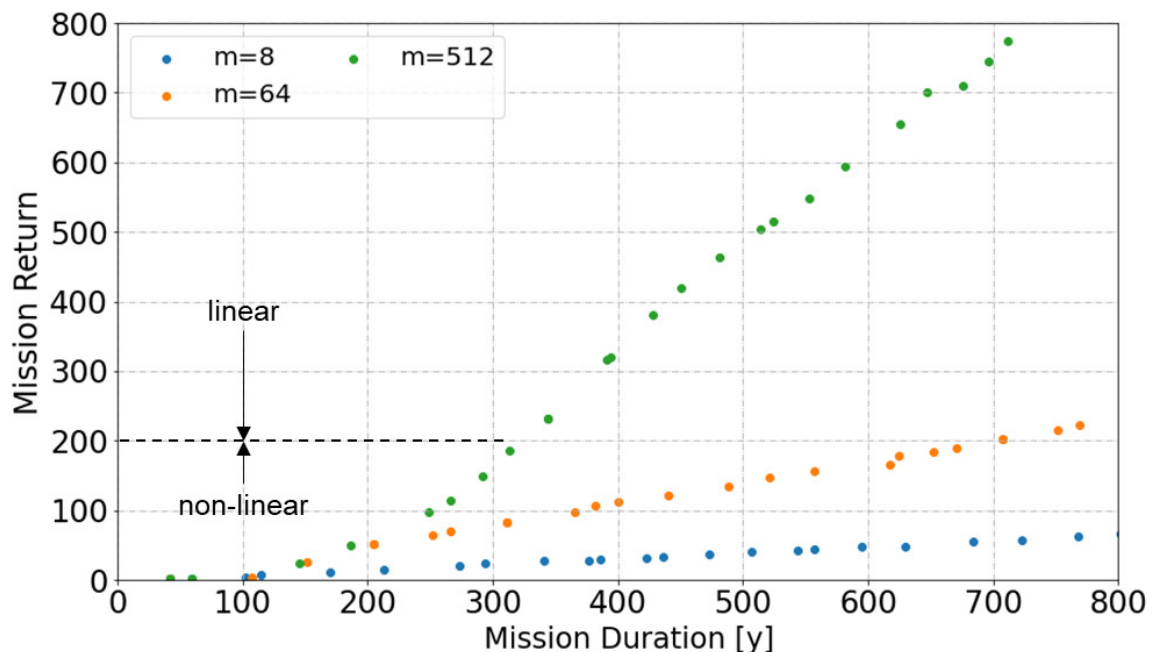


Figure 7-7: Mission return vs. mission duration for selected runs considering short-term missions

Considering the high probe number run ($m=512$) in Figure 7-7, the linear course of the curve sets in roughly from a mission return of 200 upwards. Below that limit, the curve approaches the curves with lower probe numbers, which can be explained as follows: In this short-term mission regions not all probes of the available set are deployed. Therefore, the obtained solutions for high probe number runs are similar to the results

from runs with lower probe number, as effectively the same probe number is used. This effect amplifies with further reduction of the mission return. Another observation is, that due to the high probe number the short-term missions typically consist of one-target missions. This is illustrated in Figure 7-8, where two example solutions from different runs are compared with respect to the suggested routes.

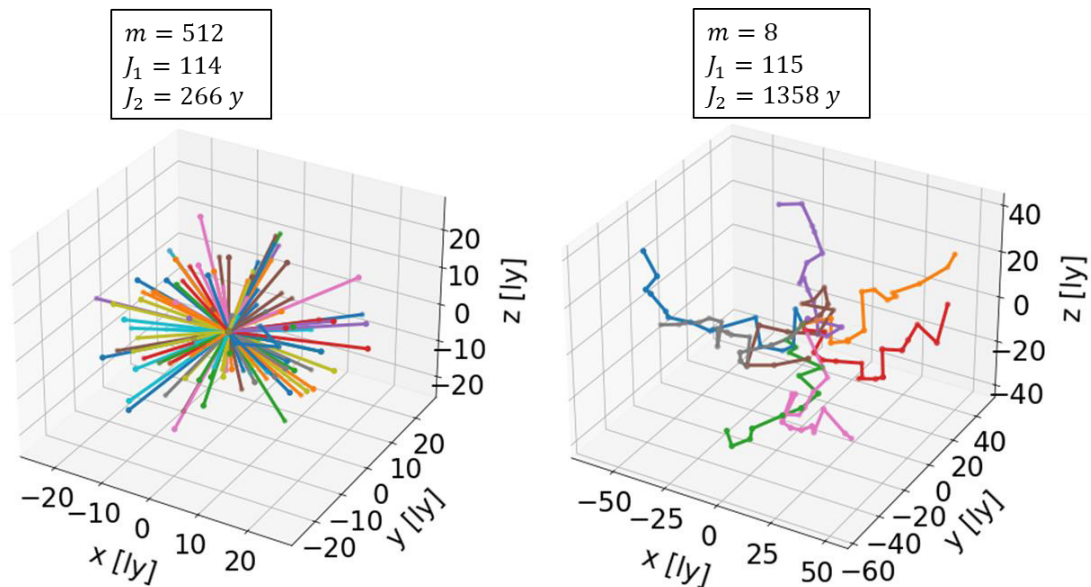


Figure 7-8: Visualization of selected solutions with similar mission return, each color refers to one route, each node indicates an explored star - left: run for 512 probes, right: run for 8 probes

As visualized, though yielding almost the same mission return both solutions reveal a very different mission structure: In the left plot, the probes are sent omnidirectionally trying to find the nearest star from sol. Note that due to the selected mission return value not all 512 probes are deployed. With each probe being launched, the distance to the nearest star which is still unexplored increases. Still, the selected stars are within a distance range of up to 20 light years to Sol. In the right plot, contrarily, also more distant stars are included. Due to the lower probe number, routes with suitable star sequences need to be build. Hence, the distance from sol becomes less relevant with increasing route length and more distant stars are selected when they allow a favorable transfer from the current departure star.

High probe number missions focus on the immediate solar neighborhood, whereas low probe number missions include more distant stars.

The question, how many stars are considered at minimum to deploy all available probes is addressed in Figure 7-9. It shows the ratio between the minimum number of stars, where all available probes are deployed, and the probe number. For instance, a ratio of 1.5 for a probe number of 128 indicates, that only if more than 192 stars are considered, each of the 128 probes is assigned to at least one star. For lower star numbers, empty routes are created, hence some probes will remain unused (as for the 512 probes case in Figure 7-8).

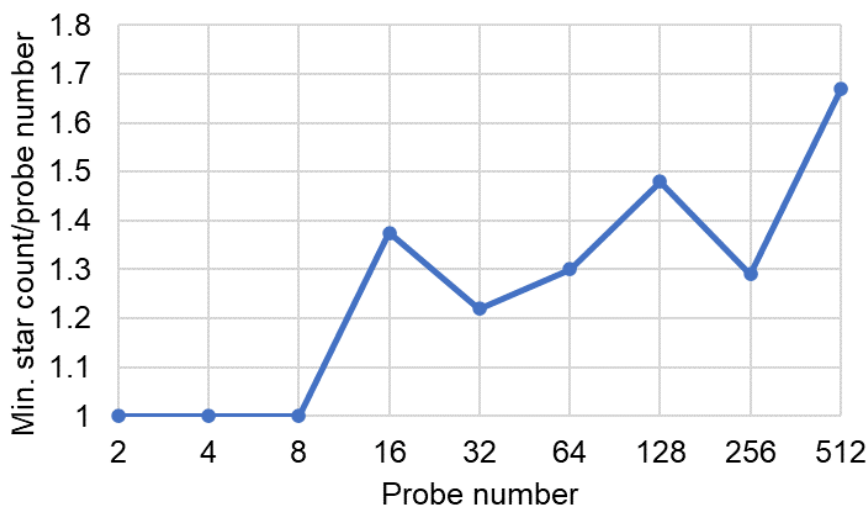


Figure 7-9: Ratio of minimum number of stars required to deploy all available probes and probe number

From Figure 7-9 a general trend towards higher ratios with increasing probe number is observed: For low probe numbers the minimum star number is equal to the probe number, which corresponds to single-target travels. Regarding higher probe numbers, contrarily, the ratio increases. Hence, single-target travels appear to be less attractive or at least equivalent compared to multi-target travels, which represent routes that contain more than one star. Considering the maximum probe number of 512 as an example, more than 850 stars need to be included into the mission to deploy all 512 probes.

This is an interesting observation as single-target missions are expected to represent the fastest exploration approach. The reason behind this behavior has already been delivered in the previous discussion on the route structure (see again Figure 7-8): Assuming single-target missions, the entire mission duration for a given number of explored stars is determined by the longest transfer distance. With increasing probe number, the transfer distance increases, as there are less unexplored stars in the immediate solar neighborhood. Hence, after a certain threshold of probes it is possible to assign several stars to one probe without increasing the overall mission duration. The resulting solution is then equivalent to single-target missions with respect to the considered objectives.

This is visualized by means of an example sketch in Figure 7-10, where two different hypothetical missions A and B are considered. Each color refers to one probe, blue dots represent explored stars.

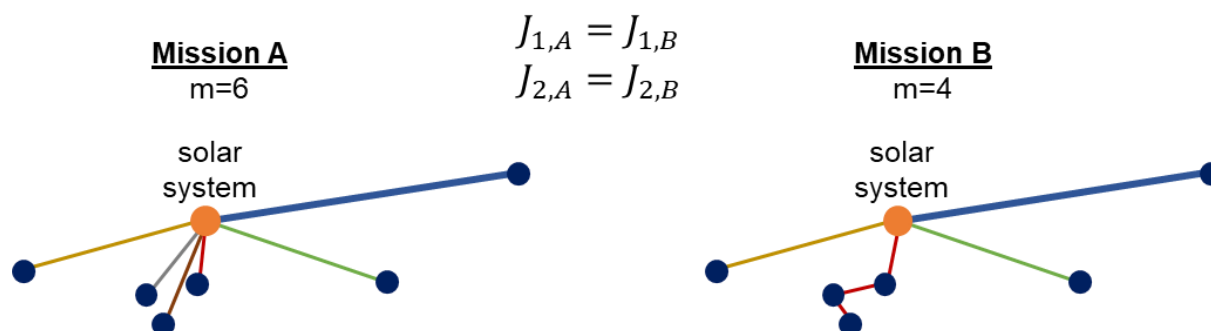


Figure 7-10: Comparison of two example missions with different probe number but equivalent mission return and duration

Mission A consists of single-target travels with 6 probes, where the longest travel determines the entire mission duration (indicated by blue, thick line). In mission B, three of the single-target travels are merged into one route (red), which allows a reduction of the probe number to 4 without affecting the mission return. Due to the small transfer distances along the red route, the overall mission duration is still determined by the blue route. Therefore, both missions are equivalent with respect to the objectives.

As there is no additional criterion (such as average transfer length or minimum probe number) to distinguish further between both missions, they appear as duplicates in the solution space. Hence, if necessary, the algorithm will select randomly between both missions without assessing any further characteristics of the mission. This is important to consider when interpreting the observations from Figure 7-9: Given the random selection in case of duplicates, the ratios are not representing the actual thresholds. Instead, they represent only a lower bound; the actual thresholds are expected to be higher.

7.1.2.3 Doubling Factor Effect

The effect of doubling the probe number with respect to the mission return for a given mission duration is analyzed in Figure 7-11. The figure has to be read counterclockwise starting with the plot in the upper right, which is already known from section 7.1.2.1. From this plot, selected solutions with mission durations of 2000 years and 4000 years are extracted and transferred into a new plot (upper left), as implied by the arrows. This new plot visualizes the impact of probe number doubling on the mission return for the considered mission durations. In the final subplot (below), the factorial increase of mission return after doubling is shown, again differentiated for both selected mission durations.

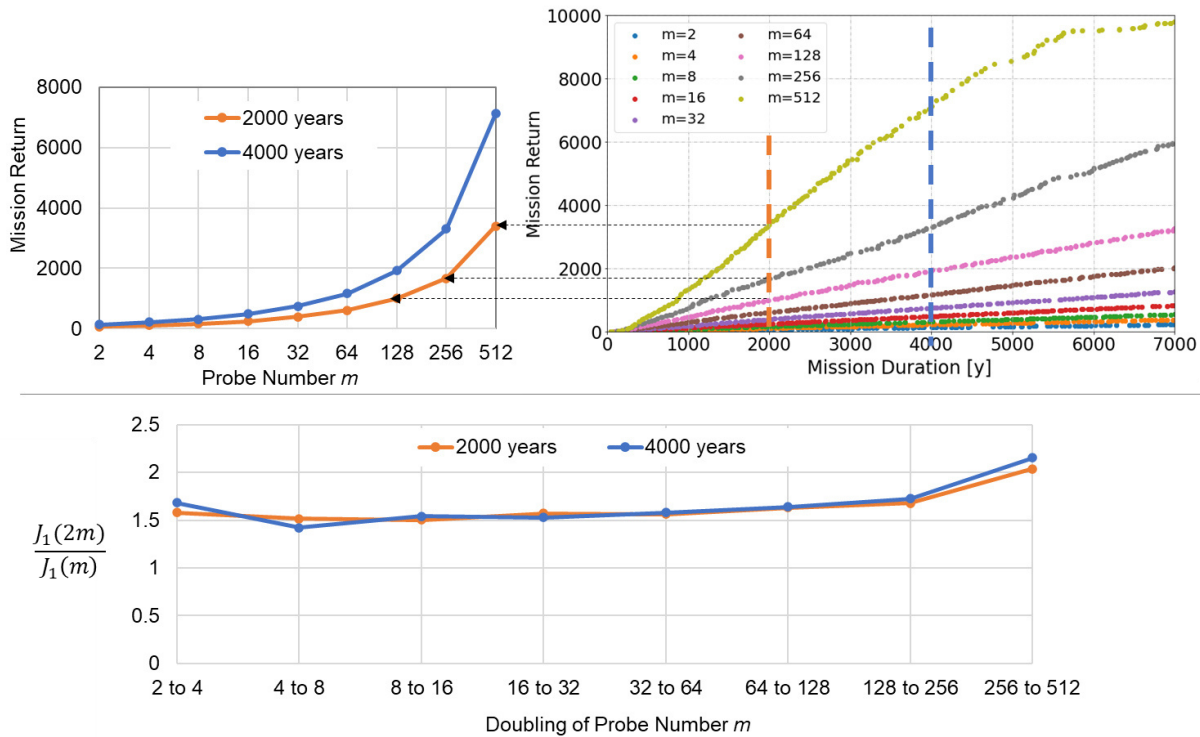


Figure 7-11: Effect of probe number doubling on the mission return – upper right plot: Mission return vs. mission duration for different probe numbers; upper left plot: extraction of selected solutions at 2000 and 4000 years mission duration; lower plot: increase in mission return after doubling the probe number

As shown in Figure 7-11, the doubling factor $\frac{J_1(2m)}{J_1(m)}$ can be assumed as nearly constant apart from the last run with 512 probes. There, the doubling factor is significantly higher for both considered curves (> 2). This unexpected behavior requires further investigation and will be discussed later.

Excluding the last run and averaging the doubling factor over the runs yields a value of 1.58. Hence, considering the lower probe runs, the relation between mission return and probe number for a given mission duration can be approximated as following:

$$J_1 (J_2 = const) \sim m^{0.66} \tag{Eq. (7-1)}$$

Note that this correlation does not hold in the non-linear case and is less accurate for high probe numbers.

By following, a further analysis of the derived relation is conducted. Differentiating Eq. (7-1) with respect to the probe number yields the first derivative:

$$\frac{d}{dm} J_1 \sim \frac{d}{dm} m^{0.66} = 0.66 m^{-0.34} \tag{Eq. (7-2)}$$

The second derivative, again with respect to the probe number, is:

$$\frac{d^2}{dm^2} J_1 \sim \frac{d^2}{dm^2} m^{0.66} = -0.22 m^{-1.34} \tag{Eq. (7-3)}$$

Due to the negative exponent both derivatives are approaching 0 for large probe numbers. Furthermore, as the second derivative is negative for all probe numbers, the

first derivative is strictly decreasing with increasing probe number. These observations appear to be similar to the law of diminishing returns, which is a concept in economics in the production context: Roughly speaking, diminishing returns denote the effect when an increase of the input yields progressively lower or even reduced increase in output [197]. In the considered case, the input is defined by the probe number (as mission duration is assumed to be constant in Eq. (7-1)) while the output is represented by the mission return.

In Figure 7-12 the first derivative (Eq. (7-2)) is plotted considering a maximum probe number of 250.

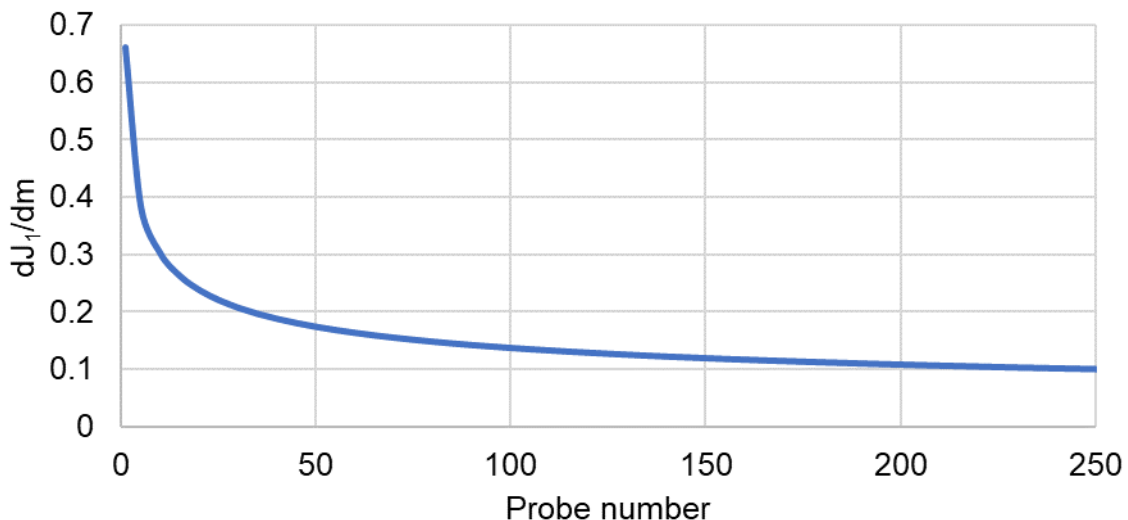


Figure 7-12: Plot of the first derivative of the scaling law with respect to probe number (Eq. (7-2))

The plot in Figure 7-12 shows a strong decline of the first derivative when low probe numbers (say up to 10 probes) are considered. Afterwards, the curve is further decreasing but with a lower rate, as the second derivative is strictly negative and approaches zero for high probe numbers. Based on these observations it can be stated, that in the very beginning each additional probe allows for a substantial increase of the mission return. However, this effect holds only for a small range of probe numbers and becomes less significant with each additional probe. Considering higher probe numbers, the curve flattens at a low level, indicating that the impact of additional probe numbers on the mission return is low, regardless of the probe number.

This behavior can be explained by a crowding-like effect, which has already been observed during earlier analyses (see again the previous chapter 7.1.2.2, particularly Figure 7-8): When many probes are launched from the solar system, long initial transfers are required to assign each probe an unexplored star. Regarding low probe numbers, contrarily, there are still enough nearby stars left which have not been explored yet and thus can be assigned to new probes. Moreover, in case of very long initial transfers of one probe, it is possible to merge shorter routes of other probes, which further reduces the benefits of high probe numbers (see again Figure 7-9).

An increase of the probe number correlates with a substantial higher mission return only for low probe numbers.

7.1.2.4 Convergence Behavior

The convergence behavior is analyzed by means of the mean fitness ratio over the generations (see Figure 7-13).

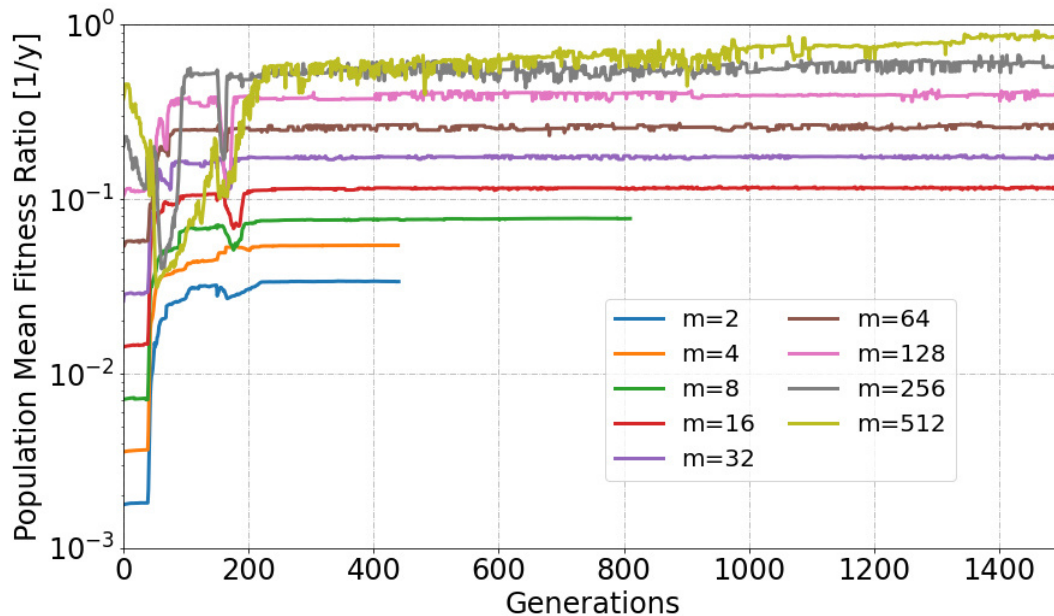


Figure 7-13: Population mean fitness ratio vs. generations for runs with varied probe number, note the logarithmic y-axis scale

From Figure 7-13 earlier observations on the convergence behaviour are confirmed: For the low probe number runs the solution stabilizes and satisfies the given convergence criterion. Contrarily, with increasing probe number the solution behaves less stable and appears to be more noisy over time. This is assumed to be an effect of the non-linearity of the fitness curve, which becomes more significant with increasing probe number (see again Figure 7-7): As the population mean fitness ratio is by definition an averaged value which represents the derivation of the solution curve, it is only constant for strictly linear curves. Since this condition is not given for higher probe numbers, the mean fitness ratio varies depending on the distribution of solutions along the Pareto curve. The distribution is intended to be balanced by means of the crowding distance criterion, however, small fluctuations may still occur. Hence, the implemented convergence criterion with the current settings works only for small probe numbers where linearity is provided, for higher probe an adaption e. g. of the moving average settings might be required.

Leaving the fluctuations aside, it can be further observed, that run 9 with 512 probes is still improving its population mean fitness ratio. Hence, the resulting fitness curve for run 9 in Figure 7-6 can be assumed to be not optimal and bears potential for further improvements. This aspect is addressed in the following subchapter, where algorithm parameters are varied for a given probe number.

7.1.3 Variation of Algorithm Parameter for Given Probe Number

7.1.3.1 Runs with 4 Probes

Table 7-3 provides the input data and algorithm parameters which are fixed during this set of runs.

Table 7-3: Specification of input data and constant algorithm parameter, 'X' indicates a parameter variation

Input Data					
Model	Gaia Star Model	m	4		
n	10,000	v	0.1 c		
s_i	1				
Algorithm Parameter					
$T_{max,g=0}$	∞	g_{max}	X	r_{mut}	0.4
$T_{max,g=g_{cut1}}$	100,000 y	P_{max}	X	r_{swap}	0.8
$T_{max,g=g_{cut2}}$	7000 y	r_{cross}	1	r_{merge}	X
g_{cut1}	100 gen.	r_{imp_cut}	X	$r_{shuffle}$	0.3
g_{cut2}	150 gen.	r_{loc_search}	40		

The parameters are varied as indicated in Table 7-4. From run 1 to 3 the population size is increased. Between run 4 to 6 the population size is kept constant while the mutation and improvement rates are varied. For run 7 the parameters from run 6 are adopted with changing the maximum generation number to 3000.

Note that for run 7 the convergence check was suspended to ensure the number of 3000 generations.

Table 7-4: Variation of parameter for given probe number of 4

Run	P_{max}	r_{merge}	r_{imp_cut}	g_{max}
1	200	0.5	0.05	1500
2	300	0.5	0.05	1500
3	400	0.5	0.05	1500
4	300	0.8	0.05	1500
5	300	0.5	0.01	1500
6	300	0.8	0.01	1500
7	300	0.8	0.01	3000

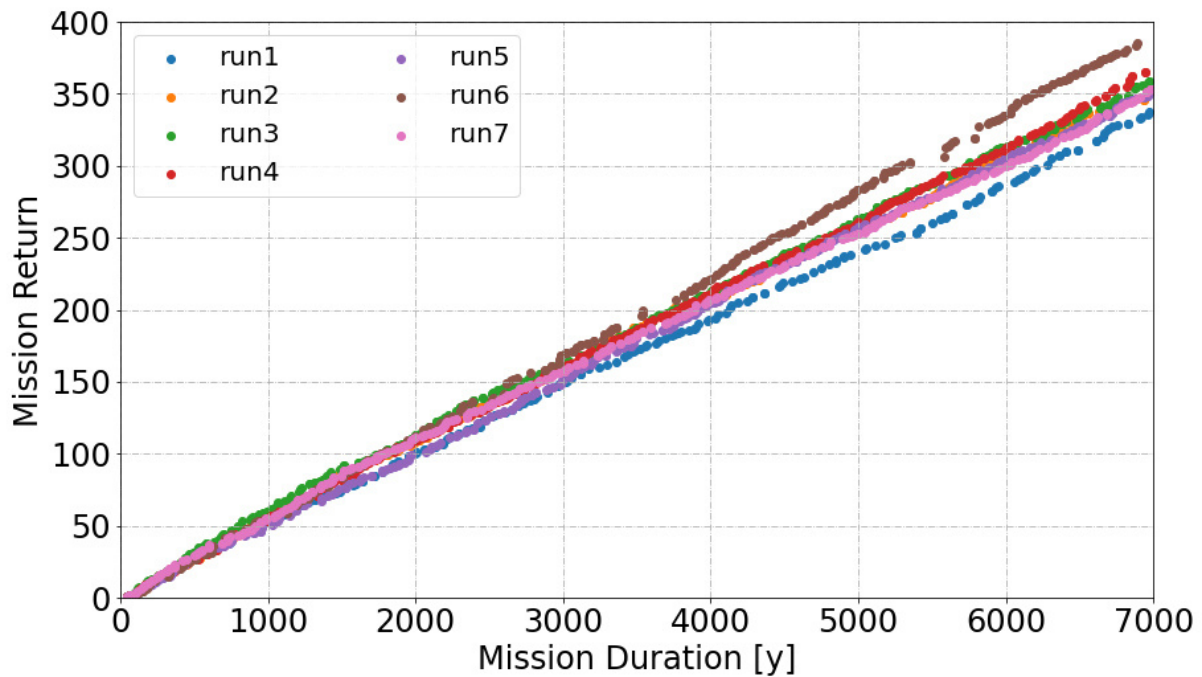


Figure 7-14: Results for algorithm parameter variation for a given probe number of 4

As shown in Figure 7-14, the modification of algorithm parameters can lead to slightly different fitness curves. In general, the best solution is obtained for run 6, the worst for run 1. Comparing both runs, the maximum deviation of mission return for a given mission duration is about 20 %. As it is difficult to distinguish between the runs in Figure 7-14, the further analysis is conducted by means of the mean population fitness ratio over time (see Figure 7-15).

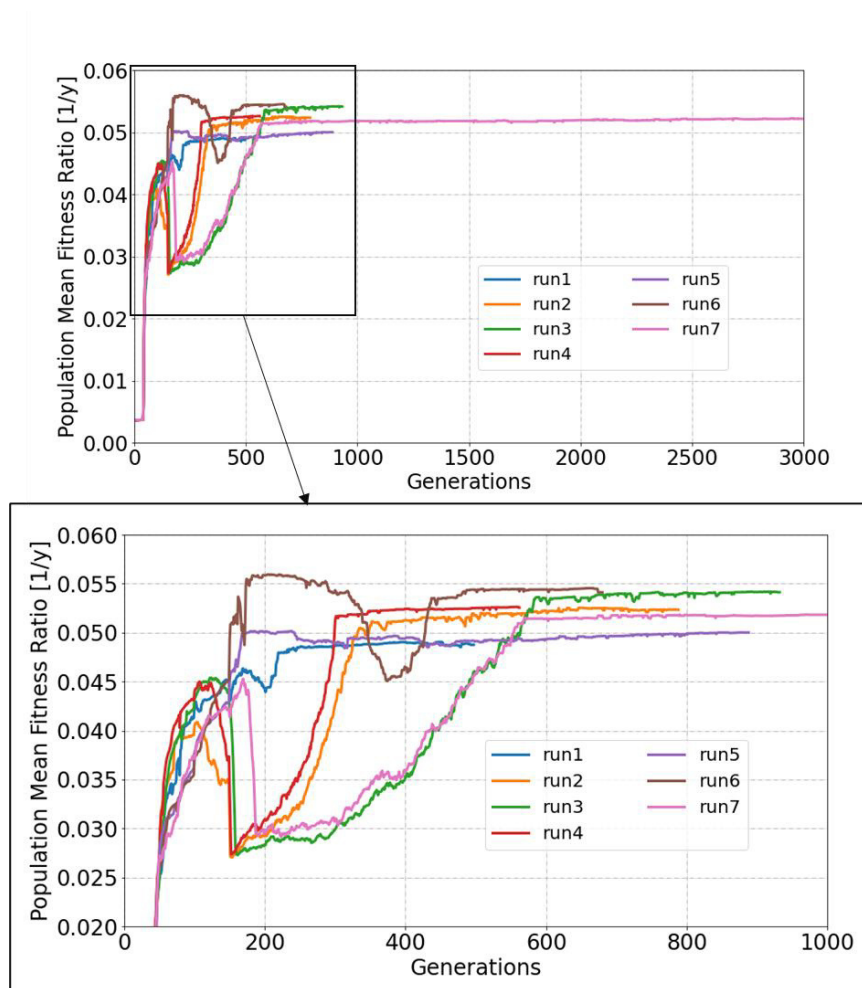


Figure 7-15: Population mean fitness ratio over generations for runs with constant probe number of 4

For all runs, the final mean fitness ratio is ranging in an interval from 0.049 y^{-1} to 0.054 y^{-1} . The deviation between the runs is below 10 % when comparing run 2 to 7 and only slightly higher considering run 1. From comparing the first three runs it can be stated that the final solution quality is increased by enlarging the population size. However, increasing the population size requires more generations to converge. Regarding the variation of the mutation and improvement parameter, run 6 yields the best result, as already observed from Figure 7-14. Interestingly, by repeating run 6 with increased generation number and disabled convergence check, a slightly worse solution is obtained. This indicates the entrapment in a local optimum.

7.1.3.2 Runs with 512 Probes

Table 7-5 specifies the input data and algorithm parameter which are kept constant along this set of runs.



Table 7-5: Specification of input data and constant algorithm parameter, 'X' indicates a parameter variation

Input Data					
Model	Gaia Star Model		m	512	
n	10,000		v	0.1 c	
s_i	1				
Algorithm Parameter					
$T_{max,g=0}$	∞	g_{max}	X	r_{mut}	0.4
$T_{max,g=g_{cut1}}$	100,000 y	P_{max}	X	r_{swap}	0.8
$T_{max,g=g_{cut2}}$	7000 y	r_{cross}	1	r_{merge}	X
g_{cut1}	100 gen.	r_{imp_cut}	X	$r_{shuffle}$	0.3
g_{cut2}	150 gen.	r_{loc_search}	40		

The undefined algorithm parameters from Table 7-5 are varied according to Table 7-6. From run 1 to 3 the population size is increased. Between run 4 to 6 the population size is kept constant while the mutation and improvement rates are varied, in addition the maximum generation number is doubled. For run 7 the parameters from run 6 are adopted with changing the generation number to 5000.

Table 7-6: Variation of parameter for given probe number of 512

Run	P_{max}	r_{merge}	r_{imp_cut}	g_{max}
1	200	0.5	0.05	1500
2	300	0.5	0.05	1500
3	400	0.5	0.05	1500
4	300	0.5	0.05	3000
5	300	0.8	0.05	3000
6	300	0.8	0.01	3000
7	300	0.8	0.01	5000

The result of each run is plotted in Figure 7-16.

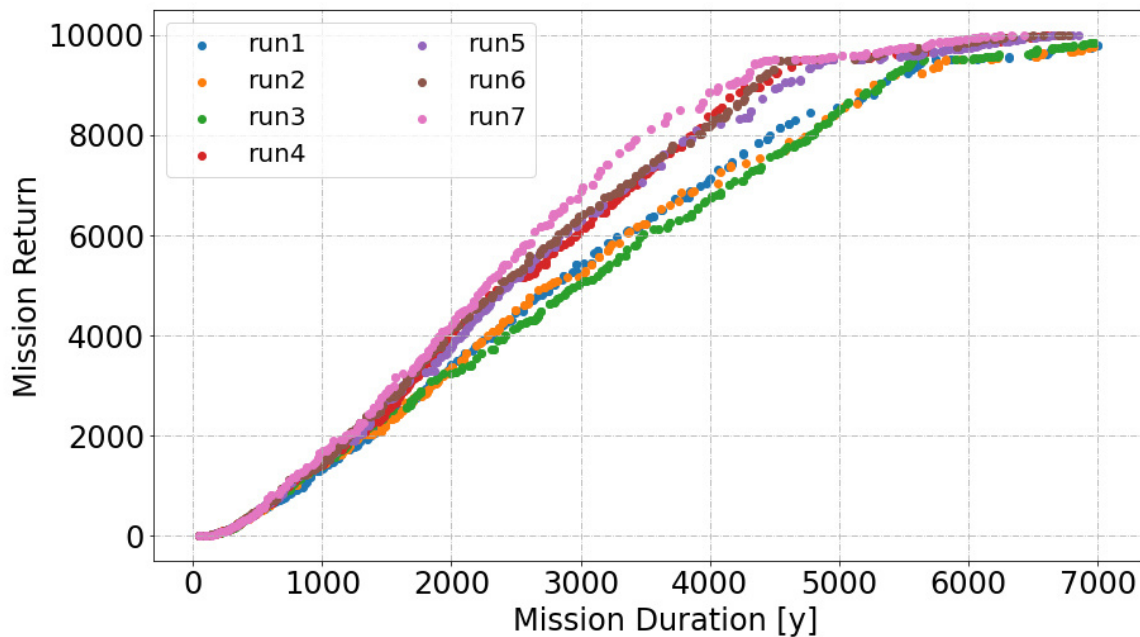


Figure 7-16: Results for algorithm parameter variation for a given probe number of 512

As shown in Figure 7-16, in a certain range the solution can be improved by more than 30 % by increasing the generation limit. This observation confirms the presence of a premature, non-converged solution in Figure 7-6, which was already presumed based on the behavior of the mean fitness ratio (see section 7.1.2.4). The effect of the variation of mutation and improvement parameters (run 4 to 6) is negligible.

The population size, which is increased from run 1 to 3 turns out to have no significant effect on the solution. This possibly can be explained by the limited generation number: As already observed in section 7.1.3.1 for 4 probes, increasing the population size requires more generations to yield better solutions.

Due to the improved solution the non-linear effects are more evident now. As explained earlier, in those cases the population mean fitness ratio must be interpreted with caution and is therefore not analyzed here.

7.2 Results for 1,000 Stars

The results for the 1,000 stars model are structured similar to the large-sized case: Firstly, the model is analyzed with respect to the spatial star distribution. Then the parameter variation is performed, which focus on the probe number.

7.2.1 Preliminary Analysis of the Model - Spatial Star Distribution

By following, the spatial star distribution in the 1,000 stars model is analyzed. Since the procedure is equivalent to 7.1.1, the results are summarized in Figure 7-17 without further explanations on the underlying approach.

The upper left plot contains the histogram indicating the distribution of the galactic longitude (5° interval size), the same is shown in the lower left plot regarding the galactic latitude (2° interval size). The upper right plot provides a cumulative histogram considering the estimated distance from Sol (1 ly steps). Finally, in the lower right plot the distribution of the transfer distances from the stars to their nearest neighbors are analyzed by means of another histogram (0.25 ly interval size).

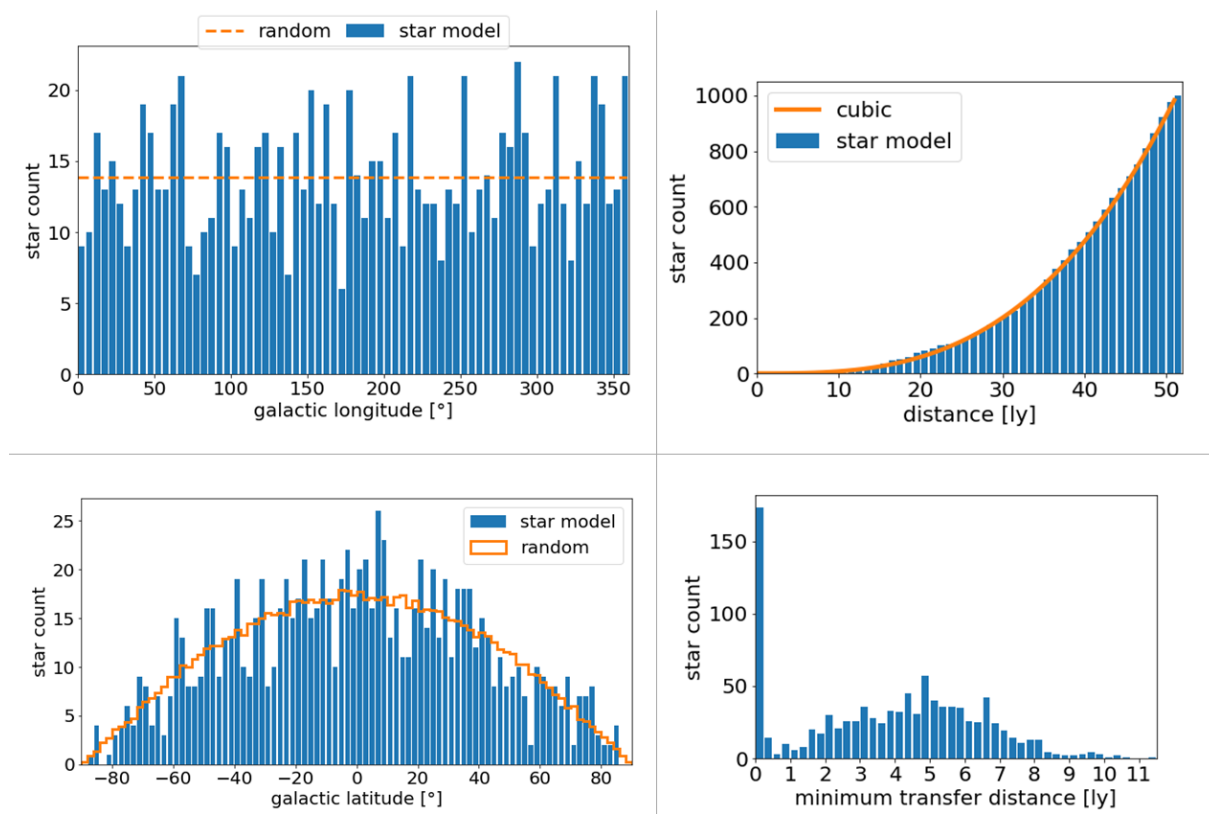


Figure 7-17: Analysis of the spatial star distribution in the 1,000 stars model

Both the latitude and the longitude show some fluctuations and thus deviate from the ideal uniform distribution. This is assumed to be an effect of the low star number, where statistical outliers are more evident. The distribution of the distance to sol appears to be more uniform, which is due to the cumulative nature of the histogram.

The minimum transfer distances (lower right plot) are in a range of 0-12 ly. Again, there is a strong increase in star systems with very small minimum transfers (< 0.5 ly), indicating the presence of binary or multiple star systems.

7.2.2 Variation of Probe Number for Given Algorithm Configuration

The parameters which are kept constant along the runs are given in Table 7-7. As indicated, only the probe number is varied.

Table 7-7: Fixed input parameters and algorithm parameters

Input Data					
Model	Gaia Star Model	m	X		
n	1000	v	0.1 c		
s_i	1				
Algorithm Parameter					
$T_{max,g=0}$	∞	g_{max}	1500	r_{mut}	0.4
$T_{max,g=g_{cut1}}$	100,000 y	P_{max}	200	r_{swap}	0.8
$T_{max,g=g_{cut2}}$	7000 y	r_{cross}	1	r_{merge}	0.5
g_{cut1}	100 gen.	r_{imp_cut}	0.05	$r_{shuffle}$	0.3
g_{cut2}	150 gen.	r_{loc_search}	40		

Based on the results from the large star model with 10,000 stars it is decided to include only probe numbers up to 64 for the smaller model, as higher probe numbers would lead to very short routes or even one-target missions. Between the runs the probe number is doubled again; hence, starting with a probe number of 2 yields a set of 6 runs. The resulting solution fitness is given in Figure 7-18.

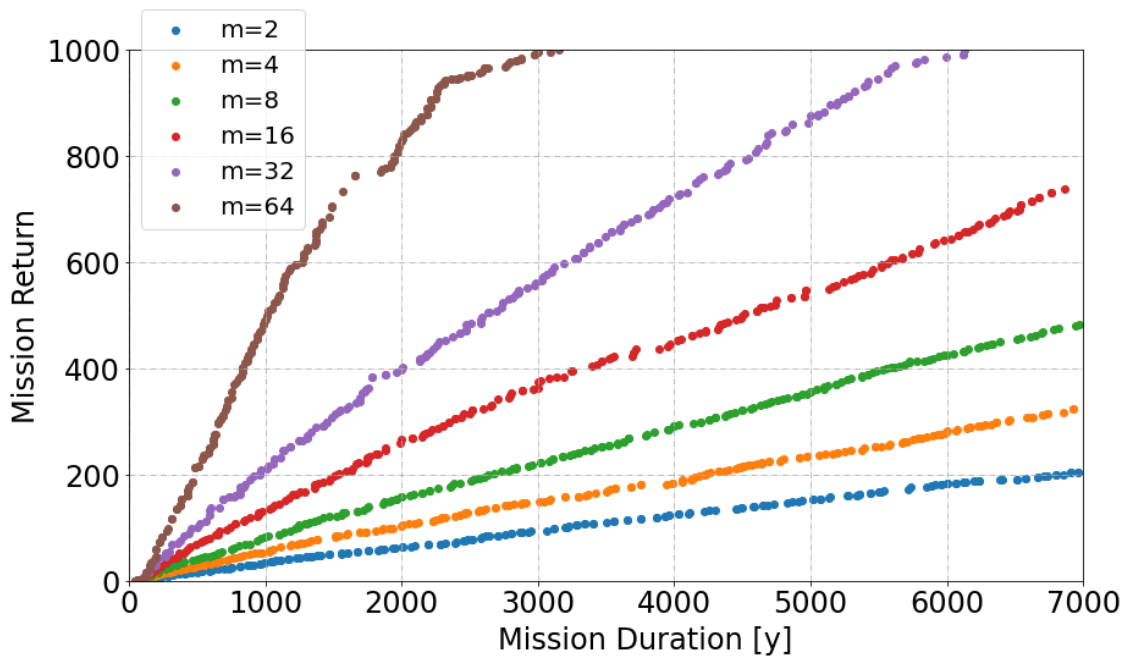


Figure 7-18: Resulting solution fitness for various probe numbers considering a model with 1000 stars

The pattern shown in Figure 7-18 is similar to the results obtained considering the 10,000 stars model. As before, there appears to be a linear relation between mission duration and mission return. Exceptions to this behavior are found again in the higher probe number runs, when either the maximum mission return is approached or, at the other extreme, towards very short-term missions.

7.2.2.1 Doubling Factor Effect

In Figure 7-19, the doubling effect of the probe number is analyzed. As done already for the 10,000 stars model, selected solutions for each run at certain mission durations are extracted from Figure 7-18 (see upper left plot in Figure 7-19). Based on this data, the doubling factor $\frac{J_1(2m)}{J_1(m)}$ is derived, which represents the change in mission return for a given mission duration when the probe number is doubled.

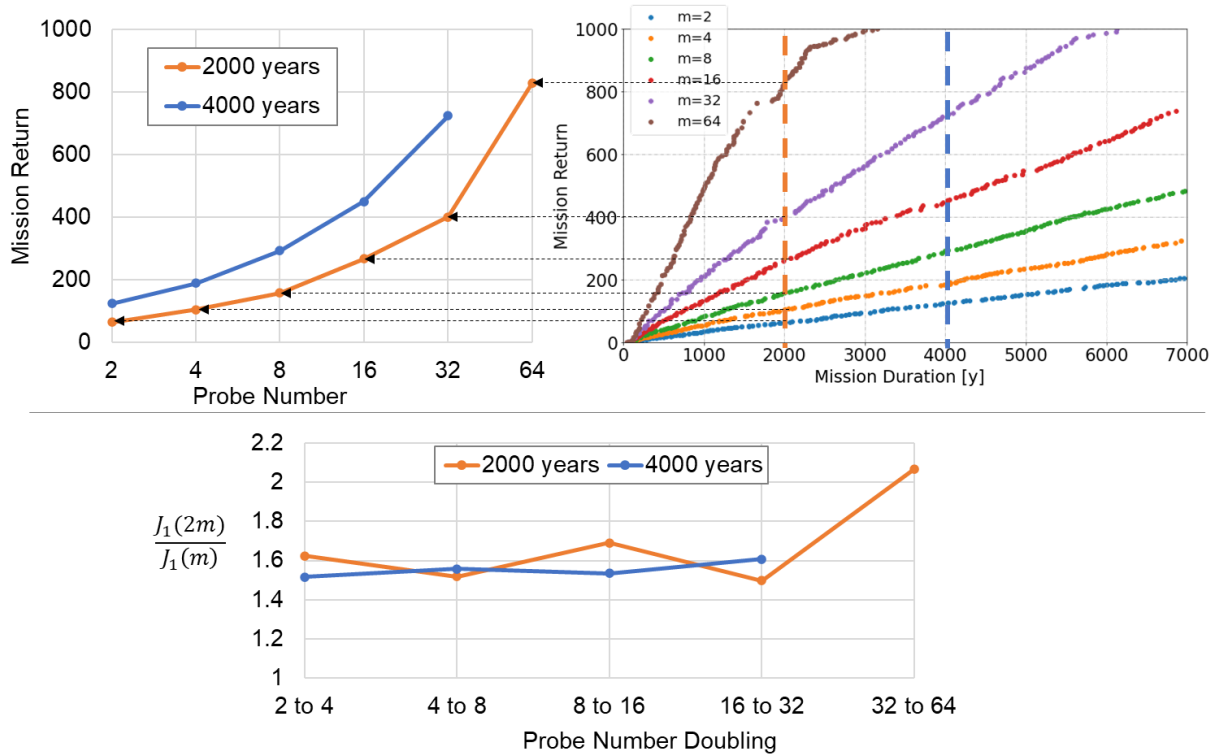


Figure 7-19: Effect of probe number doubling on the mission return considering 1000 stars model – upper right plot: Mission return vs. mission duration for different probe numbers; upper left plot: extraction of selected solutions for 2000 and 4000 years mission duration; lower plot: increase in mission return after doubling the probe number

The doubling factor varies only slightly for the first runs but increases significantly from run 32 to 64. This aspect is reconsidered when comparing the results of both models in section 7.3. Excluding the last run and averaging the doubling factors yields a mean value of 1.58. Hence, the relation between mission return and probe number for a given mission duration can be approximated by:

$$J_1 (J_2 = const) \sim m^{0.66} \quad \text{Eq. (7-4)}$$

7.2.2.2 Convergence and Further Solution Behavior Analysis

The convergence behavior of the solutions is shown in Figure 7-20 by means of the fitness ratio.

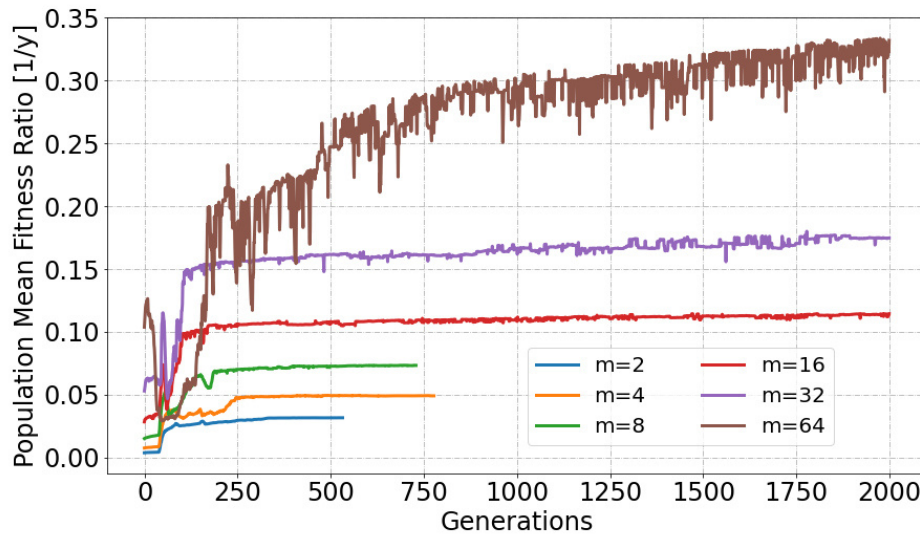


Figure 7-20: Population mean fitness ratio over time for 1000 stars model with varying probe number

The convergence criterion is satisfied only for the first three runs (until a probe number of 8). Considering higher probe numbers, the algorithm stops when the maximum generation number is reached. Hence, in particular the curve of last run with 64 probes in Figure 7-18 can be assumed to bear further potential for improvement.

By following, the behavior of the solution over the generations is further analyzed, focusing on the distribution of solutions within one generation with respect to the mission return. Therefore, another quantity needs to be introduced. It is based on the average mission return of a generation:

$$J_{1,mean} = \frac{1}{P_{max}} \sum_{i=1}^{P_{max}} J_1(i) \quad \text{Eq. (7-5)}$$

To enable a comparison between runs with different probe numbers, the result is normalized with the maximum mission return of the considered generation, yielding the normalized mission return distribution factor $\varepsilon(j)$ with respect to a generation j :

$$\varepsilon(j) = \frac{J_{1,mean}(j)}{\max(J_1(j))} \quad \text{Eq. (7-6)}$$

Assuming uniformly distributed solutions, this value equals 0.5. If there are more solutions located along the upper region of the Pareto curve (towards higher mission return) the distribution factor increases to maximum 1. Conversely, in case of more short-term missions it approaches 0. It is emphasized, that the distribution factor is different to the mean fitness ratio, which is calculated similarly but cannot be used to analyze the distribution of solutions within a generation.

In Figure 7-21, the distribution factor is plotted over the generations for the considered runs.

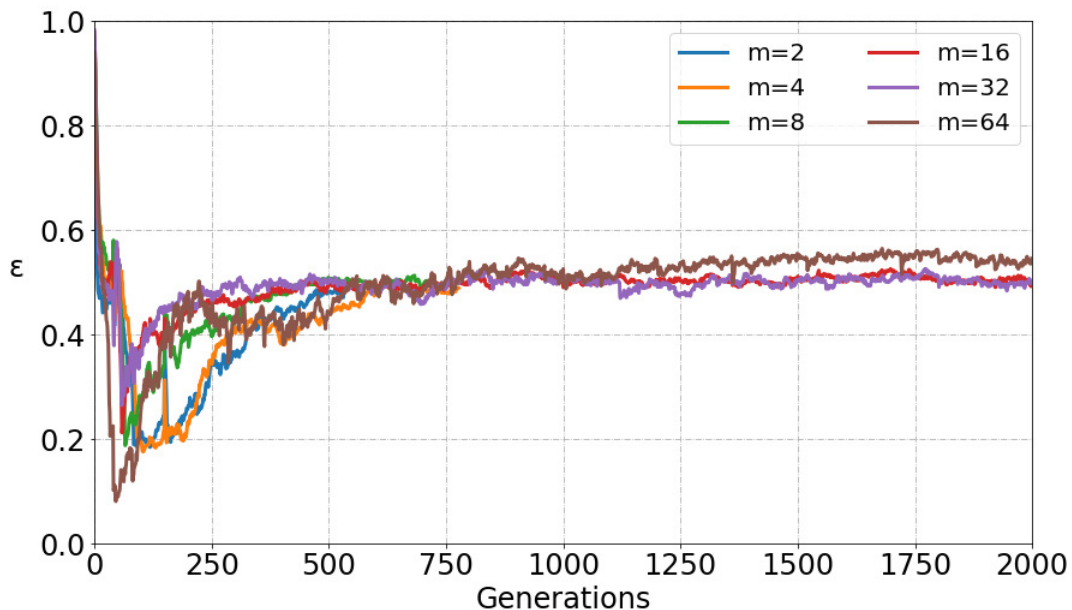


Figure 7-21: Normalized mission return distribution for the considered runs

As shown in Figure 7-21, the curves for different runs follow a similar pattern: They start with a distribution factor value of 1, as the initial generation consists of individuals with the highest mission return. By means of the mutation and improvement operations, the solutions are spread subsequently within the search space, yielding a reduction of the distribution factor. This results in a drop of the distribution factor, which indicates the presence of many short-term missions. In fact, the algorithm produces many duplicates with very short mission durations. Since during the evolving procedure the Pareto rank is prioritized over the crowding distance, those solutions, being non-dominated, are preliminarily kept. However, with increasing generations also the upper region of the search space is gradually populated with non-dominated solutions. Once the number of non-dominated solutions passes the maximum population size, the crowding distance selection is also applied within the non-dominated subpopulation. As a result, solutions in the lower, dense search space are substituted by others from the upper, rarely populated region. This finally yields a balanced distribution of the mission return, indicated by a distribution factor of $\varepsilon \approx 0.5$.

7.2.2.3 Analysis of the Transfer Distances

In this subsection, the transfer distances along the selected exploration sequences are analyzed. The transfer distance represents the distance traveled by the probe between two stars along its route and thus depends on the star locations. Together with the travel velocity the sum of transfer distances for one route determines the required travel time for the considered route.

Figure 7-22 shows the average transfer distances per mission, differed by probe number.

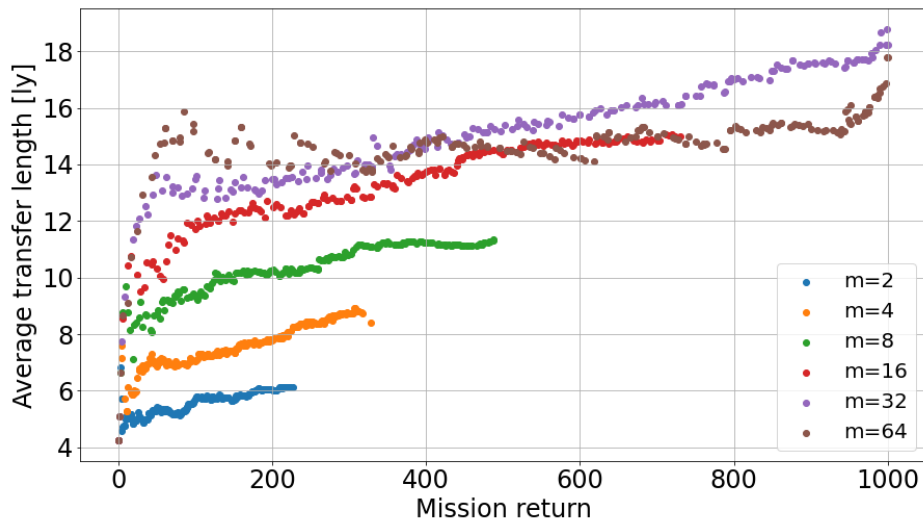


Figure 7-22: Average transfer distances vs. mission return for various probe numbers

As already stated in chapter 7.1.2.2 based on the route structure analysis, the average transfer distances increase with probe number. An exception to this behavior is found for the 64 probes run considering higher mission return. This is in line with the observations concerning the probe number doubling (chapter 7.2.2.1), where the doubling effect becomes more significant when doubling from 32 to 64 probes. The reason behind this phenomenon needs further investigation and will be reconsidered in the discussion section.

Another observation from Figure 7-22 is the slight increase of transfer distance with mission return. This contradicts earlier observations on the linear relation between both objectives, from which a constant average transfer is anticipated. Hence, it can be assumed that the non-linearity, which is induced by the model limit, has also an impact on lower probe numbers. As the increase in transfer distance is rather small, it is not evident in the plot of the solution fitness curves, which was shown in the beginning of this chapter (Figure 7-18).

The dependence of the transfer distances on the probe number is also observable when analyzing the distribution of transfers for selected solutions. For that purpose, two solutions are extracted from Figure 7-22 and investigated by means of a histogram. The histogram indicates the number of transfers with a certain distance (see Figure 7-23). Both solutions, one with 4 probes and the other with 64 probes, provide a similar mission return. One bin in the histogram represents an interval size of 1 ly. For instance, the first bin counts all transfers in the considered mission with 0-1 ly distance.

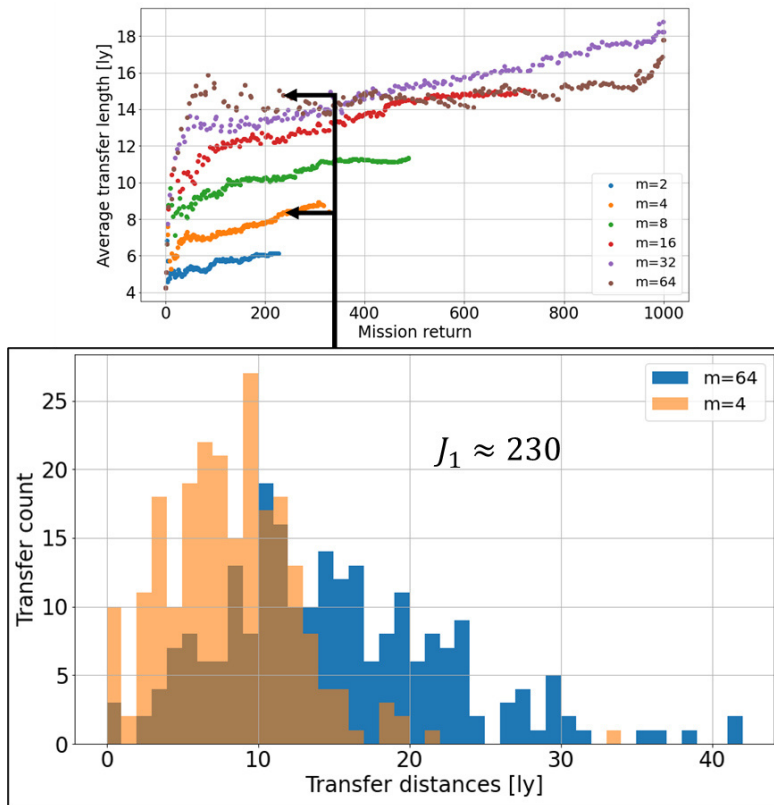


Figure 7-23: Distribution of the transfer distances for selected solutions, each bin represents an interval size of 1 ly

As shown in Figure 7-23, the transfer distances are lower when less probes are deployed, which is in line with earlier observations. The very short transfers (0-1 ly) indicate the exploration of binary or multiple star systems. Interestingly, the fraction of those systems is much higher in the lower probe number case. Hence, the presence of multiple star systems appears to be more advantageous for low probe numbers.

Small probe numbers allow for shorter transfers and a higher fraction of multiple star systems compared to large probe numbers.

7.3 Comparison of Different Model Results

For the comparison of the two different models, runs with probe numbers higher than 64 are not considered due to the limit of the smaller model. Note that the results may differ slightly from previous subchapters, as the runs have been repeated. Table 7-8 provides the used input data and algorithm parameters.

Table 7-8: Input data and algorithm configuration

Input Data					
Model	Gaia Star Model	m	X		
n	X	v	0.1 c		
s_i	1				
Algorithm Parameter					
$T_{max,g=0}$	∞	g_{max}	2000	r_{mut}	0.4
$T_{max,g=g_{cut1}}$	100,000 y	P_{max}	200	r_{swap}	0.8
$T_{max,g=g_{cut2}}$	7000 y	r_{cross}	1	r_{merge}	0.5
g_{cut1}	100 gen.	r_{imp_cut}	0.05	$r_{shuffle}$	0.3
g_{cut2}	150 gen.	r_{loc_search}	40		

7.3.1 Comparison of the Models

In Figure 7-24 the spatial star distribution of both models is compared. The distribution of the distance estimations to Sol is omitted, as the histogram for the small model represents an extract from the histogram of the large model. To enable a comparison between both models, the counts for the larger model are reduced by a factor of 10.

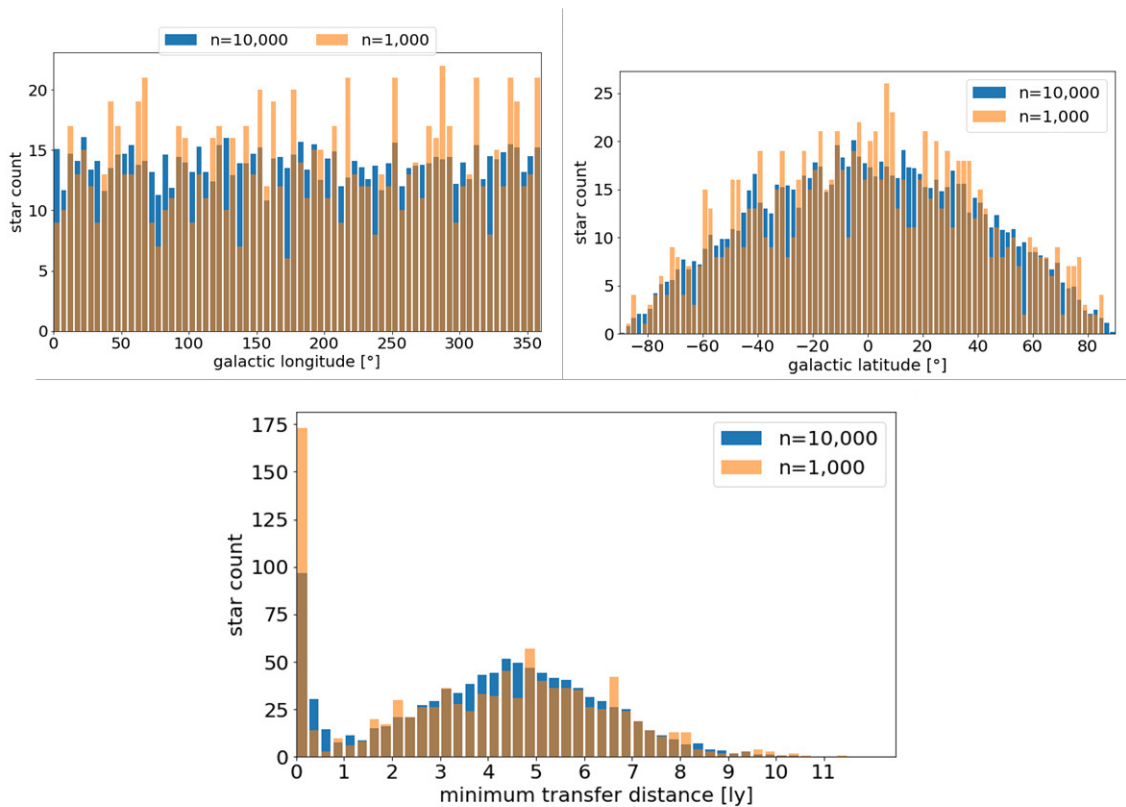


Figure 7-24: Comparison of spatial star distribution between both model

As already stated in chapter 7.2.1, the distribution of the coordinates (latitude and longitude) in the smaller model appears to be less uniform, which is due to the lower star number. An interesting observation is made from the lower histogram, where the transfer distances to the nearest neighbors are plotted: Compared to the large model, the fraction of closely neighboring stars (<0.25 ly) in the small model is significantly higher, indicating an increased occurrence of binary or multiple star systems. This is assumed to have technical reasons, as due to the restriction to the 1,000 nearest stars more multiple systems can be resolved.

7.3.2 General Comparison of the Solutions and Linearity Effects

In Figure 7-25, the solution fitness curves for different probe numbers with respect to the used models are plotted. Star symbols indicate the usage of the 10,000 stars model, while the results from the 1,000 stars model are represented with dots.

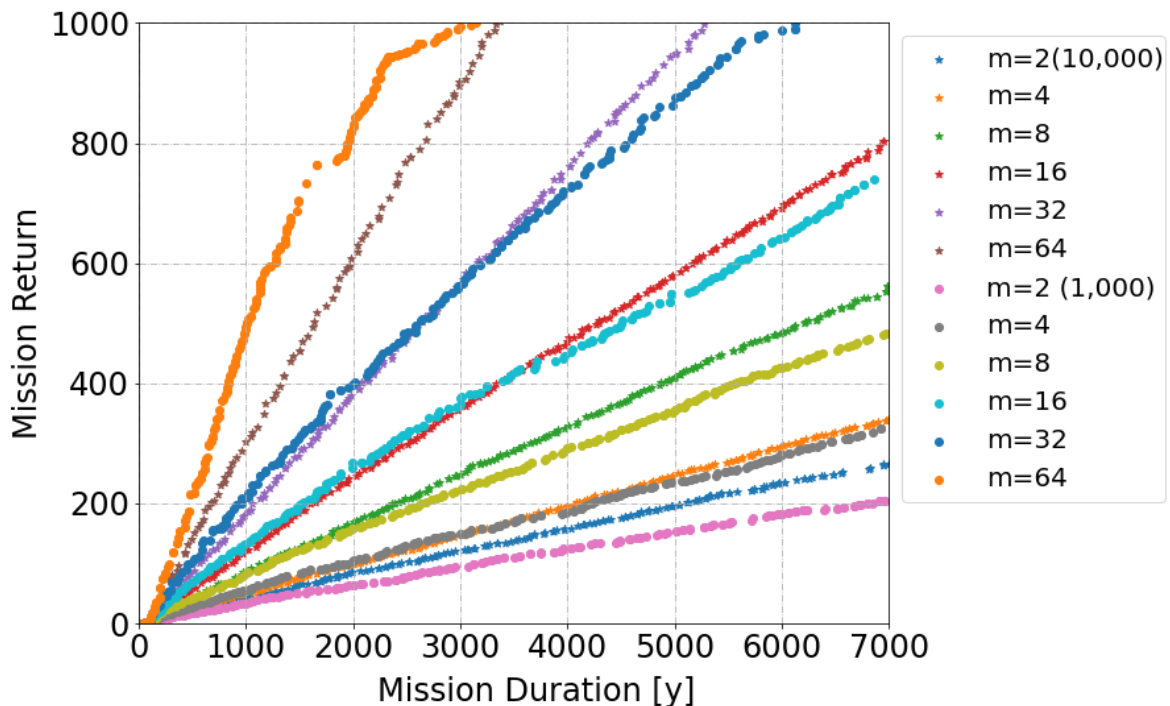


Figure 7-25: Comparison of solution fitness for different probe numbers with respect to the star models (dots indicate the usage of the 1,000 stars model, star symbols represent runs from the 10,000 stars model)

The non-linearity of the curves when approaching the maximum mission return sets in already for lower probe numbers, which is due to the reduction of the star number: It is strongly evident for a probe number of 64 but also observable for 32 probes. Even for lower probe number runs it becomes apparent as the curves are slightly skewed: For low mission durations, the smaller model runs are superior to the corresponding large model runs, while with increasing mission duration the larger model delivers better solutions, yielding higher mission return for the same time. This is in line with results from the transfer distance analysis (subchapter 7.2.2.3), where a slight increase of transfer distance with mission return is observed.

An exception to these observations is the run with 64 probes from the smaller model, which outperforms the corresponding run from the larger model significantly. The extraordinary behavior of the 64 probes run has already been noted earlier, however, there is still no explanation found.

7.3.3 Probe Number Doubling Effects

In Figure 7-26, the doubling factors for the two different models are compared. The methods have already been described in the previous subchapters and therefore are not repeated here.

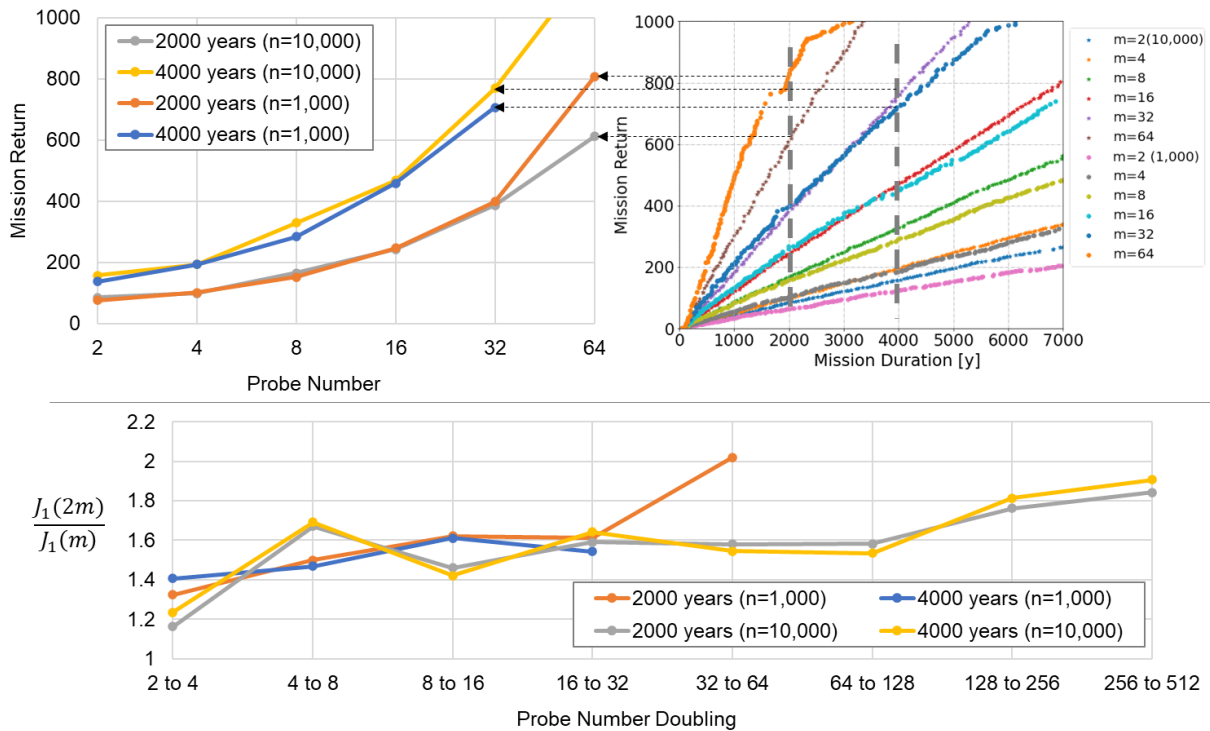


Figure 7-26: Comparing doubling factors for different star models

Considering runs with probe numbers from 2 to 32, the resulting mission return is similar (upper left plot in Figure 7-26). With respect to 64 probes there is a significant increase in mission return when both models are compared. This deviation in mission return is also apparent in the lower plot, where the doubling factors are compared. The fluctuations for lower probe numbers are assumed to be due to the probabilistic nature of the algorithm, reconsidering the results of previous runs (see again Figure 7-11), where the doubling factor is almost constant for lower probe numbers. However, there appears to be a general trend of a disproportionate increase in mission return when considering probe number runs which are reaching the star model limit. This effect is not fully understood and later addressed in the discussion (chapter 8.2.2).

As done earlier, the doubling factors from the low probe number runs (up to 32) are averaged, which yields a value of about 1.51. This allows the derivation of the following relation, which is independent from the model:

$$J_1 (J_2 = const) \sim m^{0.6} \tag{Eq. (7-7)}$$

Note that the exponential growth factor of 0.6 deviates by 10 % from the factor based on earlier runs.

Together with the observations on linearity, the following scaling law between both objectives and the probe number can be derived:

$$J_1 \sim J_2 m^{0.6} \tag{Eq. (7-8)}$$

Note that this relation is valid for the considered models with constant star values (hence $s_i = 1$) and within the linear regions described earlier. Furthermore, it is less accurate for probe numbers that are approaching the limit of the star model.

This becomes evident, when the scaling law is included in the upper left plot from Figure 7-26, as done in Figure 7-27.

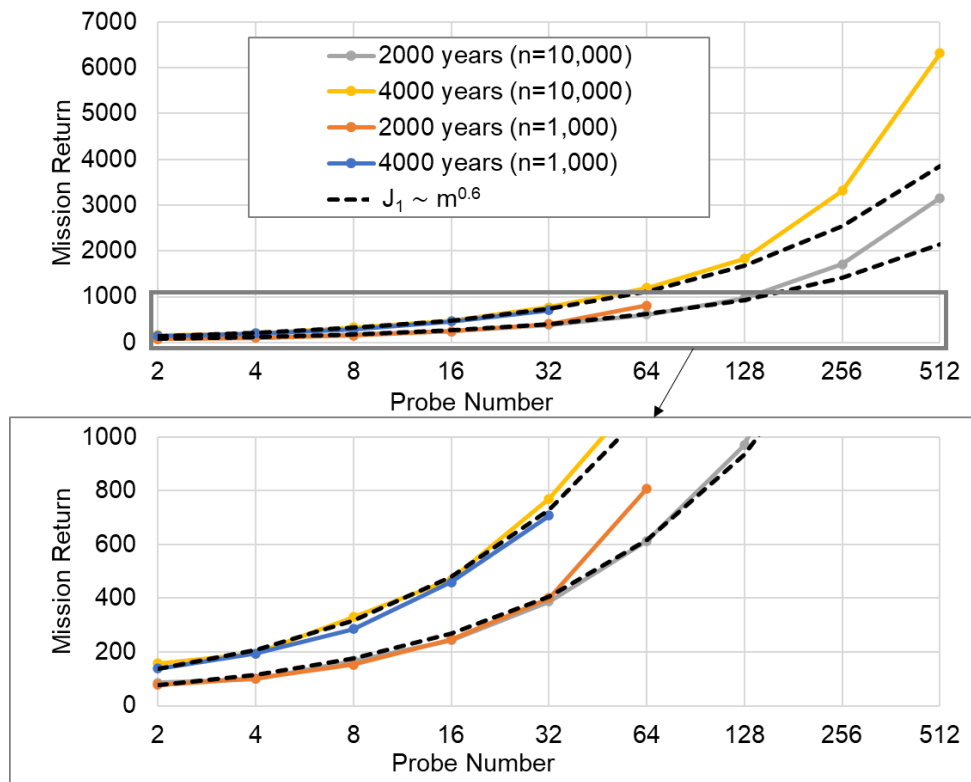


Figure 7-27: Comparison of the derived scaling law with the algorithm results obtained for given mission duration and from different models

Given these observations, it can be stated, that the relation as formulated above represents a conservative estimation.

Considering lower probe numbers, the relation between the two objectives and the probe number can be approximated by $J_1 \sim J_2 m^{0.6}$.

7.3.4 Convergence Behavior

The effects of the star number restrictions due to the different models are also observable in the behavior of the mean fitness ratio. In Figure 7-28 only a selection of runs is compared for better clarity.

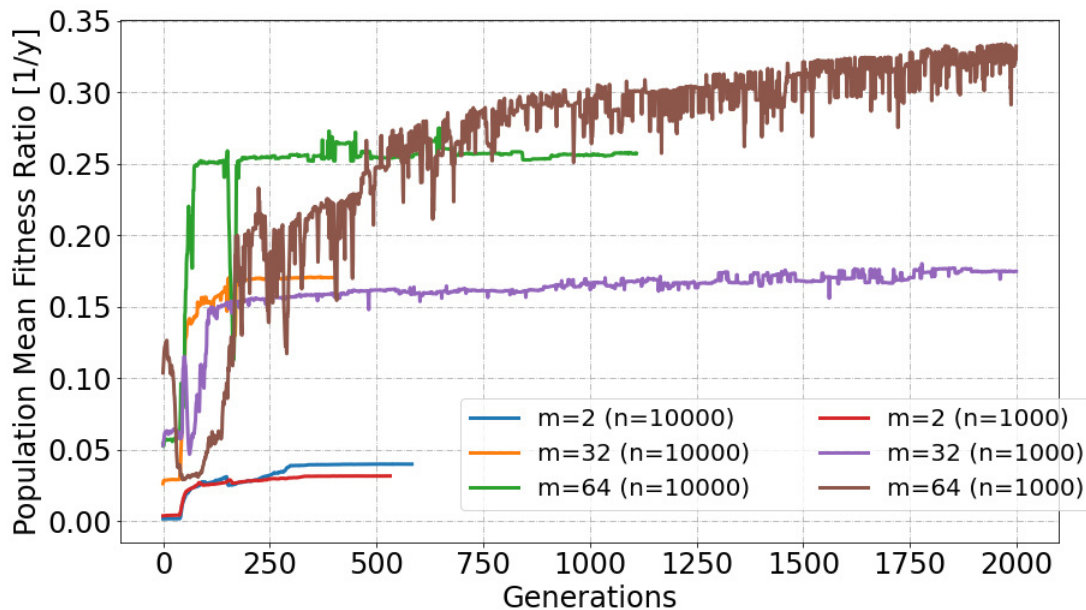


Figure 7-28: Mean fitness ratio for selected runs considering the two models with different star number

Considering the 64 probes run, both curves differ strongly: While for the larger model the solution is stable and converges, the same run based on the smaller model is noisy and keeps improving over time. This behavior is very similar to the observations in section 7.1.2.4 with respect to the 512 probes run. Regarding the low probe number run the curves do not differ significantly, while for the 32 probes run differences become observable. Reconsidering the above observations on the non-linearity of the 64 and 32 probes runs, the previously made assumptions on the non-linearity impact on the mean fitness ratio and thus convergence are confirmed.

7.3.5 Star Selection Analysis

7.3.5.1 Star Selection and Routes within the Final Generation

To analyze the differences in star selection, the final population of each run is considered. Firstly, the individuals from each population are ranked according to the mission return (starting with the lowest). Then each individual is compared with its higher ranked neighbor with respect to the set of explored stars as follows: The intersection between both sets is calculated, which gives the number of stars that are adopted by the next individual. Dividing this number by the entire star number of the corresponding individual yields the fraction of stars that are reused. For instance, assume an individual A with routes including the star set $\{1,2,3,5\}$ and another individual B with the star set $\{2,5,7,8,10\}$. The intersection of both sets yields a new set consisting of $\{2,5\}$, which represents the stars in B that are adopted from A. The fraction of stars in B that have been adopted from A is then the size of the intersection set (here equals 2) divided by the size of the B star set (here equal to 5), yielding 0.4.

In Figure 7-29 the described factor is plotted for selected runs.

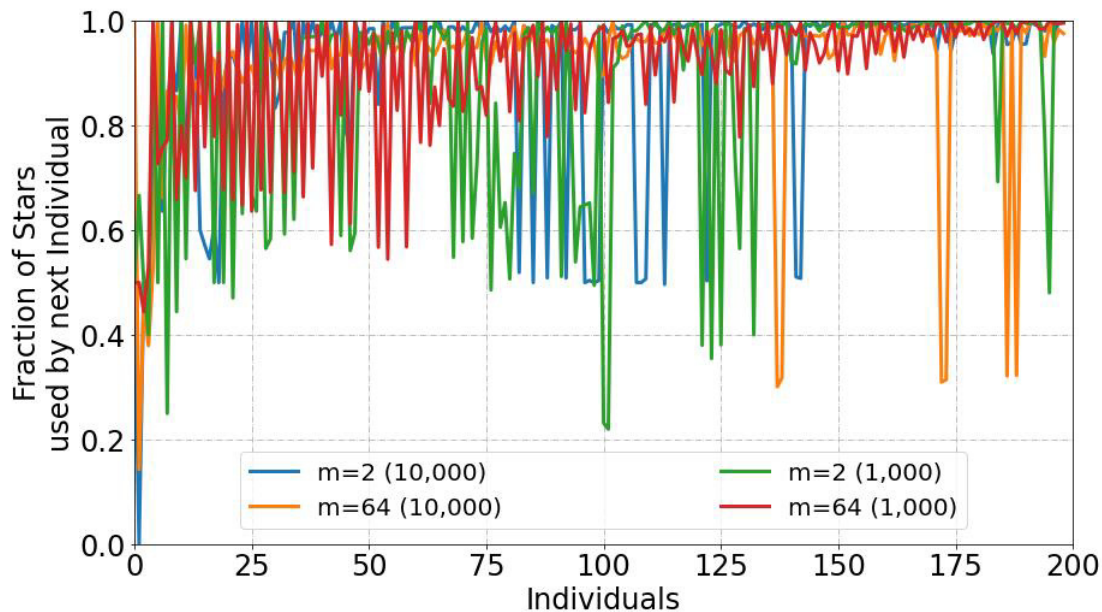


Figure 7-29: Star fraction used by subsequent individual

From Figure 7-29 follows that within one population the individuals tend to reuse stars from their neighbor individuals. Considering the 64 probes run from the smaller model, this is a trivial observation, as due to the restriction to 1,000 stars with increasing mission duration the individuals are forced to reuse the existing stars. However, the same behavior is observed for the 2 probes run based on the large model, which offers much more stars to choose from.

The differences in star selection become also evident when analyzing the route structures. In Figure 7-30, four different plots are provided which illustrate the routes from two solutions along the Pareto front ($J_1 \approx 150$, $J_1 \approx 300$) considering both models and assuming 4 probes.

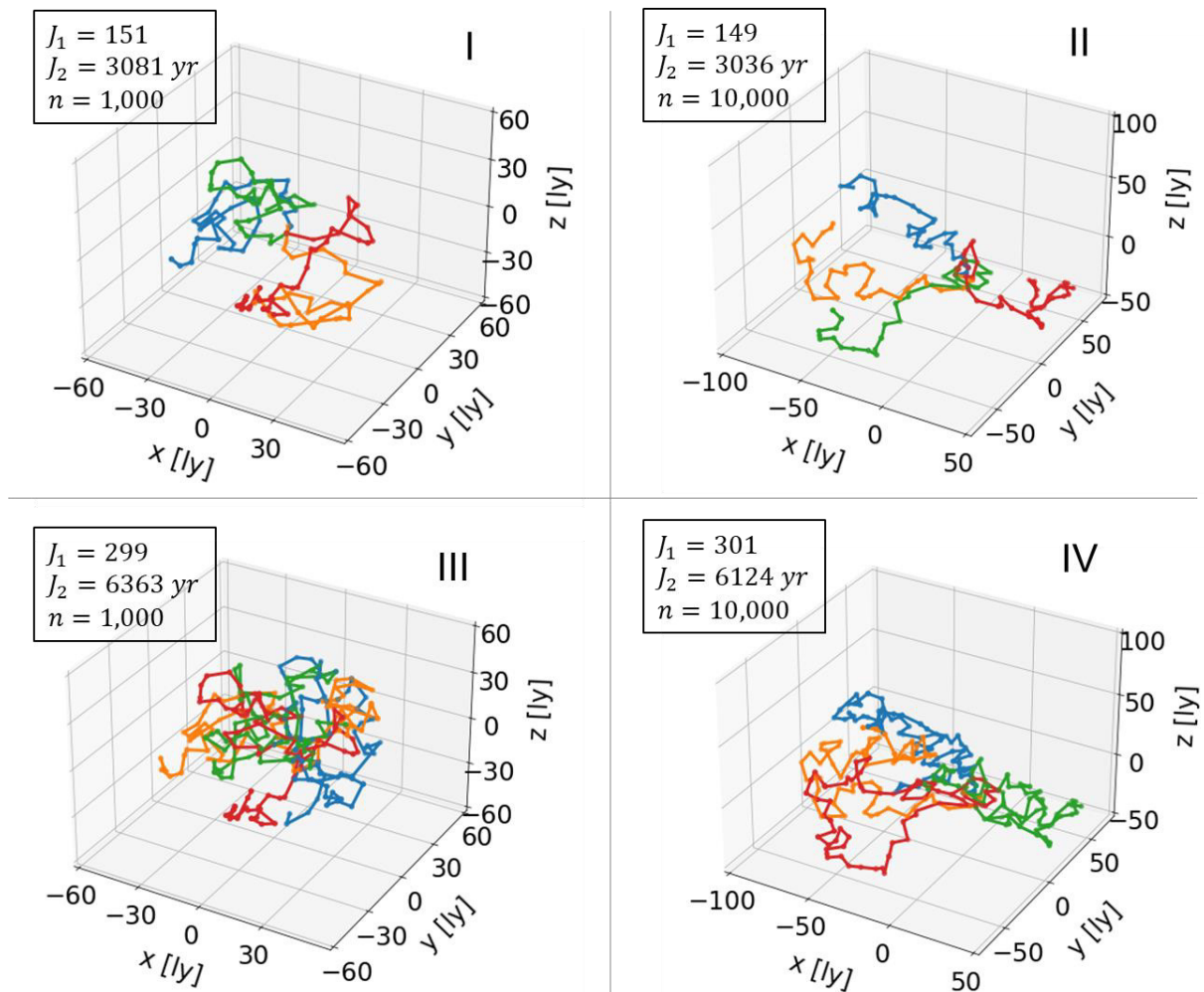


Figure 7-30: Routes comparison for different solutions from both models considering 4 probes

Comparing plot I with II reveals the first difference in the route structure: While both missions yield a similar return in similar time, the second one includes also more distant stars. Accordingly, the routes tend to follow a straight shape, whereas in I the routes are more curved. For higher mission return, this tendency towards curved, winding routes continues (plot III). Considering the larger model (plot IV), this behavior is also observable, but less apparent. Due to the differences between both models, the curvature effect can be assumed to be determined by the model borders: After launching the probes in different directions, the algorithm tends to produce straight-lined routes to further increase the distance between the probes. By means of this technique an overlap of the routes is avoided. However, after a certain time the border of the star model is approached, which requires a deflection of the route. In case of the smaller model, this occurs earlier, which finally leads to a higher occupation of the entire star model volume (see plot III) compared to the larger model (plot IV).

Reconsidering Figure 7-25 from the beginning of this chapter, these observations explain why solutions from the larger model outperform the corresponding solution from the smaller model with increasing mission duration. However, it cannot explain the difference between both runs with 64 probes.

Beside these described observations, Figure 7-30 provides also suitable examples on the reusability of stars and routes within one generation (as analyzed in Figure 7-29). For instance, considering the left two plots (I + III), the red route in III is generated by merging the red and the green route in I. The right plots (II + IV) show how existing route are extended to increase the mission return (e. g. the red route in IV represents an extension of the green route in II, likewise the orange route).

7.3.5.2 Star Selection along the Optimization Procedure

In Figure 7-31, the variation of the considered star sets over the generations is shown. The focus is on lower probe numbers, as for higher probe numbers the considered star set approaches the limit of the smaller star model.

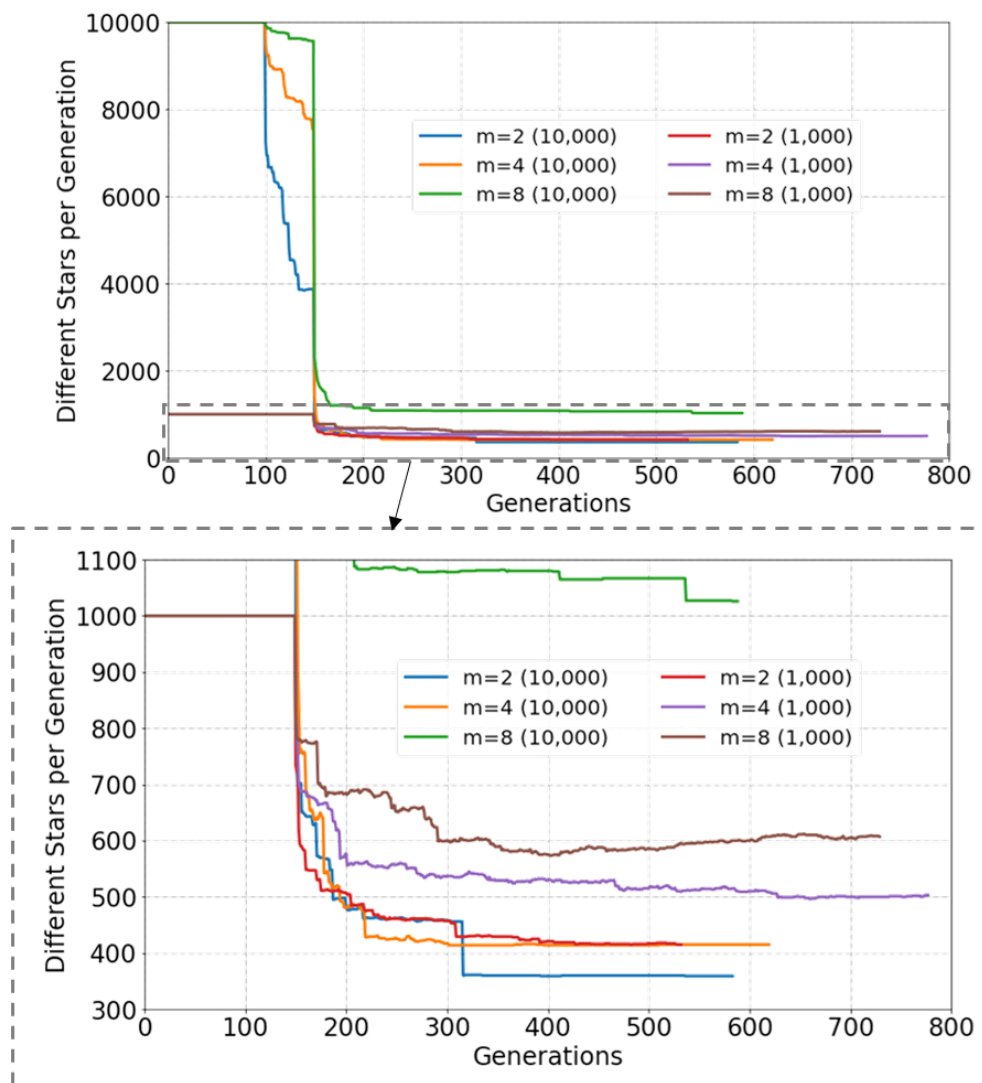


Figure 7-31: Number of different stars within one generation for different probe numbers and star models over the optimization procedure

As shown in the upper plot in Figure 7-31 the number of different stars considered within one generation is initially equal to the model star number. This is due to the initial relaxation of the time constraint. When the cutting operations are applied (in particular the second one at 150 generations), the star number is reduced significantly. Within

subsequent generations, the star number decreases further (see the zoomed section provided by the lower plot in Figure 7-31) and stabilizes until the convergence criterion is met. Interestingly, the two runs with low probe numbers ($m = 2$ and $m = 4$) based on the smaller star model reach higher values compared to the corresponding runs from the large model. For increasing probe number (8 upwards) this behavior is reversed.

In Figure 7-32, two runs are selected and compared with respect to the number of new stars that are included in the next generation.

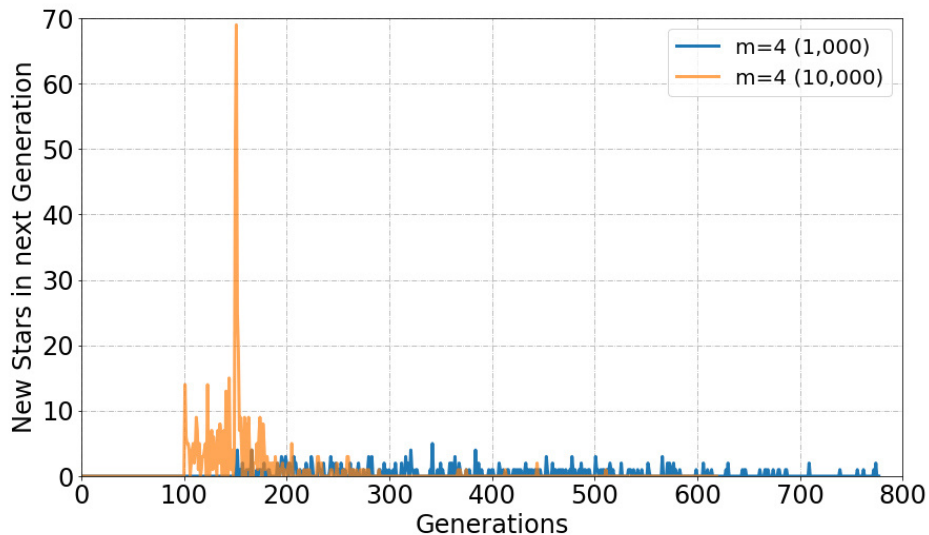


Figure 7-32: Number of new stars in next generation compared to previous generation considering runs with 4 probes from different models

As shown in Figure 7-32, there are no new stars included until the first cut operation is applied and the time constraint is activated. This is expected as from the beginning the entire set of stars is available within the generations (see again Figure 7-31). Along with the cutting operations, the star number used in the generations is reduced (as shown in Figure 7-31). From here, new stars are included, as temporarily also worse solutions are considered (see explanations on the impact of cutting on the solution quality in chapter 6.2.1.2). The cutting operations have a stronger impact on the run based on the large-sized model, as it enables much longer routes.

Reconsidering the lower plot in Figure 7-31, within this generation regime (say from 100 to 200) the entire star number of the set is still reduced. Hence, the new stars either replace existing stars from the set or are removed in the subsequent generation. With further generations, the number of new stars added to the existing set is close to zero (considering the large model run) or within a range between 1 to 5 for the small model. This deviation between both models is assumed to result from the different probabilities of choosing a suitable star due to the random selection process: Compared to the large model, the probability of randomly selecting a star which is compatible to the existing star set is much higher in case of the smaller model.

Based on these observations it can be stated that the star selection procedure is completed after 200 generations, independent of the underlying star model. Further generations are then used to distribute the selected set of stars among the probes and optimize the sequences by means of the local search operations.

8 Discussion

8.1 Discussion on Selected Models and Algorithm

8.1.1 Assumption on Mission Concept and Probe Technology

The strong simplifications on mission concept and probe technology made during the definition of the optimization framework (section 3.1) must be definitely considered in the discussion and interpretation of the results: Regarding the probe concept, only the travel velocity is included in the optimization problem. It is provided as input parameter and set based on the literature, where different probe concepts are suggested. Additional parameters, such as probe mass, or relevant probe subsystems, e. g. propulsion system or communication systems back to earth, are not considered. This entails the advantage, that the derived results are valid across a large range of concepts proposals from literature. In turn, however, the simplified probe model does not allow to derive strategies and recommendations with respect to certain technologies and mission concepts, such as effects of replicability.

Another aspect not discussed here is the feasibility of probe and mission concept. Even when refining the current probe and mission model it is evident, that given the existing technologies, the missions proposed here are at least questionable. For instance, one cannot expect that probes are working without failure over more than several hundreds or even thousands of years.

Along with the probe concept also the mission and trajectory models are simplified: The departure trajectory from the solar system, where the probes are accelerated to near-relativistic speed, is not treated separately. Furthermore, transfers between stars are assumed to follow straight trajectories, which is shown to be a valid assumption and in line with the literature. However, the gravity of a star is an important factor concerning the stellar exploration sequence selection: A common practice, currently only in interplanetary travel, but probably also relevant for interstellar travel, is the usage of the stellar gravity and velocity to change the probe trajectory. This is particular of interest with respect to the trajectory deflection during the flyby, which is also not considered in the model and thus represents another weakness of the model: At the considered velocity regime it can be expected that the possible deflection angles only by means of gravity are limited (for instance, see [188]). Hence, to enable high deflection angles a deceleration of the probe may be required, e. g. by means of a photogravitational assist as suggested for small-scale probes in [58]. If such deceleration maneuvers are not feasible (e. g. due to probe concept restrictions), the general travel velocity needs to be reduced. However, the reduction of the travel velocity affects other parameters and requires further trade-offs. For instance, consider the minimum encounter distance between probe and star which is determined by the maximum heat flux the probe can resist and the stellar luminosity [26]: Decreasing the probe velocity increases the heat load, as the probe will spend more time close to the star. To encounter this effect, either the probe shielding needs to be improved, which may entail a higher probe mass or the periastron distance must be increased, which in turn affects the deflection angle.

Alternatively, regarding large probe concepts with fusion based engines such as Project Icarus, the option of resource harvesting can be considered: Assuming to be

capable of propellant mining and processing, these probes are decelerated to harvest the required resources to provide sufficient propellant and then continue their travel to the next star system. As further advantage, the temporary deceleration extends the observation period and thus may increase the scientific return of the mission. However, this requires an extension of the mission architecture by including rendezvous maneuvers, which are not considered here.

Based on these discussions, it can be stated that the used mission model represents an ideal scenario. However, it is emphasized that the made assumptions and simplifications do not impair the validity of the outcomes and derived recommendations with respect to the exploration strategies: Aspects such as linearity and star selection preferences are expected to be not affected, which indicates a high model robustness.

8.1.2 Star Model Limitations

Compared to the probe and mission model, the star model represents a very realistic approximation of the solar neighborhood: It is based on observations from the ongoing Gaia mission, which is assumed to provide the most accurate and complete star catalogue. However, there are also some limitations on the Gaia data:

- Firstly, very bright stars are not included due to restrictions on the observable magnitude. The effect of this limitation can be examined by checking lists of very bright stars. One of those lists is provided by Kaler [198], covering more than 170 stars with magnitudes smaller than 3. Of those stars, about 60 are within the distance considered in the large-sized model. This represents a fraction of less than 1 %, that is not represented in the model. Based on this estimation, the magnitude limit of the underlying star data can be expected to be negligible for the results.
- Secondly, the Gaia catalogue is known to contain several data artifacts, particularly with respect to the immediate solar neighborhood. To encounter this issue, a very strict filtering procedure is applied, based on suggestions from literature, to obtain a clean dataset. However, due to the strict filtering also confirmed data sources are eliminated. As outlined in section 4.2.3, this effect is assumed to be less harmful to the results than the presence of spurious stars that may mislead the algorithm.
- Thirdly, all observations on star characteristics and position estimates by nature contain some uncertainty, which is induced in the model. However, compared to the made assumptions and given the formulated objective of deriving trends instead of planning a mission in detail, the uncertainty of data can be assumed to be negligible.
- Fourthly, each source is considered as single star. Hence, binary or multiple star systems are not treated as such, even when being resolved, which is not possible in all cases due to technical reasons. Furthermore, some of the binaries which are not fully resolvable cause errors, as observations may assigned to the wrong component [192]. This issue, which may produce spurious data is addressed by the filtering procedure.

Like the Gaia catalogue, the model does not account for binary or multiple star systems, hence, each star is treated as single target. As a result, the probe receives multiple rewards when visiting a multiple star system. Since the probe tries to maximize the return while limiting the mission duration, it favors stars that are forming multiple

star systems over isolated stars. By merging multiple star systems into one star, this effect can be eliminated, which is recommended for future work.

Another simplification of the star model is the neglect of stellar motion. This assumption is shown to be valid within a certain timeframe, which is represented by the time constraint in the problem formulation. As mentioned earlier, the model of fixed stars together with neglecting gravity effects eliminates the possibility of performing slingshot maneuvers. This is certainly one important aspect that has been omitted here and thus a weakness of the model, as it is expected to impact the selection of stars and exploration sequences.

Furthermore, the concept of the stellar metric which assigns each star an individual score as suggested in 4.2.4 has not been implemented yet. Hence the mission return equals the number of explored stars.

8.1.3 Algorithm Limitations: Remarks on Solution Quality and Reliability

The used algorithm is a metaheuristic method. Hence, by definition the generated solutions are not guaranteed to represent the global optimum and, even worse, might be located at any distance from the true optimum. This aspect is addressed by means of a test model with very simple star distribution: As in this special case the true optimum can be estimated analytically, it enables a quantitative assessment of the algorithm at least for a limited probe number. Considering a probe number of 4, the deviation between global optimum and algorithm solution is about 10 %.

However, considering high probe numbers, the solution quality cannot be assessed by means of the test problem, as in those cases the analytical approach is not feasible anymore. The only possibility to obtain an estimate of the deviation is by considering the maximum possible fitness ratio. The maximum fitness ratio is obtained for a hypothetical mission, where the number of stars is equal to the number of probes and thus each probe is sent to one star. In this case, the fitness ratio is determined by the max. obtainable mission return, the travel distance to the most distant star $\max(d_{ij})$ and the average travel velocity v :

$$\sigma_{\max} = \frac{v}{\max(d_{ij})} \sum_{i=1}^n s_i \quad \text{Eq. (8-1)}$$

Assuming $s_i = 1$ for all stars, the max. mission return is equal to the number of stars n . Considering the large model consisting of 10,000 stars, the maximum fitness ratio is then about 9 y^{-1} , assuming a travel speed of 10 % of the speed of light. In the considered runs, the highest fitness ratio of approximately 1 y^{-1} is reached when 512 probes are assumed. Hence, the derived solution for higher probe numbers can be expected to be at least in the same order of magnitude compared to the global optimum.

Another aspect to be emphasized is that due to the probabilistic nature of the algorithm the reliability of the results is limited. For instance, consider the derived relations between objectives and probe number: Comparing two sets of runs, the resulting growth rate deviates by 10 %. This effect is typically encountered by repeating runs several times and averaging or choosing the best one, but not done here due to the limited time resources.

Furthermore, the algorithm parameters have been shown to impact the solution quality. For high number runs, the maximum generation number has the largest impact, yielding deviations of more than 30 %. Considering lower probe numbers, the mutation and improvement probability rates turned out to bear more relevance (20 % max. deviation). Given these observations and the previous discussion on the algorithm reliability it is stated that the derived results need to be considered rather as trends or tendencies instead of exact solutions.

The solution deviates by 10 % from the ideal solution (considering a test case) and is generally expected to range at least in the same order of magnitude.

8.2 Implications of the Results for Exploration Strategies and Mission Planning

8.2.1 Linearity vs. Non-Linearity

Under the assumption that the mission return represents the number of explored stars, the mission return correlates linearly with the mission duration for a given probe number, hence $J_1 \sim J_2$. This is expected, as the stars are found to follow an approximately uniform spatial distribution.

The linear correlation can be described by means of the fitness ratio, which is calculated from the ratio of both objectives and thus represents the derivation of the fitness curve. Hence, it can be interpreted as the average mission return obtained within one year mission time. For instance, assuming a number of four probes yields a fitness ratio of about 0.05 y^{-1} . Due to the linear characteristics of the curve, this value can be used to estimate the required time to explore a certain number of stars, or, alternatively, how many stars can be explored within a given time. E. g., a mission duration of 1,000 years allows for an exploration of about 50 stars.

A further effect of the linearity is that by doubling the mission duration also the mission return is doubled. This finding is in line with a conclusion drawn by Cartin [26], who states that doubling the targets requires twice the exploration time. Note that compared to his work, where each target from a given set must be visited, in the presented approach the probes can choose their targets from the model.

However, the assumption of linearity does not hold in general, as there are two exceptions to this behavior:

- The first exception is observed when approaching the maximum mission return provided by the model. In this case, a saturation effect occurs, which makes a further increase in mission return comparatively expensive with respect to the mission duration. By comparing two runs with the identical probe number but considering different models (one with 10,000 and the other with 1,000 stars), it can be shown that this effect is caused by the model. Therefore, it has no implications on true, physical missions, which may be realized one day. However, this aspect definitely has to be accounted for when building and implementing models for similar applications: In order to avoid the presence of non-linearities in the results, the model should be designed in a way that the

limits of the model are not reached. Note that the non-linearity effects due to small models are also observed for low probe number runs, which appear to be far from reaching the model limits.

- The second exception is found at the other side of the time-scale, which concerns short term missions. Assuming a high probe number, it is not necessary to launch each probe when only few target stars are considered. In those cases, an increase in probe number does not correlate with a decrease in mission duration, as the few considered stars cannot be further distributed among the probes. The linear relation is only true once a certain threshold of mission return is passed and enough probes are launched. An analysis of the minimum star number which is required to deploy all available probes efficiently revealed that there is no constant factor between both parameters. Instead, the ratio of probe number and minimum star number to deploy all probes increases towards higher probe numbers: For 512 probes the ratio reaches its maximum value of 1.67, indicating that probes may remain unused when the mission includes less than 830 stars. This means in turn, that missions with less than 830 stars can be conducted with less than 512 probes without increasing the mission duration. However, it is emphasized, that these derivations need to be seen as trend instead of strict values, as the algorithm does not distinguish between missions with equivalent objective values and performs a random selection in those cases. Consequently, the actual thresholds are assumed to be much higher than the values calculated here. Contrarily to the first exception, this effect is not artificially induced by the model. Hence, it needs to be involved in the mission design and planning procedure in order to make fully use of the benefits of higher probe numbers, otherwise the mission might suffer from inefficiency.

8.2.2 The Relation between Probe Number, Mission Duration and Mission Return

8.2.2.1 General Discussion on the derived Scaling Law

Extending the linearity considerations by involving the effect of probe number, it is found that the mission return correlates with mission duration and probe number according to $J_1 \sim J_2 m^{0.6}$. However, this relation must be treated with caution: It is only valid in the linear case and when assuming constant star scores (e. g. $s_i = 1$). Furthermore, it is not accurate, when considering probe numbers that collide with the star model size (512 probes for large model, 64 probes for small model). In those cases, surprisingly the factor is even higher - due to the non-linearity effects actually a decrease of the factor is expected. By comparing two runs with the same probe number but based on two different models, it could be shown that this unexpected increase is induced by the model. Further investigations on finding the exact reason behind this phenomenon did not succeed, hence this effect is not fully understood. Some ideas that have been considered and discarded are described by following:

- Difference in convergence: As described earlier, the restriction of the star number in the model may lead to a non-linear behavior of the fitness curve when high probe numbers are considered. This non-linearity destabilizes the mean fitness ratio, which is used to measure the solution convergence. As a result,

the solution will never satisfy the convergence criterion and run until the maximum generation number is reached. Depending on the run, an increase in generation number may improve the solution significantly (shown in section 7.1.3.2). Hence, one may expect that for the large model the solution does not reach its optimum as it is interrupted earlier due to the assumption of convergence. This hypothesis is disproven by repeating the corresponding run for the large model with suspended convergence check.

- Random nature of the algorithm: Due to the algorithm characteristics, the results from runs with identical parameters may differ. However, repeating the corresponding run with 64 probes yielded similar results. Hence, the probabilistic algorithm characteristics are assumed to be not responsible for the observed effect.
- Model differences:
 - Spatial star distributions: Regarding the 1,000 stars model the stars appear to follow a less uniform distribution. This is due to the lower star number, which makes deviations from an ideal uniform distribution in form of statistical outliers more evident. Less uniformly distributed stars indicate the presence of clusters. Assuming, that missions with low probe number benefit from those clusters, an opposite effect to the observed results is expected. Furthermore, as the irregularities are still comparatively low, it is not expected that they influence the results that significantly. This is confirmed by the comparison of lower probe number runs for both models, which are very similar.
 - Higher occurrence rate of binary or multiple star systems: By analyzing both models, the fraction of binary or multiple stars systems is found to be much higher in the smaller model compared to the large model. In general, this could lead to differences in the solution curves when the same probe number is considered. As contradiction to this hypothesis, again one can refer to the smaller probe number runs, which deliver similar results. Furthermore, it could be shown, that typically small probe numbers benefit from the presence of those systems.

Given these considerations and the results from another set of runs with slightly differing growth factor ($J_1 \sim J_2 m^{0.66}$), it is emphasized that the derived relation must not be interpreted as an exact equation. Instead, it needs to be considered as a trend which serves as an orientation and requires further investigations to ensure higher reliability. Furthermore, as the higher probe number runs are not involved in its calculation, it is assumed to represent a rather conservative estimation.

Nevertheless, a first verification approach is intended by following. Again Carter [26] is considered as reference, who derives a similar scaling law. Rewritten with respect to the objectives used in here and neglecting the impact of velocity his result can be roughly approximated by $J_1 \sim J_2 m^{0.8}$.

Hence, he derives a higher growth factor which deviates by roughly 20 - 30 % compared to the results presented here. However, it must be noted that there are some differences between both approaches. Firstly, while both are based on true star data the used models differ strongly in size: Whereas Carter considers a maximum of 60 stars (based on the RECONS database), the smallest star model considered here consists of 1,000 stars. The other main difference was already mentioned along the

linearity discussions and concerns the exploration strategy: While the approach presented here allows the probes to select suitable stars and thus to skip unfavorable stars, Carter forces the probes to explore each star from the model.

Given these differences in modelling and accounting for the rather conservative nature of the scaling law derived here, it can be stated that at least the trend of the results is confirmed.

8.2.2.2 Scaling Law Implications for the Exploration Strategy

To derive possible implications for the exploration strategy, the scaling law has been further analyzed. For that purpose, the derivatives with respect to the probe number were determined under the assumption of a given mission duration.

Based on the derivatives, a strong similarity to the concept of diminishing returns from economics has been observed. Accordingly, the effect of a mission return increase by deploying more probes becomes less significant with increasing probe number. More precisely, there is only a substantial increase of mission return for very low probe numbers. This is assumed to be caused by a crowding-like effect: All probes are launched from the solar system, which entails large initial transfer distances when many probes are deployed. To avoid those large initial transfers due to crowding effects, one can either reduce the probe number or consider swarm-based mission concepts: For instance, a mother ship can be used to transport a fleet of smaller probes to a distant star or just a distant region. Once arrived, the probes are released and start to explore nearby stars.

In Figure 8-1 this idea is visualized by means of a sketch of two hypothetical missions A and B: Mission A represents a set of 17 probes which are launched from the solar system while mission B considers only 13 probes including one mother ship (red, dotted trajectory). The mother ship transports a small fleet of 5 probes to a distant star, where they are released to explore the neighboring stars. Furthermore, suitable routes from mission A are merged, which allows for a further reduction of the initial transfer distances.

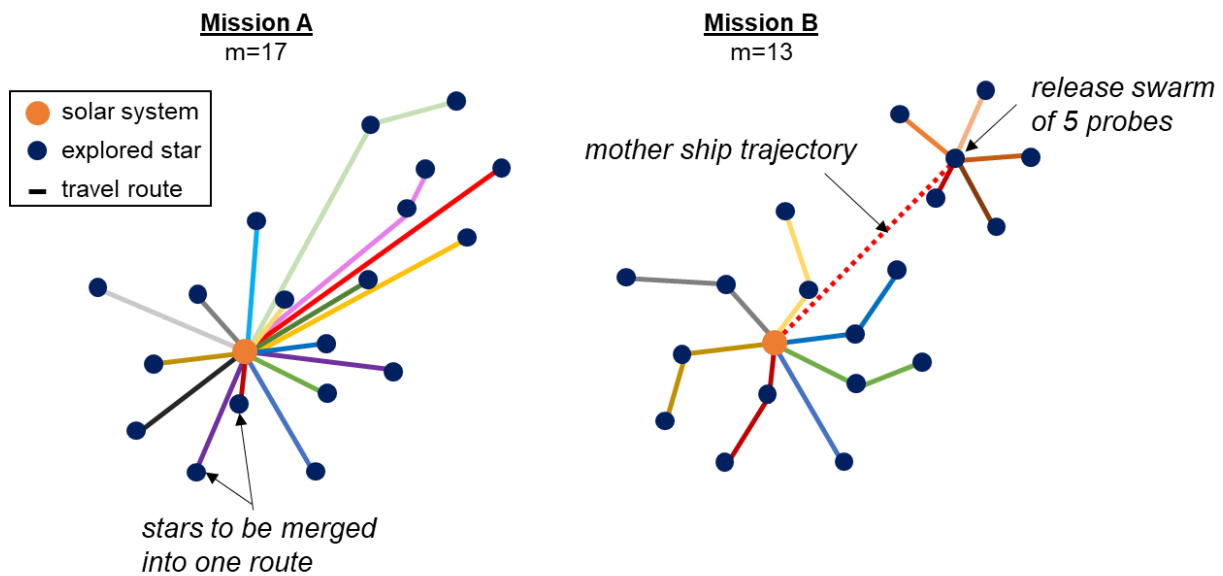


Figure 8-1: Comparison of two different missions A and B with swarm-based concept to avoid crowding effects - each color represents one probe, the blue dots indicate explored stars

As shown in the sketch in Figure 8-1 the initial transfer distances are significantly reduced by means of the merging procedure and the mother ship. As in both missions the longest routes have similar lengths, the time required for completing both missions is roughly equal. Note that a similar, de-crowding effect can be yielded by using self-replicable space probes. However, in those cases the time required for the replication needs to be taken into account.

Hence, with respect to optimal exploration strategies the following can be stated:

- Launching a high number of probes from the solar system bears the risk of crowding effects. These effects cause high initial transfer distances and thus lead to an inefficient deployment of probes. As possible mitigation strategies swarm-based or self-replicable probe concepts are suggested.
- For very low probe numbers, contrarily, increasing the probe number is still comparably efficient with respect to the corresponding increase in mission return. However, it is emphasized that the efficiency declines already from the beginning. Note that there is no strict threshold concerning the probe number efficiency: Based on Figure 7-12 from chapter 7.1.2.3, which is again given here for convenience (Figure 8-2), only ranges can be provided.

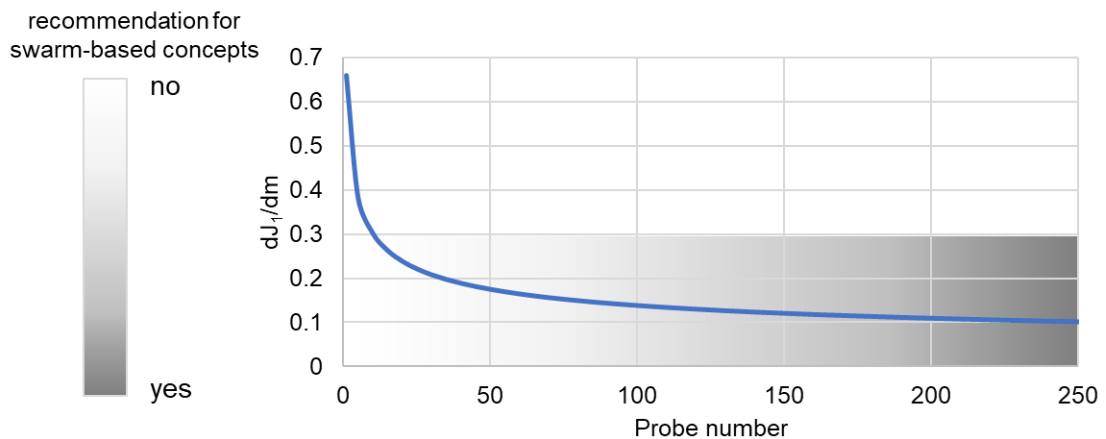


Figure 8-2: First derivative of the scaling law with respect to the probe number and recommendation for swarm-based concepts based on qualitative analysis of the scaling law

Up to a probe number of 10 - 20, the mission return can be increased efficiently by deploying more probes. From a range of 20 - 100 probes upwards, the launch of additional probes becomes less efficient. Hence, considering this probe number range, the usage of a swarm-based concept might be beneficial. This holds especially for higher probe numbers, as the efficiency decreases continuously, although at a very low rate. In Figure 8-2 this is indicated by the grey color gradient, which represents the recommendation for swarm-based concepts based on a qualitative analysis of the scaling law derivation curve.

Note that the given recommendations are based solely on the scaling law under the assumption that the crowding effects are responsible for the observed behavior of diminishing returns. A verification of this hypothesis is left for further research.

8.2.3 The Effect of Probe Number on the Star Selection

Beside its general impact on the mission return, the probe number is also found to affect the star selection procedure. This has been shown by comparing two runs with very different probe number but similar mission return, which is illustrated again in Figure 8-3.

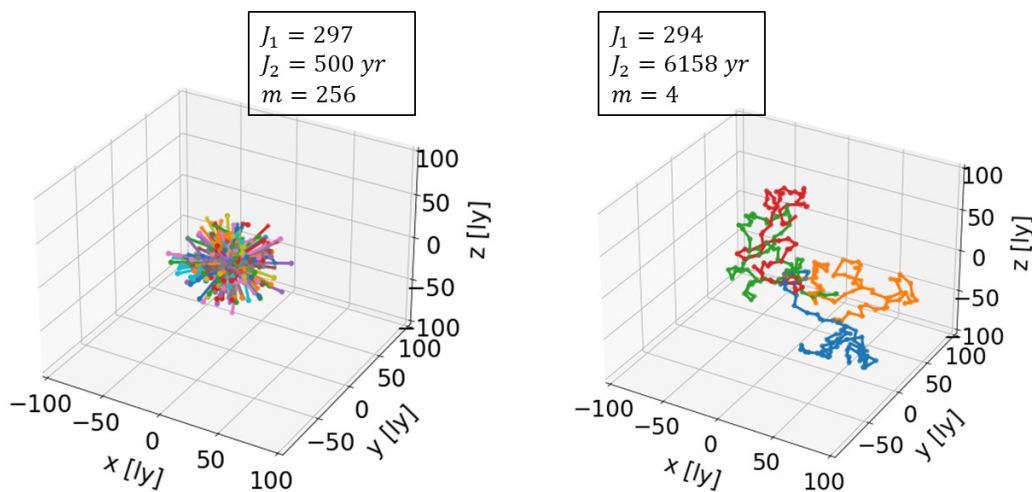


Figure 8-3: Comparing runs with similar mission return but different probe number

Though providing the same mission return, in case of higher probe numbers the focus is on nearby stars, while for lower probe number also more distant stars are included. Furthermore, the low probe number missions allow for shorter average transfer distances along the routes and includes a higher fraction of binary or multiple star systems. Note, that even though the number of explored stars is higher than the probes, in the left mission not all 256 probes are used: There is still a fraction of 15 probes which are not assigned with a star. This is confirmed by earlier observations on the effect of non-linearity.

Hence, with respect to possible exploration strategies the following can be stated:

- If the mission is supposed to explore many stars in the immediate solar neighborhood, higher probe numbers are favorable. In those cases, higher probe numbers entail a further advantage: As each probe visits only few or even one star (single-target missions), the probe can be customized according to the target star. In particular, this concerns the scientific instrumentation and equipment, which can be tailored to increase the scientific return. However, the probe number needs to be chosen carefully to avoid that there are probes remaining which are not assigned with any star (see previous discussions in chapter 8.2.1)
- When the probe number is limited (e. g. due to high production costs), it is recommendable to include also more distant stars, as this allows more efficient routing. Note that the reduction of the probe number leads to a significant increase in mission duration.
- In general, smaller probe numbers are more efficient in terms of travel distances for a given mission return. This needs to be considered e. g. when fuel costs are relevant, as in those cases it may be recommendable to deploy a smaller number of probes.
- With respect to the mission success probability, the shorter travel distances for low probe numbers at the cost of higher mission duration entail two opposite effects:
 - Assuming a failure probability of the probe per traveled distance (as done in [26]), the shorter travel distances can help to increase the mission success rate.

- Contrarily, the increase of mission duration, which leads to longer runtimes, can be expected to reduce the mission success probability. Therefore, it is not possible to give a general recommendation on this aspect. However, swarm-based concepts may be advantageous, as they enable a decrease of the travel distances without reducing the probe number (see again the previous discussion on the implications of the scaling law in chapter 8.2.2.2).
- If the exploration mission is focusing on binary or multiple star systems, smaller probe numbers appear to be more efficient.

Hence, suitable probe concepts for low probe number mission may be similar to the Daedalus spaceprobe or its successors, e. g. as suggested by the Icarus project group. Considering high probe number missions, contrarily, small-scale concepts such as Breakthrough Starshot appear to be more suitable. In Figure 8-4 the described relations between probe number and mission considerations are summarized. The discussion on swarm-based concepts is not included, as it is mostly based on hypotheses and requires further verification.

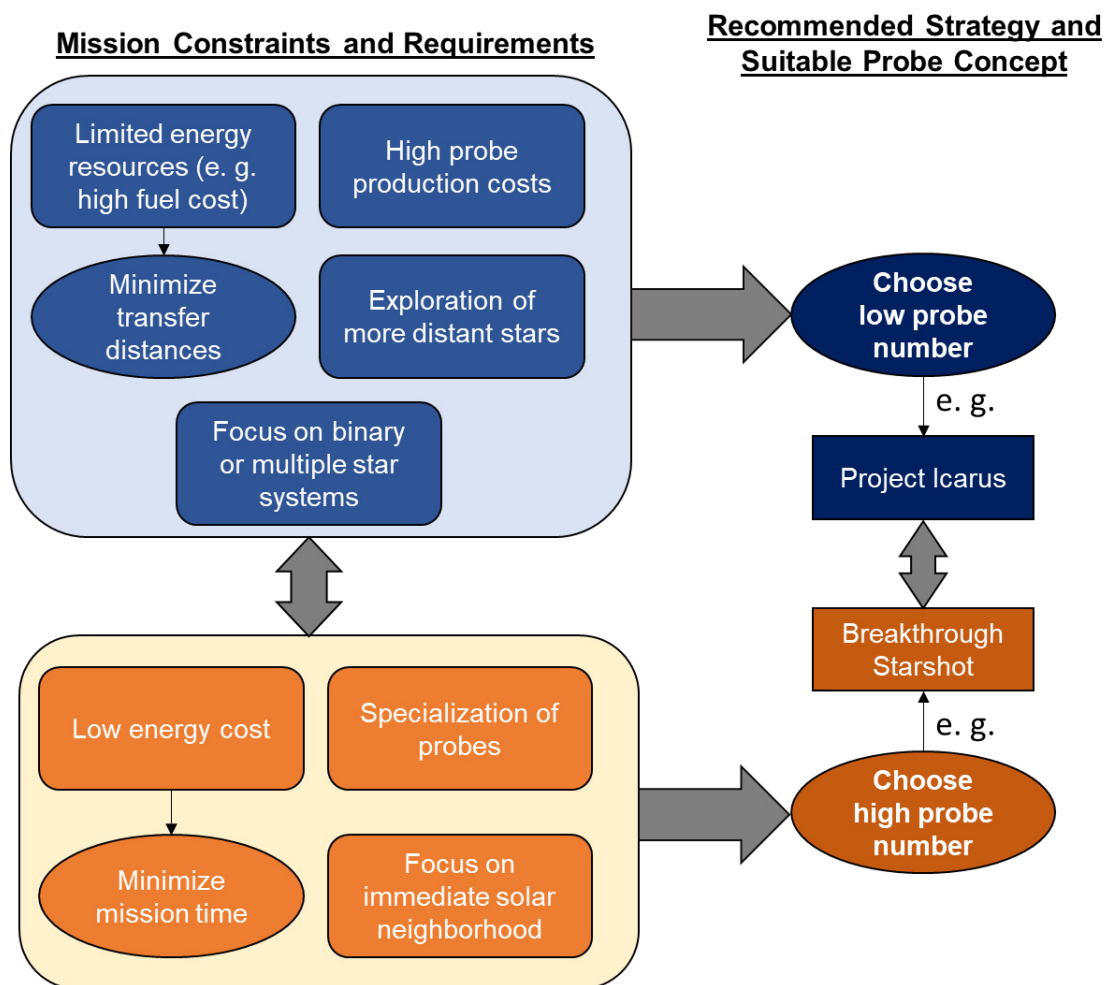


Figure 8-4: Strategy recommendations based on mission constraints and requirements including suitable probe concepts from literature

8.3 Further Implications for Star Model and Algorithm

8.3.1 Implications for Star Model: Remark on the Spatial Star Distribution

Based on the preliminary analyses of the spatial star distribution, the star coordinates are found to be distributed uniformly within the model sphere - the more stars are considered, the more accurate. However, it must be noted that there is a significant fraction of binary and multiple star systems. Hence, unlike in the test model, the stars are not arranged with constant distance to their neighbors. Compared to their expected occurrence in the Milky Way, multiple star systems are still underrepresented in the model, which is due to the limited resolution capabilities. This becomes more evident, when more distant stars are included.

Given the described observations, the following implications on the star modeling can be stated:

- In the considered distance range, the assumption of a uniform spatial star distribution is valid. This holds especially for models with high star numbers. However, if an exact model is required, one needs to use real data (as e. g. from the Gaia DR2) to account for binary and multiple star systems.
- The fraction of binary and multiple star systems decreases towards larger models, which is due to the limited resolution capabilities. This model effect must be considered when those systems are relevant.
- The model size impairs the linearity of the solution - the smaller the model, the higher the impact. The effects of the non-linearity induced by the model are observed very early (also for low probe number runs), even when the mission appears to be far from the model limits. This aspect is very important when choosing the size of the model to avoid false conclusions for the exploration strategy.

8.3.2 Implications for Algorithm: Initial Relaxation of the Time Constraint

With respect to the optimization procedure implemented in the algorithm, the initial relaxation of the time constraint allows a significant improvement of the performance. Generally, the idea of relaxing constraints does not represent a novelty in the optimization field – in some applications it is common practice. However, typically the relaxation method is used to transform the given problem into a related problem with known solution or which is at least easier to solve (for instance Lagrangian relaxation described in [199, p. 132]).

In the presented approach, contrarily, the relaxation does not change the problem itself, but enlarges the search space substantially: More precise, the relaxation opens access to the entire set of stars, which are selectable by initial generations and used to build routes. This method may be interpreted as a top-down approach, as the large set of stars available from the beginning is subsequently reduced until it stabilizes once the solution is converged (see Figure 8-5). Without the relaxation of the time constraint, the initial set of stars available within the generations is limited from the beginning: The initial generation is created randomly, which leads to poor routes with large mission durations, where stars which are not located within the close neighborhood are excluded. Due to the algorithm characteristics and the selection process, the inclusion of new stars from outside of the generation set is possible but rather improbable and

thus requires many generations. Hence, contrarily to the top-down approach, the star set is enlarged subsequently, and accordingly can be interpreted as bottom-up approach.

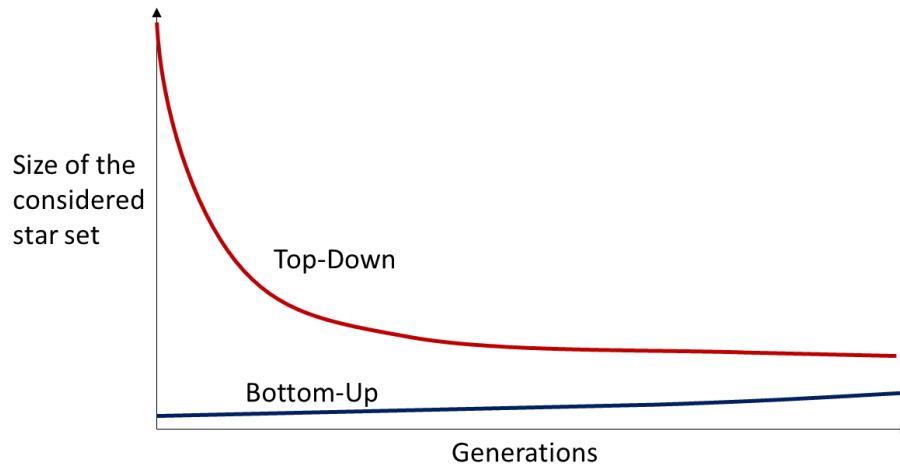


Figure 8-5: Principle of different approaches to select/build the generation star set – top-down corresponds to initial relaxation of the time constraint, bottom-up refers to active time constraint from the beginning

Note that at a certain point in the optimization procedure the time constraint must be activated, additionally a cut operation is necessary. Otherwise, the final generation will contain invalid solutions. To avoid a very harsh transition between two generations, the cut operation and time constraint activation can be performed stepwise.

The approach introduced here may be adopted in various applications, whenever the problem consists of a large search space, which is significantly restricted by an optimization constraint.

9 Conclusions and Remarks on Future Work

9.1 Summary and Main Outcomes

9.1.1 Main Results

This thesis presented an approach to derive optimal strategies for interstellar exploration missions considering nearby stars. The problem of interstellar exploration has been categorized as bi-objective multi-vehicle open routing problem with profits, assuming a minimum set of variables. The problem has been addressed by means of a hybrid multi-objective genetic algorithm. Applied on a test model with exact uniform star distribution, the algorithm generated a solution with a deviation of 10 % to the ideal value. Based on the test model results, it has been found that by means of an initial relaxation of the time constraint the solution quality improves significantly. Furthermore, a convergence check has been implemented to save computing resources.

The star models used for the actual optimization of the exploration strategies are based on the Gaia DR2 and revealed an approximately uniform distribution of the stars in the solar neighborhood. This has been found via a qualitative analysis of the coordinate distribution. However, there is a significant fraction of binary or multiple star systems (10 - 20 %), which is lower than expected due to the limited resolution capabilities. A generic stellar metric to assign each a star a score (profit) has been suggested but is not included yet in the optimization models.

With respect to the optimization results on the real star models, several observations are made:

- In most cases, a linear relation between mission duration and number of explored stars is obtained. This is assumed to be a result of the uniform star distribution.
- The general relation between mission duration, explored stars and probe number can be approximated by $J_1 \sim J_2 m^{0.6}$. This relation is less accurate for high probe number runs when reaching the star model limits. In those cases, an increase of the growth factor has been observed, which has been proven to be a modelling effect.
- The choice of the probe number turned out to influence the star selection and route structure:
 - Assuming a given number of explored stars, small probe number missions include more distant stars while high probe number solutions focus on the immediate neighborhood.
 - In general, the average transfer distances between two subsequent stars within a route increase with higher probe number.
 - Furthermore, the fraction of explored binary or multiple star systems is higher in case of small probe numbers.

9.1.2 Simplifications and Known Weaknesses

Along the modelling and optimization procedure several simplifications have been made: The probes travel at a constant velocity of 10 % of the speed of light along straight-lined trajectories. This has been proven to be a valid simplification for flyby missions, as the impact of the galactic potential can be neglected in this velocity regime. However, the feasibility of the required trajectory deflections when travelling with near-relativistic velocities is not regarded. Furthermore, the probes are assumed to operate without failure, which is not realistic for long time missions, given the current state of technology. With respect to the probe concept and technology, no further restrictions have been made. Hence, the results are valid across various exploration concepts. On the downside, the generic probe and mission model does not allow to investigate the impact of various technologies on the exploration strategy, e. g. the effect of replicability or different propulsion techniques.

In the star models the effect of stellar motion has been neglected, hence stars are assumed to maintain constant positions. This has been proven to be a valid simplification for mission timeframes up to 7000 years. Furthermore, the gravitational effects are not considered, which eliminates the possibility of performing slingshot maneuvers. As the models are based on the Gaia DR2, they are assumed to represent a very realistic approximation of the solar neighborhood.

Due to the nature of the used genetic algorithm, which belongs to the class of meta-heuristics, the optimization results are not guaranteed to represent the true optimum. This is encountered by means of the test problem with known ideal solution. Furthermore, a verification approach based on literature results confirmed the trend of the derived relation.

9.1.3 Main Conclusions for Future Optimization Procedures and Interstellar Exploration Strategies

Based on the results, the following main conclusions on modelling and optimization procedures can be drawn: Stars in the solar neighborhood (up to 110 ly distance) can be assumed to follow a uniform spatial distribution but are not equally spaced due to the presence of binary or multiple star systems. The improvement of the algorithm by means of an initial relaxation of the time constraint may be adopted in future optimization problems with similar structure: In particular, when the problem features a large search space, which is restricted by an outer constraint, the described approach may be advantageous.

Implications for possible exploration strategies concern primarily the effect of probe number: High probe numbers are beneficial when the mission focus is on the immediate solar neighborhood. As further advantage, a higher specialization of the probes is possible, as each probe explores only few stars. This allows for significant time savings, which is described by means of the derived relation between optimization objectives and probe number. Those kinds of missions are suitable for lightweight, small-scale probes which rely on remote propulsion, e. g. the Breakthrough Starshot concept.

Lower probe numbers, contrarily, allow a more resource-optimal exploration, which is due the reduced transfer distances. As further difference to high probe number missions, they conclude also more distant stars and appear to be more efficient when

focusing on binary or multiple star systems. However, missions with small probe number typically consist of long routes, which entails an increase of the mission duration. As the probe number is limited, more sophisticated probes can be deployed, e. g. with a high degree of intelligence. Due to the long mission durations, also a high robustness is required, ideally paired with self-repairing capabilities. Given the shorter transfer distances, the energy costs are minimized, which allows for large-scale probes with integrated propulsion systems. A suitable probe concept for those missions might be similar to the Daedalus spaceprobe and its successor projects, e. g. as suggested by the Icarus project [32].

The derived scaling law and found solution metric (fitness ratio), which is constant for a given probe number, can be used for preliminary estimations in the mission design process. This can help to support some basic considerations during the mission planning, such as the number of stars that can be explored within a given time for a certain probe number. Furthermore, the scaling law is found to reveal strong similarities to the law of diminishing returns from economics. Hence, an increase of the probe number correlates with a substantial higher mission return only for low probe numbers. As this behavior is expected to result from a crowding-like effect, which occurs when many probes are launched from the solar system, swarm-based concepts may help to mitigate this effect. Swarm-based concepts are further assumed to increase the mission success probability, as they are expected to allow for small transfer distances without reducing the probe number.

9.2 Evaluation of the Research Questions

Before concluding this thesis with remarks on future work, the research questions introduced in chapter 1.2 are reconsidered and linked to the results and findings presented previously. For each question, the corresponding thesis chapters are given together with a concise summary of the answer:

- *What are relevant optimization parameters and typical values in the interstellar exploration context?* This question has been addressed in chapter 2 and 3.1: The minimum set of parameters to describe the interstellar exploration problem are found to be the probe number, the travel velocity and the star exploration sequence including the underlying the star system data (such as position and stellar characteristics). Typical values for travel velocities in the related literature range from 10 - 20 % of the speed of light, however, with respect to the probe concept itself high differences in scale (from gram to hundreds of tons) are found.
- *How can interstellar exploration strategies be formulated as optimization problem and what is the corresponding problem class?* This question is answered in sections 3.2 - 3.4: The problem of developing interstellar exploration strategies has been defined as bi-objective multi-vehicle open routing problem with profits. As such, it belongs hierarchically to the class of vehicle routing problems and is found to be very similar to the subclass of team-orienting problems.
- *Is it possible to quantify the value of a star system for a given mission?* This aspect is addressed in subchapter 4.2.4: A concept of a stellar metric is suggested based on a relative ranking of the considered stars which allows to

evaluate each star's contribution to the entire mission return. Note that the stellar metric has not been included yet in the optimization procedure.

- *How can current knowledge on nearby stars contribute to the exploration strategy development?* This aspect is addressed in chapter 4.2 and in chapter 8.3.1: Instead of relying on simple distribution models, the used star model is built from the Gaia DR2, which is considered to be the most recent and complete star catalogue. Hence, the derived strategies are based on true star data. Further information on star systems can be incorporated by means of the suggested stellar metric.
- *What type of algorithm can be used to solve this kind of problem?* This question is primarily addressed in chapter 3.3.3: Given the large solution space, heuristics or metaheuristics need to be considered. Furthermore, due to the bi-objectivity of problem, population-based algorithms are regarded as an appropriate approach to analyze the relation between both objectives. In this work, a hybrid genetic algorithm was used; other examples which are expected to perform similar are Particle Swarm Optimization or Ant Colony Optimization methods.
- *How do mission design parameters affect the exploration strategy and the star selection?* This question, which represents the overarching thesis objective, is addressed explicitly in chapter 8.2 based on the results described in chapter 7. As it comprises various aspects, only two examples are given here: The explored star number increases linearly with mission duration and, furthermore, an increase of the probe number leads to higher transfer distances.

Table 9-1 provides an overview of the research questions and the corresponding chapters in the thesis.

Table 9-1: Research questions and corresponding thesis chapters

Research question	Corresponding thesis chapter
What are relevant optimization parameters and typical values in the interstellar exploration context?	Generally addressed by the literature survey in chapter 2 and more specifically within the variable identification in chapter 3.1
How can interstellar exploration strategies be formulated as optimization problem and what is the corresponding problem class?	Addressed through chapters 3.2 - 3.4
Is it possible to quantify the value of a star system for a given mission?	Addressed in chapter 4.2.4
How can current knowledge on nearby stars contribute to the exploration strategy development?	Addressed in chapter 4.2 and the discussion in chapter 8.3.1 based on analyses from chapter 7
What type of algorithm can be used to solve this kind of problem?	Addressed in chapter 3.3.3 based on the literature survey results on optimization algorithms in chapter 2.3
How do mission design parameters affect the exploration strategy and the star selection?	Addressed in chapter 8.2 based on the results from chapter 7

9.3 Future Work

Given the limited research on interstellar exploration, there are still various opportunities left for future research:

The generic probe and mission model can be refined by including more variables, such as probe mass or allowing for rendezvous. This would extend the previous analysis on the trade-off between mission return and time. Another aspect, which has not been regarded here but is commonly discussed in literature, is the capability of replication and how it affects the exploration strategy. In a similar manner, swarm-based concepts may be considered to verify the presumptions made during the discussion section, e. g. with respect to the transfer distances. To resolve differences in the propulsion technology, also the star model needs to be refined, for instance by including the luminosity of the stars, which is relevant for light sail based propulsion or deceleration. In this context, the effects of gravity could be included together with the stellar motions, which would allow the probes to perform slingshot maneuvers. With respect to gravitational effects, also the feasibility of trajectory deflections at the given velocity regime might be investigated.

A further refinement of the star model can be obtained by applying the suggested stellar metric to the optimization model. Interesting outcomes are expected from the analysis of the selected stars and their distribution (are there regions with higher or lower interest in the solar neighborhood?) and the comparison of the results with the solutions presented here; in particular, with respect to the validity of the derived relation between the objectives and the conclusions on the optimal exploration strategies. Moreover, by identifying binary or multiple star systems and treating them as single targets, a preference of those systems in the exploration strategy could be avoided.

Regarding the algorithm, further improvements are possible, e. g. by replacing the static algorithm configuration with dynamical algorithm parameters: The population size may be varied along the optimization procedure depending on the density of the current generation (e. g. based on the crowding distance) for higher efficiency. The probability rates of the mutation rates could be adapted to force the production of solutions in a certain region of the search space: E. g. by increasing the probability of the merge rate, more solutions in the upper search space are obtained. Furthermore, the efficiency can be increased by eliminating duplicate individuals from the lowest Pareto rank, e. g. by considering the crowding distance already in the Pareto ranking. The convergence check could be refined by including the success rate of the local search operations: When during the local search no further improvement of the routes is possible, the solutions can be assumed to be converged. This could help in case of non-linear fitness curves, where the fitness ratio is not a suitable indicator of convergence. Another aspect left for further research is the unexpected solution behavior for high probe numbers. This has been discussed and shown to be a modelling effect, but the exact reason has not been found yet. Finally, it would be interesting to apply an alternative optimization algorithm to the problem (e. g. PSO or ACO) and check, whether the results are similar to the ones obtained from the genetic algorithm.

Given the large challenges which need to be mastered, one might question the feasibility of interstellar travel, particularly when considering travel routes consisting of several, distant stars as suggested in this work. However, those doubts are encountered by the second of Clarke's three laws: The only way of discovering the limits of the possible is to venture a little way past them into the impossible.

A References

- [1] J. H. Mauldin, "Prospects for interstellar travel," *American Astronautical Society*, vol. 93, 1992.
- [2] *McGraw-Hill Dictionary of Scientific & Technical Terms*. [Online]. Available: <https://encyclopedia2.thefreedictionary.com/interstellar+travel> (accessed: Mar. 8 2021).
- [3] M. Scholz, *Die Physik der Sterne*. Berlin, Heidelberg: Springer Berlin Heidelberg, 2018.
- [4] A. Unsöld and B. Baschek, *Der neue Kosmos: Einführung in die Astronomie und Astrophysik*, 7th ed.: Springer Berlin Heidelberg, 2002.
- [5] Deutsches Zentrum für Luft- und Raumfahrt, *New Horizons und andere Raumsonden an den Grenzen des Sonnensystems*. [Online]. Available: <https://www.dlr.de/content/de/bilder/2020/03/new-horizons-und-andere-raumsonden-an-den-grenzen-des-sonnensystems.html> (accessed: Feb. 21 2021).
- [6] Jet Propulsion Laboratory, *Voyager - Mission Status*. [Online]. Available: <https://voyager.jpl.nasa.gov/mission/status/> (accessed: Mar. 10 2021).
- [7] T. Radford, *Stephen Hawking and Yuri Milner launch \$100m star voyage*. [Online]. Available: <https://www.theguardian.com/science/2016/apr/12/stephen-hawking-and-yuri-milner-launch-100m-star-voyage>
- [8] European Southern Observatory, *Planet Found in Habitable Zone Around Nearest Star: Pale Red Dot campaign reveals Earth-mass world in orbit around Proxima Centauri*. [Online]. Available: <https://www.eso.org/public/news/eso1629/> (accessed: Mar. 1 2021).
- [9] K. L.G. Parkin, "The Breakthrough Starshot system model," *Acta Astronautica*, vol. 152, pp. 370–384, 2018, doi: 10.1016/j.actaastro.2018.08.035.
- [10] K. F. Long, *Deep Space Propulsion*. New York, NY: Springer New York, 2012.
- [11] S. Gong and M. Macdonald, "Review on solar sail technology," *Astrodyn*, vol. 3, no. 2, pp. 93–125, 2019, doi: 10.1007/s42064-019-0038-x.
- [12] O. Borgue and A. M. Hein, "Near-Term Self-replicating Probes -- A Concept Design," May. 2020. [Online]. Available: <http://arxiv.org/pdf/2005.12303v2>
- [13] D. Stephenson, "Models of Interstellar Exploration," *Quarterly Journal of The Royal Astronomical Society*, no. 23, pp. 236–251, 1982.
- [14] A. M. Hein and S. Baxter, "Artificial Intelligence for Interstellar Travel," 2018.
- [15] R. L. Forward, "Feasibility of interstellar travel: A review," *Acta Astronautica*, vol. 14, pp. 243–252, 1986, doi: 10.1016/0094-5765(86)90126-8.
- [16] N. Kulkarni, P. Lubin, and Q. Zhang, "Relativistic Spacecraft Propelled by Directed Energy," *AJ*, vol. 155, no. 4, 2018, doi: 10.3847/1538-3881/aaafd2.
- [17] R. L. Forward, "Roundtrip interstellar travel using laser-pushed lightsails," *Journal of Spacecraft and Rockets*, vol. 21, no. 2, pp. 187–195, 1984, doi: 10.2514/3.8632.

- [18] A. Bond *et al.*, "Project Daedalus - The Final Report on the BIS Starship Study," *Journal of the British Interplanetary Society*, 1978.
- [19] C. Elachi *et al.*, "A Road Map for the Exploration of Neighboring Planetary Systems (ExNPS)," 1996.
- [20] P. Gilster, *Centauri Dreams: Imagining and Planning Interstellar Exploration*. New York, NY: Springer, 2004.
- [21] X. Zeng, K. T. Alfriend, J. Li, and S. R. Vadali, "Optimal Solar Sail Trajectory Analysis for Interstellar Missions," *J of Astronaut Sci*, vol. 59, no. 3, pp. 502–516, 2012, doi: 10.1007/s40295-014-0008-y.
- [22] E. Baumann, "Swarm-Based Concepts for Resilient Autonomous Interstellar Exploration Systems," *INSIGHT*, vol. 18, no. 1, pp. 34–40, 2015, doi: 10.1002/inst.12009.
- [23] A. M. Hein *et al.*, "The Andromeda Study: A Femto-Spacecraft Mission to Alpha Centauri," Aug. 2017. [Online]. Available: <http://arxiv.org/pdf/1708.03556v1>
- [24] R. L. Forward, "Starwisp - An ultra-light interstellar probe," *Journal of Spacecraft and Rockets*, vol. 22, no. 3, pp. 345–350, 1985, doi: 10.2514/3.25754.
- [25] S. A. Cohen *et al.*, "Direct fusion drive for interstellar exploration," *Journal of the British Interplanetary Society*, no. 72, pp. 37–50, 2019.
- [26] D. Cartin, "Exploration of the local solar neighbourhood I: Fixed number of probes," *International Journal of Astrobiology*, vol. 12, no. 4, pp. 271–281, 2013, doi: 10.1017/S1473550413000098.
- [27] R. Bjørk, "Exploring the Galaxy using space probes," *International Journal of Astrobiology*, vol. 6, no. 2, pp. 89–93, 2007, doi: 10.1017/S1473550407003709.
- [28] C. Cotta and Á. Morales, "A Computational Analysis of Galactic Exploration with Space Probes: Implications for the Fermi Paradox," *J.Br.Interplanet.Soc.62(3):82-88*. [Online]. Available: <http://arxiv.org/pdf/0907.0345v1>
- [29] F. Valdes and R. A. Freitas, *Comparison of Reproducing and Nonreproducing Starprobe Strategies for Galactic Exploration*. [Online]. Available: <http://www.rfreitas.com/Astro/ComparisonReproNov1980.htm> (accessed: Aug. 11 2020).
- [30] D. H. Forgan, S. Papadogiannakis, and T. Kitching, "The Effect of Probe Dynamics on Galactic Exploration Timescales," Dec. 2012.
- [31] Extreme Optimization, *Optimization Model Basics*. [Online]. Available: <https://www.extremeoptimization.com/Documentation/Mathematics/Optimization/Optimization-Model-Basics.aspx> (accessed: Mar. 1 2021).
- [32] K. F. Long *et al.*, "PROJECT ICARUS: Son of Daedalus, Flying Closer to Another Star," [Online]. Available: <http://arxiv.org/pdf/1005.3833v1>
- [33] H. Garrett, I. Jun, and A. Shapiro, "Interstellar Space Missions: Ultra-Reliability Requirements and Engineering Issues," in *Aerospace Sciences Meetings: 45th AIAA Aerospace Sciences Meeting and Exhibit*, Reno, Nevada, 2007.

- [34] G. F. Bignami and A. Sommariva, *A Scenario for Interstellar Exploration and Its Financing*. Milano: Springer Milan, 2013.
- [35] P. Lubin and W. Hettel, "The Path to Interstellar Flight," 2020, doi: 10.5281/ZENODO.3747263.
- [36] M. Huo, G. Mengali, and A. A. Quarta, "Mission design for an interstellar probe with e-sail propulsion system," vol. 68, pp. 128–134, 2015.
- [37] G. L. Matloff, *Deep-space probes: To the outer solar system and beyond*, 2nd ed. Berlin, New York, Chichester UK: Springer; Published in association with Praxis Pub, 2005.
- [38] D.-I. Moon *et al.*, "Sustainable electronics for nano-spacecraft in deep space missions," in *2016 IEEE International Electron Devices Meeting (IEDM)*, San Francisco, CA, USA, Dec. 2016 - Dec. 2016, 31.8.1-31.8.4.
- [39] P. Lubin, "A Roadmap to Interstellar Flight," *Journal of the British Interplanetary Society*, no. 69, pp. 40–72, 2016.
- [40] D. Messerschmitt, P. Lubin, and I. Morrison, "Relaying Swarms of Low-Mass Interstellar Probes," Jul. 2020.
- [41] G. L. Matloff, "Laser-light sailing and non-stationary power stations applied to robotic star probes," in *AIP Conference Proceedings*, Seoul (Korea), Feb. 2001, pp. 993–997.
- [42] I. A. Crawford, "Direct Exoplanet Investigation using Interstellar Space Probes," in *Handbook of Exoplanets*, H. J. Deeg and J. A. Belmonte, Eds., New York NY: Springer Berlin Heidelberg, 2018, pp. 3413–3431. [Online]. Available: <http://arxiv.org/pdf/1707.01174v2>
- [43] M. G. Millis, "Energy, incessant obsolescence, and the first interstellar missions," *Presented at the 61st International Astronautical Congress*. [Online]. Available: <http://arxiv.org/pdf/1101.1066v1>
- [44] A. Jones, "Self-replicating probes for galactic exploration," 1991.
- [45] R. A. Freitas, "A Self-Reproducing Interstellar Probe," *Journal of the British Interplanetary Society*, no. 33, pp. 251–264, 1980.
- [46] A. Nicholson and D. Forgan, "Slingshot Dynamics for Self Replicating Probes and the Effect on Exploration Timescales," *International Journal of Astrobiology*, vol. 12, no. 4, pp. 337–344, 2013, doi: 10.1017/S1473550413000244.
- [47] G. Munévar, "Self-Reproducing Automata and the Impossibility of SETI," in *Imagining Outer Space: European Astroculture in the Twentieth Century*, A. C. T. Geppert, Ed., London: Palgrave Macmillan UK, 2012, pp. 267–284.
- [48] M. T. Barlow, "Galactic exploration by directed self-replicating probes, and its implications for the Fermi paradox," *International Journal of Astrobiology*, vol. 12, no. 1, pp. 63–68, 2013, doi: 10.1017/S1473550412000419.
- [49] J. Suthakorn, A. B. Cushing, and G. S. Chirikjian, "An autonomous self-replicating robotic system," in *2003 IEEE*, Kobe, Japan, 2003, pp. 137–142.
- [50] A. M. Hein, "Artificial Intelligence Probes for Interstellar Exploration and Colonization," 2016.

- [51] R. A. Freitas, T. J. Healy, and J. E. Long, "Advanced automation for space missions," *Journal of the Astronautical Sciences*, no. 30, 1982, doi: 10.1016/0165-6074(81)90105-8.
- [52] E. Özkural, *Artificial Intelligence and Brain Simulation Probes for Interstellar Expeditions*, 2018.
- [53] V. Graziano *et al.*, "Artificial Curiosity for Autonomous Space Exploration," *Acta Futura*, pp. 41–51, 2011.
- [54] M. Sievers and A. M. Madni, "Agent-Based Flexible Design Contracts for Resilient Spacecraft Swarms," 2016.
- [55] D. Andrews and R. Zubrin, "Magnetic Sails and Interstellar Travel," *Journal of the British Interplanetary Society*, no. 43, pp. 265–272, 1990.
- [56] N. Perakis and A. M. Hein, "Combining magnetic and electric sails for interstellar deceleration," *Acta Astronautica*, vol. 128, pp. 13–20, 2016, doi: 10.1016/j.actaastro.2016.07.005.
- [57] C. Gros, "Why planetary and exoplanetary protection differ: The case of long duration genesis missions to habitable but sterile M-dwarf oxygen planets," *Acta Astronautica*, vol. 157, pp. 263–267, 2019, doi: 10.1016/j.actaastro.2019.01.005.
- [58] R. Heller and M. Hippke, "Deceleration of high-velocity interstellar photon sails into bound orbits at α Centauri," *ApJ*, vol. 835, no. 2, 2017, doi: 10.3847/2041-8213/835/2/L32.
- [59] R. Heller, M. Hippke, and P. Kervella, "Optimized Trajectories to the Nearest Stars Using Lightweight High-velocity Photon Sails," *AJ*, vol. 154, no. 3, 2017, doi: 10.3847/1538-3881/aa813f.
- [60] M. Lingam and A. Loeb, "Electric sails are potentially more effective than light sails near most stars," *Acta Astronautica*, vol. 168, pp. 146–154, 2020, doi: 10.1016/j.actaastro.2019.12.013.
- [61] I. A. Crawford, "Project Icarus: A Review of Local Interstellar Medium Properties of Relevance for Space Missions to the Nearest Stars," *Acta Astronautica*, vol. 68, 7-8, pp. 691–699, 2011, doi: 10.1016/j.actaastro.2010.10.016.
- [62] T. Hoang, A. Lazarian, B. Burkhart, and A. Loeb, "The Interaction of Relativistic Spacecrafts with the Interstellar Medium," *ApJ*, vol. 837, no. 1, pp. 5–21, 2017, doi: 10.3847/1538-4357/aa5da6.
- [63] G. Vulpetti, "On the viability of The Interstellar Flight," *Acta Astronautica*, vol. 44, 7-12, pp. 769–792, 1999, doi: 10.1016/S0094-5765(99)00096-X.
- [64] R. N. BRACEWELL, "Communications from Superior Galactic Communities," *Nature*, vol. 186, no. 4726, pp. 670–671, 1960, doi: 10.1038/186670a0.
- [65] R. Frisbee, "Impact of Interstellar Vehicle Acceleration and Cruise Velocity on Total Mission Mass and Trip Time," in *Joint Propulsion Conferences: 42nd AIAA/ASME/SAE/ASEE Joint Propulsion Conference & Exhibit*, Sacramento, California, 2006.

- [66] A. K. Singh, K. Vishwakarma, and U. Guven, “Case Study of An Interstellar Mission To Luhman 16: Unmanned Interstellar Probe Powered by Gas Core Nuclear Reactors,” 2019.
- [67] V. Surdin, “Launch of a galactic probe using a multiple perturbation maneuver,” *Solar System Research*, vol. 19, no. 4, pp. 229–231, 1986.
- [68] A. Hanslmeier, *Einführung in Astronomie und Astrophysik*. Berlin, Heidelberg: Springer Berlin Heidelberg, 2020.
- [69] ESA/Gaia Data Processing and Analysis Consortium, *Gaia's Hertzsprung-Russell Diagram*. [Online]. Available: <https://sci.esa.int/web/gaia/-/60198-gaia-hertzsprung-russell-diagram> (accessed: Aug. 21 2020).
- [70] ESO, *Artist's impression of the Milky Way (updated - annotated)*. [Online]. Available: <https://www.eso.org/public/images/eso1339e/> (accessed: Aug. 22 2020).
- [71] W. Demtröder, *Experimentalphysik 4*. Berlin, Heidelberg: Springer Berlin Heidelberg, 2010. Accessed: Aug. 22 2020.
- [72] G. Kaplan, “The IAU Resolutions on Astronomical Reference Systems, Time Scales, and Earth Rotation Models,” 2006.
- [73] E. Fantino and S. Casotto, “Study on Libration Points of the Sun and the Interstellar Medium for Interstellar Travel,” 2004.
- [74] D. Boubert, J. Guillochon, K. Hawkins, I. Ginsburg, N. W. Evans, and J. Strader, “Revisiting hypervelocity stars after Gaia DR2,” *Monthly Notices of the Royal Astronomical Society*, vol. 479, no. 2, pp. 2789–2795, 2018, doi: 10.1093/mnras/sty1601.
- [75] W. R. Brown, “Hypervelocity stars in the Milky Way,” *Physics Today*, vol. 69, no. 6, pp. 52–58, 2016, doi: 10.1063/PT.3.3199.
- [76] ESA, *The Hipparcos Space Astrometry Mission*. [Online]. Available: <https://www.cosmos.esa.int/web/hipparcos/home> (accessed: Aug. 23 2020).
- [77] ESA, *Summary of the Hipparcos and Tycho Catalogues*. [Online]. Available: <https://www.cosmos.esa.int/web/hipparcos/catalogue-summary> (accessed: Feb. 1 2021).
- [78] M. C. Turnbull and J. C. Tarter, “Target Selection for SETI. I. A Catalog of Nearby Habitable Stellar Systems,” *The Astrophysical Journal Supplement Series*, vol. 145, no. 1, pp. 181–198, 2003, doi: 10.1086/345779.
- [79] Astronomisches Rechen-Institut Heidelberg, *Sechster Katalog von Fundamentalsternen FK6*. [Online]. Available: <https://www.add.zah.uni-heidelberg.de/datenbanken/fk6/index.php.de> (accessed: Aug. 24 2020).
- [80] Astronomisches Rechen-Institut Heidelberg, *Databases*. [Online]. Available: <https://zah.uni-heidelberg.de/institutes/astronomisches-rechen-institut/databases> (accessed: Aug. 24 2020).
- [81] Research Consortium on Nearby Stars, *The one hundred nearest star systems*. [Online]. Available: <http://www.recons.org/TOP100.posted.htm> (accessed: Aug. 23 2020).

- [82] C. W. Allen and A. N. Cox, *Allens astrophysical quantities*, 4th ed. New York: AIP Press; Springer, 2002.
- [83] K. von Braun and T. Boyajian, *Extrasolar Planets and Their Host Stars*. Cham: Springer International Publishing, 2017.
- [84] W. Knapp, “Star Systems in the Solar Neighborhood up to 10 Parsecs Distance,” *Journal of Double Star Observations*, vol. 16, no. 3, pp. 229–288, 2020.
- [85] ESA, *Gaia Data Release 1 (Gaia DR1)*. [Online]. Available: <https://www.cosmos.esa.int/web/gaia/dr1> (accessed: Aug. 23 2020).
- [86] ESA, *Gaia Early Data Release 3 (Gaia EDR3)*. [Online]. Available: <https://www.cosmos.esa.int/web/gaia/earlydr3> (accessed: Jan. 10 2021).
- [87] ESA, *Gaia Data Release 2 (Gaia DR2)*. [Online]. Available: <https://www.cosmos.esa.int/web/gaia/dr2> (accessed: Aug. 22 2020).
- [88] D. Boubert and A. Everall, “Completeness of the Gaia verse II: what are the odds that a star is missing from Gaia DR2?,” *Monthly Notices of the Royal Astronomical Society*, vol. 497, no. 4, pp. 4246–4261, 2020, doi: 10.1093/mnras/staa2305.
- [89] C. A. L. Bailer-Jones, J. Rybizki, M. Fouesneau, G. Mantelet, and R. Andrae, “Estimating distances from parallaxes IV: Distances to 1.33 billion stars in Gaia Data Release 2,” *AJ*, vol. 156, no. 2, 2018, doi: 10.3847/1538-3881/aacb21.
- [90] R. Andrae *et al.*, “Gaia Data Release 2: first stellar parameters from Apsis,” *A&A*, vol. 616, 2018, doi: 10.1051/0004-6361/201732516.
- [91] M. Johnson, *Kepler and K2: Mission overview*. [Online]. Available: https://www.nasa.gov/mission_pages/kepler/overview/index.html (accessed: Aug. 23 2020).
- [92] US Naval Observatory, *Catalog Information*. [Online]. Available: <https://www.usno.navy.mil/USNO/astrometry/information/catalog-info> (accessed: Aug. 23 2020).
- [93] *Sloan Digital Sky Survey: Mapping the Universe - Webpage*. [Online]. Available: <https://www.sdss.org/> (accessed: Aug. 24 2020).
- [94] I. A. Crawford, “The Astronomical, Astrobiological and Planetary Science Case for Interstellar Spaceflight,” *Journal of the British Interplanetary Society*, 2009. [Online]. Available: <http://arxiv.org/pdf/1008.4893v1>
- [95] F. Fressin *et al.*, “The false positive rate of Kepler and the occurrence of planets,” *ApJ*, vol. 766, no. 2, p. 81, 2013, doi: 10.1088/0004-637X/766/2/81.
- [96] G. D. Mulders, I. Pascucci, and D. Apai, “A stellar-mass-dependent Drop in Planet Occurrence Rates: A STELLAR-MASS-DEPENDENT DROP IN PLANET OCCURRENCE RATES,” *ApJ*, vol. 798, no. 2, p. 112, 2015, doi: 10.1088/0004-637X/798/2/112.
- [97] A. Maliuk and J. Budaj, “Spatial distribution of exoplanet candidates based on Kepler and Gaia data,” *A&A*, vol. 635, 2020, doi: 10.1051/0004-6361/201936692.
- [98] S. H. Dole, “Habitable Planets for Man,” 1964.

- [99] H. Lammer *et al.*, “What makes a planet habitable?,” *Astron Astrophys Rev*, vol. 17, no. 2, pp. 181–249, 2009, doi: 10.1007/s00159-009-0019-z.
- [100] V. S. Meadows and R. K. Barnes, “Factors Affecting Exoplanet Habitability,” in *Handbook of exoplanets*, H. J. Deeg and J. A. Belmonte, Eds., Cham, Switzerland: Springer, 2018, pp. 2771–2794.
- [101] J. F. Kasting, “When Methane Made Climate,” *Scientific American*, pp. 78–87, 2004.
- [102] S. N. Raymond, J. Scalo, and V. S. Meadows, “A Decreased Probability of Habitable Planet Formation around Low-Mass Stars,” *ApJ*, vol. 669, no. 1, pp. 606–614, 2007, doi: 10.1086/521587.
- [103] A. Gronstal, *An Inner Edge for Habitable Planets around Low-Mass Stars*. [Online]. Available: <https://astrobiology.nasa.gov/nai/articles/2016/5/9/an-inner-edge-for-habitable-planets-around-low-mass-stars/index.html> (accessed: Aug. 20 2020).
- [104] J. R. Cantrell, T. J. Henry, and R. J. White, “The Solar Neighborhood XXIX: The Habitable Real Estate of our Nearest Stellar Neighbors,” *AJ*, vol. 146, no. 4, 2013, doi: 10.1088/0004-6256/146/4/99.
- [105] R. k. Kopparapu *et al.*, “The inner edge of the habitable zone for synchronously rotating planets around low-mass stars using general circulation models,” *ApJ*, vol. 819, no. 1, 2016, doi: 10.3847/0004-637X/819/1/84.
- [106] R. k. Kopparapu, “A revised estimate of the occurrence rate of terrestrial planets in the habitable zones around kepler m-dwarfs,” *ApJ*, vol. 767, no. 1, 2013, doi: 10.1088/2041-8205/767/1/L8.
- [107] J. Scalo *et al.*, “M stars as targets for terrestrial exoplanet searches and biosignature detection,” *Astrobiology*, vol. 7, no. 1, pp. 85–166, 2007, doi: 10.1089/ast.2006.0125.
- [108] G. N. Arney, “The K Dwarf Advantage for Biosignatures on Directly Imaged Exoplanets,” *ApJ*, vol. 873, no. 1, L7, 2019, doi: 10.3847/2041-8213/ab0651.
- [109] R. Garner, *Goldilocks Stars Are Best Places to Look for Life*. [Online]. Available: <https://www.nasa.gov/feature/goddard/2020/goldilocks-stars-are-best-places-to-look-for-life> (accessed: Jan. 9 2021).
- [110] D. Atri, “Stellar Proton Event-induced surface radiation dose as a constraint on the habitability of terrestrial exoplanets,” *Monthly Notices of the Royal Astronomical Society: Letters*, 2019, doi: 10.1093/mnrasl/slz166.
- [111] A. Petropoulos, E. Gustafson, G. Whiffen, and B. Anderson, “GTOC X, The 10th Global Trajectory Optimisation Competition - Settlers of the Galaxy,” 2019.
- [112] D. Izzo *et al.*, “GTOC-X: Our Plan to settle the Galaxy (ESA-ACT),” 2019.
- [113] A. Zavoli, L. Federici, B. Benedikter, L. Casalino, and G. Colasurdo, “GTOC X: Solution Approach of Team Sapienza-PoliTo,” Sep. 2019.
- [114] C. Zhang, H. Zhang, H. Peng, C.-H. Yang, and Y. Gao, “Settlers of the Galaxy: The CSU Solution to GTOCX,” 2019.

- [115] Y.-Z. Luo *et al.*, “GTOC X: Results and Methods of National University of Defense Technology and Xi'an Satellite Control Center,” 2019.
- [116] S. Li, X. Huang, and B. Yang, “Review of optimization methodologies in global and China trajectory optimization competitions,” *Progress in Aerospace Sciences*, vol. 102, pp. 60–75, 2018, doi: 10.1016/j.paerosci.2018.07.004.
- [117] D. Izzo, D. Hennes, L. F. Simões, and M. Märten, “Designing Complex Interplanetary Trajectories for the Global Trajectory Optimization Competitions,” in *Springer Optimization and Its Applications, Space Engineering*, G. Fasano and J. D. Pintér, Eds., 1st ed.: Springer International Publishing Switzerland, 2016, pp. 151–176.
- [118] V. Maiwald, “Evolutionary Algorithms in Astronautic Applications,” 2010.
- [119] O. Abdelkhalik and D. Mortari, “N-Impulse Orbit Transfer Using Genetic Algorithms,” *Journal of Spacecraft and Rockets*, vol. 44, no. 2, pp. 456–460, 2007, doi: 10.2514/1.24701.
- [120] G. A. Rauwolf and V. L. Coverstone-Carroll, “Near-optimal low-thrust orbit transfers generated by a genetic algorithm,” *Journal of Spacecraft and Rockets*, vol. 33, no. 6, pp. 859–862, 1996, doi: 10.2514/3.26850.
- [121] K. K.H. Fung, G. F. Lewis, and X. Wu, “The optimisation of low-acceleration interstellar relativistic rocket trajectories using genetic algorithms,” *Acta Astronautica*, vol. 133, pp. 258–268, 2017, doi: 10.1016/j.actaastro.2017.01.033.
- [122] T. Vinkó and D. Izzo, “Global Optimisation Heuristics and Test Problems for Preliminary Spacecraft Trajectory Design,” 2008.
- [123] B. Addis, A. Cassioli, M. Locatelli, and F. Schoen, “A global optimization method for the design of space trajectories,” *Computational Optimization and Applications*, vol. 48, no. 3, pp. 635–652, 2011, doi: 10.1007/s10589-009-9261-6.
- [124] S. Wagner and B. Wie, “Hybrid Algorithm for Multiple Gravity-Assist and Impulsive Delta-V Maneuvers,” *Journal of Guidance, Control, and Dynamics*, vol. 38, no. 11, pp. 2096–2107, 2015, doi: 10.2514/1.G000874.
- [125] J. W. Hartmann, V. L. Coverstone-Carroll, and S. N. Williams, “Optimal Interplanetary Spacecraft Trajectories via a Pareto Genetic Algorithm,” *Journal of the Astronautical Sciences*, vol. 46, no. 3, pp. 267–282, 1998, doi: 10.1007/BF03546237.
- [126] S. Selvaraj, “Interplanetary Trajectory Optimization of Solar Sails,” 2018.
- [127] M. Vasile and P. DePascale, “On the Preliminary Design of Multiple Gravity-Assist Trajectories,” *Journal of Spacecraft and Rockets*, vol. 42, no. 4, pp. 794–805, 2006. [Online]. Available: <http://arxiv.org/pdf/1105.1822v1>
- [128] M. Vasile and M. Locatelli, “A hybrid multiagent approach for global trajectory optimization,” *Journal of Global Optimization*, vol. 44, no. 4, pp. 461–479, 2009, doi: 10.1007/s10898-008-9329-3.
- [129] B. Dachwald, “Low-Thrust Trajectory Optimization and Interplanetary Mission Analysis Using Evolutionary Neurocontrol,” 2004.

- [130] F. Schoutetens, "Photon-Sail Trajectory Optimization in Alpha Centauri using Evolutionary Neurocontrol," 2019.
- [131] B. Dachwald, "Evolutionary Neurocontrol: A Smart Method for Global Optimization of Low-Thrust Trajectories," in *Guidance, Navigation, and Control and Co-located Conferences: AIAA/AAS Astrodynamics Specialist Conference and Exhibit*, Providence, Rhode Island, 2004.
- [132] A. Ohndorf, "Multiphase Low-Thrust Trajectory Optimization Using Evolutionary Neurocontrol," 2016.
- [133] J. Olympio, "Optimisation and optimal control methods for planet sequence design of low-thrust Interplanetary transfer problems with gravity-assists," École Nationale Supérieure des Mines de Paris, 2008. [Online]. Available: <https://pastel.archives-ouvertes.fr/tel-00365115>
- [134] S. W. Napier, J. W. McMahon, and J. A. Englander, "A Multi-Objective, Multi-Agent Transcription for the Global Optimization of Interplanetary Trajectories," *The Journal of the Astronautical Sciences*, 2020, doi: 10.1007/s40295-020-00215-2.
- [135] D. Izzo, M. Märten, and B. Pan, "A Survey on Artificial Intelligence Trends in Spacecraft Guidance Dynamics and Control," Dec. 2018.
- [136] D. Izzo, C. Sprague, and D. Taylor, "Machine learning and evolutionary techniques in interplanetary trajectory design," Feb. 2018.
- [137] P. Di Lizia and G. Radice, "Advanced Global Optimisation Tools for Mission Analysis and Design," 2004.
- [138] P. Di Lizia, G. Radice, D. Izzo, and M. Vasile, *On the Solution of Interplanetary Trajectory Design Problems by Global Optimisation Methods*, 2005.
- [139] D. Myatt, V. Becerra, S. Nasuto, and J. Bishop, "Advanced global optimisation for mission analysis and design," 2004.
- [140] V. Becerra, D. Myatt, S. Nasuto, J. Bishop, and D. Izzo, "An Efficient Pruning Technique for the Global Optimisation of Multiple Gravity Assist Trajectories," 2005.
- [141] B. Yang, Q. LI, S. Li, and H. YANG, "Autonomous multi-target rendezvous mission planning using artificial intelligence," 2019.
- [142] Y. Liu, J. Yang, Y. Wang, Q. Pan, and J. Yuan, "Multi-objective optimal preliminary planning of multi-debris active removal mission in LEO," *Science China Information Sciences*, vol. 60, no. 7, 2017, doi: 10.1007/s11432-016-0566-7.
- [143] H.-X. Shen, T.-J. Zhang, L. Casalino, and D. Pastrone, "Optimization of Active Debris Removal Missions with Multiple Targets," *Journal of Spacecraft and Rockets*, vol. 55, no. 1, pp. 181–189, 2018, doi: 10.2514/1.A33883.
- [144] T. Zhang, H. Shen, Y. Yang, H. Li, and J. Li, "Ant Colony Optimization-based Design of Multiple-target Active Debris Removal Mission," *TRANSACTIONS OF THE JAPAN SOCIETY FOR AERONAUTICAL AND SPACE SCIENCES*, vol. 61, no. 5, pp. 201–210, 2018, doi: 10.2322/tjsass.61.201.

- [145] M. Cerf, "Multiple Space Debris Collecting Mission—Debris Selection and Trajectory Optimization," *Journal of Optimization Theory and Applications*, vol. 156, no. 3, pp. 761–796, 2013, doi: 10.1007/s10957-012-0130-6.
- [146] A. BAREA, H. URRUTXUA, and L. CADARSO, "Optimal large-scale object selection and trajectory planning for active space debris removal missions," 2019.
- [147] H. Li, S. Chen, and H. Baoyin, "J2-Perturbed Multitarget Rendezvous Optimization with Low Thrust," *Journal of Guidance, Control, and Dynamics*, vol. 41, no. 3, pp. 802–808, 2018, doi: 10.2514/1.G002889.
- [148] J. Yang, Y. H. Hu, Y. Liu, X. Hou, and Q. Pan, "On the Application of Reinforcement Learning in Multi-debris Active Removal Mission Planning," in *2019 IEEE 28th International Symposium on Industrial Electronics (ISIE 2019): Vancouver, British Columbia, Canada, 12-14 June 2019*, Vancouver, BC, Canada, 2019, pp. 605–610.
- [149] H. Li and H. Baoyin, "Optimization of Multiple Debris Removal Missions Using an Evolving Elitist Club Algorithm," *IEEE Trans. Aerosp. Electron. Syst.*, vol. 56, no. 1, pp. 773–784, 2020, doi: 10.1109/TAES.2019.2934373.
- [150] D. Izzo, I. Getzner, D. Hennes, and L. F. Simões, "Evolving Solutions to TSP Variants for Active Space Debris Removal," in *GECCO'15 companion: Proceedings of the 2015 Annual Conference on Genetic and Evolutionary Computation, Madrid, Spain, July 11 - 15, 2015*, Madrid, Spain, 2016, pp. 1207–1214.
- [151] B. W. Barbee, S. Alfano, E. Pinon, K. Gold, and D. Gaylor, "Design of spacecraft missions to remove multiple orbital debris objects," in *Aerospace Conference, 2011 IEEE*, Big Sky, USA, 2011, pp. 1–14.
- [152] M. Di Carlo, J. M. Romero Martin, and M. Vasile, "Automatic trajectory planning for low-thrust active removal mission in low-earth orbit," *Advances in Space Research*, vol. 59, no. 5, pp. 1234–1258, 2017, doi: 10.1016/j.asr.2016.11.033.
- [153] J. Bang and J. Ahn, "Multitarget Rendezvous for Active Debris Removal Using Multiple Spacecraft," *Journal of Spacecraft and Rockets*, vol. 56, no. 4, pp. 1237–1247, 2019, doi: 10.2514/1.A34344.
- [154] M. Kanazaki, Y. Yamada, and M. Nakamiya, "Trajectory optimization of a satellite for multiple active space debris removal based on a method for the traveling serviceman problem," in *21st Asia Pacific Symposium on Intelligent and Evolutionary Systems (IES)*, 2017, pp. 61–66.
- [155] A. Zhou, L. Kang, and Z. Yan, "Solving dynamic TSP with evolutionary approach in real time," in *CEC 2003: The 2003 Congress on Evolutionary Computation : [proceedings] : Canberra, Australia, 8-12 December*, Canberra, Australia, 2003, pp. 951–957.
- [156] J. Zhang, Y. Luo, H. Li, and G. Tang, "Analysis of multiple asteroids rendezvous optimization using genetic algorithms," in *2015 IEEE Congress on Evolutionary Computation (CEC)*, Sendai, Japan, 2015, pp. 596–602.

- [157] A. Peloni, M. Ceriotti, and B. Dachwald, "Solar Sail Trajectory Design for a Multiple Near-Earth Asteroid Rendezvous Mission," 2016.
- [158] Y. Song and S. Gong, "Solar-sail trajectory design for multiple near-Earth asteroid exploration based on deep neural networks," *Aerospace Science and Technology*, vol. 91, pp. 28–40, 2019, doi: 10.1016/j.ast.2019.04.056.
- [159] K. ZHU, F. JIANG, J. Li, and H. Baoyin, "Trajectory Optimization of Multi-Asteroids Exploration with Low Thrust," *Trans. Japan Soc. Aero. S Sci.*, vol. 52, no. 175, pp. 47–54, 2009, doi: 10.2322/tjsass.52.47.
- [160] L. Federici, A. Zavoli, and G. Colasurdo, *Impulsive Multi-Rendezvous Trajectory Design and Optimization*, 2019.
- [161] N. Ganganath, C.-T. Cheng, K.-Y. Fok, and C. K. Tse, "Trajectory planning for 3D printing: A revisit to traveling salesman problem," in *2016 2nd International Conference on Control, Automation and Robotics (ICCAR)*, Hong Kong, Hong Kong, 2016, pp. 287–290.
- [162] M. Caserta and S. Voß, "A hybrid algorithm for the DNA sequencing problem," *Discrete Applied Mathematics*, vol. 163, pp. 87–99, 2014, doi: 10.1016/j.dam.2012.08.025.
- [163] D. Davendra, Ed., *Traveling Salesman Problem, Theory and Applications*: InTech, 2010.
- [164] G. Gutin and A. P. Punnen, Eds., *Traveling salesman problem and its variations*: Springer, 2007.
- [165] A. Larsen, "The Dynamic Vehicle Routing Problem," 2000.
- [166] V. Pillac, M. Gendreau, C. Guéret, and A. Medaglia, "A review of dynamic vehicle routing problems," *European Journal of Operational Research*, vol. 225, pp. 1–11, 2013, doi: 10.1016/j.ejor.2012.08.015.
- [167] A. Lim and F. Wang, "Multi-Depot Vehicle Routing Problem: A One-Stage Approach," *IEEE Trans. Automat. Sci. Eng.*, vol. 2, no. 4, pp. 397–402, 2005, doi: 10.1109/TASE.2005.853472.
- [168] J. Nalepa, Ed., *Smart delivery systems: Solving complex vehicle routing problems*, 1st ed. Cambridge: Elsevier, 2019.
- [169] P. Vansteenwegen and A. Gunawan, *Orienteering Problems*. Cham: Springer International Publishing, 2019. Accessed: Feb. 17 2021.
- [170] B. L. Golden, L. Levy, and R. Vohra, "The orienteering problem," *Naval Research Logistics*, vol. 34, no. 3, pp. 307–318, 1987, doi: 10.1002/1520-6750(198706)34:3<307::AID-NAV3220340302>3.0.CO;2-D.
- [171] K. C. Tan, T. H. Lee, Y. H. Chewand, and L. H. Lee, "A multiobjective evolutionary algorithm for solving vehicle routing problem with time windows," in *SMC '03 Conference proceedings: October 5-8, 2003, Crystal City Hyatt Regency, Washington, D.C., USA*, Washington, DC, USA, 2003, pp. 361–366.
- [172] H. Bederina and M. Hifi, "A hybrid multi-objective evolutionary algorithm for the team orienteering problem," in *2017 4th International Conference on Control*,

- Decision and Information Technologies (CoDIT)*, Barcelona, Apr. 2017 - Apr. 2017, pp. 898–903.
- [173] Y.-C. Liang and A. E. Smith, “An ant colony approach to the orienteering problem,” *Journal of the Chinese Institute of Industrial Engineers*, vol. 23, no. 5, pp. 403–414, 2006, doi: 10.1080/10170660609509336.
- [174] R. Montemanni, D. Weyland, and L. M. Gambardella, “An Enhanced Ant Colony System for the Team Orienteering Problem with Time Windows,” in *2011 International Symposium on Computer Science and Society (ISCCS 2011): Kota Kinabalu, Malaysia, 16-17 July 2011*, Kota Kinabalu, Malaysia, 2011, pp. 381–384.
- [175] D. Gavalas, C. Konstantopoulos, K. Mastakas, and G. Pantziou, “A survey on algorithmic approaches for solving tourist trip design problems,” *J Heuristics*, vol. 20, no. 3, pp. 291–328, 2014, doi: 10.1007/s10732-014-9242-5.
- [176] N. Siddique and H. Adeli, “Physics-based search and optimization: Inspirations from nature,” *Expert Systems*, vol. 33, no. 6, pp. 607–623, 2016, doi: 10.1111/exsy.12185.
- [177] E. Elbeltagi, T. Hegazy, and D. Grierson, “Comparison among five evolutionary-based optimization algorithms,” *Advanced Engineering Informatics*, vol. 19, no. 1, pp. 43–53, 2005, doi: 10.1016/j.aei.2005.01.004.
- [178] D. Wang, H. Wang, and L. Liu, “Unknown environment exploration of multi-robot system with the FORDPSO,” *Swarm and Evolutionary Computation*, vol. 26, pp. 157–174, 2016, doi: 10.1016/j.swevo.2015.09.004.
- [179] K. Premalatha and A. M. Natarajan, “Hybrid PSO and GA for global maximization,” *Int. J. Open Problems Compt. Math*, vol. 2, no. 4, pp. 597–608, 2009.
- [180] M. Settles and T. Soule, “Breeding Swarms: A GA/PSO Hybrid,” in *Proceedings of the 7th Annual Conference on Genetic and Evolutionary Computation*, 2005, pp. 161–168.
- [181] C. K. Monson and K. D. Seppi, “The Kalman Swarm,” in *Genetic and Evolutionary Computation – GECCO 2004*, Berlin, Heidelberg, 2004, pp. 140–150.
- [182] M. Løvbjerg, “Improving Particle Swarm Optimization by hybridization of stochastic search heuristics and Self-Organized Criticality,” 2002.
- [183] P. Moscato, “On Evolution, Search, Optimization, Genetic Algorithms and Martial Arts - Towards Memetic Algorithms,” *Caltech Concurrent Computation Program*, 2000.
- [184] P. Merz and B. Freisleben, “Memetic Algorithms for the Traveling Salesman Problem,” *Complex Syst*, vol. 14, 2002.
- [185] J. N. Winn and D. C. Fabrycky, “The Occurrence and Architecture of Exoplanetary Systems,” *Annu. Rev. Astron. Astrophys.*, vol. 53, no. 1, pp. 409–447, 2015, doi: 10.1146/annurev-astro-082214-122246.
- [186] J. Kovalevsky, *Fundamentals of astrometry*. Cambridge: Cambridge University Press, 2004.

- [187] J. Kennewell, *The Sun and Solar Activity: Solar Escape Velocity*. [Online]. Available: <https://www.sws.bom.gov.au/Educational/2/1/4> (accessed: Mar. 30 2021).
- [188] R. Moir and W. Barr, "Analysis of Interstellar Spacecraft Cycling Between the Sun and the Near Stars," *Journal of the British Interplanetary Society*, vol. 58, pp. 332–341, 2005.
- [189] S. J. Kenyon, B. C. Bromley, M. J. Geller, and W. R. Brown, "Hypervelocity Stars: From the Galactic Center to the Halo," *ApJ*, vol. 680, no. 1, pp. 312–327, 2008, doi: 10.1086/587738.
- [190] T. A. Collaboration *et al.*, "The Astropy Project: Building an inclusive, open-science project and status of the v2.0 core package," *AJ*, vol. 156, no. 3, p. 123, 2018, doi: 10.3847/1538-3881/aabc4f.
- [191] T. A. Collaboration *et al.*, "Astropy: A Community Python Package for Astronomy," *A&A*, vol. 558, A33, 2013, doi: 10.1051/0004-6361/201322068.
- [192] L. Lindegren *et al.*, "Gaia Data Release 2 - The astrometric solution," *A&A*, vol. 616, A2, 2018, doi: 10.1051/0004-6361/201832727.
- [193] C. Y. Cheong, K. C. Tan, D. K. Liu, and J. X. Xu, "A Multiobjective Evolutionary Algorithm for Solving Vehicle Routing Problem with Stochastic Demand," in *IEEE Congress on Evolutionary Computation, 2006. CEC 2006*, Vancouver, BC, Canada, 2006, pp. 1370–1377.
- [194] C. M. M. d. Fonseca, "Multiobjective Genetic Algorithms with Application to Control Engineering Problems," PhD Thesis, The University of Sheffield, 1995.
- [195] K. Deb, A. Pratap, S. Agarwal, and T. Meyarivan, "A fast and elitist multiobjective genetic algorithm: NSGA-II," *IEEE Trans. Evol. Computat.*, vol. 6, no. 2, pp. 182–197, 2002, doi: 10.1109/4235.996017.
- [196] E. Weisstein, *Sphere Point Picking*. [Online]. Available: <https://mathworld.wolfram.com/SpherePointPicking.html> (accessed: Feb. 10 2021).
- [197] Encyclopedia Britannica, *Diminishing return*. [Online]. Available: <https://www.britannica.com/topic/diminishing-returns> (accessed: Mar. 18 2021).
- [198] J. B. Kaler, *The 172 Brightest Stars: Through Magnitude 3.00*. [Online]. Available: <http://stars.astro.illinois.edu/sow/bright.html> (accessed: Feb. 14 2021).
- [199] B. Korte and J. Vygen, *Kombinatorische Optimierung*. Berlin, Heidelberg: Springer Berlin Heidelberg, 2018.